REFERENCE ONLY

UNIVERSITY OF LONDON THESIS

Degree PhD Year 2006 Name of Author CROSS J.U.

Regulation of the pro-apoptotic protein Bax

Justin R Cross

A thesis is submitted towards the degree of:

Doctor of Philosophy

February 2006

Signal Transduction Laboratory,
Cancer Research UK – London Research Institute,
44 Lincoln's Inn Fields, London.

Department of Biochemistry and Molecular Biology,
University College London,
Gower Street, London.

ProQuest LLC
789 East Eisenhower Parkway
P.O. Box 1346
Ann Arbor, MI 48106-1346

Abstract:

Apoptosis is essential for correct development and tissue homeostasis of multi-cellular organisms as well as providing a critical safety mechanism to remove unwanted and damaged cells throughout life. Apoptosis is also relevant to human pathologies: many cancers acquire lesions in apoptotic pathways whilst inappropriate activation of apoptosis occurs in degenerative disease. This thesis studies the regulation and function of a key regulator of apoptosis and mitochondrial dysfunction, the Bcl-2 family member, Bax.

Bax is shown to be a cytoplasmic protein that, upon activation, rapidly translocates into mitochondrially-associated foci. The timing and possible causes of Bax activation have been studied. Live cell video microscopy reveals that this is a rapid and co-ordinated process and is accompanied by loss of the mitochondrial membrane potential. Two viral proteins, E1B19k from Adenovirus and BHRF1 from Epstein Bar Virus, are shown to block Bax activation at different steps. Using these proteins it is shown that changes in mitochondrial ultrastructure occur prior to Bax activation.

In the second part of this thesis, a structure / function analysis of the Bax protein leads to the identification of a novel mutation that promotes its activation. Subsequently, this mutation is used, in combination with E1B19k, in a proteomic strategy to isolate and identify candidate Bax interacting proteins at a critical step in the protein's activation. The results of this, and a similar screen with another Bcl-2 family protein, Bcl-XL, are reported. The data set contains known interacting proteins and proteins previously implicated in apoptosis control. In addition a range of metabolic and transport proteins not previously implicated in the control of Bcl-2 family proteins are identified and their relevance discussed.

Dedication:

To my family,

and especially Mum and Dad.

Acknowledgements:

The work presented in this thesis would not have been possible without the assistance of many people. Firstly, I would like to thank my advisor, Julian Downward, for his steadfast support though out every stage of the development of this work and also for giving me the freedom to try new experiments and freely explore avenues of investigation suggested by the data.

I would also like to thank all the members of the Signal Transduction Laboratory, past and present, for their contributions scientifically, intellectually and socially which have made the past few years in London so enjoyable. In particular I would like to thank David Hancock, Miguel Martins and Ingram Iaccarino for advice and insights that have helped the progress of this work and Antonio Postigo in the Cell Motility Laboratory for fruitful discussions and collaboration.

I would also like to thank staff of the wonderful research services, formerly of the Imperial Cancer Research Fund, and now Cancer Research UK. In particular: Graham Clark and Olga O'Neill in the Equipment Park, Ken Blight in the Electron Microscopy Unit, Gary Warnes in the FACS Laboratory, Colin Gray and Peter Jordan in the Light Microscopy Laboratory, Sarah Haranhan, Nicholas Michael, Malcolm Saxton and Nick Totty in the Protein Analysis Laboratory, and Peter Sheehan for IT support.

Finally, I would like to thank my friends and family who have made the past few years so enjoyable. I would like to thank Kathy for her encouragement and understanding in everything I have done. In particular, I would like to thank my Mum and Dad for their constant support and encouragement when I was working and for providing a refuge when I was not.

Table of Contents:

Abstract *2*

Dedication *3*

Acknowledgements *4*

Table of Contents *5*

List of Figures *9*

List of Tables *12*

Abbreviations *13*

Chapter 1 – Introduction

1.1 The origins of the apoptosis field **16**

1.2 Defining a genetic pathway for programmed cell death **16**

1.3 The Bcl-2 family and their place in cell death pathways **18**

1.4 Extrinsic cell death pathways **19**

1.5 BH3 only proteins – initiators of intrinsic cell deaths **21**

1.5.1 Bid 21

1.5.2 Bim 21

1.5.3 Bmf 21

1.5.4 Noxa and Puma 22

1.5.5 Bad 22

1.6 Bax and Bak **23**

1.7 Mitochondrial permeabilisation **24**

1.8 Execution of apoptotic cell deaths **25**

1.9 Final rites - DNA degradation and cell engulfment **26**

1.10 The structure of Bcl-2 family proteins: **28**

1.11 Bcl-2 proteins show structural similarity to bacterial pore-forming toxins **30**

1.12 Models for Bcl-2 family action and questions remaining 31

1.13 Outline of subsequent chapters 34

Chapter 2 – Materials and Methods

2.1 General buffers and solutions 44

2.2 Reagents and drug treatments 45

2.2.1 Drugs and reagents used to induce apoptosis 45

2.2.2 Antibiotics used for cell selection 46

2.2.3 Antibodies 46

2.2.4 Oligonucleotide primers 50

2.3 DNA methods 51

2.3.1 Basic DNA manipulations 51

2.3.2 DNA gel electrophoresis 51

2.3.3 Plasmid mutagenesis 51

2.3.4 Transformation of DNA into competent *E.coli* by heat shock 52

2.3.5 Purification of plasmid DNA 52

2.3.6 DNA sequencing 52

2.3.7 DNA constructs 53

2.4 Mammalian cell culture 54

2.4.1 Sources of cell lines used in this study 54

2.4.2 Cell growth conditions 54

2.4.3 Transfection methods 55

2.4.4 Retroviral infections 55

2.4.5 Production of stable inducible 293 T-REx cell lines 56

2.5 Protein methods 58

2.5.1 Determination of protein concentrations 58

2.5.2 SDS PAGE and western blotting 58

2.5.3 Co-immunoprecipitation 58

2.5.4 Gel filtration 59

2.5.5 Tandem affinity purifications 59

2.5.6 Concentration and visualisation of TAP purified proteins 60

2.5.7 Addition of cross-linkers to TAP purifications 60

2.6 Mass spectrometry 61

2.7 Fluorescence activated cell sorting (FACS) methods 62

2.7.1 Bax and Bak activation staining 62

2.7.2 Analysis of DNA content – SubG1 apoptosis assay 62

2.7.3 Annexin V staining – measuring apoptosis in GFP transfected cells 63

2.8 Immunofluorescence and confocal microscopy 64

2.9 Live cell video microscopy 65

2.9.1 Basic live cell recording experimental setup 65

2.9.2 Specific modifications for caspase 3/7 activity reporter experiments 67

2.9.3 Specific modifications for Pericam Ca^{2+} imaging experiments 68

2.10 Electron microscopy 69

Chapter 3 – Behaviour of the Bax protein

3.1 Introduction 70

3.2 Characterisation of conformationally sensitive Bax and Bak antibodies 71

3.3 Characterisation of Bax antibodies by immuofluorescence 73

3.4 GFP-Bax can be used to monitor Bax activation in live cells 74

3.5 Rapid and synchronised Bax activation appears to be locally initiated 76

3.6 Further consideration of the timing of GFP-Bax activation 78

3.7 Increased mitochondrial calcium is detectable prior to Bax activation 80

3.8 Discussion 82

Chapter 4 – Viral pro-survival proteins

4.1 Introduction 117

4.2 Characterisation of cell lines expressing pro-survival proteins 118

4.3 The effect of E1B19k and BHRF1 on Bax (and Bak) activation 120

4.4 Activation of GFP-Bax can also be blocked by E1B19k 124

4.5 Characterisation of the E1B19k block to GFP-Bax activation in live cells 125

4.6 Spreading loss and partial recovery of $\Delta\psi_m$ in E1B19k-expressing cells 128

4.7 Mitochondrial ultrastructural analysis in protected MCF10A cells 129

4.8 Discussion 133

Chapter 5 – Bax structure function analysis

5.1 Introduction **174**

5.2 Selection of Bax mutations **174**

5.3 Analysis of the effect of Bax mutations on protein localisation **176**

5.4 The toxicity of Bax mutations correlates with their localisation **179**

5.5 Discussion **180**

Chapter 6 – Bax interacting proteins

6.1 Introduction **200**

6.2 Design of the purification strategy **201**

6.3 Characterisation of 293 T-REx cells TAP-tagged Bax clonal cell lines **202**

6.4 Tandem Affinity Purifications with Bax **205**

6.5 Tandem Affinity Purifications with Bcl-XL **208**

6.6 Preliminary validation of candidate Bax and Bcl-XL interacting proteins **209**

6.7 Discussion **210**

6.7.1 Known interactions - E1B19k and the BH3 only proteins 211

6.7.2 F1F0 ATP Synthase complex and other inner membrane proteins 211

6.7.3 The Ribophorin / OST48 / DAD1 complex 212

6.7.4 VDAC and ANT 212

6.7.5 Rab7/JM4 and secretory pathway proteins 212

6.7.6 Proteins involved in Ca^{2+} regulation 212

Chapter 7 – General discussion

7.1 Progress made in this thesis: **233**

7.2 Concluding remarks: **244**

References ***248***

Appendix – Supplementary data figures ***267***

List of figures:

Figure 1.1 The sub-families of the Bcl-2 family and related viral pro-survival proteins. 36
Figure 1.2 Extrinsic and intrinsic apoptotic pathways. 38
Figure 1.3 Protein structures of Bcl-2 family members and related proteins. 40
Figure 1.4 Models for the action of Bcl-2 family proteins. 42

Figure 2.1 T-REx system (Invitrogen) inducible protein expression. 57
Figure 2.2 Representative clonal cell lines used for Tandem Affinity Purifications. 57
Figure 2.3 Summary of the Tandem Affinity Purification (TAP) method. 60
Figure 2.4 FACS analysis for dead cells with sub-G1 DNA content. 63
Figure 2.5 Basic design of filter system used for low light live cell microscopy. 66
Figure 2.6 Schematic outline of the Caspase 3 reporter construct (Clontech). 67
Figure 2.7 The mitochondrial pericam – a conformation sensitive permuted AFP protein. 68

Figure 3.1 Bax activation can be monitored using conformationally sensitive antibodies. 85
Figure 3.2 Bak activation can be monitored using conformationally sensitive antibodies. 87
Figure 3.3 Characterisation of commercially available anti-Bax and -Bak antibodies. 89
Figure 3.4 N-terminally directed anti-Bax antibodies reveal post-activation distributions. 92
Figure 3.5 The Bax 43-61 antibody reveals mitochondrially localised Bax in a distribution distinct from the bright Bax foci correlating with Cyt-c release. 94
Figure 3.6 GFP-Bax recapitulates the distributions observed for endogenous Bax. 96
Figure 3.7 Initial characterisation of GFP-Bax activation in live cells. 98
Figure 3.8 Translocation of GFP-Bax into clusters occurs synchronously with $\Delta\psi_m$ loss. 100
Figure 3.9 Local initiation of GFP-Bax activation is followed by spreading loss of $\Delta\psi_m$. 103
Figure 3.10 Local Bax activation appears to rapidly trigger Bax activation in a neighbouring region. .. 105
Figure 3.11 In low GFP-Bax expressing cells loss of $\Delta\psi_m$ occurs before GFP-Bax foci are detectable. 108
Figure 3.12 Bax activation precedes significant caspase 3/7 activity. 110
Figure 3.13 Flickering of $\Delta\psi_m$ is occasionally observed but does not correlate with the onset of complete $\Delta\psi_m$ loss. 113
Figure 3.14 An increase in mitochondrial calcium is detectable prior to Bax activation. 115

Figure 4.1 Generation of stable MCF10A cell lines expressing pro-survival proteins. 139
Figure 4.2 E1B19k and BHRF1 strongly protect against Fas/CHX induced apoptosis. 141
Figure 4.3 Pre-mitochondrial events occur in all cell lines whereas post-mitochondrial events are effectively blocked in the most strongly protected lines. 143
Figure 4.4 E1B19k and BHRF1 differ in their ability to block Bax and Bak activation. 145

Figure 4.5 The Bax conformational change takes place at the same rate in E1B19k and E.V. control cells. 147
Figure 4.6 Bak conformational change is also blocked in BHRF1-, but not in E1B19k- expressing cells. 149
Figure 4.7 Gel filtration confirms E1B19k and BHRF1 block Bax oligomerisation. 151
Figure 4.8 Additional biochemical characterisation of the action of BHRF1 and E1B19k. 153
Figure 4.9 GFP-Bax is also blocked at mitochondria in E1B19k-expressing cells. 155
Figure 4.10 GFP-Bax steadily accumulates at mitochondria of E1B19k-expressing cells. 157
Figure 4.11 The ability of E1B19k to block Bax activation is dependent upon expression level of GFP-Bax. 159
Figure 4.12 Further characterisation of E1B19k block forming and being breached. 161
Figure 4.13 E1B19k-expressing cells exhibit a spreading loss followed by partial recovery of $\Delta\psi_m$. 163
Figure 4.14 E1B19k-expressing cells exhibit rapid flickering and incomplete loss of $\Delta\psi_m$. 165
Figure 4.15 Characterisation of the changes in mitochondrial ultrastructure occurring following the induction of apoptosis. 167
Figure 4.16 Neither E1B19k nor BHRF1 prevent changes in mitochondrial ultrastructure. 171
Figure 4.17 Model for the block in Bax activation conferred by BHRF1 and E1B19k. 172

Figure 5.1 Schematics showing the positions of Bax mutations characterised in this study. 184
Figure 5.2 Analysis of the effect of mutations on N-terminal GFP-Bax localisation. 186
Figure 5.3 C-terminally tagged GFP-Bax mutants are predominantly cytoplasmic. 192
Figure 5.4 Bax-GFP L25P and Bax-GFP AAA show altered distributions in MCF10A E1B19k cells. 194
Figure 5.5 Summary of the localisation of the GFP Bax constructs analysed in this study. 196
Figure 5.6 Analysis of the toxicity of GFP Bax mutants. 198

Figure 6.1 Distribution of TAP-tagged Bax proteins in 293 T-REx clonal cell lines. 214
Figure 6.2 Expression of TAP-tagged Bax proteins does not change mitochondrial morphology in 293 T-REx clonal cell lines. 216
Figure 6.3 The gel filtration profile of TAP-tagged Bax is altered by Bax mutations. 218
Figure 6.4 Effect of detergents on the profile of proteins purified with TAP-tagged Bax. 220
Figure 6.5 The Bax-TAP L25P construct enhances the profile of purified proteins. 222
Figure 6.6 Summary of proteins identified by mass spectrometry in a preparative scale TAP purification with Bax-TAP L25P. 224
Figure 6.7 Western blot confirmation of the presence of proteins identified by mass spectrometry. 226
Figure 6.8 HeLa cells over-expressing TAP-Bcl-XL are protected from apoptosis and can be used for TAP purifications. 228
Figure 6.9 Preliminary validation of interactions identified in TAP experiments by co-immunoprecipitation. 231

Figure 7.1 Model for the regulation of Bax activation. 246

Supplementary Movie Figures:

The accompanying DVD will run on either Mac or PC and contains Supplementary Movie Figures for Chapter 3: M3.1 - M3.12 and Chapter 4: M4.1 - M4.8. The movies are best viewed from the within the Microsoft Powerpoint files included. However, the raw data files are also included as .avi files and can be viewed individually on any Quicktime or Microsoft compatible video player.

List of tables:

Table 2.1 Selective antibiotics used in this study. 46

Table 2.2 Details of primary antibodies appearing in this study. 47

Table 2.3 Details of secondary antibodies appearing in this study. 49

Table 6.1 Proteins identified in TAP purifications using HeLa TAP-Bcl-XL and 293 T-REx Bax-TAP L25P cells. 230

Abbreviations:

A	Alanine
aa	amino acid
ATP	Adenosine 5'-triphosphate
ATP	Adenosine triphosphate
BSA	Bovine serum albumin
°C	Centigrade
C	Carboxy
Ca^{2+}	Calcium
cAMP	Cyclic andenosine monophosphate
CBP	Calmodulin binding peptide
CFP	Cyan fluorescent protein
CHX	Cyclohexamide
CMV	Cytomegalovirus (promoter)
Cyt-c	Cytochrome c
DD	Death domain
ddH_2O	Double distilled H_2O
DED	Death effector dominan
DISC	Death-Inducing Signaling Complex
DKO	Double knocked out
DNA	Deoxyribose Nucleic Acid
Dox	Doxycycline
DSS	Disuccinimidyl suberate
DT	Diphtheria toxin
DTT	Dithiothreitol
E	Aspartic acid
E.V.	Empty Vector
EBV	Epstein Barr Virus
ECL	Enhanced chemiluminescence
ER	Endoplasmic reticulum
FACS	Flourescence activated cell sorting
Fas	Anti-Fas IgM antibody
FBS	Foetal bovine serum

FSG	Fish skin gelatin
G	Glycine
g	gramme
GFP	Green fluorescent protein
H_2O_2	Hydrogen peroxide
HRP	Horseradish peroxidase
hrs	hours
IAP	Inhibitor of apoptosis
IF	Immunofluorescence
IgG	Immunoglobulin G subclass
IgM	Immunoglobulin M subclass
IP	Immunoprecipitation
IP3R	Inositol 1,4,5-trisphosphate receptor
kDa	kilodalton
L	Leucine
l	litre
LB	Luria-Bertani
m	milli
M	Molar
MEF	Murine embryonic fibroblasts
MIM	Mitochondrial inner membrane
mins	minutes
MOM	Mitochondrial outer membrane
N	Amino
n	nanomolar
NES	Nuclear Export Signal
NLS	Nuclear Localisation Signal
O/N	Overnight
OD	Optical density
OHT	4-hydroytamoxifen
P	Proline
PAGE	Polyacrylamide gel electrophoresis
PBS	Phosphate buffered saline
PCR	Polymerase Chain Reaction
PI	Propidium iodide
ProA	Protein A
RFP	Red fluorescent protein

RNA	Ribonucleic acid
ROI	Region of interest
rpm	Revolutions per minute
RT	Room temperature
RyR	Ryanodine receptor
S	Serine
SDS	Sodium dodecyl sulphate
Ser	Serine
SR	Sarcoplasmic reticulum
STS	Staurosporine
TAP	Tandem affinity purification (tag)
TBS	Tris-buffered saline
TetR	Tetracycline repressor protein
TEV	Tobacco Etch Virus protease
TMRE	tetramethylrhodamine methyl ester
TO	Tetracycline operator sequence
UV	Ultraviolet
V	Volts
w.t.	wild type
YFP	Yellow fluorescent protein
$\Delta\psi_m$	Mitochondrial membrane potential
μ	micro

Chapter 1 – Introduction

1.1 The origins of the apoptosis field:

Nineteenth century anatomists, histologists and developmental biologists were the first to observe cells dying in a regulated and predictable manner. In the earliest instance these observations related to the metamorphosis of tadpoles and insects and the disappearance of transient embryonic structures such as the notocord (Clarke and Clarke, 1996).

The term programmed cell death was first coined by Richard Lockshin working with Carroll Williams at Harvard in the early 1960s (Lockshin and Williams, 1965). It captured the notion of a predictable and controlled series of events occurring in dying cells which could now be examined in detail with improving histological and biochemical techniques. Saunders also reported similar observations in a chick limb system (Saunders, 1966). By the late 1960s the Australian pathologist John Kerr observed that these dying cells were dying by 'shrinkage necrosis'. Necrotic cells are predicted to undergo swelling and lyse by rupture due to a failure of their ability to maintain their internal osmotic environment. Cell shrinkage is the reverse of this and implies an active process. Later it was Kerr, together with Andrew Wyllie and A.R. Currie who coined the term apoptosis to describe the specific pattern of cell death characterised by shrinkage, coalescence of chromatin and fragmentation of the nucleus and cell. The word itself is derived from the Greek words apo = from and ptosis = falling, as is reminiscent of the dropping of petals or of leaves from deciduous trees. However, their contribution went further than merely another description of the process, in their 1972 paper they argued that cell death or apoptosis was as much of a controlled cell process as mitosis, migration or differentiation (Kerr et al., 1972). They suggested the process is naturally occurring during development and for tissue homeostasis and may also be responsible for therapeutically-induced tumour regression.

1.2 Defining a genetic pathway for programmed cell death:

Ever since these initial descriptions of regulated cell death intensive work has focused on unravelling its genetic and biochemical basis. During the 1970s the role of lysosomal death

pathways in systems such as metamorphosing of tadpole tails and the involution of mammary glands were given the most attention. Lysosomes are now recognised to play an important role in regulated autophagic and necrotic cell death pathways, an area that is receiving increased attention because of its role in cancer therapeutics (Zong and Thompson, 2006).

By 1976 the application of modern genetic techniques had lead to the first breakthrough in proving apoptosis was a genetically controlled cell fate. Sydney Brenner envisioned that the nematode worm, *Caenorhabditis elegans* would be an ideal model organism to define the genes responsible for cell fate. John Sulston and Robert Horvitz were able to undertake a complete cell lineage analysis and discovered that in addition to 959 cells generated during worm development a further 131 cells were generated but were not present in the adult (Sulston, 1976). These cells were absent because they undergo programmed cell death and therefore identify programmed cell death as a legitimate cell fate. They reasoned that there should be genes controlling both the decision to die and the implementation of the death program and such genes should be identifiable by genetic screening. By 1983 the first of these had been identified and were named ced-1 and ced-2, for cell death abnormal (Hedgecock et al., 1983). These genes turned out not to control the cell autonomous death program but instead to control engulfment, or phagocytosis, the process which normally removes dying cells from multicellular organisms. The identification of these mutations solved a significant problem in the cell death field; how to study cells which may disappear completely in the space of an hour. In a ced-1 mutant background dead corpses were not removed and could therefore be detected by Nomarski optics in living worms. Over the next decade, a complete genetic pathway was defined:

Egl-1 --| Ced-9 --| Ced-4 → Ced-3 → Cell death.

Where ced-3 is responsible for the execution of apoptotic cell death, ced-4 is necessary to promote the activity of ced-3 and ced-9 is an inhibitor apoptosis, protecting cells by preventing ced-4 from activating ced-3. egl-1 is the gene positioned to activate the pathway by relieving the inhibition of ced-9 on ced-4. These experiments illustrate the power of a tractable genetic system in identifying key molecular players in a molecular pathway. However, the true significance of these experiments, which earned Robert Horvitz, John Sulston and Sydney Brenner the Nobel Prize in 2002, only became clear as the number of sequences deposited in the protein databases began to increase and homologous mammalian genes could be identified. ced-3 had homology to interleukin-1-beta converting enzyme (ICE), a protease responsible for converting the pro-form of the cytokine interleukin-1-beta into an active molecule (Miura et al., 1993). ICE and ced-3 became the founding members of the family of cysteine proteases now known as the caspases (Degterev et al., 2003). ced-4 had homology to the human APAF1

protein (Zou et al., 1997), and ced-9 was found to be homologous to the human proto-oncogene Bcl-2 (B cell lymphoma) (Hengartner and Horvitz, 1994).

The evasion of apoptosis is now recognised as a key step in oncogenesis. The link between deregulated apoptosis and cancer was initially identified by the finding that in human follicular lymphoma, the BCL-2 gene becomes translocated to the immunoglobulin locus, t(14;18), resulting in constitutive over–expression of Bcl-2 (Tsujimoto et al., 1984). Traditionally, the activation oncogenes, like Myc (Lutz et al., 2002), through over–expression or mutation, were thought to promote oncogenesis by promoting unrestrained cell cycle progression. However, unlike all other oncogenes known at the time, Bcl-2 did not promote cell proliferation. Instead, it was the founding member of a new category of proteins that could block cell death in response to multiple physiological and pathological triggers (Vaux et al., 1988). It is now widely accepted that activation of apoptosis, by proliferation–inducing oncogenes (Harrington et al., 1994b), functions as a tumour–suppressive mechanism to prevent unrestrained cell proliferation (Harrington et al., 1994a), and defects in the apoptotic pathway are considered a prerequisite for tumour formation. Recapitulation of the t(14;18) translocation seen in human follicular lymphoma in transgenic mouse models was the first demonstration that perturbations of the apoptotic pathway promotes oncogenesis. These mice contain a BCL-2-immunoglobulin minigene and developed polyclonal follicular lymphoma comprised of resting B cells that accumulate because of extended survival, not increased proliferation (McDonnell et al., 1989). These mice went on to develop spontaneous high-grade monoclonal lymphoma following spontaneous activation of c-myc (McDonnell and Korsmeyer, 1991). Bcl-2/myc double transgenic mice were also created, and they develop undifferentiated hematopoietic leukaemia (Strasser et al., 1990). Thus demonstrating that synergy between two genetic lesions, one promoting proliferation and the other suppressing apoptosis, is a central component of tumour development (Hanahan and Weinberg, 2000; Johnstone et al., 2002). Bcl-2, became the founding member of a family of related apoptotic regulators in mammals. It is the regulation and action of these Bcl-2 proteins that forms the main subject for this thesis.

1.3 The Bcl-2 family and their place in cell death pathways:

In the two decades since the discovery of Bcl-2 the family of related genes has continued to expand and now includes members that can be both pro- and anti-apoptotic. The family is now divided into three groups defined, in part, by four short stretches of relatively conserved sequence, or Bcl-2 Homology (BH) domains (Figure 1.1, left panel).

Bcl-2 has been joined by four others, Bcl-XL (Boise et al., 1993), Bcl-w (Gibson et al., 1996), A1 (Choi et al., 1995) and Mcl-1 (Kozopas et al., 1993) all of which promote cell survival, protecting cells from a wide variety of cytotoxic insults, such as cytokine deprivation, UV- and γ-irradiation. They share all four of the BH domains (BH1 - BH4) and are therefore referred to as the multi-domain pro-survival proteins.

Bax, the founding member of the pro-apoptotic sub-family, was identified by its ability to interact with Bcl-2 (Oltvai et al., 1993). Bax, together with two close relatives, Bak (Chittenden et al., 1995b; Kiefer et al., 1995), and Bok (Hsu et al., 1997a) share three domains (BH1, BH2 and BH3). These proteins act, at least in part, by perturbing intracellular membranes.

The remaining family members, the BH3-only proteins, are more diverse, lacking sequence homology amongst themselves and to the wider Bcl-2 family, outside of their signature BH3 interaction domain. There are now at least 13 of these BH3-only proteins, although the function of several of these is not yet clear. They are all pro-apoptotic and the BH3 domain is necessary, and probably sufficient, to mediate both their killing activity and their interaction with other family members (Cory et al., 2003).

Apoptotic signal transduction has traditionally been divided into two pathways, extrinsic or intrinsic. Both eventually lead to the same caspase-dependent pathways mediating the dismantling of the cell and its eventual engulfment; they differ in the way the signals are initially processed. The extrinsic pathway is initiated by the activation of death receptors on the cell's surface and is summarised Figure 1.2 A. This will be considered in more detail in section 1.4. The intrinsic pathway is initiated in response to a wide variety of cellular metabolic and physiological stresses. The pathway is currently thought to be initiated primarily by the activation of BH3-only proteins and is summarised in Figure 1.2 B. This is considered in more detail in section 1.5. The Bcl-2 family of proteins constitute a critical cellular checkpoint in all intrinsic and many extrinsic death pathways, acting at a level proximal to mitochondrial dysfunction, which will be considered in more detail in section 1.6.

1.4 Extrinsic cell death pathways:

The extrinsic cell death pathway is responsible for the elimination of cells during development, in the immune system programming and in immuosurveillance throughout life. The pathway is initiated by engagement of a tumour necrosis factor type I superfamily transmembrane death receptor, the best-studied member of this family of Fas (CD95/APO-1) (Ashkenazi and Dixit,

1998). Binding of the Fas ligand to the Fas receptor, which is preassembled as a timer, causes a conformational change the receptor's cytoplasmic tail. This results in recruitment of the adaptor molecule FADD (Fas-Associated protein with Death Domain), mediated by death domains (DDs) contained in both molecules. FADD then recruits caspase-8 zymogens via Death Effector Domains (DEDs), present in both proteins (Kischkel et al., 1995). The resulting complex is known as the Death-Inducing Signalling Complex (DISC), and caspase-8 becomes active according to an 'induced proximity' model whereby a low intrinsic degree of caspase-8 activity, in the confined space of the DISC, leads to cleavage *in trans* of caspase-8 dimers. Recent data suggests that, unlike for effector caspases, cleavage of caspase-8 is not required for formation of the caspase-8 active site, but adds stability to active dimmers created at the DISC; in this case 'induced proximity' becomes the driving force for recruited monomers to dimerise (Boatright and Salvesen, 2003). Once active caspase-8 as an initiator caspase can then activate the effector caspases-3 and -7, responsible for cleaving key cellular substrates and the execution phases of apoptosis (discussed above). Interestingly, following cleavage casapse-8 is released from the DISC complex and translocates to mitochondria, where it may have additional roles in coordinating apoptotic signalling which have yet to be fully investigated (Chandra et al., 2004).

Apoptotic signalling via the extrinsic pathway can be modulated at various levels: antagonistic decoy receptors have also evolved which capture death ligands but fail to propagate the signal downstream due to non-functional or absent death domains (LeBlanc and Ashkenazi, 2003). FLIP (FLICE-like inhibitory protein) is a proteolytically inactive homology of capase-8 (originally called FLICE), due to the lack of a catalytic cysteine. Interestingly low levels of FLIP expression enhance casapse-8 activation at the DISC by helping to drive formation of FLIP/caspase-8 heterodimers, which are active. In contrast, high levels of FLIP expression, as found in some tumours, inhibit caspase-8 activation, presumably through competing caspase-8 recruitment to the DISC. FLIP can heterodimerise with capase-8 when it presumably blocks caspase-8 recruitment to the DISC (Chang et al., 2002). In addition, there are other death receptors including DR4/5 that are responsive to the ligand TRAIL (TNF-related apoptosis inducing ligand). In some settings engagement of death receptors has been reported to activate cell proliferation, and survival signalling through the NFkB pathway. These significance of these observations is not yet not fully understood but is likely to involve different adaptor complexes forming downstream of activated receptors (Micheau and Tschopp, 2003).

In response to Fas-induced apoptosis, cells have traditionally been categorised as Type I and Type II (Scaffidi et al., 1998). Type I cells, such as thymocytes, are not protected by Bcl-2 proteins since sufficient caspase-8 activity is generated to cleave and activate caspases-3 and -7. Type II cells, such as hepatocytes, are protected by Bcl-2 expression since a mitochondrial

amplification loop initiated by the cleavage caspase-8 dependent cleavage of the BH3-only protein Bid is also required to generate sufficient caspase activity to kill these cells (Li et al., 1998; Luo et al., 1998).

1.5 BH3 only proteins – initiators of intrinsic cell deaths:

The BH3-only proteins members of the Bcl-2 family connect a wide variety of death signals to the core apoptotic pathway at mitochondria. There are currently at least 11 recognised members of this group, the best known of which are introduced below:

1.5.1 Bid

As mentioned in the previous section, the Bid is a component of the extrinsic cell death-signalling pathway. Activation of p22 Bid involves cleavage by caspase-8, followed N-myristoylation, resulting in translocation of p7/Myr-p15 Bid to mitochondria (Li et al., 1998; Luo et al., 1998; Zha et al., 2000). In a reconstituted mitochondrial assay p15 tBid has been shown to trigger oligomerisaiton of Bax and rapid Cyt-c release, a process dependent on its BH3-domain (Desagher et al., 1999; Eskes et al., 2000; Kluck et al., 1999). tBid also induced oligomisation of Bak in mitochondria isolated from hepatocytes (Wei et al., 2000). The role of Bid in direct activation of Bax and Bak is discussed in more detail in Section 1.12.

1.5.2 Bim

Bim was found to be a complex with the dynein motor complex on microtubules via an interaction with dynein light chain-1 (DL-1 or LC8) (Puthalakath et al., 1999). However, this may be cell type specific since in healthy hematopoietic cells it has also been reported to associate with the mitochondria and not microtubules (Zhu et al., 2004). Bim responds to a diverse range of apoptotic stimuli, for example, the protein is required for the deletion of autoreactive thymocytes *in vivo* and for apoptosis of T-cells *in vitro* following treatment cytokine deprivation, treatment and treatment with taxol (Bouillet et al., 1999; Bouillet et al., 2002). Bim has also been seen to be transcriptionally up-regulated in haematopoietic and neuronal cells in response to cytokine deprivation (Dijkers et al., 2000; Putcha et al., 2001) and is thought to be regulated by phosphorylation events which can act to enhance its degradation following growth factor stimulation or promote its activation in when growth factors are withdrawn (Ley et al., 2005).

1.5.3 Bmf

Bmf is bound to the myosin V motor complex through interaction with dynein light chain-2 (DLC2) and may play a role in detachment-induced death of epithelial cells, called anoikis

(Puthalakath et al., 2001). Through their sequestration to the cytoskeleton it is thought both Bim and Bmf are able to monitor cytoskeletal integrity. Interestingly, Bim, but not Bmf, is released in response to treatment with taxol, which prevents tubulin depolarisation and thereby disrupts normal regulation of the microtubule cytoskeleton (Puthalakath et al., 2001). Both proteins have been reported to be released in response to UV irradiation through a mechanism that may involve their phosphorylation (Lei and Davis, 2003)

1.5.4 Noxa and Puma

Noxa and Puma/bbc3 are transcriptionally induced by p53 following DNA damage (Oda et al., 2000; Vousden and Lu, 2002; Yu et al., 2001). Both have been genetically demonstrated to be important in p53-mediated cell death following drug-induced genotoxic damage (Jeffers et al., 2003; Villunger et al., 2003) and down-regulation of Puma by an RNA interference strategy has been shown to promote transformation in a primary murine fibroblast tumour model (Hemann et al., 2004). This mode of regulation has direct parallel with that seen in *C. elegans*, where transcriptional regulation predominates. In this organism the BH3-only homologue EGL-1 is induced in all somatic cells fated to die (Conradt and Horvitz, 1998), and in response to the worm p53 homologue CEP-1, in germline cells which have suffered DNA damage (Hofmann et al., 2002).

1.5.5 Bad

Bad is regulated by phosphorylation by kinases such as Akt/PKB and PKA in response to growth factors leading to its sequestration by 14-3-3 scaffold proteins (Zha et al., 1996). Bad activation is promoted by dephosphorylation, for example by calcineurin (Wang et al., 1999). Interestingly Bad has also recently been found in a complex with protein kinase A, protein phosphatase 1 catalytic units, WAVE-1 and glucokinase which may have novel roles in coordinating glycolysis and apoptosis in situations of glucose deprivation (Danial et al., 2003).

Currently little is known about the regulation of mechanism of action of the other BH3-only proteins, which include: Bik/Nbk, Hrk/DP5, Boo/Dive, Bcl-B, Bcl-G, Bcl-Rambo and Bfk. However, further characterisation of these proteins is expected to reveal they also act to promote apoptosis in particular cell types or in response to physiological stresses.

The activation of BH3-ony proteins leads, directly or indirectly, to the activation of Bax and Bak; their place in the apoptotic pathway is introduced in the next section. Current models and remaining uncertainties regarding their regulation and mechanism of activation is discussed in a later section (Section 1.9).

1.6 Bax and Bak:

The multi-domain pro-apoptotic members of the Bcl-2 family consist of Bax, Bak and Bok (Figure 1.1). Bax and Bak are widely expressed and have been extensively studied, whist the expression pattern of the third member of this sub-family, Bok, is restricted to reproductive tissues and it has consequently been studied in much less depth (Hsu et al., 1997a).

Significant insights into the role of these proteins have recently been obtained through the study of mice lacking one or both of them. Bax-deficient mice have a range of abnormalities, specifically lymphoid hyperplasia, decreased cell death in the central and peripheral nervous systems and abnormal gametogenic development (Knudson et al., 1995). Nevertheless, they are viable, showing the Bax is not essential for development. Disruption of Bak in mice had no discernible effect, with no reported developmental or age-related defects (Lindsten et al., 2000). However, when *Bax-/-Bak-/-* doubly knocked out (DKO) mice were generated fewer than 10% of animals survived to adulthood, and those that did displayed multiple phenotypic abnormalities including: retained inter-digital and females had imperforate vaginal canals, multiple neurological abnormalities including deafness, circling behaviour and persistence of many undifferentiated cells, progressive accumulation of mature B and T cells leads to massive enlargement of the spleen and lymph nodes and infiltration into parenchymal organs (Lindsten et al., 2000). These findings suggested that the Bax and Bak proteins have largely redundant roles in regulating apoptosis, but the lack of both proteins causes a widespread failure of cells to undergo apoptosis leading to the inappropriate accumulation of cells which should either die during development or during the normal regulation of tissue homeostasis. Subsequent characterisation of murine embryonic fibroblasts (MEFs) showed them to be resistant to tBid-induced Cyt-c release as well as multiple apoptotic stimuli including staurosporine (STS), ultraviolet (UV) irradition, etoposide and thapsigargin (Wei et al., 2001). These finding place Bax and Bak as essential regulators of mitochondrial dysfunction in response to diverse signals and also implicate the mitochondrial dysfunction as a required step in apoptotic cell deaths mediated by the intrinsic cell death pathway. Significantly, the defects reported in *Bax-/-Bak-/-* animals are more severe than for either Apaf1 or Caspase-9 deficient animals, leading to the conclusion that whilst there may be redundancy in the execution of apoptotic cell death the Bcl-2 proteins are the critical regulators of the program, a characteristic that also makes them of potential interest as pharmaceutical targets.

The formation of oligomeric clusters of Bax and Bak is temporally indistinguishable from the initiation of mitochondrial dysfunction and the release of mitochondrial inter-membrane space proteins (Korsmeyer et al., 2000). It is therefore considered likely that the former is the cause of

the later, although the molecular mechanism by which this occurs is still unclear and under active investigation. Over-expression of Bax in cells, as well as the addition of purified recombinant Bax to mitochondria, can trigger the release of Cyt-c (Eskes et al., 2000; Jurgensmeier et al., 1998; Rosse et al., 1998). Further investigation showed recombinant Bax purified in the presence of detergent to induce oligomerisation is active, whereas monomeric Bax purified in the absence of detergent is not (Antonsson et al., 2000; Hsu and Youle, 1997; Hsu and Youle, 1998). Bax has been reported to form pores in synthetic lipid membranes and liposomes (Antonsson et al., 1997) and a novel channel has been detected by patch-clamping experiments in the mitochondrial membrane of apoptotic cells and Bax expressing yeast (Pavlov et al., 2001) and can be prevented by Bcl-2 and blocked by Bax antibodies (Dejean et al., 2005). Strong supporting evidence that it is the dimerisation of Bax molecules which is the key event in Bax activation came from experiments in which enforced dimerisation of Bax molecules resulted in cell death and was able to override the protection from Bcl-XL (Gross et al., 1998). Other studies have attempted to address the exact nature of the Bax-induced pore. It has been claimed this would require at least a tetramer of Bax molecules to form a pore with diameter 22Å, capable of transporting a 12kD Cyt-c molecule with Stokes diameter of 12Å (Saito et al., 2000). There have also been reports of much larger pores requiring lipid components (Epand et al., 2002; Terrones et al., 2004). The nature of the lipid composition of the outer membrane lipid is also thought to play a role (Kuwana et al., 2002).

1.7 Mitochondrial permeabilisation:

The first reports connecting mitochondria with apoptotic cell death emerged in the mid-1990s (Marchetti et al., 1996; Newmeyer et al., 1994; Petit et al., 1995; Zamzami et al., 1995), and soon after Cytochrome-c (Cyt-c) was implicated as a necessary component for caspase-3 activation, being released from mitochondria into the cytosol during apoptosis (Liu et al., 1996). A consensus now exists that it is the Bcl-2 proteins Bax and Bak trigger Cyt-c release when they become activated and oligomerise and in most cases this is likely to be the pivotal event in committing the cell to die by apoptosis. The most studied consequence of Bax and Bak activation is the permeabilisation of the MOM and release of inter-membrane space proteins into the cytoplasm including: Cyt-c (Liu et al., 1996), Smac/DIABLO (Du et al., 2000; Verhagen et al., 2000), HtrA2/Omi (Suzuki et al., 2001), apoptosis-inducing factor (AIF) (Susin et al., 1999) and Endonuclease G (Li et al., 2001).

The Membrane Permeability Transition Pore (MPTP) is a Ca^{2+}-, voltage-, pH- and redox-gated channel traversing both the outer and inner mitochondrial membranes. Although the exact

molecular composition and function of this channel remains unclear it is thought to have three main components: (1) the voltage dependent anion transporter (VDAC) in the outer mitochondrial membrane, (2) the adenine nucleotide transporter (ANT) which maintains ATP/ADP exchange across the inner mitochondrial membrane and (3) Cyclophilin D (CypD), a small soluble molecule found in the mitochondrial matrix and identified because it binds to the immunosuppressant Cyclosprorin A (CsA).

MPTP has been observed during apoptotic and necrotic cell deaths, where it was presumed to not only be responsible for mitochondrial depolarisation but would also allow water and solutes less than 1500 Da in mass from the cytosol to enter the matrix and cause swelling and rupture of the outer membrane, hence explaining the release of Cyt-c (Lemasters et al., 1998; Vander Heiden et al., 1997). The mitochondrial inner membrane (MIM) is highly folded into cristae and so matrix swelling could have the potential to exceed the constrains of the mitochondrial outer membrane (MOM) and result in its rupture. Such models have since fallen out of favour as in vivo evidence for swelling or rupture of mitochondria in the early stages of apoptotic cell death has remained scant and controversial.

1.8 Execution of apoptotic cell deaths:

Cyt-c, together with Apaf-1, procaspase-9 and ATP/dATP, form the apoptosome caspase activating complex. Activation of the apoptosome is initiated by the binding of Cyt-c to the WD40 domains of Apaf-1, making Apaf-1 competent to recruit pro-caspase-9 in an ATP/dATP-dependent manner via caspase recruitment domains (CARD) present in both Apaf-1 and caspase-9 (Li et al., 1997).

Caspases are synthesised as inactive zymogens or procaspases. Active caspases are dimers consisting of two identical units, each with a single active site. Each unit is composed of one large and one small subunit derived from the zymogen precursor by internal cleavage at a linker region (Shi, 2002). Procaspases contain N-terminal pro-domains of varying length: upstream or initatior capases, such as caspase-9, have long pro-domains which are involved in their regulation and autocatalytic activation. The zymogens of initiator caspases exist as inactive monomers and it has recently been shown that cleavage of the zymogen is neither required nor sufficient for activation of the initiator caspases. Instead they require dimerisation to assume the active conformation, which occurs in multi-protein activating complexes to which the zymogens are recruited by their N-terminal domains – the apoptosome in the case of Caspase-9 (Boatright and Salvesen, 2003; Rodriguez and Lazebnik, 1999; Stennicke et al., 1999).

Downstream or executioner caspases, such a caspase-3, -7 and -6, exist within the cytosol as inactive dimers (Boatright and Salvesen, 2003). To become active, these caspases require processing by an initiator caspase within their linker region, a process which has been structurally defined in the most detail for caspase-7 (Chai et al., 2001). The basis for zymogen activation is shared amongst all caspases, but the driving forces differ: for effector caspases cleavage within the linker segment is necessary for ordering of the active site whilst for initator caspases the reordering of their structures requires dimerisation alone and cleavage is a secondary event which stabilises the active dimers (Boatright and Salvesen, 2003). This distinction is important as explains how a proteolytic pathway can be initiated without proteolysis itself, the initiator caspases rely on induced proximity driven by co-factors. Once activated the effector caspases are responsible for the proteolytic cleavage of cellular substrates which ultimately leads to cell death and the associated characteristic morphological changes.

In *Drosophila*, direct regulation of caspases seems to be the major strategy by which apoptosis is regulated and they are held in check by inhibitors of apoptosis (IAPs). Originally identified in baculovirus (Clem et al., 1991), the family now includes many cellular homologs, including DIAP1, which bind to and inhibit both initiator and effector caspases through a baculoviral IAP repeat (BIR) motif (Salvesen and Duckett, 2002). IAPs also contain RING domains, which recruit E2 ubiquitin–conjugating enzymes, which mediates ubiquitylation and destruction of IAP interacting proteins, and IAPs themselves, by the 26S proteasome (Vaux and Silke, 2005). Although the *in vivo* targets of IAP ring fingers have not been characterized, IAP may potentially play an important role in regulating the abundance of various components of the apoptotic machinery. Mammalian IAPs, such as XIAP (Deveraux et al., 1997), are controlled by antagonists: Smac/DIABLO (Verhagen et al., 2000) and HtrA2/Omi (Suzuki et al., 2001), two proteins which are released from the mitochondrial intermembrane space. In general mammalian cells are not as dependent on IAPs and their antagonists for the regulation of apoptosis: Smac, HtrA2, XIAP deletion in mice do not show obvious defects in apoptosis indicating this role is dispensable (Harlin et al., 2001; Okada et al., 2002), although HtrA2 has other roles, potentially relating to mitochondrial functions prior to its release (Deshmukh et al., 2002).

1.9 Final rites - DNA degradation and cell engulfment:

Condensation and fragmentation of nuclei was observed as one of the original defining hallmarks of apoptosis. DNA degradation, which occurs downstream of caspase activation, is

mediated by caspase activated DNase (CAD) (Enari et al., 1998; Liu et al., 1997). CAD becomes activated when its inhibitor ICAD is cleaved by the effector caspases. DNaseII, held within the lysosomes of phagocytes also plays a role after engulfment (McIlroy et al., 2000). In mammalian cells, the other two proteins mentioned as being released from the mitochondria: EndoG (Li et al., 2001) and AIF (Susin et al., 1999) translocate to the nucleus upon their release and are believed to contribute to caspase-independent DNA degradation. Translocation of AIF into the nucleus and activity is believed to involve cooperation with poly(ADP-ribose) polymerase-1 (PARP-1) which attaches poly ADP-ribose to nuclear proteins including histones (Yu et al., 2002). Exactly how AIF and EndoG function is not fully understood. Genetic studies in *C. elegans* indicate they may work in concert, but in a caspase dependent manner. The *C. elegans* genes nuc-1 (DNaseII), wah-1 (AIF) and cps-6 (EndoG) are conserved.

Dying cells produce "eat me" signals, for mammalian cells, of which the best characterised is exposure of phosphatidylserine on the outer leaflet of the plasma membrane (Fadok et al., 2000). This signal is recognized by engulfment receptors on phagocytosing cells (Savill and Fadok, 2000). The engulfment of apoptotic cell corpses is an essential continuum of the apoptotic process and ensures the lack of inflammatory response – a fundamental difference between cell death by apoptosis over cell necrosis. *C. elegans* has again been useful in defining the core genetic elements of this pathway, which depends on CED-3 caspase activity (Hoeppner et al., 2001). This process consists two overlapping pathways in *C. elegans* with mammalian homologues. The first pathway recognizes apoptotic cells and consists of: ced-1, an engulfment receptor (Zhou et al., 2001), ced-6, an adaptor which is homologous to the mammalian GULP protein (Liu and Hengartner, 1998), and ced-7, which is homologous to the ABC-2 transporter (Wu and Horvitz, 1998b). The other category is involved in cytoskeletal remodelling and is composed of: Ced-2 (CrkII) (Reddien and Horvitz, 2000), ced-5 (DOCK180) (Wu and Horvitz, 1998a), ced-10 (Rac) (Reddien and Horvitz, 2000) and ced-12 (ELMO) (Gumienny et al., 2001. Cells from the immune system play an essential role in removal of apoptotic cells {Ekert, 1997 #296). Macrophages are important regulators of pro-inflammatory responses releasing cytokines, such as TNFα, but macrophages engaged in engulfing apoptotic cell corpses also release anti-inflammatory factors, such as TGF-beta and IL-10, to help prevent unwanted immune reactions. In addition, phagocytosing dendritic cells present peptides from apoptotic corpses to not initiate activation of T cells. Defects in these clearance pathways are a major cause of inflammation and also pre-dispose to autoimmune disorders.

1.10 The structure of Bcl-2 family proteins:

Structural studies of the Bcl-2 proteins have given many important clues as to their functions. The first published structure was that of human Bcl-XL solved by both X-ray crystallography and NMR spectroscopy (Muchmore et al., 1996) and since then structures of the anti-apoptotic family members: Bcl-2 (Haldar et al., 1998), Bcl-w (Denisov et al., 2003) and Mcl-1 (Day et al., 2005) and pro-apoptotic members Bax (Suzuki et al., 2000) and Bid (Chou et al., 1999) have been reported. The structures all show strikingly a striking degree of similarity, despite considerable divergence in their primary amino acid sequence and, in some cases, opposing biological functions (Figure 1.3).

Bcl-XL and Bcl-2 both consist of eight α-helices connected by loops of varying length. Two helices, α5 and α6, form the core of the protein and are predominantly hydrophobic. Amphipathic helices α3 and α4 on one side and α1 and α2 on the other flank the central pair. In general, the alpha helices roughly correspond to the conserved BH domains: α1 to BH4 and α2 to BH3. The BH1 domain is between α4 and α5 so just ahead of the core α5/ α6 hydrophobic helices. The BH2 domain maps to. α7/α8. A long loop between α1 and α2 is unstructured and dispensable for protective function of Bcl-XL (Muchmore et al., 1996). However, the loop may be important for regulation: phosphorylation of Ser 70 in the analogous loop in Bcl-2 blocks its protective function (Haldar et al., 1998) and caspase-3 cleavage at Asp 34 within the loop converts Bcl-2 from anti-apoptotic to pro-apoptotic (Cheng et al., 1997).

The Bcl-XL structure helped to provide the first insights in the function of the BH domains. The BH1, BH2 and BH3 come together to form an elongated hydrophobic groove on the protein surface and this was postulated to form the binding surface for BH3 domains of a pro-apoptotic protein. This explained earlier findings that mutations in all of these regions affected the ability of Bcl-XL to interact with pro-apoptotic proteins, where as in the pro-apoptotic proteins only the BH3 domain was required (Cheng et al., 1996; Chittenden et al., 1995a). There are only minor differences between the Bcl-XL and Bcl-2 structures; the α3 helix, which contributes residues to the BH3 binding cleft is slightly differently positioned and this creates a slightly wider cleft in Bcl-2 (Petros et al., 2001).

The BH3 binding cleft model was soon confirmed by the NMR structure of the Bcl-XL/Bak peptide complex (Sattler et al., 1997) and Bcl-XL/Bad peptide complex (Petros et al., 2000). The BH3 domain peptides do indeed sit across the hydrophobic groove with key conserved residues of the BH3 domain pointing directly into the binding pocket. This provides a molecular basis for the observed dimerisation between BH3 proteins.

The BH3 only proteins have extremely divergent sequences outside the short 9-16aa BH3 domain motif, they are therefore not expected to have similar structures to the multi-domain proteins. The limited stretch of sequence between the Bim BH3 domain and the predicted C-terminal membrane interaction domain is certainly insufficient to form the core helical arrangement described above, or to sequester the BH3 region. This raises the possibility that, for Bim at least, the BH3 domain would be constitutively exposed.

To date no structure of a complex between two full length Bcl-2 family proteins has been reported, although a recent report of the structure of Bcl-XL with a longer peptide from Bim does provide some additional insights (Liu et al., 2003). In this study the Bim fragment formed an extended alpha helix of at least 29 amino acids (amino acids 85-115 of BimL, and encompassing the BH3 domain). This is consistent with other experiments which have shown residues outside the BH3 motif also contribute to BH3-only proteins binding multi-domain proteins (Petros et al., 2000). Hydrophobic residues observed to contact Bcl-XL in the extended Bim alpha helix are also found in similar positions in other BH3-only proteins. It is therefore possible that extended helices encompassing the BH3 motifs may contribute to the binding of other BH3-only proteins to their multidomain partners.

Considering the other pro-survival proteins whose structures are solved: Mcl-1 is a larger protein with a unique N-terminal domain, however the structure reported lacked this unique 151aa N-terminal extension. The remaining Bcl-2-like core of the protein looked very similar to that described for Bcl-2 and Bcl-XL above and a 23aa C-terminal truncation was also necessary to increase solubility of the protein (Day et al., 2005). Finally, the Bcl-w structure showed that, in contrast to Bcl-2 and Bcl-XL, the C-terminal domain of Bcl-w was found to fold back across the protein and bind in the hydrophobic pocket and the BH3-binding pocket is therefore not constitutively available (this is also the case for Bax, see below) (Hinds et al., 2003).

Of the multi-domain pro-apoptotic Bcl-2 family members only the Bax structure has so far been solved (Suzuki et al., 2000). Bax also has seven amphipathic helices clustered around two central predominantly hydrophobic helices (α5 and α6). However, the α9 helix of Bax, which corresponds to the TM domain of Bcl-2 and Bcl-XL, binds across the hydrophobic groove. This has two important implications: firstly the groove is not constitutively available for binding the BH3-domains of other family members and secondly the shielding of the hydrophobic surface leads to an increase in the proteins solubility and contributes to it being predominantly located in the cytoplasm prior to an apoptotic stimulus.

Of the BH3-only proteins only Bid has been solved (Chou et al., 1999; McDonnell et al., 1999). The overall fold of Bid is very similar to the multi-domain proteins and described above, although there is an additional helix in the N-terminus before the unstructured loop and no helix corresponding to the Bcl-XL α7. However, the hydrophobic groove on Bid is much shorter and shallower than in Bcl-XL and Bcl-2 since Bid lacks the BH1 and BH2 domains, which, in the Bcl-XL structure, contribute key residues to the BH3 binding cleft. This may explain why Bid is unable to bind BH3 domain peptides, despite having an overall similar fold (Chou et al., 1999). However, as highlighted in Figure 1.1, the primary sequence of Bid is unique amongst the BH3-only group with predicted helices in analogous positions to the multi-domain members. It is more likely the Bim peptide bound to Bcl-XL is more generally representative of the mechanism by which BH3-only proteins engage the pro-survival Bcl-2 family members.

1.11 Bcl-2 proteins show structural similarity to bacterial pore-forming toxins:

A striking observation made in the very first structural study was how the fold of Bcl-XL closely resembled that of the colicins and diphtheria toxin (Muchmore et al., 1996) (Figure 1.3). Colicins are made by some bacteria to kill other bacteria strains. They contain three domains for (a) receptor binding, (b) translocation of the toxin, (c) the toxin itself that kills by making pores in the bacterial membrane (Stroud et al., 1998). The Bcl-XL structure closely resembled the toxin domain. The colicins form pores in the membranes leading to the release of essential metabolites and in the influx of water, which causes rupture of the cell. This led to early models suggesting that Bcl-2 protein might function in an analogous fashion.

It has been shown that Bcl-XL, like the bacterial toxins, can insert into either synthetic lipid vesicles or planar lipid bilayers and form an ion-conducting channel. The channel was shown to be pH-sensitive and becomes cation-selective at physiological pH. This led to the suggestion that Bcl-2 proteins might regulate the permeability of the membranes where they are located (Minn et al., 1997). Bax and Bcl-2 have been reported to have similar properties (Schlesinger et al., 1997). However, there are significant problems in interpreting the similarities with the colicins too literally and extrapolating a similar function for Bcl-2 proteins. The colicins insert into bacterial membranes, but this is the evolutionary equivalent of the MIM, not the MOM, where the Bcl-2 proteins are thought to act. The MOM is already porous to water and most metabolites due to the presence of non-selective ion channels.

Diphtheria toxin (DT) kills mammalian cells by a different mechanism to the way the colicins kill bacteria. DT is a member of the two domain AB family of toxins: the A domain contains

enzymatic activity that is toxic to the cell. In the case of DT this is an ADP-ribosyl transferase, which inactivates an elongation factor required for protein synthesis. The B domain is a receptor binding and translocation domain, which can move the A domain across the membrane and into the cell (Falnes and Sandvig, 2000). When the B domain of DT binds a receptor it is endocytosed and then, in the more acidic environment of the endosomes, a conformational change takes place leading to membrane insertion and the translocation of the A domain into the cytoplasm. The final step is the reduction in the cytoplasm of a sulfhydril bond which links the two domains, freeing the A domain. The translocation domain can also behave as a cation-selective channel but it is not clear that this activity is required for translocation of the A domain. It seems more likely the B domain acts as a chaperone to unfold the A domain and pass it through the channel (Falnes and Sandvig, 2000).

There is some direct evidence to support an analogous role for Bcl-XL. It has been demonstrated that a hybrid protein, in which the Diptheria toxin B chain was deleted and the translocation domain replaced with Bcl-XL, was able to protect the cells, presumably by translocating itself following endocytosis and proving that Bcl-XL could functionally substitute for the translocation domain (Liu et al., 1999). However, another AB toxin anthrax the A domain is transported without a requirement for covalent linkage to the B domain (Falnes and Sandvig, 2000), it is not clear whether Bcl-XL would be able to translocate proteins other than itself though the membrane.

A significant problem posed by these structural homology studies is how Bax and Bcl-XL, which have very similar structures and *in vitro* properties as ion channels, have opposing biological functions *in vivo*. However, the structural similarities between multi-domain Bcl-2 proteins and bacterial toxins are striking and it remains likely that the proteins share at least some common functions in relation to their ability to form pores in membranes (Lazebnik, 2001).

1.12 Models for Bcl-2 family action and questions remaining:

This introduction has summarised current views regarding the place of Bcl-2 family proteins, and specifically Bax, in the mammalian apoptotic pathway. At this point it is pertinent to consider current models concerning the regulation of Bcl-2 family proteins and highlight remaining areas of uncertainty.

The apoptotic program can be invoked by intrinsic cell signalling indicating cytotoxic damage or infection and by extrinsic cell signalling mediated via the engagement of death receptors. In addition it can be initiated in response to developmentally regulated cues. The emerging consensus from structural and binding studies and from mouse models is that, in almost ever case, it is the BH3-proteins appear to provide the upper level of regulation upon apoptotic decisions mediated by the Bcl-2 family. Some BH3-only proteins are expressed in a limited subset of cell types, whilst other appear to monitor a particular subcellular compartment, stress signal or damage response (see section 1.5 and Figure 1.4 A). These diverse mechanisms of regulation are thought to provide fine-tuning to the apoptotic response and reflect the diverse range of conditions under which apoptosis may be initiated.

Whilst the BH3-only proteins are regulated by diverse mechanisms, some common themes have recently emerged concerning their mode of action. Evidence accumulated from structural studies (discussed in section 1.10) and binding studies (Cheng et al., 2001) has led to a model by which multi-domain anti-apoptotic proteins protect cells by sequestration of active BH3-only proteins. Initially, this binding was envisioned to be promiscuous but more recent data suggests that some BH3-only proteins, namely Bim, Puma and Bid, have a more prominent role than others. An explanation for this became apparent when a systematic study of the binding affinities between eight BH3-only peptides and five Bcl-2 pro-survival proteins revealed over 10,000-fold differences existed between different pairings (Chen et al., 2005). This implies that under physiological conditions only certain binding combinations were likely (Figure 1.4 B). Of the BH3-containing peptides tested, only those from Bim and Puma showed high affinity for all five pro-survival proteins. Bad and Bmf appeared specific for Bcl-2, Bcl-XL and Bcl-w, whilst Noxa binds to Mcl-1 and A1. These findings imply that there may, in fact, be two classes of Bcl-2 pro-survival proteins, those neutralised by Bad and Bmf (Bcl-2, Bcl-XL and Bcl-w), and those neutralised by Noxa (Mcl-1 and A1) (Chen et al., 2005). Bim and Puma are more potent killers since they are able to target both classes (Figure 1.4 B).

Models in which BH3-only proteins target the pro-survival proteins are consistent with the genetically established ordering of the apoptotic pathway in *C. elegans* where the BH3-only protein egl-1 is genetically upstream of the multi-domain ced-9 pro-survival molecule (Conradt and Horvitz, 1998). However, in the mammalian system, it is Bax and Bak which are required for apoptosis (Lindsten et al., 2000; Wei et al., 2001), and in their absence, the binding of BH3-only proteins to pro-survival Bcl-2 family members fails to induce apoptosis (Zong et al., 2001). This leads directly to the question of how Bax and Bak are regulated, and of the nature of the inhibition Bcl-2 pro-survival proteins impose upon them.

Despite their sequence homology, Bax and Bak exist in different subcellular locations prior to the receipt of an apoptotic stimulus; Bax is largely cytosol and Bak localises to the mitochondria. This suggests their regulation is likely to differ. Bak has recently been shown to be complexed with both Mcl-1 and Bcl-XL in healthy cells, but not with Bcl-2, Bcl-w or A1 (Willis et al., 2005). It was determined that whilst Noxa alone could release Bak from Mcl-1, Bak killing required the addition of a second BH3-only protein such as Bad (Figure 1.4 C) (Willis et al., 2005). This data also supports the model shown in Figure 1.4 B, defined based on BH3-only protein binding affinities (Chen et al., 2005), that inhibition of both classes of pro-survival proteins is necessary before Bak becomes active.

Whether Bax is regulated in a similar manner is less certain, since in healthy cells Bax is predominantly a cytosolic monomer (Antonsson et al., 2000; Hsu et al., 1997b). One possibility is that a small, but crucial pool of Bax molecules exist at the mitochondria and is sequestered in an analogous manner to Bak. However, this has not yet been demonstrated in the absence of non-ionic detergents.

An alternative explanation for Bax activation has been suggested based on structural similarities with pro-survival Bcl-2 family proteins complexed with BH3-peptides (Liu et al., 2003; Suzuki et al., 2000). The model suggests that some BH3-only proteins, namely tBid and Bim, are able directly engage Bax and Bak and function as 'activators', whilst others are 'sensitiser' which bind to the pro-survival proteins and displace tBid and Bim, allowing them to engage Bax and Bak (Figure 1.4 D) (Letai et al., 2002). These observations were based on the ability of Bim and Bid BH3 peptides to initiate Cyt-c release from isolated mitochondria, whilst those from other BH3-only proteins, the sensitisers, also required the presence of limiting amounts of Bim or Bid BH3 peptide. In this study the effect of the BH3 peptides Bcl-2 pro-survival proteins was not investigated. However, more recently it has been reported that Bid and Bim BH3 peptides co-operate with Bax to permeabilise artificial liposomes, and in this situation a role on pro-survival proteins can be excluded (Kuwana et al., 2005). However, interpretation of such data has been complicated by the lack of a detectable interaction between Bid and Bax. This has often been explained in terms of a 'hit-and-run' mechanism whereby the activating interaction between Bid would be transient and unstable, and therefore not detectable (Sundararajan and White, 2001; Wei et al., 2000). More recently, an interaction between the BH3 peptides from Bid and Puma and the N-terminal helix (hα1) of Bax as been reported (Cartron et al., 2004). However, this data is difficult to reconcile based on the BH3-binding cleft model developed for the other family members (see Section 1.10). Finally, reports placing Bid as an important Bax activator must be reconciled with the minimal phenotype observed in Bid deficient animals (Yin et al., 1999).

There leads to the conclusion that, as yet, there is no comprehensive mechanistic description of how Bax is regulated and becomes activated *in vivo* (Figure 1.4 E). Direct inhibition of Bax by Bcl-2 pro-survival proteins to block oligomerisation of Bax has suggested based on the ability of the proteins to heterodimerise (Oltvai et al., 1993) (Figure 1.4 E). However, this interaction has only been seen following the addition of non-ionic detergents (Hsu and Youle, 1997; Hsu and Youle, 1998) and has yet to be validated *in vivo*. An alternative mechanism is that Bcl-2 pro-survival proteins may have an as yet undefined role in inhibiting Bax activation through an unknown intermediary, this could encompass modification of the mitochondrial microenvironment (Figure 1.4 E). Finally, there have been suggestions that the pro-survival proteins may be able to compete with Bax for an as yet unidentified shared target. In such a model the pro-survival proteins would protect by sequestering a protein required to drive Bax activation (Hsu et al., 1997b; Polcic and Forte, 2003; Wilson-Annan et al., 2003) (Figure 1.4 E). The experimental work reported in this thesis was designed to further investigate these issues by taking unbiased microscopic and proteomic approaches to the study of Bax regulation.

1.13 Outline of subsequent chapters:

In this chapter I have tried to place the Bcl-2 family, and in particular Bax, into the complex and ever-growing field of apoptosis research. At this time many of issues in this field remain controversial. I have tried to present the consensus views of the currently available data. In late 2000, when this work was begun, much less was known about the regulation of Bcl2 family proteins. At that time it was decided to take two unbiased approach to address the problem of Bax regulation and the subsequent chapters outline how these studies progressed.

The first approach perused was a detailed microscopy-based analysis of Bax activation. The premise behind this work was that by observing Bax activation in high spatial and temporal resolution might reveal clues as to how Bax was regulated. The data collected is presented in Chapter 3 and resulted in evidence that, whilst Bax activation was a rapid event, it may be locally initiated within the cell. The data suggest that once the first Bax molecules become active the process rapidly propagated across the cell to ensure complete and co-ordinated recruitment of all mitochondria into the apoptotic program.

Viral proteins have often proved to be useful in identifying and perturbing key cellular processes; they can also be used to gain insights into cellular apoptotic mechanisms. The data presented in Chapter 4 characterises the impact of two viral proteins, BHRF1 from Epstein Bar Virus and E1B19k from Adenovirus, on Bax and Bak activation. The data demonstrates that

whilst both proteins are able to potently block full Bax and Bak activation, they do so by acting at different steps. Furthermore, even both viral proteins are able to prevent Bax/Bak oligomerisation and irreversible mitochondria dysfunction, analysis of mitochondrial ultrastructure reveals that changes still occur. Thereby demonstrating that mitochondrial changes in response to the receipt of an apoptotic stimulus are not solely the result of Bax and Bak activation.

The mitochondrial distribution in which E1B19k is able to stabilise N-terminally active Bax and prevent full activation may be directly comparable to a state that, in wild type cells, exists only transiently. This property E1B19k, together with a novel Bax mutation identified in Chapter 5 as promoting activation, was subsequently used as the basis for an unbiased proteomic approach in an attempt to identify proteins interacting with Bax at a critical step in the molecule's activation. In Chapter 6 the results of this screen, together with that for a similar screen conducted to identify proteins interacting with Bcl-XL, are presented. The data set contains known Bcl-2 interacting proteins and proteins previously implicated in apoptosis. In addition, a range of major metabolic and transport proteins not previously implicated in the control of apoptosis were also identified. This data suggests that Bax regulation, and that of the Bcl-2 family more widely, may be more closely integrated into the control of cell metabolism and physiology than previously anticipated.

Figure 1.1 The sub-families of the Bcl-2 family and related viral pro-survival proteins.
The Bcl-2 family are divided into three major groups, the Bcl-2 group promote cell survival, the Bax and BH3-only groups promote apoptosis. BH homology domains (BH1-BH4) are shown and helical regions are indicated where known. Hydrophobic C-terminal transmembrane (TM) domains are also shown (TM). Viral Bcl-2 homologues are grouped into those with sequence homology to the cellular proteins (sequence homologues) and those which target Bax/Bak but lack significant sequence homology to the cellular proteins (function homologues) Figure adapted from Cory et. al, 2003 to show viral proteins with sequence and functional homology.

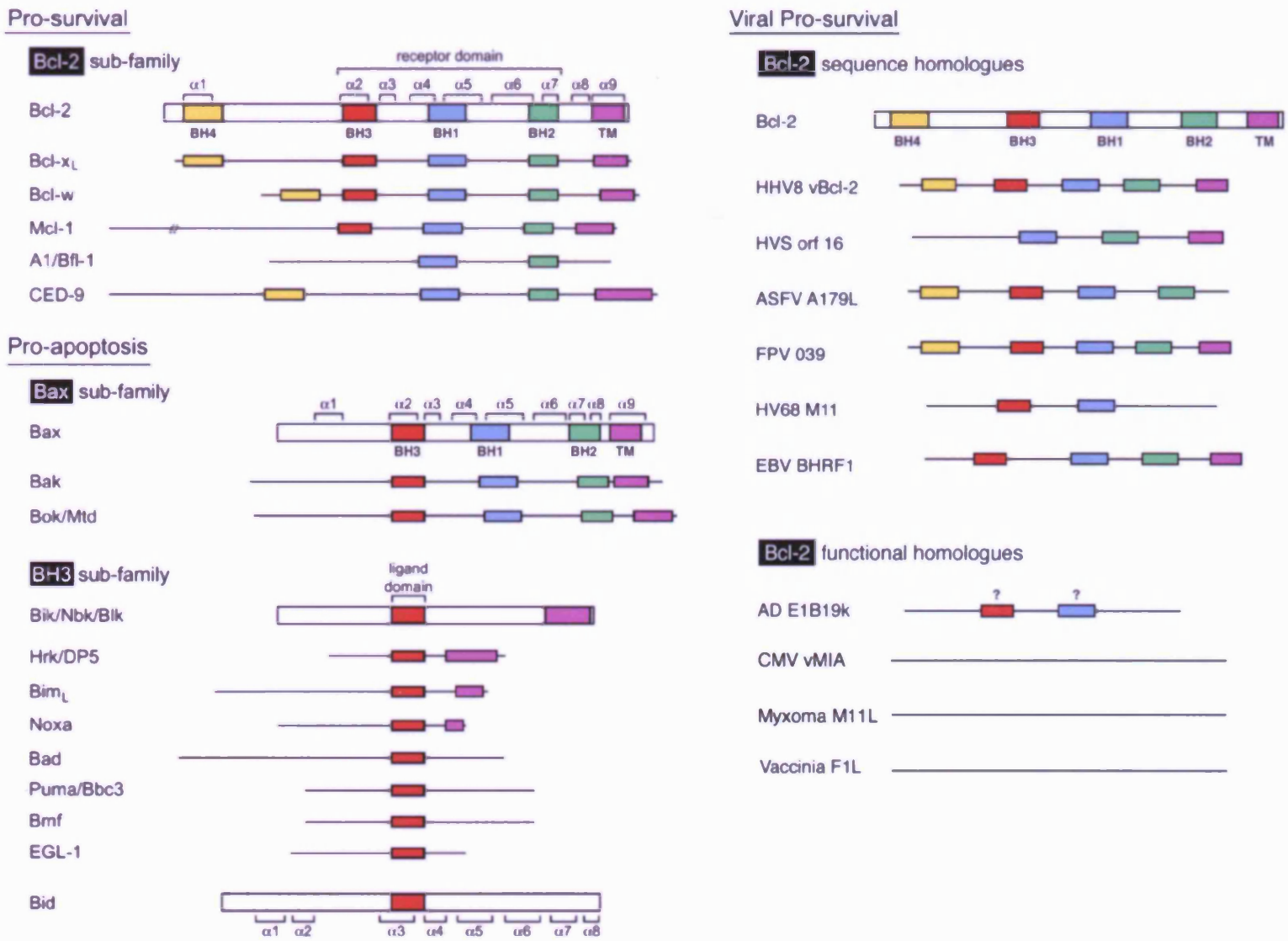
Pro-survival
Bcl-2 sub-family
receptor domain
α1 α2 α3 α4 α5 α6 α7 α8 α9
Bcl-2
BH4 BH3 BH1 BH2 TM
Bcl-xL
Bcl-w
Mcl-1
A1/Bfl-1
CED-9
Pro-apoptosis
Bax sub-family
Bax
Bak
Bok/Mtd
BH3 sub-family
ligand domain
Bik/Nbk/Blk
Hrk/DP5
BimL
Noxa
Bad
Puma/Bbc3
Bmf
EGL-1
Bid
Viral Pro-survival
Bcl-2 sequence homologues
HHV8 vBcl-2
HVS orf 16
ASFV A179L
FPV 039
HV68 M11
EBV BHRF1
Bcl-2 functional homologues
AD E1B19k
CMV vMIA
Myxoma M11L
Vaccinia F1L

Figure 1.2 Extrinsic and intrinsic apoptotic pathways.

Apoptosis can be initiated through either extrinsic or intrinsic apoptotic signalling pathways. **(A)** Activation of the extrinsic pathway is triggered by ligation of death receptors and results in formation of the DISC complex and activation of caspase-8 and then effector caspases leading to apoptosis. Bid cleavage by caspase-8 provides cross-talk with the mitochondrial pathway. **(B)** Activation of the intrinsic pathway is triggered by BH3 only proteins and results in Bax / Bak mediated mitochondrial dysfunction, leading to the release Cyt-c and activation of the apoptosome caspase-9 complex and then effector caspases leading to apoptosis. Figure from Igney et. al., 2002.

A

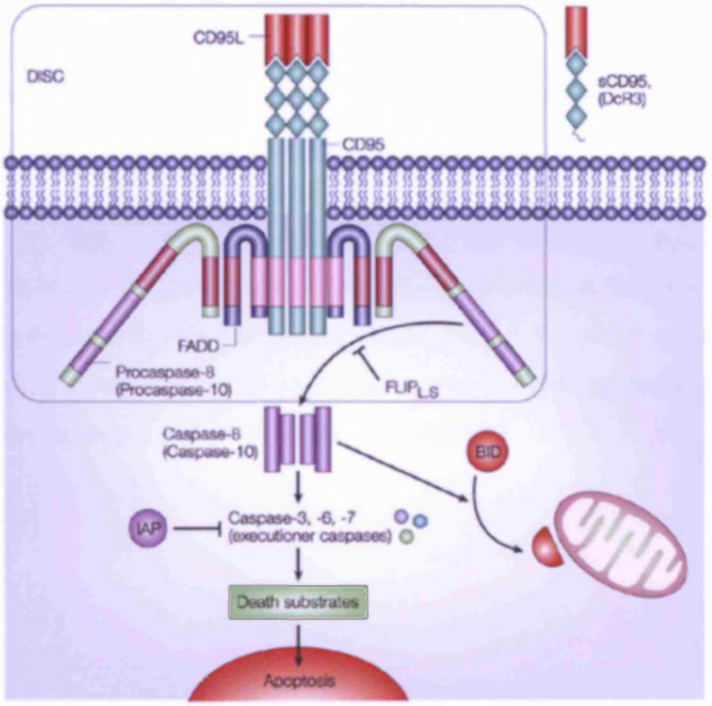
CD95L
DISC
sCD95,
(DcR3)
CD95
FADD
Procaspase-8
(Procaspase-10)
FLIP$_{L,S}$
Caspase-8
(Caspase-10)
BID
IAP
Caspase-3, -6, -7
(executioner caspases)
Death substrates
Apoptosis

B

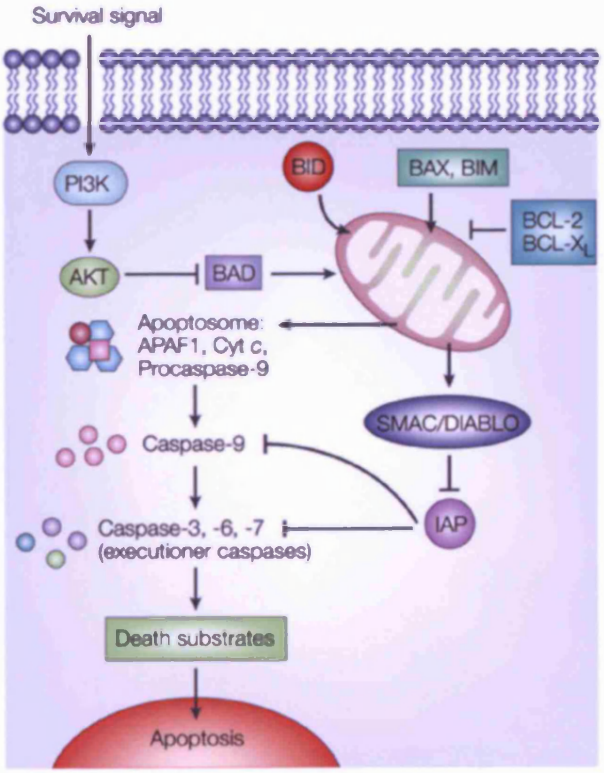
Survival signal
PI3K
BID
BAX, BIM
BCL-2
BCL-X$_L$
AKT
BAD
Apoptosome:
APAF1, Cyt c,
Procaspase-9
SMAC/DIABLO
Caspase-9
IAP
Caspase-3, -6, -7
(executioner caspases)
Death substrates
Apoptosis

Figure 1.3 Protein structures of Bcl-2 family members and related proteins.

Bcl-2 cellular proteins have structure which closely resemble viral Bcl-2 sequence homologues bacterial pore-forming toxins. Cartoon structures of cellular Bcl-2 (1G5H), Bax (1F16), Bcl-XL+Bak peptide (1BXL), Bcl-w (1MK3) and Bid (2BID), the viral Bcl-2 homolgoue BHRF1 (1Q59) and the Collicin toxin (1COL) are shown. For clarity N-terminal helices are in yellow, C-terminal helices are in red and the central helical hairpin (α5/α6 in Bax) is shown in cyan. The Bak peptide is shown in purple. Cartoons generated using RasMol software and the Protein Data Bank (PDB) record numbers indicated (www.rcsb.org/pdb).

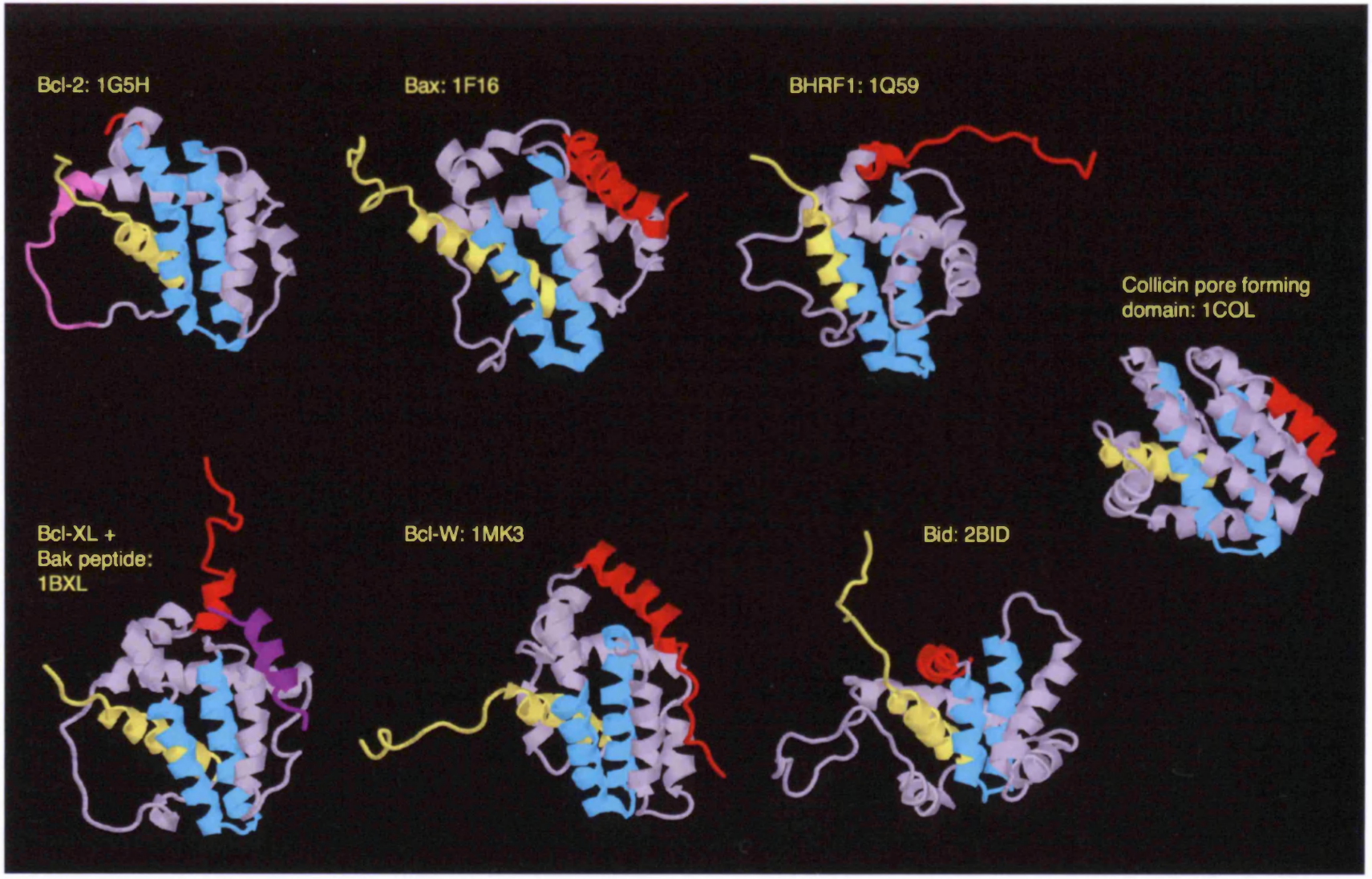
Bcl-2: 1G5H
Bax: 1F16
BHRF1: 1Q59
Collicin pore forming domain: 1COL
Bcl-XL + Bak peptide: 1BXL
Bcl-W: 1MK3
Bid: 2BID

Figure 1.4 Models for the action of Bcl-2 family proteins.

(A) BH3-only proteins are regulated by diverse mechanisms; **(B)** Bcl-2 pro-survival proteins show specificity for subsets of BH3-only proteins; **(C)** Bak can be held in check Mcl-1 and Bcl-XL prior to release due to a BH3-only protein; **(D)** tBid, along with Bim (not shown) has been suggested to directly activate Bax, whilst other BH3-only proteins target the pro-survival family members; **(E)** Suggest models and current uncertainties regarding Bax activation – see main text for details. Figure from Willis et. al., 2005 (parts A to C) and Cory et. al., 2003 (parts D and E).

A

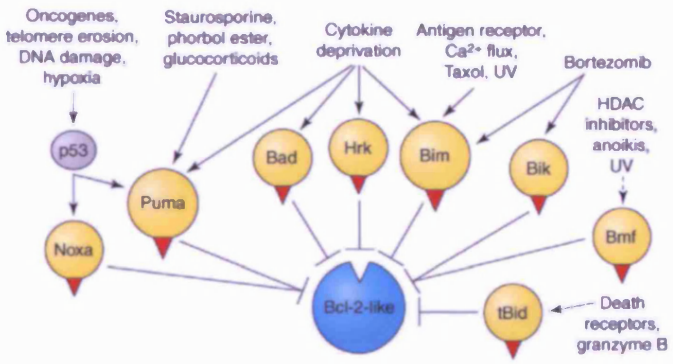
Oncogenes, telomere erosion, DNA damage, hypoxia
Staurosporine, phorbol ester, glucocorticoids
Cytokine deprivation
Antigen receptor, Ca2+ flux, Taxol, UV
Bortezomib
HDAC inhibitors, anoikis, UV
p53
Puma
Noxa
Bad
Hrk
Bim
Bik
Bmf
Bcl-2-like
tBid
Death receptors, granzyme B

B

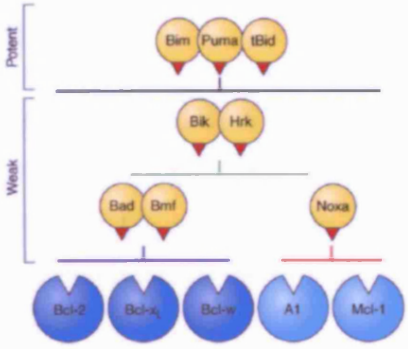
Potent
Weak
Bim
Puma
tBid
Bik
Hrk
Bad
Bmf
Noxa
Bcl-2
Bcl-xL
Bcl-w
A1
Mcl-1

C

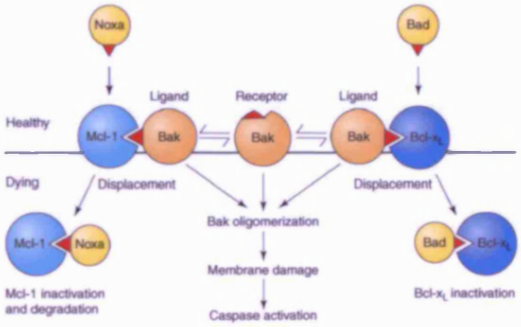
Noxa
Bad
Ligand
Receptor
Ligand
Healthy
Mcl-1
Bak
Bak
Bak
Bcl-xL
Dying
Displacement
Displacement
Bak oligomerization
Mcl-1
Noxa
Membrane damage
Bad
Bcl-xL
Mcl-1 inactivation and degradation
Caspase activation
Bcl-xL inactivation

D


Bad
Bcl-2
tBid
Bax
Caspase

E

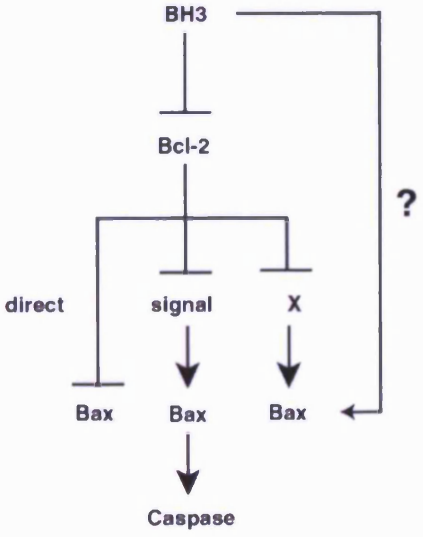
BH3
Bcl-2
?
direct
signal
X
Bax
Bax
Bax
Caspase

Chapter 2 – Materials and Methods

2.1 General buffers and solutions:

All laboratory chemicals were of analytical grade and purchased from Sigma-Aldrich unless stated otherwise. Buffers and solutions were prepared with Millipore purified, autoclaved distilled water (ddH_2O). * indicates solutions supplied centrally by Cancer Research UK central research services.

• **Luria-Bertani (LB) bacterial liquid growth media*:** 10 g/l bactotryptone, 5 g/l yeast extract, 170 mM (10g/l) NaCl. Made up to 1 litre in ddH_2O and adjusted to pH 7.0. For solid media plates: 1.5% w/v agar was added to above solution. Molten L-agar was poured into plastic culture dishes (20 ml per 10 cm dish).

• **Tris solution:** 1 M Tris stock solution was 121.1 g Trizma base per litre, pH 7.5 with HCl.

• **NaCl stock solution:** 5 M NaCl stock solution was prepared as 292.2 g/l.

• **Phosphate buffered saline (PBS)*:** 137 mM NaCl (8 g/l), 3 mM KCl (0.25 g/l), 10 mM Na_2HPO_4 (1.43 g/l), KH_2PO_4 (0.25 g/l), pH 7.2.

• **Tris buffered saline (TBS)*:** 137 mM NaCl (8 g/l), 25 mM Trizma Base (3 g/l), pH 7.4.

• **Tris-acetate-EDTA buffer (TAE):** A 50X stock solution was prepared as 242 g/l Trizma base (2 M), 57.2 ml/l glacial acetic acid and 100 ml/l 0.5 M EDTA, pH8.0*.

• **20X MES SDS PAGE running buffer (NuPAGE buffer):** 97.6 g MES (2-(N-morpholino) ethane sulphonic acid, 1.0 M), 60.6 g Tris Base (1.0 M), 10.0 g SDS (69.3 mM), 3.0 g EDTA (20.5 mM) and then ddH_20 to 500ml. pH 7.3.

• **10X SDS PAGE wet transfer buffer:** 250 mM Trizma base (30.3 g/l), 1.92M glycine (144.2 g/l), 1% SDS (10 g/l).

• **1% CHAPS mammalian cell lysis buffer:** 50 mM Tris HCl, 150 mM NaCl, 1% CHAPS, 2 mM EDTA, 5% glycerol. pH 8.0. Complete protease inhibitors (Roche, Lewes, East Sussex) were added to 1X final concentration immediately before use. This buffer was used for all immunoprecipitation and mammalian cell lysis, including the initial lysis step during TAP purifications (section 2.5.5). For gel filtration experiments the glycerol was omitted.

• **TEV cleavage buffer (for TAP purifications):** 10 mM Tris HCl, 150 mM NaCl, 0.1% CHAPS, 0.5 mM EDTA, 1 mM dithiothreitol (DTT), pH 8.0.

• **Calmodulin binding buffer (for TAP purifications):** 10 mM Tris HCl, 150 mM NaCl, 0.1% CHAPS, 1 mM magnesium acetate, 1 mM imidazole, 2 mM $CaCl_2$, 10mM beta-mercaptoethanol (BME), pH 8.0.

• **Calmodulin elution buffer (for TAP purifications):** 10 mM Tris HCl, 150 mM NaCl, 0.1% CHAPS, 1 mM magnesium acetate, 1 mM imidazole, 2 mM EGTA, 10mM BME, pH 8.0.

• **10X DNA loading buffer:** 2.5 g Ficoll type 400, 0.001 g bromophenol blue, 0.001 g xylene cyanol FF made up to 10ml in ddH_2O.

• **4X SDS sample buffer:** 200mM Tris pH 6.8, 8% SDS, 40% glycerol and 0.01 g bromophenol blue. DTT added to a final concentration of 100 mM immediately before use.

2.2 Reagents and drug treatments:

2.2.1 Drugs and reagents used to induce apoptosis:

• **Anti-Fas IgM / Cyclohexamide (CHX):** Anti-Fas IgM (human, activating), clone CH11 (Upstate, Lake Placid, NY) was purchased at 0.5 mg/ml and stored at -20°C. CHX (Sigma) was prepared as a 2 mg/ml stock in 100% ethanol and stored at -20°C. To induce apoptosis a final concentration of 250 ng/ml (1:2000 dilution) anti-Fas IgM and 2 μg/ml CHX (1:1000 dilution) was added to cells. Unless stated otherwise the abbreviation Fas/CHX is used throughout the test to indicate these conditions. For MCF10A cells Fas/CHX was prepared in minimal media supplemented only with 5% horse serum and lacking other supplements. For all other cell lines complete media was used.

• **Ultra violet irradiation (UV):** Media was removed and cells were briefly rinsed with PBS to remove traces of phenol red. PBS was removed by tipping the dish and cells were then rapidly exposed to 30 J/m^2 UVC irradiation in a UV crosslinker (Hoefer, San Francisco). Media was then replaced: for MCF10A cells minimal media supplemented only with 5% horse serum and lacking other supplements, for other cell lines this was serum free media.

• **Staurosporine (STS):** STS (Calbiochem, San Diego, CA) was prepared as 1mM stock in DMSO and stored at -20°C. A final concentration of 250nM diluted in complete media was routinely used to induce apoptosis.

• **Hydrogen peroxide (H_2O_2):** 30% stock solution (BDH chemicals, Poole, UK) was diluted to a final concentration of 1mM diluted in complete media to induce apoptosis.

2.2.2 Antibiotics used for cell selection:

Drug selections were performed using the antibiotics shown in Table 2.1.

Table 2.1 Selective antibiotics used in this study.

Antibiotic	Manufacturer	Stock concentration	Working concentration	Cells selected
Ampicillin	Sigma	50 mg/ml	50 - 100 μg/ml	Bacterial cells
Kanamycin	Sigma	10 mg/ml	25 - 50 μg/ml	Bacterial cells
Blasticidin S HCl	Invitrogen	5 mg/ml	2 - 10 μg/ml	293 T-REx cells
Zeocin	Invitrogen	100 mg/ml	500 - 1000 μg/ml	293 T-REx cells
Neomycin (G418)	Gibco (Invitrogen)	100 mg/ml	0.5 - 1 mg/ml	MCF10A cells Jurkat cells
Puromycin	Calbiochem	10 mg/ml	1 - 2 μg/ml	MCF10A cells Jurkat cells
Hygromycin B	Calbiochem	385 mg/ml	300 μg/ml	MCF10A cells

2.2.3 Antibodies:

Primary antibodies used in this work are catalogued in Table 2.2 and secondary antibodies in Table 2.3. For western blotting primary antibodies were used at dilutions of 1:1000 unless stated otherwise. For immunofluorescence primary antibodies were used at dilutions of 1:200 unless stated otherwise. Working dilutions for secondary antibodies are indicated in Table 2.2.

Table 2.2 Details of primary antibodies appearing in this study.

Name appearing in this study	Distributor or source	Product code & other details	Species and quantity	Epitope information
(A) Bax antibodies:				
Bax 6A7	Trevigen Also: BD, Merck	2281-MC-100 Y2H-6A7	Mouse 100 μg in 100 μl	12-24 hBax N-terminus
Bax N20	Santa Cruz	sc-493	Rabbit 200 μg in 1 ml	11-30 hBax N-terminus
Bax N20 AC	Santa Cruz	sc-493AC	Rabbit 500 μg / 250 μl agarose	11-30 hBax N-terminus
Bax NT	Upstate	06-499	Rabbit 200 μg in 200 μl	1-21 hBax N-terminus
Bax 2D2	Oncogene (Merck)	AM32 (Ab3)	Mouse 100 μg in 1 ml	3-16 hBax N-terminus
Bax N19	Santa Cruz	sc-526	Rabbit 200 μg in 1 ml	1-19 mBax N-terminus
Bax AF820	R&D Systems	AF820	Rabbit 30 μg in 100 μl	12-33 hBax N-terminus
Bax Loop	BD PharMingen (Neomarkers)	554101	Rabbit 100 μl serum	43-61 hBax α1 to α2 loop
Bax Mid	BD Transduction Labs	610983	Mouse 250 μg in 600 μl	55-178 hBax α2 to α9
Bax TL41	Gift from Evan Lab, ICRF, UK.	Serum (not purified)	Rabbit 100 μl serum	57-72 hBax BH3 domain
Bax Ab4	Oncogene (Merck)	PC103 (Ab4)	Rabbit 100 μg in 1ml	98-117 hBax BH1 domain
Bax α7/α8	Oncogene (Merck)	PC66 (Ab1)	Rabbit 100 μg in 1ml	150-165 hBax BH2 domain
Bax FL-TM	Santa Cruz	sc-6236 (Δ21)	Rabbit 200 μg in 1ml	1-171 mBax Full length - TM
(B) Bak antibodies:				
Bak Ab1	Oncogene *discontinued*	AM03 *discontinued*	Mouse *discontinued*	1-52 hBak N-terminus
Bak N-term	Calbiochem	196150	Rabbit 100 μg	2-14 hBak N-terminus
Bak NT	Upstate	06-536	Rabbit 200 μg in 200 μl	23-37 hBak N-terminus
Bak BD	BD PharMingen	556396	Rabbit 100 μl serum	14-36 hBak N-terminus, 1:500

Bak sc-832	Santa Cruz	sc-832	Rabbit 200 μg in 1 ml	Unspecified internal epitope
Bak B0055	US Biological	B0055-02	Mouse 0.5 mg/ml, 100 μl	41-54 hBak N-terminal
Bak AF816	R&D Systems	AF816	Rabbit 100 μg in 100 μl	53-72 hBak N-terminal
Bak Ab3	Calbiochem *discontinued*	AM15 *discontinued*	Mouse *discontinued*	82-135 hBak BH1 domain
Bak N20	Santa Cruz	sc-1035	Goat 200 μg in 1 ml	Unspecified N- terminal epitope
Bak FL	Santa Cruz	sc-7873	Rabbit 200 μg in 1 ml	1-211 hBak full length
Bak TC100	Calbiochem *replaces Ab1*	AM03 *replaces Ab1*	Mouse 100 μg	Full length hBak minus TM.
(C) ATP synthase components:				
ATP synthase alpha subunit	Molecular Porbes	A-21350	Mouse, 100 μg	Clone: 7H10
ATP synthase beta subunit	Molecular Porbes	A-21351	Mouse, 100 μg	Clone: 3D5
ATP synthase d subunit	Molecular Porbes	A-21353	Mouse, 100 μg	Clone: 7F9 1:500
ATP synthase OSCP subunit	Molecular Porbes	A-21354	Mouse, 100 μg	Clone: 4C11 1:500
ATP synthase IPing Ab	R.Capaldi (gift) & Mitosciences	MS501 (Aggeler et. al., 2002)	Mouse, 250 μg agarose coupled	Clone: 12F4AD8AF8
(D) Endoplasmic reticulum (ER) proteins:				
Ribo I	Santa Cruz	sc-12164	Goat, 200 μg	C-terminal
Ribo II	Santa Cruz	sc-12165	Goat, 200 μg	N-terminal
Ost48	Santa Cruz	sc-12171	Goat, 200 μg	C-terminal
Calnexin	Transduction Labs	610524	Mouse, 150 μg	116-301 hCanx
(E) Caspases:				
Caspase 8 (1C12)	Cell Signaling NEB	9746 18, 43, 57kDa	Mouse 200μl purified	C-terminal peptide from hCasp8
Caspase 9	Cell Signaling NEB	9502 17,35,37,47kDa	Rabbit 100 μl purified	Peptide around Asp315 hCasp9
Caspase 3 (3G2)	Cell Signaling NEB	9668 17,19,35kDa	Mouse 100 μl purified	Residues 28-44 of hCasp3
Cleaved Caspase 3 (Asp175)	Cell Signaling NEB	9661 17, 19kDa	Rabbit 100 μl purified	N-terminal, around Asp175

(F) Pro-survival proteins:				
E1B19k	Oncogene	DP07L	Rat, 100 μg	Clone: 1G11, 1:500
BHRF1	Chemicon	MAB8188	Mouse, 100 μg	Clone: 5B11
Bcl-2	Santa Cruz	sc-509	Mouse, 200 μg	41-54 hBcl-2
Bcl-XL	Transduction Labs	B61220 (610746)	Mouse, 50 μg	18-233 rBcl-XL
Bid (FL-195)	Santa Cruz	sc-11423	Rabbit, 200μg	1-195 hBid, 1:500
(G) Other miscellaneous antibodies:				
Cyt-c (native)	BD Pharmingen	556432	Mouse, 100 μg	Clone: 6H2.B4
PARP	BD Pharmingen	556362	Mouse, 0.1ml	Clone: C2-10
Actin	Santa Cruz	sc-1615	Goat, 200μg	C-terminus hActin

Table 2.3 Details of secondary antibodies appearing in this study.

Name appearing in this study	Distributor or source	Product code	Species Pack size	Regular working dilutions
HRP-linked anti-mouse IgG	Amersham	NA931V	Donkey 1.0 ml	1:3000
HRP-linked anti-rabbit IgG	Amersham	NA934V	Donkey 1.0 ml	1:3000
HRP-linked anti-goat IgG	Pierce	31433	Rabbit 1.5 ml	1:1000
HRP-linked anti-rat IgG	Amersham	NA935V	Goat 1.0 ml	1:1000
HRP-linked anti-rabbit Fc_γ	Jackson Labs (Stratech UK)	315-035-008	Rabbit 1.5 ml	1:75,000 Fcγ fragment specific
HRP-linked anti-rabbit Fc_γ	Jackson Labs (Stratech UK)	111-035-008	Goat 1.5 ml	1:75,000 Fcγ fragment specific
FITC anti-mouse IgG (H+L)	Jackson Labs (Stratech UK)	715-095-150	Donkey 0.5 mg, 0.6 μg/μl	1:200 range 1:50-1:200
FITC anti-rabbit IgG (H+L)	Jackson Labs (Stratech UK)	711-095-152	Donkey 0.5 mg, 0.6 μg/μl	1:200 range 1:50-1:200
Cy3 anti-mouse IgG (H+L)	Jackson Labs (Stratech UK)	715-165-150	Donkey 0.5 mg, 0.6 μg/μl	1:200 range 1:100-1:800
Cy3 anti-rabbbit IgG (H+L)	Jackson Labs (Stratech UK)	711-165-152	Donkey 0.5 mg, 0.6 μg/μl	1:200 range 1:100-1:800
Cy5 anti-mouse IgG (H+L)(Cytc)	Jackson Labs (Stratech UK)	715-175-150	Donkey 0.5 mg, 0.6 μg/μl	1:200 range 1:100-1:800
FITC anti-rat IgG (H+L)(E1B)	Jackson Labs (Stratech UK)	712-095-153	Donkey 0.5 mg, 0.6 μg/μl	1:200 range 1:100-1:800

2.2.4 Oligonucleotide primers:

All primers were synthesised by the CR-UK oligonucleotide facility, resuspended in ddH_2O and stored as 5μM stocks at -20°C. All primer sequences are written in the 5' to 3' direction.

(A) Sequencing primers:

pcDNA4/TO forward primer: CGCAAATGGGCGGTAGGCGTG

pcDNA4/TO reverse primer: TAGAAGGCACAGTCGAGG

pBABE forward primer: CGTCTCTCCCCCTTGAACCTCCTCTTTCG

pBABE reverse primer: CCACACCCTAACTGACACACATTCCACAGG

pEGFPN3 forward primer: GGCGTGTACGGTGGGAGGTCTATATAAGCA

pEGFPN3 reverse primer: TCGCCGTCCAGCTCGACCAGGATG

pEGFPC3 forward primer: CATGGTCCTGCTGGAGTTCGTGACCG

pEGFPC3 reverse primer: CAGGTTCAGGGGGAGGTGTGGGAGG

(B) Primers for PCR amplification of Bax:

pEGFPN3 forward primer: GAGCCGAGATCTATGGACGGGTCCGGGGAGCA

pEGFPN3 reverse primer: GAGCTACTCGAGTCAGCCCATCTTCTTCCAGATGGTGA

pECFPC1 forward primer: GATGCGAAGCTTATGGACGGGTCCGGGGAGCAGCCCAG

pECFPC1 reverse primer: CTACGCGAATTCTTAGCCCATCTTCTTCCAGATGGTGAGCGA

pcDNA RFP(N) forward primer: GATGCGAAGCTTATGGACGGGTCCGGGGAGCAGCCCAG

pcDNA RFP(N) reverse primer: CTACGCCTCGAGTTAGCCCATCTTCTTCCAGATGGTGAGCGA

pcDNA4TO/NTAP forward primer: GAGCCGGGATCCGCCACCATGGACGGGTCCGGGGAGCA

pcDNA4TO/NTAP reverse primer: GAGCTATCTAGATCAGCCCATCTTCTTCCAGATGGTGA

pcDNA4TO/CTAP forward primer: GAGCCGGAATTCATGGACGGGTCCGGGGAGCA

pcDNA4TO/CTAP reverse primer: GAGCTATCTAGATCAGCCCATCTTCTTCCAGATGGTGA

(C) Bax mutagenesis primers (positions of mutant codons are marked in **BOLD**):

Bax S184V Forward: GCGGGAGTGCTCACCGCC**GTG**CTCACCATCTGGAAGAAG

Bax S184V Reverse: CTTCTTCCAGATGGTGAG**CAC**GGCGGTGAGCACTCCCGC

Bax L25P Forward: ATCATGAAGACAGGGGCC**CCT**TTGCTTCAGGGTTTCATC

Bax L25P Reverse: GATGAAACCCTGAAGCAA**AGG**GGCCCCTGTCTTCATGAT

Bax K119A, K123A, K128A (AAA) Forward:

CCCTTTTCTACTTTGCCAGC**GCA**CTGGTGCTC**GCG**GCCCTGTGCACC**GCG**GTGCCGGAACTGATCAG

Bax K119A, K123A, K128A (AAA) Reverse:

CTGATCAGTTCCGGCAC**CGC**GGTGCACAGGGC**CGC**GAGCACCAG**TGC**GCTGGCAAAGTAGAAAAGGG

Bax K119A, K123E, K128E (AEE) Forward:

CCCTTTTCTACTTTGCCAGC**GCA**CTGGTGCTC**GAG**GCCCTGTGCACC**GAG**GTGCCGGAACTGATCAG

Bax K119A, K123E, K128E (AEE) Reverse:

CTGATCAGTTCCGGCAC**CTC**GGTGCACAGGGC**CTC**GAGCACCAG**TGC**GCTGGCAAAGTAGAAAAGGG

2.3 DNA methods:

2.3.1 Basic DNA manipulations:

DNA amplification by polymerase chain reaction (PCR) was performed in a 50μl reaction according to the general scheme: 400 ng DNA template, 5 μM forward and reverse primers (section 2.2.4), 5 μl 10X Pfu buffer, 1 μl dNTP mix and 1 μl Pfu polymerase (Stratagene) made up to 50 μl with ddH_2O. Thermocycling parameters were: 95°C for 1 min; (95°C for 30 sec, 54°C for 1 min, 68°C for 3 min) repeated for 30 cycles; 68°C for 10 min, then held at 4°C. PCR grade deoxynucleoside triphosphates (dNTPs, Roche) were combined and diluted to a 50X stock solution containing dATP, dCTP, dGTP and dTTP at 10 mM each.

Restriction enzyme digests were performed according to the manufacturer's protocol (New England Biolabs (NEB), Hitchin, Herts) in a total volume of 20 μl and then analysed by DNA gel electrophoresis (section 2.3.2). DNA fragments were excised form agarose gels and recovered using QIAquick Gel Extraction kit (Qiagen). DNA ligation reactions were performed in 10 μl total volume as DNA vector (0.5 μl), DNA insert (0.5 μl), T4 DNA ligase (1 μl) (NEB), 10X T4 ligase buffer (1 μl) and 7 μl ddH_2O, for 1-2 hrs at RT and then 2 μl of the ligation reaction was use to transform competent *E.coli* as described in section 2.3.4.

2.3.2 DNA gel electrophoresis:

Agarose gels were prepared by dissolving 1% agarose in 1X TAE buffer and heating until boiling. Ethidium bromide was added to a final concentration of 0.5 μg/ml before the gel was cast. PCR reactions and DNA digests were supplemented with DNA loading buffer to a final 1X concentration and loaded. DNA molecular weight markers (1kb ladder, Invitrogen) were included on all gels. Electrophoresis was at 5-10 V/cm in TAE buffer and bands were visualised on a UV transilluminator.

2.3.3 Plasmid mutagenesis:

Plasmid DNA mutagenesis was performed by an adapted QuickChange method (Stratagene, La Jolla, CA) as a 50 μl reaction: 50 ng parental DNA template, 3.2 pmol of the appropriate forward and reverse primers (section 2.2.4), 5 μl 10X Pfu buffer, 1 μl 50X dNTP mix and 1 μl Pfu polymerase made up to 50 μl with ddH_2O. Thermocycling parameters were: 95°C for 30 sec; (95°C for 30 sec, 55°C for 1 min, 68°C for 16 min) repeated for 16 cycles; then held at 4°C. 1 μl DpnI restriction enzyme (NEB) was then added to the PCR reaction and incubated for 1 hr at 37°C to digest methylated parental DNA strands. 1 μl of the resulting reaction was used to

transform competent *E.coli* as Section 2.3.4. A control reaction with no Pfu polyermerase was performed in parallel and colonies only picked for analysis if the control plate was clear of colonies.

2.3.4 Transformation of DNA into competent E.coli by heat shock:

20 ng of plasmid DNA, 2 μl of ligation reactions or 1 μl of mutagenesis reactions was incubated with 30 μl competent XL10 gold *E.coli* bacteria (Stratagene) on ice for 30 mins. The bacteria were then heat shocked by transfer to a 42°C hot-block for 45 seconds and then returned to ice for a further 2 mins. 1 ml fresh LB medium was added and bacteria were allowed to recover by 1hr incubation at 37°C with gentle shaking. Bacteria were then pelleted in a microcentrifuge, resuspended in 100 μl LB medium and spread onto LB agar plates containing the appropriate selective antibiotic. Plates were incubated overnight at 37°C and then stored at 4°C.

2.3.5 Purification of plasmid DNA:

Single bacterial colonies picked from LB agar plates containing the appropriate selection antibiotic, were used to inoculate 5 ml cultures of LB medium also containing antibiotic and incubated overnight at 37°C with shaking. For small scale (mini prep) plasmid purification the 5 ml overnight culture was pelleted by centrifugation and plasmid DNA isolated using DirectPrep 96 MiniPrep automated plasmid purification system (Qiagen) according to the manufacturer's instructions. For large scale (maxi prep) plasmid DNA purification 1ml of the overnight culture was used to inoculate 400 ml of LB / antibiotic and incubated at 37°C overnight with shaking. Cells were harvested by centrifugation and used for Maxi-prep plasmid purification kit (Qiagen) according to the manufacture's instructions. Purified plasmid DNA was resuspended in ddH_2O and the concentration and purity assessed using an Eppendorf spectrophotometer (Hamburg, Germany) by measuring optical density at 260nm (OD_{260nm}) according to the equation: Concentration (mg/ml) = OD_{260nm} x 50 x dilution factor x pathlength.

2.3.6 DNA sequencing:

Sequencing PCR reactions were performed according to the general scheme: 8.0μl of Big Dye Terminator reaction mix, 3.2 pmol of primer, 150-200 ng of double stranded primer template in a total reaction volume of 20 μl. Thermocycling parameters were: 2.5°C/sec to 96°C, 96°C for 1 min; (96°C for 10 sec, 1°C/sec to 48°C, 48°C for 5 sec, 1°C/sec to 60°C, 60°C for 4 mins) repeated for 24 cycles; then held at 12°C. Dye-terminator removal was achieved either with DyeEx2.0 spin columns (Qiagen), according to the manufacturer's instructions or manually by ethanol/EDTA/sodium acetate precipitation, briefly: 2 μl 125 mM EDTA, 2 μl 3 M sodium

acetate and 50 μl 100% ethanol were added to each 20 μl reaction, vortexed, and spun in a microcentrifuge at 14,000 rpm for 15 mins at RT. Supernatant was removed by tube inversion and precipitant washed with 200 μl 70% ethanol. Samples were then spun again in a microcentrifuge at 14,000 rpm for 15 mins at 4°C and supernatant again removed by tube inversion. Finally samples was dried in a Speed Vac microcentrifuge and stored at -20°C until run. Sequences were read by capillary sequencing using an ABI Prism 3730 DNA analyser (Applied Biosystems, Foster City, CA). DNA sequence reads were aligned and manipulated using the DNA strider (http://www.cellbiol.com/soft.htm).

2.3.7 DNA constructs:

• **Fluorescent protein Bax constructs:** The N-terminally tagged green fluorescent protein (GFP) vector, pEGFPC3 GFP-Bax, was a gift from R.Youle, NIH, Bethesda, USA. The human Bax insert was amplified by PCR and inserted (BglII / EcoRI) into pECFPC1 (Clontech) to produce the N-terminally tagged cyan fluorescent protein (CFP) variant CFP-Bax. The Bax insert was amplified by PCR and inserted (HindIII / XhoI) into pcDNA RFP-N (a gift from R.Tsien, Stanford, USA) to create the red fluoresent protein (RFP) variant RFP-Bax. The Bax insert was also amplified by PCR and inserted (BglII / XhoI) into pEGFPN3 (Clontech) to create the C-terminally tagged variant Bax-GFP. All vectors contain Kanamycin/Neomycin resistance cassettes except pcDNA RFP-Bax which has Ampicillin/Neomycin resistance cassettes.

• **TAP tag Bax constructs:** pcDNA4/TO TAP-Bax and pcDNA4/TO Bax-TAP were constructed based on pcDNA4/TO tetracycline inducible vector (T-REx system, Invitrogen). This vector has Ampicillin/Zeocin resistance cassettes. The C-TAP tag template sequence was obtained from B.Seraphin, EMBL, Heidelberg, Germany and sub-cloned into pcDNA4/TO (EcoRI / XbaI). The human Bax coding sequence was amplified by PCR and inserted immediately upstream (5') of the TAP tag (HindIII / EcoRI) to create Bax-TAP. The N-TAP tag template sequence was obtained from Euroscarf (the EUROpean Saccharomyces Cerevisiae ARchive for Functional analysis, Frankfurt, Germany) and sub-cloned into pcDNA4/TO (HindIII / EcoRI). The human Bax coding sequence was amplified by PCR and inserted immediately downstream (3') of the TAP tag (EcoRI / XbaI) to create TAP-Bax.

• **Retroviral constructs containing pro-survival proteins:** pBABE puro Bcl-2, pBABE hygro Bcl-XL, pBABE puro E1B19k and pBABE puro BHRF1 were all obtained from D.Hancock, CR-UK.

• **Other constructs:** A retroviral expression vector containing the Ecotropic receptor, pBABE neo EcoR, was obtained from P.Warne, CR-UK. The pEGFPC3 GFP-Bax, pEGFPN3 Bax-GFP, pcDNA4/TO TAP-Bax and pcDNA4/TO Bax-TAP constructs listed above were used as templates in mutagenesis reactions, as described in section 2.3.3 and using primers listed in section 2.2.4, to generate the series of four mutants: S184V, L25P, AAA and AEE which are characterised in Chapters 5 and 6. All constructs were sequence verified.

2.4 Mammalian cell culture:

2.4.1 Sources of cell lines used in this study:

• 293 T-REx cells: Human embryonic kidney cells expressing pcDNA6/TR. Invitrogen.

• HeLa cells: Human cervical cells. CR-UK central cell services.

• Jurkat cells: Human T lymphocytes. CR-UK central cell services.

• MCF10A cells: Human mammary epithelial cells. P.Warne, CR-UK.

• MCF10A AktER: MCF10A cell line stably expressing an oestrogen receptor (ER) fusion of activated (myristoylated) human Akt1 (Kohn et al., 1998). This construct can be activated by the addition of 4-hydroxytamoxifen (OHT). P.Warne, CR-UK.

• Phoenix A/E cells: 293 based retrovial packaging cells. A gift from G.Nolan, Stanford. (Phoenix A indicates amphotropic and Phoenix E indicates ecotropic host selectivity).

• U2OS cells: Human osteosarcoma cells (HTB96). CR-UK central cell services.

2.4.2 Cell growth conditions:

Adherent epithelial cells (293 T-REx, HeLa, Phoenix and U2OS) were in Dulbecco's MEM (E4) media supplemented with 10% foetal bovine serum (FBS). Suspension cells (Jurkat) were grown in RPMI 1640 2% (RPMI) media also supplemented with 10% foetal bovine serum (FBS). MCF10A cells were grown in Ham's nutrient mixture F-12 / DMEM (1:1) media supplemented with 5% horse serum, 10 μg/ml insulin, 20 ng/ml EGF, 5 μg/ml hydrocortisone, and 100 ng/ml cholera toxin (full medium). Minimal medium consisted of Ham's nutrient mixture F-12 / DMEM (1:1) containing 5% horse serum only. All media formulations were prepared by CR-UK central cell services.

Cell lines were grown in environmentally controlled humidified incubators at 37°C and 10% CO_2. Adherent cells passaged when 80-90% confluent by removing the old growth media, rinsing cells in warm PBS and then covering the monolayer with 0.25% trypsin / versene solution (CR-UK central cell services). Cells were returned to the incubator until they detached

and the resuspended in fresh complete growth media and distributed into fresh culture dishes at 1:5 to 1:10 dilutions. In preparation for microscopy experiments cells were re-plated at higher dilutions (1:30) to allow time for them to re-adherence onto glass coverslips and transfection and still be < 75% confluent at the time of analysis. Suspension cells maintained at 0.5 - 2.0x10^6 cells/ml by diluting the culture with fresh complete media.

Expression of pcDNA4/TO tetracycline inducible constructs in 293 T-REx was achieved by the addition doxycycline (dox, Clontech, Mountain View, CA) to a final concentration of 100 ng/ml for 12 hrs. Dox was prepared as a 1 mg/ml stock solution in 70% ethanol and stored at -20°C. Doxycycline is approximately 100 times more active than tetracycline in this system and these conditions 293 T-REx cells were induced at maximal levels. Activation of the 4-hydroxytamoxifen dependent AktER fustion in MCF10A AktER cells was achieved by addition of 4-hydroxytamoxifen (OHT, Sigma Aldrich) to a final concentration of 250 nM. OHT was prepared as a 1 mM stock solution in 100% ethanol and stored at -20°C.

2.4.3 Transfection methods:

All transfections for biochemistry and microscopy experiments were preformed with Effectene (Qiagen) unless stated otherwise. Transfections were performed according to the manufacturer's instructions, briefly: cells were seeded into 6-well plates 1 day before, or onto flame sterilised glass coverslips in 6-well plates 2 days prior to transfection. The transfection mix was prepared as: 0.4 μg DNA, 3.2 μl Enhancer, 100 μl EC buffer and incubated at room temperature (RT) for 5mins. 10 μl Effectene reagent was then added and incubated for a further 10 mins at RT, during this period old media was removed from cells and replaced with 1.6 ml fresh media. Finally the transfection mix was then diluted in a further 600 μl fresh media and added to the cells.

To obtain higher transfection efficiencies in Phoenix retroviral packaging cell lines (section 2.4.4) either a Calcium Phosphate based method (Invitrogen) or Lipofectamine 2000 reagent (Invitrogen) were used according to the manufacturer's instructions. In both cases this yielded > 80% transfection efficiency as assessed by transfection of a GFP marker plasmid.

2.4.4 Retroviral infections:

MCF10A Bcl-2, Bcl-XL E1B19k and BHRF1 cell lines and Jurkat Bcl-2 cells were produced by retroviral transduction. Briefly, the pBabe constructs described in section 2.3.7 were used to transfect Phoenix packaging cells as described in section 2.4.3. At 24 and 48 hrs post-transfection virus-containing supernatant was collect from the Phoenix cells, filtered though a

0.45 μm syringe unit (Millipore) and diluted 1:1 with fresh growth media appropriate for the target cells. Viruses were then added to the cells for a total of 48hrs. After a further 24hrs (72hrs after the initial infection) cells were passaged into fresh growth media containing the appropriate selective antibiotic (Table 2.1). Selective media was replaced every 3-4 days until no more cell death was observed (~3 days for puromycin, ~6 days for hygromycin and ~14 days for G418). Stable integration of pBabe-encoded protein in the resulting cell population was confirmed by western blotting. In the interests of safety all stable cell lines were constructed using a two-step infection regime. In the first round, naive MCF10A and Jurkat cells were first infected with the pBabe Neo EcoR virus produced from Phoenix A cells to have amphotropic receptor selectivity. This conferred expression of the murine ecotropic receptor on the target cell lines. In the second round, pBabe constructs encoding the indicated pro-survival proteins were packaged using Phoenix E cells. The viruses produced therefore had more limited ecotropic host selectivity and could be safely used to infect cells produced during the initial round.

2.4.5 Production of stable inducible 293 T-REx cell lines:

293 clonal cell lines inducibly expressing TAP-tagged Bax and Bax mutants were produced using the T-REx system (Invitrogen). 293 T-Rex cells stably express the tetracycline repressor (TetR) encoded by pcDNA6/TR (selection marker: blasticidin). TAP-tagged Bax constructs were created in pcDNA4/TO as described in section 2.3.7. pcDNA4/TO is a cytomegalovirus (CMV) driven expression vector containing two copies of the tetracycline operator ($TetO_2$) sequence. In cells expressing pcDNA6/TR, TetR binds to these sequences and prevents transcription from the CMV promoter. Upon the addition of tetracycline or doxycycline (Dox) this repression is relieved resulting in transcriptional induction of the gene of interest (Figure 2.1). Prior to transfection the pcDNA4/TO TAP Bax constructs, and TAP alone control, were linearised by digestion with the single-cutting enzyme SspI (NEB) in an attempt to increase the efficiency of stable integration. Plasmid DNA was then purified on QIAquick columns (Qiagen) and transfected into 293 T-Rex cells plated in 6 cm dishes at 70-80% confluency. 24 hrs after transfection the cells were split at dilutions of 1:100, 1:500 and 1:1000 into three 15 cm plates. Cells were allowed a further 24hrs to adhere to these plates before the growth media was supplemented with Zeocin to a final concentration of 100 μg/ml. Zeocin-containing selective media was gently aspirated and replaced with fresh every 4 days until surviving clones were clearly visible to the naked eye (usually 14-16 days for discrete, well-spaced clones to become visible on the 1:500 and 1:1000 dilutions). To isolate surviving clones the media was gently aspirated from the cells and the clones covered with small circles of Whatman filter paper, autoclaved and pre-soaked in trypsin / versene solution. After returning the plates to the incubator for 5 mins the filter paper discs were recovered using sterile forceps and placed into

individual wells of a 24-well plate. Selection was maintained while cells transferred from the filter paper and expanded in the wells. Once confluent, clones were each passaged into two wells of a 6-well plate and single 6 cm dishe. When nearing confluency one well from the 6-well plate was induced with Dox (100 ng/ml for 18 hrs) and then both were lysed and analysed by western blotting for induction of the Bax TAP fusion protein. Clones exhibiting tight and high-level induction of the Bax TAP fusion were recovered from the remaining 6 cm dishes and expanded to prepare frozen stocks and for use in tandem affinity purifications. Representative western blots showing induction levels in Bax TAP expressing clones generated by this procedure are shown in Figure 2.2.

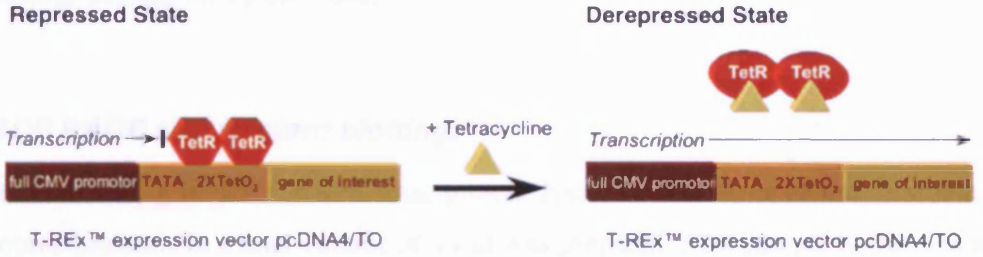

Figure 2.1 T-REx system (Invitrogen) inducible protein expression.

In cells expressing the pcDNA6/TR encoded Tetracycline repressor protein (TetR) a gene of interest encoded by pcDNA4/TO is constitutively repressed as transcription from the CMV promoter is blocked by the binding of TetR to tetracycline operator sequences ($TetO_2$) positioned immediately 3' of the promoter. The addition of tetracycline (or doxycycline) causes a conformational change in TetR and release from the operator sequences, thereby allowing transcription of the gene of interest.

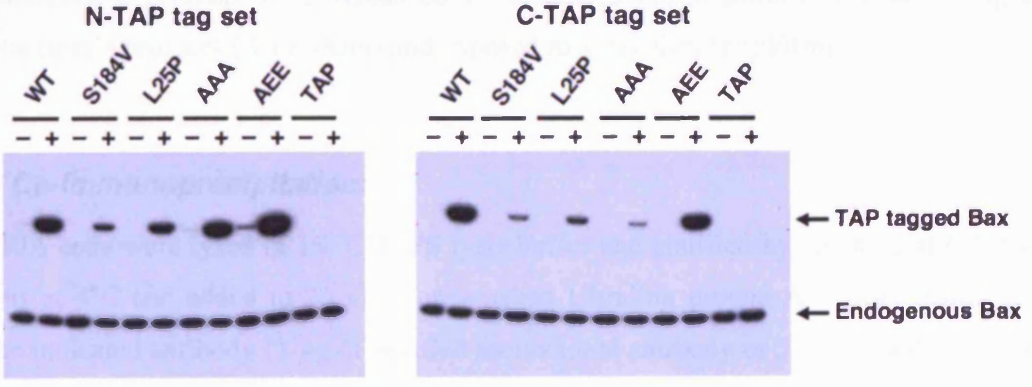

Figure 2.2 Representative clonal cell lines used for Tandem Affinity Purifications.

293 T-REx clonal cell lines containing the indicated pcDNA4/TO TAP Bax variants were treated +/- 100 ng/ml doxycycline for 18hrs. Cells were then lysed in 1% CHAPS lysis buffer and 20 μg of total protein analysed by western blotting with an anti-Bax antibody (2D2).

2.5 Protein methods:

2.5.1 Determination of protein concentrations:

Protein concentrations were measured using a modified Lowry method (Bio-Rad DC Assay, Bio-Rad, Hercules, CA). Briefly: 5 μl of 1:5 dilutions of protein lysates or of protein standards were aliquotted into a 96-well plate in triplicate. Standard samples covering the linear range of the assay (0-2.0 mg/ml) were prepared from bovine serum albumin (10 mg/ml, NEB). 25 μl Reagent A and 200 μl Reagent B were added to each well and the plate was then incubated at RT for 20 mins. Protein concentrations were then determined in relation to the standard curve by measuring OD_{750nm} on a plate reader.

2.5.2 SDS PAGE and western blotting:

In most cases 20 μg of 1% CHAPS total protein lysate or one third of the final eluate from immunoprecipitations in a total volume of 15 μl was prepared. SDS sample buffer was added to a final concentration of 1X. Full range pre-stained molecular weight markers (Amersham) were included on all gels. Samples were loaded onto 4-12% gradient Bis-Tris NuPAGE gels (Invitrogen) for electrophoresis in MES buffer at 200 volts for 35 mins. Following separation proteins were transferred to PVDF membranes (Millipore) using mini-gel wet transfer apparatus (BioRad) at 85V for 1.5 hrs at 4°C. Membranes were blocked in 5% milk in PBS for 1 hr at RT and then incubated with primary antibodies diluted in 5% milk in PBS at 4°C O/N with gentle shaking. Membranes were then washed 3 times for 10 mins in PBS with 0.1% Tween-20 and incubated with the appropriate secondary antibody diluted in 5% milk in PBS for 1 hr at RT. Finally membranes were washed 4 more times for 10 mins in PBS with 0.1% Tween-20. Immunoreactive proteins were visualised by enhanced chemiluminescence according to the manufacturer's protocol (Amersham) and exposed to x-ray film (FujiFilm).

2.5.3 Co-immunoprecipitation:

MCF10A cells were lysed in 1% CHAPS lysis buffer and clarified by spinning at 6000 x *g* for 12 mins at 4°C and added to 20 μl of pre-washed Ultralink protein A/G bead matrix (Pierce) and the indicated antibody (3 μg of purified monoclonal antibody or 5 μl of purified polyclonal sera, unless stated otherwise). Samples were incubated O/N at 4°C with rotation. Beads were recovered by centrifugation at 1000 x *g* for 3 mins at 4°C and washed 3 times with 1 ml of 1% CHAPS lysis buffer. Following the final wash immunoprecipitated proteins were eluted by the addition of 30 μl 1.5X SDS sample buffer and the eluate stored at -80°C.

2.5.4 Gel filtration:

MCF10A cells (2 x 80% confluent 10 cm dishes) were harvested by scraping into PBS and pelleted at 2000 rpm in a benchtop centrifuge. Cells were lysed in an equal volume of 2% CHAPS lysis buffer (without glycerol). Following rotation at 4°C for 20 mins, samples were clarified by spinning at 21,000 x *g* for 20 min and 40 μl loaded onto a pre-equilibrated Superdex 200 Precision Column PC 3.2/30 (2.4 ml) gel filtration column (Pharmacia). The column was calibrated using thyroglobulin (667 kDa), ferritin (440 kDa), aldolase (158 kDa), BSA (67 kDa), ovalbumin (43 kDa), chymotrypsinogen A (25 kDa) and ribonuclease A (14 kDa). The entire column volume was collected in 40 μl fractions and 10 μl analysed by SDS PAGE.

2.5.5 Tandem affinity purifications:

Each 293 T-REx TAP Bax expressing clone was expanded to 15 x 15 cm culture dishes, except for the TAP purification shown in Figure 6.6 where a total of 60 x 15 cm plates were used. When cells reached confluency the Bax TAP fusion was induced with the addition Dox to a final concentration of 100 ng/ml for 12 hrs. The growth media was then removed and cells detached by the addition of 2 ml of 2 mM EDTA in PBS for 10 mins. Cells were then collected in PBS and pelleted at 1300 rpm in a benchtop centrifuge. Cell pellets were lysed on ice in 10ml of 1% CHAPS lysis buffer with 10 strokes in a dounce homogeniser. The lysate was then cleared of nuclei and large fragments by centrifugation at 4300 x *g* for 20 mins at 4°C and then added to 15 ml tube containing 500 μl of a 50% slurry of pre-washed IgG-linked agarose (Sigma) and incubated for 2 hrs at 4°C with rotation. Beads were then recovered by centrifugation for 5 mins at 1600 rpm in a benchtop centrifuge and washed 3 x 10 ml 1% CHAPS lysis buffer and then 1 x 10ml TEV cleavage buffer. The bead matrix, resuspended in the second of these washes, was transferred to a 15 ml Poly-prep chromatography column (BioRad) to simply further handling. After TEV cleavage buffer wash the base of the column was capped and 950 μl TEV cleavage buffer and 100 μl recombinant tobacco etch virus (TEV) protease (manufactured by the CR-UK protein isolation laboratory) added. The column was then capped at the top and incubated for 2hrs at RT followed by O/N at 4°C with rotation. Following TEV cleavage the sample was eluted directly into a second column containing capped at the base and containing 500 μl of a 50% suspension of Calmodulin-linked affinity resin (Stratagene). 3.5 ml calmodulin binding buffer and 3.5 μl 1 M $CaCl_2$ were then added, the column capped at the top and incubated for 2-4 hrs at 4°C with rotation. Finally, the calmodulin resin was washed 3 x 10 ml calmodulin binding buffer and bound proteins eluted in 5 x 200 μl fractions of calmodulin elution buffer. At each step aliquots were saved for diagnostic western blotting. For TAP purifications shown in Figure 6.4 CHAPS was exchanged for Triton-X100 throughout. A summary of the TAP method is shown in Figure 2.3.

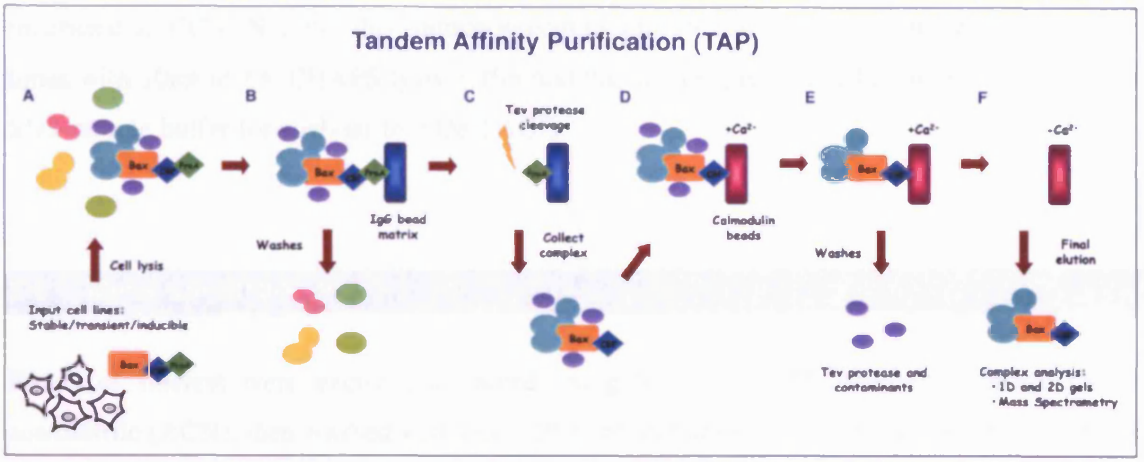

Figure 2.3 Summary of the Tandem Affinity Purification (TAP) method.

Stable cell lines expressing TAP fusion proteins were lysed **(A)** and the tagged protein bound to an IgG-linked bead matrix via the Protein A epitope of the tag **(B)**. The column was washed and the tagged protein eluted with TEV protease **(C)** and then bound to a calmodulin-linked bead matrix via the Calmodulin binding peptide (CBP) of the tag **(D)**. Following more washes **(E)**, the tagged protein was eluted by chelation of Ca^{2+} and collected for concentration and analysis **(F)**.

2.5.6 Concentration and visualisation of TAP purified proteins:

Final TAP eluates were concentrated using Microcon YM-10 columns (Millipore) operating at 5000 x *g* and 4°C from an initial volume of ~ 1 ml to a final volume of ~ 30 µl. SDS sample buffer was added to 1X final concentration and the sample run on 10-well 4-12% NuPAGE gels (Invitrogen) and fixed in 40% ethanol, 10% acetic acid, made with ddH_2O for 1 hr at RT. Gels were then stained using either SilverQuest mass spectrometry compatible silver stain (Invitrogen) or colloidal coomassie (Sigma).

2.5.7 Addition of cross-linkers to TAP purifications:

A modified TAP purification is outlined in Figure 6.9. Essential changes were that the TEV cleavage was performed in a modified buffer in which the Tris buffer was substituted for Hepes. Following the TEV cleavage the crosslinker disuccinimidyl suberate (DSS, Pierce) was added to a final concentration of 0.1 mM from a 100 mM stock prepared in DMSO. The cross-linking reaction was allowed to proceed for 30 mins at RT with rotation and then neutralised by the addition of 1 M Tris pH 7.5 to a final concentration of 50 mM. Following a further incubation for 15 mins at RT, SDS was added to a final concentration of 1% and the sample to promote dissociation of unlinked proteins and the sample was rotated for a further 15 mins at RT. Finally, the SDS was diluted to 0.1% by the addition of 1% CHAPS lysis buffer and entire sample added to 50 µl compact pre-washed Bax N20-linked agarose beads (Santa Cruz) and

incubated at 4°C O/N. After this immunoprecipitation step the Bax N20 agarose was washed 3 times with 10ml of 1% CHAPS lysis buffer and the immunoprecipitated proteins eluted in 1.5X SDS sample buffer for analysis by SDS PAGE.

2.6 Mass spectrometry:

Bands of interest were excised, destained using 50:50 25 mM ammonium bicarbonate / acetonitrile (ACN), then washed with H_2O (20 min) and dried in a SpeedVac (45 min). Porcine trypsin (Promega) was prepared in 200 μl ice-cold resuspension buffer (supplied with the enzyme; 0.1 mg/ml trypsin at 16 000 U/mg) and made up to 500 μl with 25 mM ammonium bicarbonate to give a working solution. Gel pieces were rehydrated in 5 μl of this working solution for 5 min on ice. 30 μl of 25 mM ammonium bicarbonate was then added and samples incubated for 2 hrs at 37°C. Digestion was stopped by placing the samples on dry ice. Samples were later defrosted and the supernatant transferred to a 0.2 ml siliconized thin walled tube (Bioquote, York, UK). Two further extractions were performed with 30 μl of 5% v/v formic acid, incubating in a sonicating water bath for 15 min. Peptides from the three extractions were pooled then dried in a SpeedVac. Prior to MS the peptides were desalted twice by re-suspending and washing in 50 μl H_2O and then taken to dryness in a SpeedVac to remove all volatile salts.

Immediately prior to analysis peptides were resuspended in 7 μl 1% formic acid and 5 μl injected onto a nano HPLC (high pressure liquid chromatorgraphy) system (LC Packings, Sunnyvale, CA). Separation is achieved on a nano LC column (75 μm I.D. x 150 mm) packed with Vydac C18 (5 μm particles) at a flow rate of 250 nl/min with a gradient from 0% to 95% of 0.1% acetic acid in acetonitrile and anlysed directly by tandem electrospray mass spectrometry using either a qTOF (Micromass) or API 4000 QTRAP MS/MS System (Applied Biosystems). The resulting spectra were initially collected using proprietary software supplied with the instruments. Subsequently peptide masses were searched against the National Center for Biotechnology Information (NCBI) non-redundant database using the Mascot software (Matrix Science, London). One missed cleavage per peptide and an initial mass tolerance of 10 ppm were used in all searches.

2.7 Fluorescence activated cell sorting (FACS) methods:

2.7.1 Bax and Bak activation staining:

At specific times after drug treatments cells (minimum 10^6) were harvested from suspension cultures by centrifugation or 6-well dishes by scraping into PBS. Cells were then fixed in ice cold 70% ethanol for at least 30 mins at 4°C and stored at 4°C. Prior to analysis cells were immunostained with the indicated anti-Bax and -Bak antibodies at 1:200 dilutions in 500 μg/ml digitonin in PBS, either overnight at 4°C or for 1 hr at room temperature (RT). Cells were then washed in PBS and incubated with the appropriate FITC-linked secondary antibody at 1:200 dilution in PBS for 1hr at room temperature (RT) in the dark and then washed for a final time in PBS (Griffiths et al., 1999).

Cells were then analysed by FACS using a FACSCalibur instrument fitted with an argon-ion 488 nm laser and red HeNe 633 nm red diode laser (Becton Dickinson, San Jose, CA). The instrument was configured to record 10000 events per sample in the FITC (FL-1) channel. Data handling was performed using CellQuest software (Becton Dickinson, San Jose, CA) to display histograms of the staining intensity for each sample.

2.7.2 Analysis of DNA content – SubG1 apoptosis assay:

Cells were grown in 6 cm dishes and treated with Fas/CHX as indicated to induce apoptosis. At each time point samples were harvested in triplicate by scraping into PBS and fixed with ice cold 70% ethanol for at least 30 mins and accumulated at 4°C for analysis. Cells were then washed twice in phosphate-citrate buffer (0.2 M disodium phosphate (Na_2HPO_4), 4 mM citric acid (pH 7.8)), between washes cells were collected by spinning at 2000 rpm in a benchtop centrifuge. Each sample was then treated with 50 μl of 100 μg/ml RNase followed by 200 μl of 50 μg/ml propidium iodide (PI).

Cells were then analysed by FACS using a FACSCalibur instrument fitted with an argon-ion 488 nm laser and red HeNe 633 nm red diode laser (Becton Dickinson, San Jose, CA). The instrument was configured to exclude debris and cell doublets and then record PI staining intensity (FL-3) as a measure of DNA content as shown in Figure 2.4. For each sample 10,000 events were acquired and data analysis was preformed using FlowJo software (TreeStar Inc, CA).

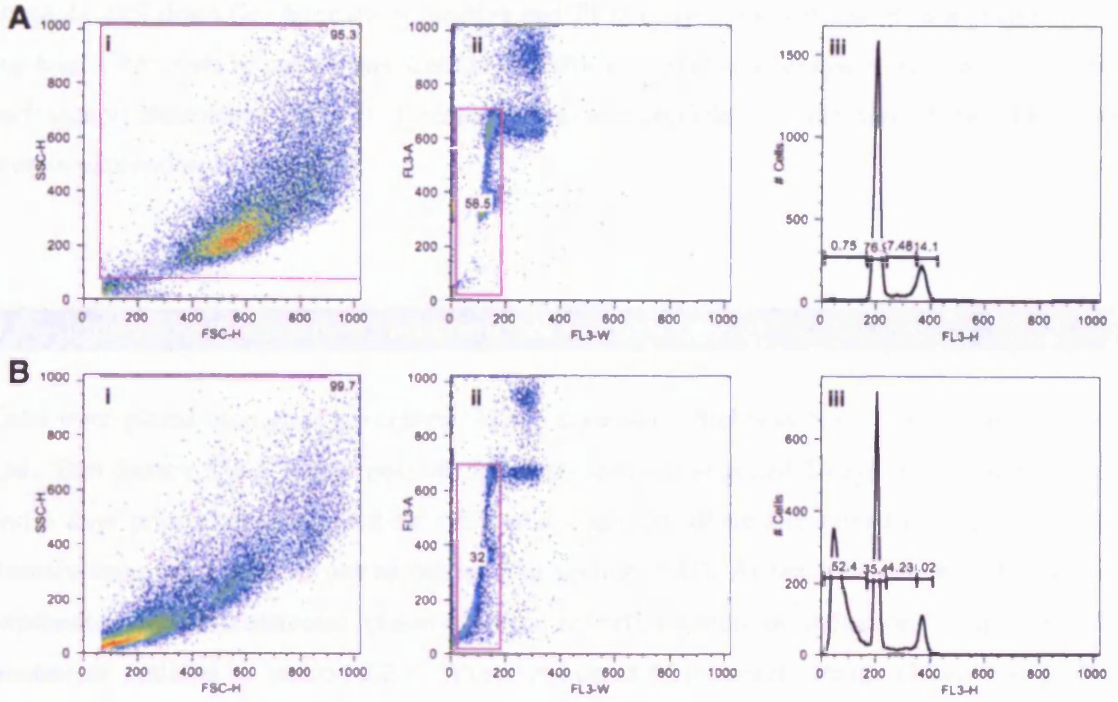

Figure 2.4 FACS analysis for dead cells with sub-G1 DNA content.

Representative FACS profiles to demonstrate how the proportion of dead cells with sub-G1 DNA content was measured. MCF10A cells were harvested and stained as described in section 2.7.2. **(A)** Untreated, **(B)** 14hrs after exposure to Fas/CHX. In both parts 3 analysis steps were performed sequentially: (i) gating of forward scatter against side scatter to discriminate whole cells; (ii) doublet discrimination was achieved by adjusting area and width parameters; (iii) finally fluorescence intensity of PI (FL-3) was measured on a linear scale and the proportion of cells with a sub-G1 DNA content was then calculated using FlowJo sowtware.

2.7.3 Annexin V staining – measuring apoptosis in GFP transfected cells:

MCF10A cells were grown in 6-well dishes and transfected with the GFP constructs indicated using Effectene reagent (Qiagen). 24 hrs after transfection, cells were harvested by scraping into PBS, collected by centrifugation and washed in PBS. Cells were then resuspended in calcium-rich buffer (Becton Dickinson, San Jose, CA) containing 2 µl Alexa 647 linked anti-Annexin V IgG (Molecular Probes, Oregon, USA) and 5 µg/ml propidium iodide (PI, Sigma Chemicals, Poole, UK) for 15 min at RT.

Cells were analysed by FACS using a FACSCalibur instrument fitted with an argon-ion 488 nm laser and red HeNe 633 nm red diode laser (Becton Dickinson, San Jose, CA). The instrument was configured to measure GFP (FL-1) fluorescence intensity on a logarithmic scale and gate 5000 GFP positive cells. This subset was then analysed for PI (FL-2/3) and Annexin V Alexa 647 (FL-4) positivity. The percentage of GFP-positive cells displaying characteristic features of

apoptotic cell death (ie. Annexin V positive and PI negative) was calculated as a proportion of the total GFP-positive cells using CellQuest software (Becton Dickinson, San Jose, CA). For each sample the median GFP (FL-1) intensity was also recorded as a measure of the GFP-fusion protein expression level.

2.8 Immunofluorescence and confocal microscopy:

Cells were plated onto glass coverslips (22mm diameter, Thickness No 1.5, Raymond A Lamb Ltd., East Sussex, UK). Where possible MCF10A cells were plated 2 days prior to transfection and 3 days prior to analysis as these cells take longer to adhere and spread on a glass surface. Transfections were carried out as outlined in section 2.4.3. At least 24 hrs was allowed for expression of the transfected plasmids prior to cell fixation or induction of apoptosis by treatments outlined in section 2.2.1. Where indicated Mitotracker Orange (Molecular probes, Carlsbad, CA) was added to the medium to a final concentration of 200 nM for 20 mins prior to fixation. Cells were then rinsed briefly with warm PBS and fixed by flooding coverslips with warm 3% paraformaldehyde solution in PBS. After 20 mins fixation at RT were washed 3 times in PBS and stored at 4°C until before immunostaining. Note: for the GFP/Mitotracker/DAPI combination used to characterise Bax mutants in Chapter 5 no additional staining was necessary and coverslips were mounted directly onto glass slides and imaged directly.

For immunostaining fixed cells were permeabilised by incubation in 0.1% Triton X-100 in PBS for 5 mins on ice and then washed 3 times in PBS. Cells were then blocked to reduce unspecific binding using 0.2% fish skin gelatine (FSG) in PBS for at least 20 mins at RT. Primary antibodies were diluted to 1:200 (unless stated otherwise) in 0.2% FSG / PBS and incubated on the cells for 1 hr at RT or overnight at 4°C. Where co-staining with more than one primary antibody was used they were added simultaneously. Coverslips were placed on pedestals made from inverted 1.5 ml tube caps mounted in a Petri dish and then kept inside a damp chamber. This arrangement meant 200 μl antibody solution was sufficient to cover the cells on each coverslip and be held in place by surface tension. Following incubation with the primary antibody coverslips picked up with forceps and drained by tilting and touching their edges onto absorbent paper. They were then rinsed by moving sequentially through a series of four baths of 0.2% FSG / PBS (50 ml each) and placed back onto pedestals. 200 μl of the appropriate secondary antibody dilutions were then added for 1 hr at RT in the dark (see table 2.2). Coverslips were then rinsed through another 4 washes of 0.2% FSG / PBS, 1 wash of PBS and 1 wash of water (to prevent PBS derived salt crystals forming between coverslip and glass slide after mounting). Finally, coverslips were mounted onto glass slides using 8 μl of ProLong Gold

anti-fade reagent containing DAPI (Molecular Probes) and left to set at 4°C overnight. Cells were visualised on an LSM510 confocal microscopy (Carl Zeiss, Thornwood, NY) equipped Argon 288 nm, HeNe 543 nm, HeHe 633 nm and blue diode 405 nm laser lines. Image acquisition was achieved using a 63X plan-apochromat Phase 3 oil immersion objective, numerical aperture 1.4 (Carl Zeiss), operating and operating at 1 airy unit (optical slice size ~0.8 μm) and image manipulation was using the LSM510 propriety software and Photoshop CS2 (Adobe, San Jose, CA).

2.9 Live cell video microscopy:

Cells were grown in 35 mm glass bottomed dishes (MatTek Corporation, Ashland, MA) for 1 day prior to transfection. Transfections were with Effectene (Qiagen) as described in section 2.4.3. 24 hrs after transfection cells were loaded with tetramethylrhodamine methyl ester (TMRE, Molecular Probes) by adding a 1 μM stock to a final concentration of 2 nM in the growth media for 20 mins. Cells were then washed and placed in fresh media and indicated treatment to induce apoptosis applied (either Fas/CHX or UV irradiation, see section 2.2.1).

2.9.1 Basic live cell recording experimental setup:

Digital time-lapse microscopy was used to record cell behaviour following the induction of apoptosis. All time-lapse experiments were conducted on the same Zeiss Axiovert 135 TV (Carl Zeiss) inverted microscope. The microscope was optimised for multi-channel digital time-lapse microscopy and to accommodate the long-term imaging of mammalian cells in culture. The microscope was fitted with tungsten and mercury lamps to enable both bright field and fluorescence imaging, and was equipped with separate bright field and fluorescence shutters (Uniblitz), a shutter controller (Sutter Instruments), and a sensitive CCD camera (Orca ER, Hamamatsu). All peripheral devices were under the control of image acquisition software (Acquisition Manager, Kinetic Imaging). The CCD camera was mounted directly under the sample on the lower camera port of the microscope in order to minimise the number of optical elements in the path from the objective to the camera, therefore maximising the fluorescence signal. Blocks containing excitation and emission filters and compatible dichromatic mirrors enabled a range of fluorophore species to be imaged and were constructed as shown in figure 2.5. In addition, motorised excitation and emission filter wheels containing a selection of different fluorescence filters enabled the rapid sequential imaging of multiple fluorophores during a single time-lapse experiment when used in conjunction with appropriate multiple dichromatic mirrors.

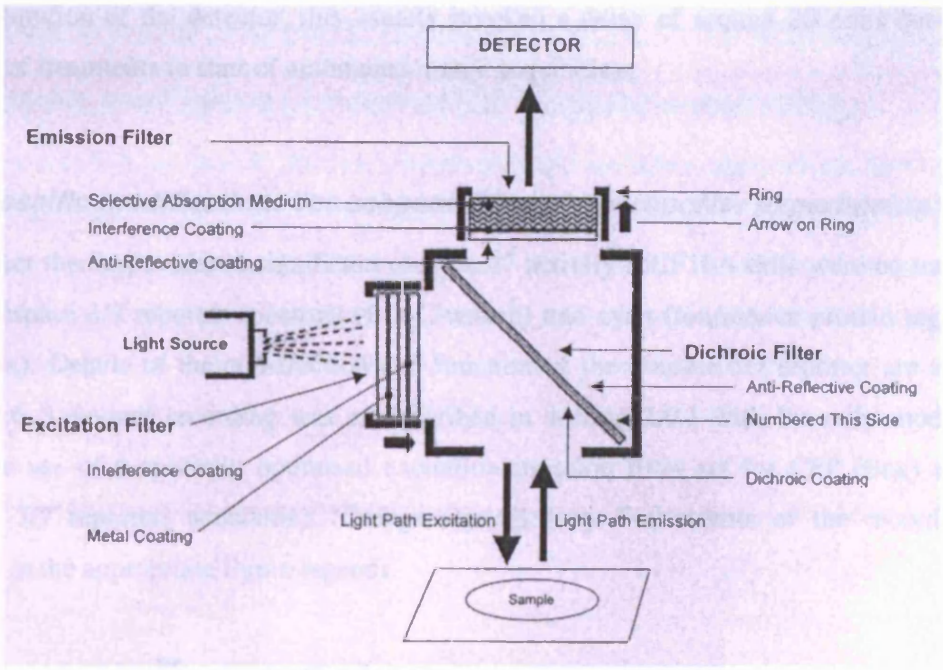

Figure 2.5 Basic design of filter system used for low light live cell microscopy.
Basic design of filter blocks containing excitation and emission filters and compatible dichromatic mirrors. During automated image acquisition a block position containing only the appropriate dichroic was used, the excitation and emission filters being contained in motorised filter wheels for automated switching.

Filters and dichromatic mirrors were purchased from Omega Optical Inc. and permitted the imaging of EGFP (FX100-2 Alpha Vivid: Ex 475 AF40, DRLP 505, Em 535 AF45) and Alexa 568/Cy3/Cy3.5 (FX108-2 Alpha Vivid: Ex 525 AF45, DRLP 560, Em 695 AF55) fluorescence, the latter being suitable for visualising TMRE. The microscope was housed in a purpose built Perspex environmental chamber accurately maintained at 37°C using a heater unit constructed in-house (CR-UK Research Services). The main body of the microscope rested on an optical table isolator (Melles Griot) in order to minimize the effects of ambient vibrations on image acquisition. The glass-bottomed culture dish was positioned on the stage of the microscope in a glass-topped, steel humidity chamber (also constructed in-house) and efficiently prevented evaporation during the course of time-lapse recording. A 63X plan-apochromat Phase 3 oil-immersion objective, numerical aperture 1.4 (Carl Zeiss) was used for all recordings.

The time-lapse interval, total duration of the recording, and filter configurations varied according to the experimental assay and are therefore described for each assay. Most commonly EGFP fluorescence, TMRE fluorescence and phase frame acquisitions were made at 1 min intervals for a total of 1000 cycles. Exposure times for each channel were set individually to

avoid saturation of the detector, this usually invoked a delay of around 20 mins between the addition of treatments to start of automated image acquisition,

2.9.2 Specific modifications for caspase 3/7 activity reporter experiments:

To monitor the first evidence significant caspase3/7 activity MCF10A cells were co-transfected with a caspase 3/7 reporter construct (BD Clontech) and cyan flouresence protein tagged Bax (CFP-Bax). Details of the construction and function of the caspase 3/7 reporter are shown in Figure 2.6. Live cell recording was as described in section 2.9.1 with the only modification being the use of a specially optimised excitation/emission filter set for CFP (Bax) and YFP (caspase 3/7 reporter) acquisition (Omega Optical Inc). Full details of the recordings are included in the appropriate figure legends.

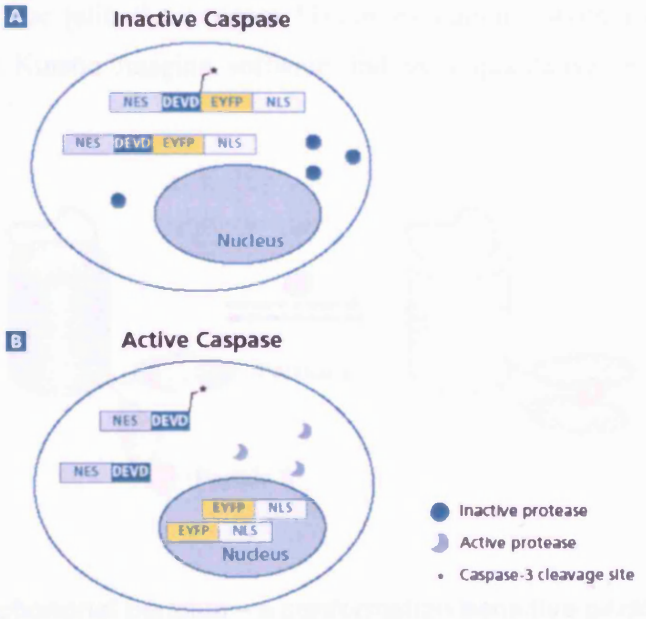

Figure 2.6 Schematic outline of the Caspase 3 reporter construct (Clontech).

The Caspase 3 sensor vector consists of a yellow fluorescent protein (YFP) fused at the N-terminus there to a Nuclear Export Signal (NES) and caspase consensus cleavage site (DEVD)*. A Nuclear Localisation Signal (NLS) is fused at the C-terminus. **(A)** In healthy cells the NES is dominant over the NLS and the fusion protein is excluded from the nucleus. **(B)** Upon activation of effector caspases cleavage at the DEVD motif releases the NLS-targeted YFP from the NES and the fluorescent protein is rapidly sequestered into the nucleus. By transiently co-transfecting this construct with an N-terminally CFP-tagged Bax it is possible address the temporal relationship between the appearance of Bax clusters and significant effector caspase enzymatic activity.

2.9.3 Specific modifications for Pericam Ca^{2+} imaging experiments:

The dual-excitation ratiometric pericam fluorescent Ca^{2+} indicator construct has been described in detail elsewhere (Nagai et al., 2001; Zhang et al., 2002). The basic principle of the construct is shown in Figure 2.7. A mitochondrially targeted version of the ratiometric pericam was a gift from M.Martins, University of Leicester and used in co-transfection experiments together with red fluorescent protein fusion of Bax (RFP-Bax). Three excitation/emission filter combinations were used to image these constructs: RFP-Bax: 560±20nm/625±25nm, pericam 410nm: 380±25nm/535±15nm and pericam 510nm: 480±20nm/535±15nm, together with a DAPI/FITC/TexasRed optimised dichromatic mirror (all from Omega Optical Inc). This enabled the live cell system described in section 2.9.1 to be adapted for the sequential acquisition of: (i) RFP-Bax, (ii) pericam excited at ~410nm, (iii) pericam excited at ~510nm, (iv) phase contrast. The ratio the pericam 510nm excitation / 410nm excitation was then calculated using the Kinetic Imaging software and as a qualitative readout of changes in mitochondria [Ca^{2+}].

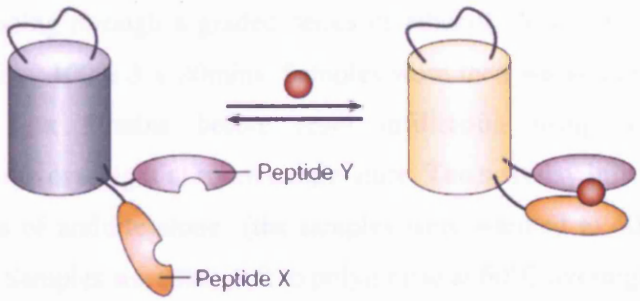

Figure 2.7 The mitochondrial pericam – a conformation sensitive permuted AFP protein. The pericam protein is based on *Aequorea* fluorescent protein (AFP) engineered to be directly sensitive to calcium ions (red circle). In this case Ca^{2+} sensitive proteins X and Y (Calmodulin and M13 peptide) have been fused to the amino- and carboxy-termini of the circularly permuted AFP. Upon binding of Ca^{2+} the pericam protein exhibits changes in excitation spectra as well as increased fluorescence emission intensity. This is detected by monitoring changes in the ratio of emissions following excitation at two different wavelengths: ~510nm excitation and ~410nm excitation and allows these proteins to report on changes in intracellular Ca^{2+}. Since such proteins can be targeted to specific subcellular locations such as organelles they enable organelle-specific Ca^{2+} measurements to be made. (Figure from Zhang et. al., 2002).

2.10 Electron microscopy:

For standard morphological analysis MCF10A were grown on 13 mm diameter Thermanox plastic coverslips (Agar scientific). 293-T-REx cells were grown in 10 cm plastic culture dishes. Following induction of apoptosis (MCF10A) or induction of Bax TAP fusions (293 T-REx) cells growth media was removed and cells were fixed for 1 hr in a modified Karnovsky's fixative: 4% paraformaldehyde, 2.5% glutaraldehyde, 2mM $CaCl_2$ in 0.1M Na Cacodylate ($Na(CH_3)_2AsO_2.3H_2O$), pH7.4. 293 T-REx cells were scraped in the fixative and pelleted using a benchtop centrifuge and processed as a loose pellet. MCF10A cells were fixed and processed on the plastic coverslips. Cells were then washed in cacodylate buffer twice for 10 mins at room temperature. Samples were then post-fixed using 1% osmium tetroxide (OsO_4) and 1% potassium ferricyanide ($K_3Fe(CN)_6$) in 0.1M Na Cacodylate pH7.4 at room temperature for 30 mins. Samples were then washed 2 x 20 mins in cacodylate buffer, 2 x 5 mins in ddH_2O. Finally 2% aqueous uranyl acetate solution was added for contrast enhancement and samples were stored at 4°C overnight.

In preparation for sectioning samples were again washed 3 x 5 mins in ddH_2O and then dehydrated by processing through a graded series of ethanol: 70% 1 x 20 mins, 80% 1 x 20 mins, 90% 1 x 20 mins, 100% 3 x 20mins. Samples were then washed in intermediate solvent (propylene oxide) 1 x 20mins before resin infiltration using a 50/50 mixture of araldite/propylene oxide overnight at room temperature. The next day infiltration was continued with 3 x 1hr changes of araldite alone (the samples were warmed to 60°C for about 10mins before each change). Samples were then left to polymerise at 60°C overnight.

Sections of approximately 90nm thickness were then cut on Leica Ultracut S Ultratome (Leica, Wetzlar, Germany) and collected on 200 mesh copper grids. Sections were further stained with a saturated solution of uranyl acetate in methanol for approximately 6 mins at RT, rinsed x 4 in methanol and then with Reynold's lead citrate stain for 4 mins RT and rinsed x 4 in ddH2O. Samples were then viewed in a JEOL 1200 TEM (JEOL, Tokyo, Japan). Each micrograph collected represented a different cell selected at random from the grid and at least 30 cells were examined in each sample. For MCF10A samples all mitochondria in the micrograph were scored for morphology and included in the analysis.

Chapter 3 – Behaviour of the Bax protein

3.1 Introduction:

In late 2000, when this work was begun, the central role of Bcl-2 family proteins in the cellular decision to initiate apoptosis was already becoming clear. Earlier in 2000, the first reports of *Bax-/-Bak-/-* doubly deficient animals provided genetic proof that the presence of at least Bax or Bak was required to initiate cell death by apoptosis (Lindsten et al., 2000; Wei et al., 2001), Yet, despite a significant body of work in this area, both the mechanism of action of these proteins, and the process by which they become active, remained a matter of debate, and does so to this day. The work described here was initiated to gain further insights into the process of Bax regulation and activation.

Several publications in the preceding years have revealed the Bcl-2 proteins, and particularly the pro-apoptotic Bax and Bak molecules, were artificially activated by commonly used non-ionic detergents such as Triton X-100 and NP-40 (Hsu and Youle, 1997; Hsu and Youle, 1998). In 2000, this was confirmed when the NMR structure showed dramatic shifts in the spectra upon the addition of detergent (Suzuki et al., 2000). Early explanations for Bcl-2 protein function were largely based around a so-called rheostat model, in which the life or death decision was a consequence of whether pro-survival or pro-apoptotic members predominated after taking into account intra-family binding by which pro-survival and pro-apoptotic members were able to neutralise each others function. As it became clear that detergent-induced activation promoted promiscuous binding between the different Bcl-2 family proteins, the physiological relevance of the earliest incarnations of the rheostat models had to be re-evaluated. Further studies have since led to revisions and modifications, but certain aspects of the rheostat model have stood the test of time. Here it is only mentioned in order to reiterate two key points: one is that it now seems most likely the BH3-only proteins are primarily ligands to neutralise pro-survival proteins, and thereby relieve inhibition on Bax and Bak. Only a minority of BH3-only proteins can directly activate Bax and Bak, and even these are not essential. The second is that although direct binding of pro-survival Bcl-2 proteins to Bak has been validated (Willis et al., 2005), it is unlikely a similar mechanism can be invoked to explain how Bax is held in check since the Bax protein is predominantly a cytoplasmic monomer and is not found

complexed with pro-survival proteins in healthy cells. Therefore, although an essential step in the initiation of apoptosis, the mechanisms by which Bax becomes activated and by which Bcl-2 pro-survival proteins prevent Bax activation remain largely unknown.

There are many possible models which can, and have, been invoked to explain Bax activation, including release from a cytoplasmic anchor (Sawada et al., 2003), hit-and-run activation by another protein (Eskes et al., 2000), recruitment to the mitochondria (Marzo et al., 1998), binding of a small molecule such as a metabolite or change in the physiological conditions of the cell such as pH (Tafani et al., 2002). However, none of these models has yet been widely accepted. Most of the previous studies of Bax activation have been carried out in cell populations. Spatial and temporal organisation of apoptotic signalling in general, and of Bax activation in particular, remains a largely uninvestigated area. With such a diverse range of possible mechanisms involved, a reasonable starting point therefore seemed to be to take an unbiased approach and see if further insights could be gained by observing the Bax protein in action, in order to characterise when and where in the cell activation takes place. This was achieved initially by using antibodies raised against the endogenous protein and later by expressing GFP-Bax to monitor changes in Bax localisation in live cells. Although some of the data presented in this chapter has been superseded by more recent publications, the results shown have not previously been reported in MCF10A cells or followed at such high resolution following the activation of apoptosis by Fas/CHX. These observations formed the basis for further attempts to interrogate and manipulate the Bax activation process, the results of which are presented in the subsequent chapter.

3.2 Characterisation of conformationally sensitive Bax and Bak antibodies:

Early reports had demonstrated that antibodies raised against the N-terminus of Bax were conformationally sensitive, meaning that they only recognised Bax subsequently to its activation (Nechushtan et al., 1999). Antibodies raised against the N-terminus of Bak behave in a similar conformationally sensitive manner and have been used to quantify the early stages of apoptosis (Griffiths et al., 1999; Makin et al., 2001; Postigo et al., 2006). The ability of these antibodies to identify individual cells undergoing apoptosis could therefore be used in assays to quantitate apoptosis. In this section an example is shown for both Bax and Bak.

To demonstrate the conformational sensitivity of the Bax 6A7 antibody, U2OS cells were treated 1 mM H_2O_2 to induce apoptosis. 4 hrs later the cells were loaded with Mitotracker to reveal the location of energised mitochondria, fixed and immunostained with the Bax 6A7

antibody. Apoptotic cells are clearly identified as being recognised by the 6A7 (12-24) anti-Bax antibody (Figure 3.1 A). A reciprocal staining pattern, whereby "Bax-positive cells" have failed to stain with Mitotracker, indicates that the mitochondria have already lost the $\Delta\psi_m$, suggesting that these cells are undergoing the early stages of apoptosis. The binary nature of this staining pattern, whereby cells are either strongly positive for 6A7 staining or remain completely unstained, makes it a useful assay with which to quantify apoptosis at a stage much earlier than other commonly used readouts, for example DNA fragmentation. This can be visualised in MCF10A mAkt-ER cells, which are protected from apoptosis by the tamoxifen-dependent activation of the pro-survival kinase Akt1. By counting the percentage of cells staining positively with the 6A7 antibody, the level of apoptosis induced by etoposide, Fas alone or Fas/CHX was clearly reduced by a 4 hr prior activation of Akt1 (Figure 3.1 B, panel i). Lysates prepared from parallel cultures were used in a western blot with a phospho-specific antibody to detect phosphorylation of residue serine 473, which indicates that the protein kinase is active.

Bak has an analogous function to Bax and was shown to be genetically redundant (Wei et al., 2001). Jurkat cells are a useful system in which to study Bak activation since they fail to express Bax, due a frame-shift mutation within a polyguanine tract in the Bax open reading frame (Brimmell et al., 1998), and are therefore reliant on Bak to mediate mitochondria dysfunction. To demonstrate the use of Bak conformationally sensitive antibodies Jurkat cells were treated with H_2O_2 to induce apoptosis and then stained using an antibody against the N-terminus of Bak, Ab1 (1-52). When staining intensity was analysed by FACS a clear shift in the Bak staining intensity could be seen in cells induced to undergo apoptosis (Figure 3.2 A, blue trace), compared to untreated cells (red trace). As with Bax 6A7 staining, the clear increase in staining intensity that accompanies Bak activation makes the Ab1 antibody ideally suitable for use as the basis for assays to monitor protection from apoptosis. This is shown for Bak Ab1 staining of Jurkat cells with and without stable over-expression of Bcl-2. The experiment reveals that Bcl-2 efficiently protected the cells against staurosporine (STS) induced Bak conformational change (Figure 3.2 B, upper row). STS is a broad specificity kinase inhibitor and therefore triggers apoptosis by 'cell intrinsic' pathways. This contrasts with Fas/CHX, which is considered an activator of 'cell extrinsic' pathways since it directly activates Fas death receptor signalling. In response to Fas/CHX the Bcl-2 expressing Jurkat cells are not protected and show the same degree of Bak conformational activation as the wild type cells (Figure 3.2 B, lower row). Jurkat cells are a human T-cell leukaemia cell line, which generate large amounts of caspase-8 and caspase-3 activity directly following death receptor activation (Strasser et al., 1995). Such cells, primarily restricted to those of lymphatic origin, are classically referred to as Type I cells, being able to activate effector caspases independently of mitochondrial involvement (Scaffidi et al., 1998). The majority of cells from other tissues, including the MCF10A cells used extensively in

this work, are defined as Type II cells which show an absolute dependence on mitochondrial dysfunction to initiate apoptosis downstream of death receptor ligation.

There are, of course, many commercially available antibodies raised against various epitopes within the human Bax and Bak proteins (Figure 3.3 A). To test the conformational sensitivity of a range of these antibodies, immunoprecipitations were performed from lysates prepared from MCF10A cells treated with Fas/CHX to induce apoptosis. It was, however, somewhat surprising to find that the conformationally sensitive behaviour of the Bax and Bak antibodies, described above, was not limited to those raised against N-terminal epitopes of the proteins. This suggests that, for Bax, at least, activation is associated with a more dramatic conformational change than just rearrangement of the N-terminus (Suzuki et al., 2000). The majority of anti-Bax and -Bak antibodies tested were in fact conformationally sensitive, only able to immunoprecipitate their respective proteins following a treatment to induce apoptosis (Figure 3.3 B-D). A notable exception to this was an antibody raised against residues 43-61 of human Bax. This was able to efficiently immunoprecipitate Bax from both healthy and apoptotic cells (Figure 3.2 C, labelled 43-61). A possible explanation for this difference is the location of the epitope; it is located in a flexible loop between helix α1 and α2 and is therefore more likely to be constitutively exposed. The Bak antibodies tested also displayed a high degree of conformational sensitivity, although there was a higher level of Bak recognition prior to the induction of apoptosis. This is an interesting result since it indicates that a pool of Bak protein exists with a constitutively exposed N-terminus, even in healthy cells, although this is substantially increased by the induction of apoptosis. This pool could be analogous to the fraction reported to be interacting with Bcl-2 pro-survival proteins (Willis et al., 2005), although this point was not investigated further.

3.3 Characterisation of Bax antibodies by immuofluorescence:

To examine the location of active Bax in cells undergoing apoptosis, the Bax antibodies characterised biochemically in Figure 3.3 were also tested in immunofluorescence experiments and examined by high-resolution confocal microscopy. U2OS cells, treated with Fas/CHX, were loaded with Mitotracker to reveal the mitochondria and immunostained with the two of the N-terminal Bax antibodies: NT (1-21) and N20 (11-30). Apoptotic cells could be clearly identified by bright mitochondrially-associated foci (Figure 3.4). This pattern was analogous to the staining pattern seen at lower resolution with the Bax 6A7 antibody (Figure 3.1). During the early stages of cell death these clusters appeared to be small (< 0.5 μm) and positioned at the tips of mitochondria and at restriction points along the mitochondrial network (Figure 3.4 A-C). Cells in the later stages of apoptosis appeared to contain larger clusters, and whilst these were

still closely associated with the mitochondrial network, they were mainly adjacent to, rather than co-localised with, mitochondria. In addition, in cells with larger Bax clusters, the mitochondria showed evidence of fragmentation, forming a more punctate and less reticular network (Figure 3.4 D).

Although these antibodies are useful in revealing the post-activation distribution of Bax, they do not report of the location of Bax immediately prior to the activating conformational change. For this reason further immunoflouresence experiments were conducted with the Bax 43-61 antibody, which was uniquely able to immunoprecipitate Bax from healthy cells (Figure 3.3 C). When U20S osteosarcoma cells were exposed to a low dose of UV irradiation (30 J/m^2) the majority of cells were still alive 18 hrs later. Whilst this mild stress trigger was insufficient to induce widespread apoptosis, immunofluorescence using the Bax 43-61 antibody under these conditions revealed a re-distribution of Bax onto the mitochondrial network, co-localising with Mitotracker Orange (Figure 3.5 A). This redistribution of Bax to mitochondria following UV irradiation was striking in that it occurred in every cell in the culture and was evenly distributed along the mitochondrial network. Both features distinguish it from full Bax activation, which involved entry into bright foci and initiated stochastically throughout the population (Figure 3.4). At longer times after UV irradiation, or following the addition of more acutely acting death stimuli, such as Fas/CHX, the Bax 43-61 was also able to recognise the bright foci associated with full activation (data not shown). In addition, it was confirmed that Cyt-c retained an exclusively mitochondrial distribution in cells exhibiting this UV-induced Bax redistribution. It was only in cells where Bax had formed bright foci where Cyt-c had been released from the mitochondria and become diffusely distributed in the cytoplasm (Figure 3.5 B and data not shown). This result demonstrates that translocation of, at least a portion of, the Bax protein to mitochondria does not result in full activation of the protein and therefore is not sufficient to initiate apoptosis.

3.4 GFP-Bax can be used to monitor Bax activation in live cells:

When considering the Bax 43-61 immunostaining shown in Figure 3.5 A, it is not possible to be certain whether the cytoplasmic staining truly represents the cytoplasmic pool of Bax or is simply unspecific background staining. It is also possible that Bax co-localisation with mitochondria following UV irradiation is the result of conformational change in the protein rather than redistribution. In an attempt to address these questions the experiments were repeated using a transiently transfected N-terminal green fluorescent protein (GFP) fusion of

Bax (GFP-Bax). This has the advantage that the total cellular pool of GFP-Bax is always visible, regardless of its activation state.

Examination of the cells 24 hrs after transfection revealed that moderate levels of GFP-Bax over-expression were well tolerated by both U2OS and MCF10A cells. In healthy MCF10A cells, GFP-Bax was predominantly cyctoplasmic (Figure 3.6 A, upper row). Following the induction of apoptosis with Fas/CHX, transfected cells underwent apoptosis in response to Fas/CHX or UV irradiation within a similar time period to surrounding untransfected cells. GFP-Bax could be seen to enter small mitochondrial-associated foci (Figure 3.6 A, middle row). At later stages of cell death, when fragmentation of the nuclei was clearly visible from the DAPI co-staining, these foci appeared considerably larger and Mitotracker staining was absent or disrupted (Figure 3.6 A, bottom row). Similar distributions were observed in U2OS cells (data not shown). In U20S cells transfected with GFP-Bax and treated with low-dose UV irradiation, enrichment of GFP-Bax evenly along the mitochondrial network, could also be clearly observed 18 hrs later (Figure 3.6 B). This latter result also confirms that mitochondrially localised Bax appearing after low doses of UV irradiation was indeed the result of partial translocation of the cytoplasmic pool to the mitochondria. Together, the data presented in Figure 3.6 also demonstrates that GFP-Bax can recapitulate the distributions observed using antibodies to the endogenous protein, thereby validating its use as a Bax reporter.

An additional advantage of GFP-Bax is that translocation and activation of the protein can be followed in live cells. To this end a low light imaging system was established with which to monitor changes in GFP-Bax distribution in transiently transfected cells following the induction of apoptosis. The position of energised mitochondria was also recorded by pre-loading the cells with the mitochondrial specific fluorescent probe tetramethylrhodamine methyl ester (TMRE). Representative recordings of U2OS and MCF10A cells undergoing apoptosis in response to UV irradiation are included as Supplementary Movie Figures M3.1 and M3.2, with static frames from M3.2 shown in Figure 3.7 C. From these initial results it was clear that the initiation of GFP-Bax clustering was a rapid event and was temporally closely linked to the loss of $\Delta\psi_m$, as detected by dissipation of TMRE sequestered in mitochondria (Figure 3.7 C, compare frames at 28 – 36 mins).

It was also possible to see enrichment of GFP-Bax onto the mitochondrial network in U2OS cells following a low dose of UV irradiation. The partial translocation itself occurred extremely slowly and was difficult to document. However, once formed, the distribution was observed to persist for several hours and was therefore not predictive that full GFP-Bax activation was imminent. An example is shown in Figure 3.8 and Supplementary Movie Figure M3.3. In this

recording, which began approximately 18 hrs after the UV dose was administered, there is no detectable further increase in GFP-Bax at the mitochondria during the first hour of recording (Movie M3.3). Strikingly, just 1 min before the onset of GFP-Bax clustering, there is no evidence of mitochondrial fragmentation or any other visible evidence of the cell's impending death (Figure 3.8 B, frame 59 mins). However, when Bax activation does occur it is rapid and associated with complete loss of $\Delta\psi_m$ within 5 mins (Figure 3.8 B, frames 60 - 64 mins). An enlargement of a small peri-nuclear region from the sequence shown in Figure 3.8 B is included as Figure 3.8 C. From these frames it is clear that there is a degree of heterogeneity in the behaviour of individual mitochondria in the same cell undergoing these events. For example, in the frames recorded at 60 mins, exactly as the first GFP-Bax become visible, the first detectable loss of $\Delta\psi_m$ occurs in just a few mitochondria. Interestingly, there is an associated increase in the TMRE staining intensity of some of the remaining mitochondria. Over the next 5 mins, as the GFP-Bax clusters increase in size, the $\Delta\psi_m$ is lost from these remaining mitochondria as well. The GFP-Bax foci then continue to increase in size throughout the next 30 mins, during which time the cell begins to change shape and round up showing the typical morphological features of apoptotic cell death (Figure 3.8 B and C, frames up 90 mins). These initial recordings indicate that when GFP-Bax activation begins, as detected by the formation of small bright foci of GFP-Bax, there is a heterogeneous response of mitochondria within the first 5 mins, with some losing their $\Delta\psi_m$ before others in the same cell. This heterogeneity was clearer in more polarised cells; two recordings from such cells are described in the next section.

3.5 Rapid and synchronised Bax activation appears to be locally initiated:

Occasionally cells were observed in which activation of GFP-Bax, and loss of $\Delta\psi_m$, appeared to initiate in one discrete sub-cellular region. This occurred in more polarised cells, where GFP-Bax activation initiated in the cell's periphery, and then spread rapidly across the rest of the cell. An example is shown in Figure 3.9 and Supplementary Movie Figure M3.4. This record shows a U2OS cell treated with UV irradiation 18 hrs previously. The cell demonstrates the partial enrichment of GFP-Bax at mitochondria described previously (Figure 3.9 C, blue arrows). GFP-Bax activation initiats in a protrusion in the lower part of the cell and there is a corresponding loss of $\Delta\psi_m$ from mitochondria in this localised region. GFP-Bax activation spreads across the whole cell, with an associated loss of $\Delta\psi_m$, within the next 3 minutes (Figure 3.9 C, yellow arrows). A few mitochondria retain their $\Delta\psi_m$, briefly gaining a higher TMRE staining intensity, before they too become depolarised (Figure 3.9 B, frames at +3 mins and +4 mins). The rapid and progressive nature of both GFP-Bax activation and loss of $\Delta\psi_m$ suggests the existence of a

feed-forward activation mechanism whereby Bax activation at one mitochondrion can rapidly trigger activation in the neighbouring cellular region.

This hypothesis is further supported by a second example which shows a particularly polarised MCF10A cell (Figure 3.10 and Supplementary Movie Figures M3.5). During the course of the experiment, and as surrounding untransfected cells die, the central GFP-Bax transfected cell undergoes morphological changes that result in the formation of a cytoplasmic projection (more clearly documented in an extended and accelerated version of the recording M3.6). GFP-Bax first becomes active, as detected by the formation of bright foci, in this projection (Figure 3.10 C, yellow arrows). This region is initially appears isolated from the rest of the cell body by the narrow neck of connecting cytoplasm. However, over the course of filming, the projection retracts towards the cell body. Exactly as the connecting neck is breached, there is a rapid and synchronous activation of GFP-Bax, and corresponding loss of $\Delta\psi_m$, throughout the rest of the cell body (Figure 3.10 C, red arrows). This is followed by a period during which the GFP-Bax clusters increase in size and the cell then dies with the distinctive morphological features of apoptosis. This recording therefore shows that Bax can be activated in one region of the cell and which then leads to the rapid activation of Bax in adjacent regions. In this case the narrow bridge of connecting cytoplasm, separating the main cell body from the region with active GFP-Bax is likely to act as a diffusion barrier, preventing communication between the two regions. It is only when the narrow neck of the projection is breached by its full retraction into the cell body that communication is restored and then the active GFP-Bax efficiently triggers activation of the remaining cellular pool.

Together the data presented in this section indicates that Bax activation may not be a globally initiated cell-wide process, whereby Bax becomes active in the cell and synchronously targets all mitochondria. Instead, Bax activation may begin in a discrete subcellular location which then initiates a feed-forward mechanism to ensure that this activation is rapidly spread across the whole cell. If correct, this interpretation has important implications for understanding Bax activation, since it would suggest that the decision to initiate apoptosis can be made at a local level, maybe at a single mitochondrion. This would connect the decision to commit to apoptosis with the local environment and mitochondrial physiology a particular subcellular region. These conclusions are reliant on the ability to detect the very first Bax molecules to become active in the cell. For this reason additional experiments were conducted to assess the sensitivity of the imaging system and these will be discussed in the next section.

3.6 Further consideration of the timing of GFP-Bax activation:

The data presented in section 3.5 and 3.6 suggests that in UV-treated U2OS and MCF10A cells the cell-wide loss of $\Delta\psi_m$ begins coincidentally with GFP-Bax activation and is complete within 5 minutes. However, some reports have suggested that loss of $\Delta\psi_m$ precedes Bax activation, for example, in Cos7 cells treated with STS, it was observed that dissipation of $\Delta\psi_m$ by at least 50% occurred before GFP-Bax was detectable at the mitochondria (Smaili et al., 2001). Occasionally in the present study recordings were made which appear to confirm that this order of events was also possible (Figure 3.11 and Supplementary Movie Figure M3.7). However, the reasons for these rare results were likely to be technical. In this example the cell expressed very low levels of GFP-Bax. For comparison, the adjacent cell, appearing in Figure 3.10, is shown in the final panel. It is likely that in such low-expressing cells there was insufficient GFP-Bax recruited into the early clusters for them to be detectable. In this record, loss of $\Delta\psi_m$ was detectable at least 2 mins before the first sign of GFP-Bax foci and it was a further 5 mins before they were prominent. (Figure 3.11, compare frames at t = 705, 707 and 714 mins). Nevertheless, it is also a long-standing observation that high levels of Bax expression will sensitise cells to more rapid apoptosis (Rosse et al., 1998; Xiang et al., 1996) and in live cell systems such cells died well in advance of surrounding untransfected cells (Smaili et al., 2001). Therefore, both these extremes were avoided in the present study and all recordings shown feature moderately expressing cells. Under these conditions, surrounding untransfected cells died in approximately the same timeframe as those transfected with GFP-Bax, indicating that significant sensitisation by Bax over-expression was not the case.

Given the controversial nature of the temporal relationship between GFP-Bax activation and the loss of $\Delta\psi_m$ it was preferable to validate the system further by correlating the appearance of the first clusters of GFP-Bax to an additional event known to be an immediate downstream consequence of Bax activation. If the system is truly detecting the first GFP-Bax to become active the bright foci should be detectable immediately before or coincidentally with such an event. The use of GFP-tagged Cyt-c has been previously reported and should fulfil these criteria (Goldstein et al., 2005; Goldstein et al., 2000). However, attempts using both N- and C-terminal GFP fusions of Cyt-c were confounded by a lack of mitochondrial import of the over-expressed protein. In fact, the previously described experiments were performed using clonal cell lines specifically selected to have mitochondrial localisation of the over-expressed tagged Cyt-c (Goldstein et al., 2000). Following transient transfection this proved to be a surprisingly rare event. The details of mitochondrial import of Cyt-c are not currently known but it is likely that either over-expression or the addition of the florescent protein tag prevented efficient mitochondrial import in the majority of cells. Cyt-c instead accumulated to high levels in the

cytoplasm. This was not yet toxic, since the active conformation is only attained following the addition of haem-groups in the mitochondrial intermembrane space (Kranz et al., 1998), nevertheless, this marker was unsuitable for use in live cell imaging.

An alternative approach was therefore employed using a fluorescent caspase reporter construct. This consisted of a YFP variant protein engineered to contain a caspase cleavage site, nuclear export signal (NES) and nuclear localisation signal (NLS). In healthy cells the protein is cytoplasmic due to the dominance of the NES over NLS. Upon activation of effector caspases-3 and -7, cleavage of the protein results in the removal of the NES, it is subsequently imported into the nucleus (for further information see section 2.9.2). This construct was transfected into MCF10A cells, together with a CFP-Bax and the cells were imaged following treatment with Fas/CHX. A representative recording is shown in Figure 3.12 and Supplementary Movie Figure 3.8. From this recording it is clear that bright foci of CFP-Bax are detectable at least 1-2 mins prior to detectable translocation of the caspase reporter into the nucleus. Recordings from two further cells are included Appendix 1 (Supplementary parts 3.12 B and 3.12 C, with accompanying movies M3.9 and M3.10). Both show the same 1 - 2 min delay between the Bax activation and the first sign of effector caspase activity. Although this experiment measures the enzymatic consequence of caspase activation, rather than activation of the caspase itself, it is still highly indicative that the first active Bax detectable does represent the first pool becoming active in the cell, before the downstream consequences of mitochondrial dysfunction become apparent.

Finally, in a few recordings spontaneous transient depolarisations of $\Delta\psi_m$, or mitochondrial flickers, were occasionally observed. Figure 3.13 A shows a flicker of 2 - 3 mins duration recorded in a UV treated MCF10A cell, and Figure 3.13 B shows a major flicker at 10 mins and minor flicker at 12 mins, both of 1 - 2 mins duration in UV treated U2OS cells. In the former example the depolarising mitochondria are still visible in the phase image showing that this is not an artefact due to the mitochondria moving out of the focal plane. Flickers were usually localised and resulted in a brief increase in the TMRE staining intensity of nearby mitochondria, followed by complete recovery of the depolarising mitochondria. Flickers of $\Delta\psi_m$ were first described in healthy neuronal cells (Loew et al., 1993) and have more recently been quantified in smooth muscle cells where they are reported to occur with an average frequency of 0.02 flickers per second (O'Reilly et al., 2003). In the system described in the present work such flickers were rarely observed, but this could be because they were too rapid to detect at the 1 frame/minute acquisition rate used. The flickers will be discussed in more detail in Chapter 4. However, they did not appear to be predictive of the onset of apoptosis. For example the cell shown in Figure 3.12 A was recorded for a further 2 hrs during which time no further flickering

or complete depolarisation was observed. Flickering of individual mitochondria was also clearly distinct from the cell-wide depolarisation that accompanied the onset of apoptosis (Figure 3.13 C).

The results presented in this chapter demonstrate that, in cells over-expressing moderate levels of GFP-Bax, the appearance of detectable foci of GFP-Bax occurs prior to detectable effector caspase activity and synchronously with $\Delta\psi_m$ loss. It is, therefore, likely that the first foci of active GFP-Bax detected using this imaging system accurately correlate with the first Bax molecules becoming active in the cell. This means that observations suggesting the existence of a feed-forward mechanism of Bax activation, namely the spreading of Bax activation (Figure 3.9) and the ability of active GFP-Bax in the cellular projection to rapidly activate Bax in another location (Figure 3.10), are also likely to be valid.

3.7 Increased mitochondrial calcium is detectable prior to Bax activation:

There are multiple examples of cellular signals that initiate in discrete cellular spatial domains and give rise to travelling signalling waves to ensure a signal is propagated at full strength to a remote location within the cell. The best known examples are cAMP and calcium (cAMP, Ca^{2+}). Of these, Ca^{2+} ions represent one of the most ubiquitous signalling pathways in all cells, regulating many short-term changes in cell function (Berridge et al., 2000). Mechanisms have been characterised for feed-forward expansion and propagation of the Ca^{2+} signal, such as the Ca^{2+}-induced-Ca^{2+}-release (CICR) from the inositol 1,4,5-trisphosphate receptors (IP3R) at the endoplasmic reticulum (ER), and the Ryanodine receptors (RyR) present at the sarcoplasmic reticulum (SR) of muscle cells (Berridge et al., 2000). During IP3R-driven Ca^{2+} signalling mitochondrial Ca^{2+} uptake can modulate propagation of the wave (Simpson and Russell, 1996; Tinel et al., 1999). In addition, isolated mitochondria immobilized in agarose gel have been shown to drive Ca^{2+} waves by CICR in their own right (Ichas et al., 1997). Ca^{2+} waves have also been reported in permeabilised myocardial myotubes following apoptosis induced by exposure to C2 ceramide (Pacher and Hajnoczky, 2001). It is therefore possible that the feed-forward mechanism causing sequential Bax activation is a result of a CICR wave. Direct measurement of mitochondrial Ca^{2+} uptake *in situ* is now possible due to the advent of selectively targetable Ca^{2+}-sensitive fluorescent proteins (Zhang et al., 2002). One of these, the mitochondrial pericam, is targeted to the mitochondrial matrix (Nagai et al., 2001) and could therefore be used in an attempt to address this hypothesis.

Ratiometric imaging of the pericam protein (ie. the ratio of emission intensities following excitation at two wavelengths) can be used to give a qualitative indication of changes in matrix Ca^{2+} levels. MCF10A cells were co-transfected with the pericam protein together with a red fluorescent protein fusion of Bax (RFP-Bax), to provide a marker for when Bax activation initiated. The cells were then treated with Fas/CHX to induce apoptosis and imaged sequentially to visualise RFP-Bax and mitochondrial pericam at 410 nm and 510 nm, allowing the ratio image to be calculated (Figure 3.14 A). In the representative recording shown, the first sign of RFP-Bax activation occurs in frame 585, 195.2 mins (Figure 3.14 B). Two small regions of interest were then defined to encompass pericam containing mitochondria and the mean integrated intensity of the RFP-Bax and pericam emissions were plotted against time (Figure 3.14 C). From this recording it is apparent that the monomeric RFP used here is prone to bleaching and this resulted in the steadily declining RFP emission signal seen throughout the recording. Nevertheless, the point when RFP-Bax begins to concentrate into mitochondrially-associated foci is shown by a rapid increase in RFP-Bax intensity at ~195 mins. An apparent increase in the level of mitochondrial Ca^{2+} is detectable from ~73 mins after the addition of Fas/CHX until the initiation of Bax activation at ~195 mins, based upon pericam Ca^{2+} recording. At around the time of RFP-Bax activation there is acceleration in the rate of Ca^{2+} uptake by the mitochondria, however this was not detectable in all experiments. Pericam measurements in the period after Bax activation must be considered unreliable due to the rapid onset of apoptosis, resulting in cell shrinkage and movement of the cell such that the static regions of interest, from which the measurements were made, no longer covered the same subcellular region. Recordings from two further cells, both showing an increase in mitochondrial Ca^{2+} in the period immediately prior to Bax activation, are included Appendix 1 (Supplementary parts 3.14 D and E).

Unfortunately, due to the technical problems encountered during these experiments, it became clear that for accurate and reproducible measurements mitochondrial Ca^{2+} a more rapid rate of image acquisition was required than the 20 sec/frame used in the examples shown. In addition, the rapid movement of both mitochondria within healthy cells and the cell as a whole, particularly in the period immediately after the onset of Bax activation, meant that it was extremely difficult to define regions of interest which remained stable for the period required to obtain useful data. Nevertheless, the data presented indicates a steady and reproducible increase in the pericam signal, following the induction of apoptosis and before Bax becomes active, suggesting that mitochondrial calcium levels are increasing. These results are included because they are considered supportive of additional data presented in the next chapter.

Discussion:

The activation of Bcl-2 proteins Bax and Bak, and resulting mitochondrial dysfunction, including the release of Cyt-c, is widely accepted to represent the point-of-no-return in the mammalian apoptotic cell death pathway. However, despite a large body of literature on both of these proteins, their mechanism of activation remains largely uncertain. The premise of this chapter was to follow Bax activation at high temporal and spatial resolution and to see if such an unbiased approach could provide further insights into the protein's activation.

Antibodies directed against the N-termini of both Bax and Bak provide robust and useful tools with which to assay the activation of these proteins (Figure 3.1 and 3.2). However, they are limited to use on fixed material and, critically for this study, they fail to report on the location of Bax immediately before it becomes active. The finding that most anti-Bax antibodies are in fact conformationally sensitive (Figure 3.3), only recognising the protein subsequent to its activation, reinforces the dramatic nature of the conformational change Bax is thought to undergo (Suzuki et al., 2000). From this analysis, only one antibody, Bax 43-61, was able to detect the inactive conformation of the protein, perhaps because this epitope maps to a flexible loop in the Bax structure between hα1 and hα2. Immunostaining with this antibody following a low dose of UV irradiation revealed an enrichment of Bax evenly distributed over the mitochondrial network (Figure 3.5 A), not seen by the antibodies which only recognise the full active conformation of Bax. In the recent literature, it is often assumed that Bax translocation to the mitochondria is synonymous with its activation, oligomerisation and permeabilisation of the MOM. However, the finding that, following a mild cellular insult, Bax can become partially localised to mitochondria prior to full activation (Figure 3.5 A), suggests that translocation alone does not explain Bax activation and that subsequent steps are likely to be required. This finding also supports early fractionation data, in which a proportion of Bax was detected at mitochondria (Desagher et al., 1999; Goping et al., 1998; Hsu et al., 1997b), and some more recent studies in which Bax was characterised at the mitochondrial membrane but not yet fully active (Annis et al., 2005; Valentijn et al., 2003).

It is possible that the partial accumulation of Bax (Figure 3.5 A) and GFP-Bax (Figure 3.6 B) at mitochondria following UV irradiation represents a snapshot of an ongoing accumulation. If mitochondria have a limited, but saturable, capacity to accommodate Bax, a threshold could be envisioned beyond which their binding capacity is saturated, or the local concentration of Bax becomes high enough, such that oligomerisation of the protein ensues. In support of such an accumulation model, it has been reported that translocation of ~20% of the cellular Bax to the MOM is sufficient to induce apoptosis (Hsu et al., 1997b) and Bax over-expression has been

widely reported to promote apoptosis (Rosse et al., 1998; Xiang et al., 1996), indicating that over-expression may shift the cellular equilibrium towards greater and faster accumulation of Bax at mitochondria. However, several lines of evidence run contrary to this model. Firstly, accumulation of GFP-Bax at mitochondria prior to full Bax activation does not occur following administration of an acutely acting death stimulus, such as Fas/CHX (see Figure 3.7 for example). Additionally, it has been reported that in HO15.19 rat fibroblasts, around 40% of Bax can translocate to mitochondria without initiating apoptosis (Soucie et al., 2001), although this may be related to the fact that these cells are Myc null and, therefore, may not be more generally applicable. Finally, live cell recordings from UV treated U2OS cells presented in this study showed no additional enrichment of GFP-Bax at mitochondria in the period immediately before full Bax activation occurred (Movie M3.3). It is therefore likely that Bax is regulated at multiple steps and that whilst the protein can become enriched at mitochondria, it is not necessarily fully active if it does so, nor is mitochondrial localisation a prerequisite step to full activation and entry into foci. Bax activation at mitochondria can also take place directly, without detectable prelocalisation or enrichment.

From observing GFP-Bax activation in live cells, a striking feature was the sudden nature of its onset. Just 1 min before full GFP-Bax activation occurred there were no visible signs of mitochondrial disruption or the cell's impending death (see Figure 3.9 for example). This is significant because a recent body of literature has accumulated on the role of mitochondrial fission and fusion proteins, which are thought to accelerate a 'thread-like' to 'grain-like' transition of the mitochondrial network, at around the time of Bax activation (Youle and Karbowski, 2005). Two of these proteins, Drp1, a large dynamin family GTPase, and Endophilin B1, a fatty acyl transferase, have been shown to translocate from the cytosol into foci on mitochondria early during apoptosis (Frank et al., 2001; Karbowski et al., 2004). Drp1 has also been shown to co-localise with Bax (Karbowski et al., 2002), in the foci that appear at tips and restriction points in the mitochondrial network (Figure 3.4). Interestingly, Endophilin B1 was originally identified in a yeast two hybrid screen as Bax Interacting Factor 1, Bif1 (Cuddeback et al., 2001). It has been suggested mitochondrial fission is a necessary physiological step to enhance mitochondrial dysfunction and accelerate apoptosis (Youle and Karbowski, 2005). However, this view has recently been challenged by a number of findings. Firstly, an inter-membrane space protein, DDP/TIMM8a has been shown to enhance Drp1-mediated mitochondrial fission, thereby placing maximal rates of mitochondrial fission downstream of the initial mitochondrial dysfunction (Arnoult et al., 2005). Secondly, expression of dominant negative DRP-1 in *C. elegans* has been reported to increase long-term survival of some cells in the organism, but the phenotype was extremely weak, indicating it may not contribute significantly to apoptotic cell deaths in this organism *in vivo* (Jagasia et al., 2005).

No evidence of mitochondrial fragmentation was observed in MCF10A and U2OS cell lines, in response to both UV- and Fas/CHX induced apoptosis prior to Bax activation. This would support the view that mitochondrial fragmentation is not required for efficient initiation of apoptosis but may play a role in the subsequent dismantling of the cell.

Finally, data presented in this chapter is consistent with the existence of a feed-forward mechanism whereby Bax activation first initiates locally and then propagates rapidly throughout the cell (Figure 3.9 and 3.10). Such a mechanism would have advantages, particularly in large cells, in co-ordinating efficient recruitment of all mitochondria into the apoptotic program. However, the propagation of Bax activation, and a corresponding loss of $\Delta\psi_m$, was only observed in particularly highly polarised wild type cells. It may be that this is a generally applicable phenomenon but occurs too rapidly to be reproducibly captured at the 1 frame/min image acquisition rate used, except in more polarised cells where it propagates over larger distances and therefore persists for longer. A candidate mechanism for the feed forward propagation of Bax activation would be a Ca^{2+} signal, since mitochondria are known to participate in Ca^{2+} signalling (Ichas et al., 1997), and apoptotic Ca^{2+} waves have been reported previously (Pacher and Hajnoczky, 2001). Whilst it was not technically possible to test this hypothesis directly, preliminary evidence of mitochondrial Ca^{2+} accumulation during the period before Bax activation was obtained. This at least indicates mitochondria may contain higher than normal levels of Ca^{2+} following prolonged exposure to an apoptotic stimulus that could be available for release when their permeabilisation occurs. The existence of such a mechanism would mean that the key signalling events resulting in Bax activation may not take place globally throughout the cell but may instead initially occur in a particular subcellular region, or maybe at a single mitochondrion.

In this chapter an initial characterisation of Bax activation has been described in relation to other characteristic features of the apoptotic program. Insights gained from examining GFP-Bax activation in live cells have included its rapid nature, that it is accompanied by a coincident loss of $\Delta\psi_m$, and the possible existence of a feed-forward mechanism to coordinate cell-wide Bax activation. The next chapter describes attempts to perturb this process by co-expressing Bcl-2 pro-survival homologues.

Figure 3.1 Bax activation can be monitored using conformationally sensitive antibodies. Antibodies raised against the N-terminus of Bax display conformational specific staining by immunofluorescence. **(A)** U20S cells grown on glass coverslips were treated with 1 mM H_2O_2 for 4 hrs to induce apoptosis and then loaded with 200 nM Mitotracker Orange for 20 mins to reveal the location of mitochondria with intact membrane potential (red). Cells were then fixed and immunostained using anti-Bax 6A7 (12-24) antibody and FITC-linked anti-mouse IgG (green) and imaged by confocal microscopy. Scale bars represents 20 μm; **(B)** The anti-Bax 6A7 antibody can be used to assay Akt-mediated protection in response to apoptotic stimuli. **(i)** MCF10A Akt-ER cells were grown on coverslips and treated +/- 250 nM 4-hydroxytamoxifen (OHT) for 18 hrs prior to incubation with either: 10 μM etoposide, 100 ng/ml anti-Fas, 100 ng/ml anti-Fas + 1 μg/ml CHX or DMSO vehicle control, all for a further 4 hrs. Cells were then fixed and stained with 6A7 anti-Bax (12-24) antibody and Cy3-linked anti-mouse IgG (red). At least 5 randomly selected fields were counted, in excess of 400 cells per treatment, were analysed and the proportion of positively staining cells expressed as a percentage of total (insets show samples of negative and positive staining). Results from a typical experiment are presented with inset depicting the typical staining pattern. **(ii)** Whole cell lystes prepared from parallel cultures were analysed by western blotting with anti-phospho-Akt (Ser 473) (P.Warne, CR-UK) to confirm Akt activation following OHT treatment; D=DMSO, E=etoposide, F=ant-Fas antibody. The blots were re-probed using anti-Bax 2D2 as controls. Data produced in collaboration with David Hancock, CR-UK.

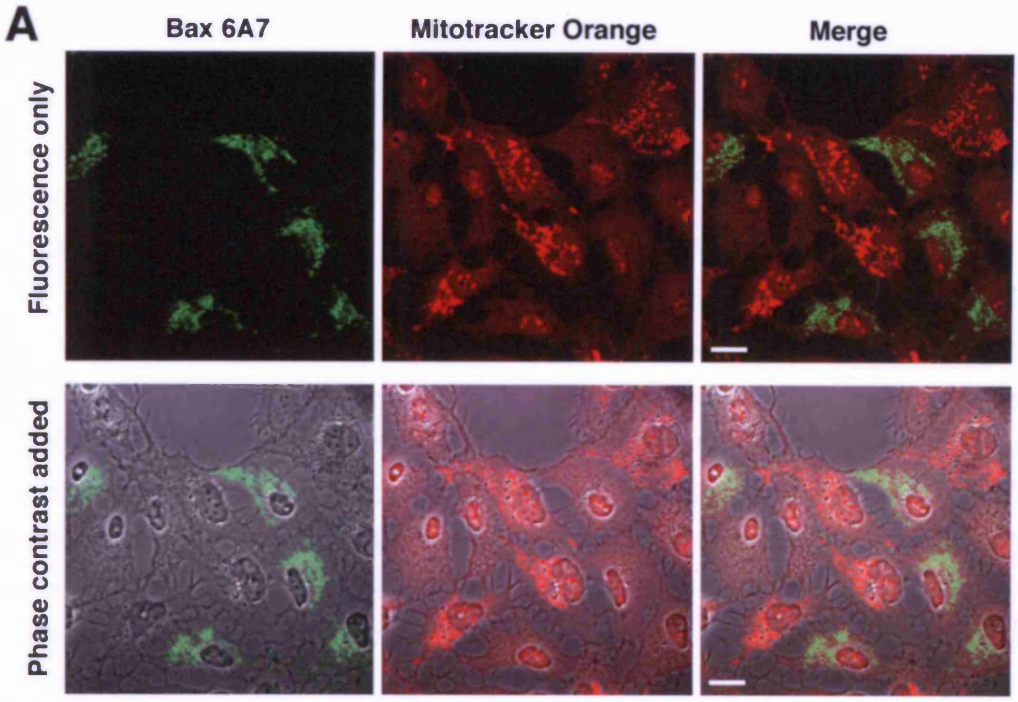
A
Bax 6A7
Mitotracker Orange
Merge
Fluorescence only
Phase contrast added

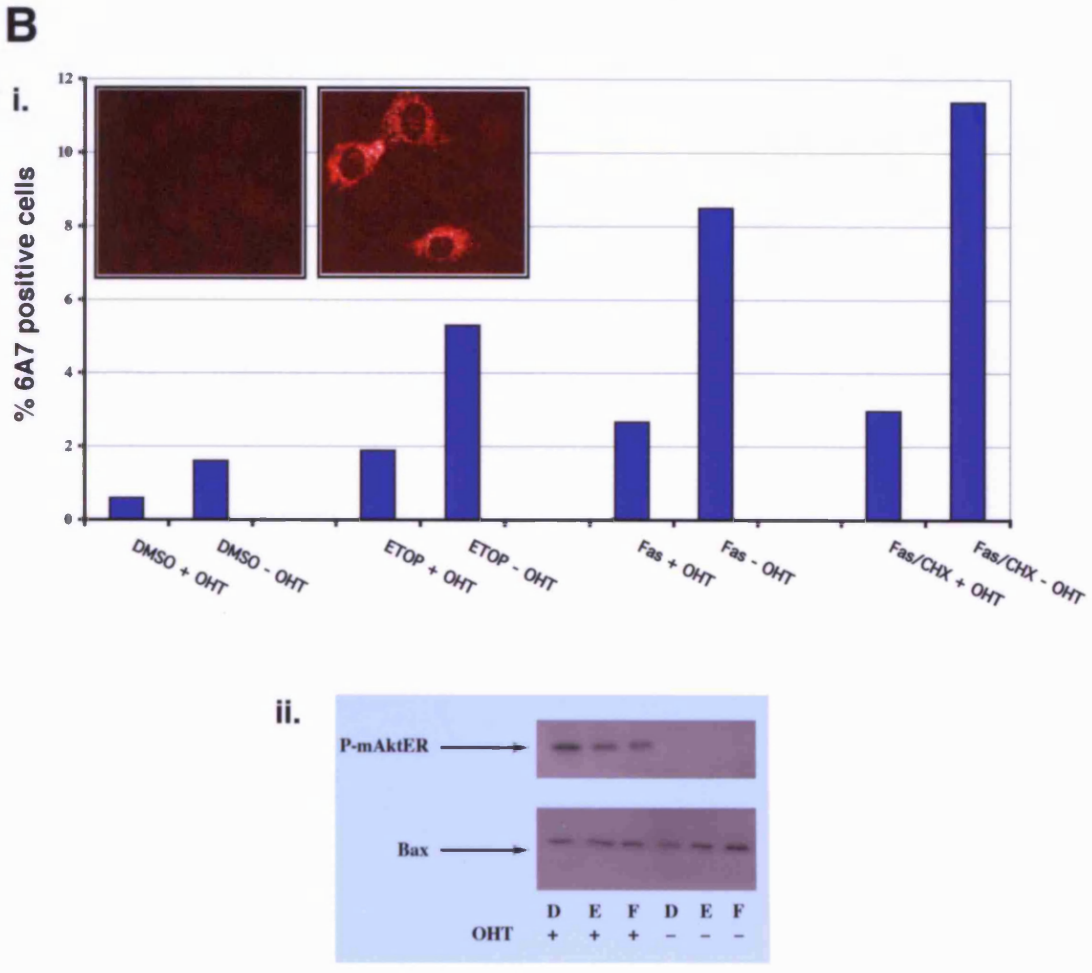
B
i.
% 6A7 positive cells
12
10
8
6
4
2
0
DMSO + OHT
DMSO - OHT
ETOP + OHT
ETOP - OHT
Fas + OHT
Fas - OHT
Fas/CHX + OHT
Fas/CHX - OHT

ii.
P-mAktER
Bax
D E F D E F
OHT + + + – – –

Figure 3.2 Bak activation can be monitored using conformationally sensitive antibodies. Antibodies raised against the N-terminus of Bak display conformation specific staining by FACS. **(A)** Jurkat cells were treated with +/- 1 mM H_2O_2 for 4 hrs to induce apoptosis. Cells were then fixed and immunostained using anti-Bak Ab1 (1-52) antibody and FITC-linked anti-mouse IgG before analysis by FACS. Untreated cells: red trace; treated cells: blue trace; **(B)** Jurkat cells with and without stable over-expression of Bcl-2 were treated with the 250 nM STS (upper panels), a broad specificity kinase inhibitor to induce apoptosis via intrinsic pathways, or Fas/CHX (100 ng/ml anti-Fas and 1 μg/ml CHX, lower panels), to activate the Fas death receptor and thereby induce apoptosis via extrinsic pathways. 4 hrs later cells were fixed and immunostained using anti-Bak Ab1 (1-52) antibody and FITC-linked anti-mouse IgG before analysis by FACS. At least 10,000 events were counted for each condition and fluorescent intensities are plotted as percentage of maximum. Untreated cells: red trace; treated cells: blue trace.

A

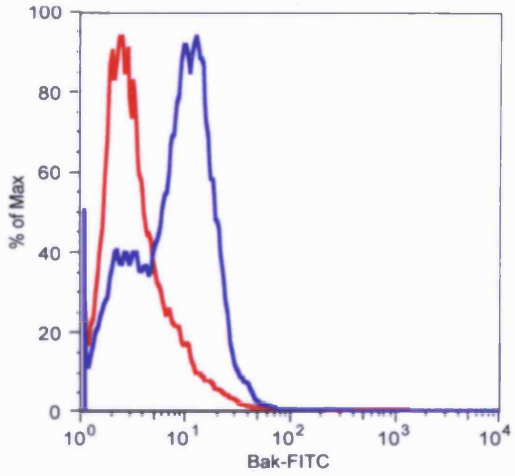
100
80
60
40
20
0
% of Max
10^0
10^1
10^2
10^3
10^4
Bak-FITC

B

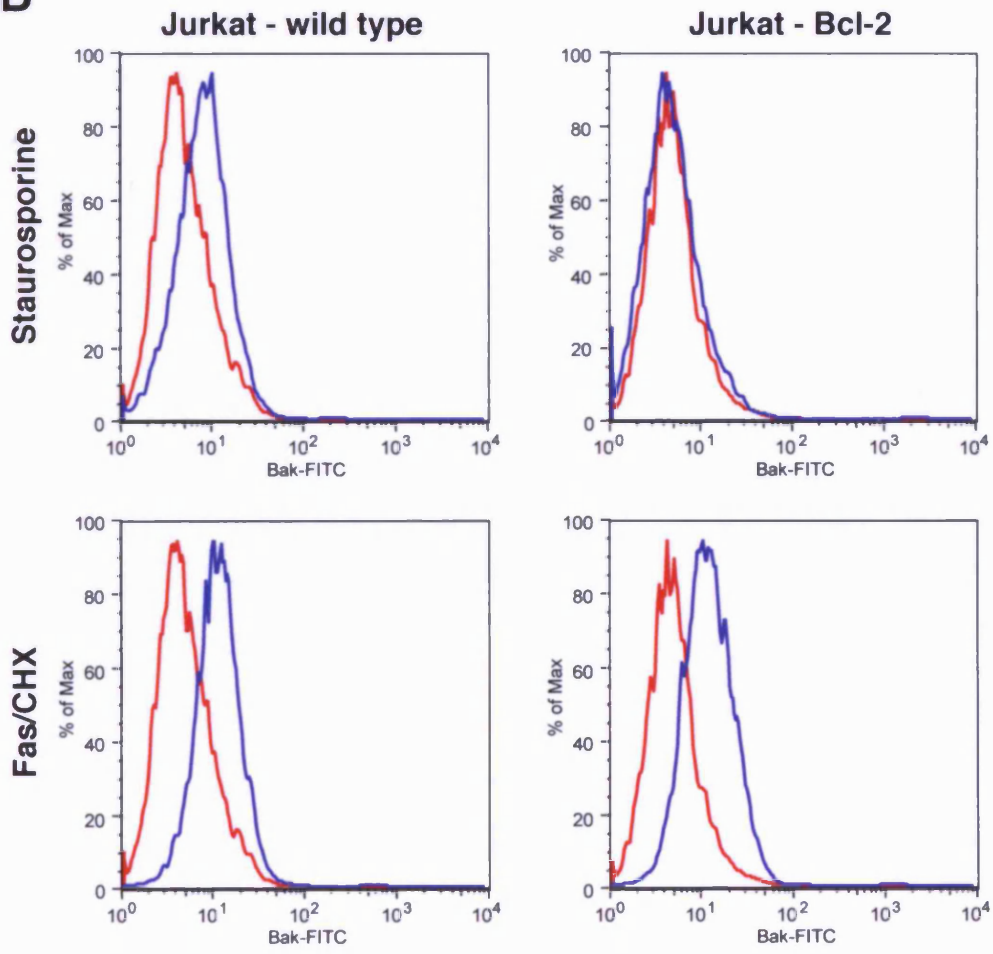
Jurkat - wild type
Jurkat - Bcl-2
Staurosporine
Fas/CHX
% of Max
Bak-FITC

Figure 3.3 Characterisation of commercially available anti-Bax and -Bak antibodies.
The majority of commercially available anti-Bax and -Bak antibodies only recognise the proteins following a treatment to induce apoptosis. **(A)** Cartoon schematic showing the epitope locations for commercially available anti-Bax and anti-Bak antibodies. Antibodies shown in **red** text have been tested in this study; full details of all antibodies are listed in Table 2.2. Bax and Bak domain boundaries were taken from their respective GeneCards entries (www.genecards.org), Bax helical boundaries were taken from Suzuki M. et. al., 2000; **(B)** Phase contrast images of MCF10A cells were treated +/- Fas/CHX for 8 hrs to induce substantial apoptosis. Whole cell lysates were prepared from these cells in 1% CHAPS buffer to preserve Bax/Bak conformation and used in subsequent immunoprecipitations (both adherent and floating cells were collected and lysed); **(C)** Bax was immunoprecipitated from the lysates generated in part (B) using the indicated antibodies; **(D)** Bax was immunoprecipitated from the lysates generated in part (B) using the indicated antibodies.

A Bax (1-192), 21.2kD:

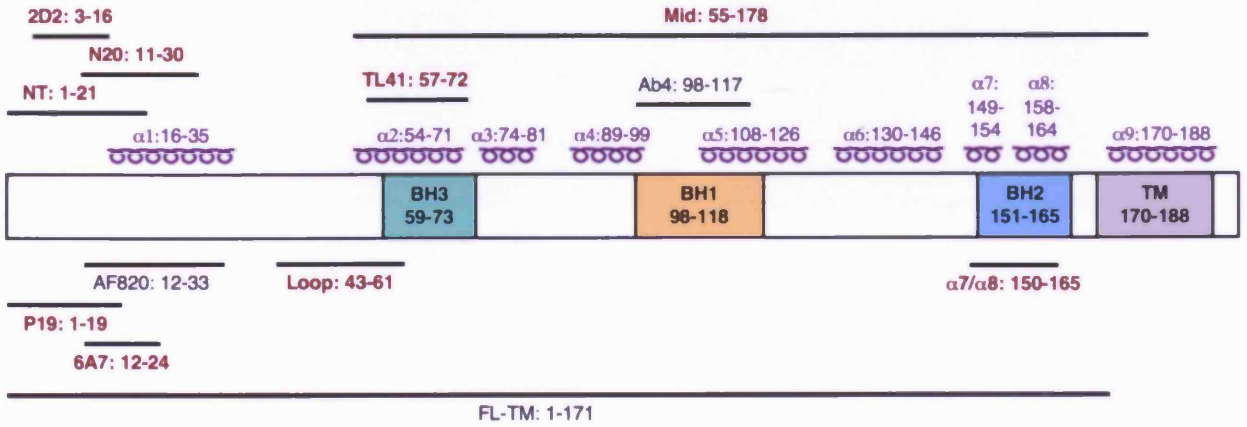

Bak (1-211), ~28kD:

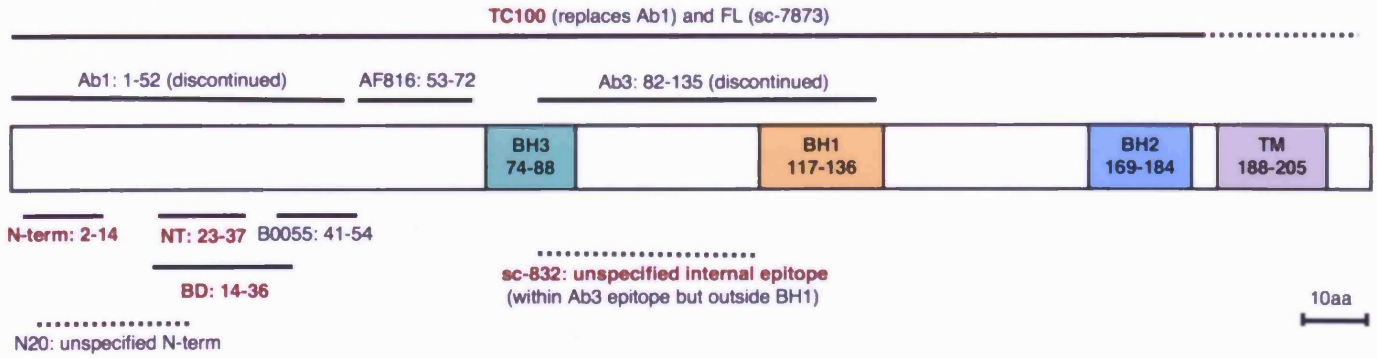

Cont.

B

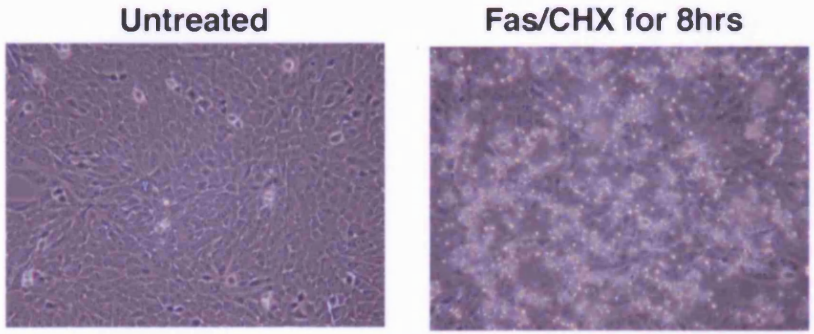
Untreated
Fas/CHX for 8hrs

C

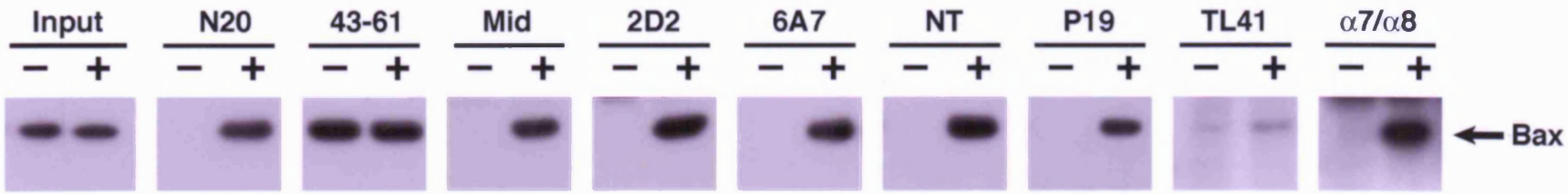
Input
N20
43-61
Mid
2D2
6A7
NT
P19
TL41
α7/α8
− + − + − + − + − + − + − + − + − + − +
Bax

D

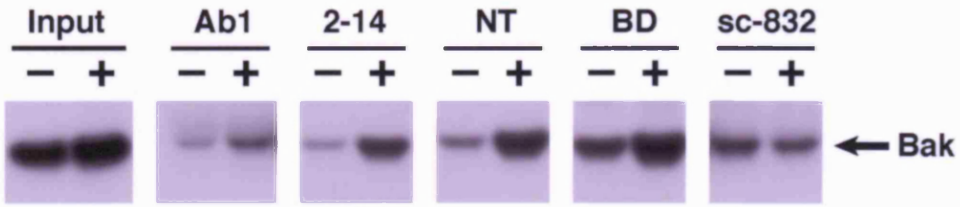
Input
Ab1
2-14
NT
BD
sc-832
− + − + − + − + − + − +
Bak

Figure 3.4 N-terminally directed anti-Bax antibodies reveal post-activation distributions. Two N-terminal Bax antibodies reveal bright mitochondrially-associated foci of Bax. **(A)** U2OS cells grown on glass coverslips were treated with Fas/CHX for 6 hrs to induce apoptosis and then loaded with 200 nM Mitotracker Orange for 20 mins to reveal the location of mitochondria (red). Cells were then fixed and immunostained using anti-Bax NT (1-21) antibody and FITC-linked anti-rabbit IgG (green) and imaged by confocal microscopy; **(B)** 2.5X enlargement of the area indicated in the merged panel of part (A). Bax clusters form at the tips and restriction points of the mitochondrial network; **(C)** HeLa cells prepared in an identical manner and stained with anti-Bax N20 (11-30) antibody also show bright Bax foci forming along the mitochondrial network during the early stages of apoptosis; **(D)** At later stages these clusters increase in size and appear adjacent to, but not coincident with, mitochondria. Inset is a 2X enlargement of the area indicated in the merged panel. In all images scale bars represent 20 μm.

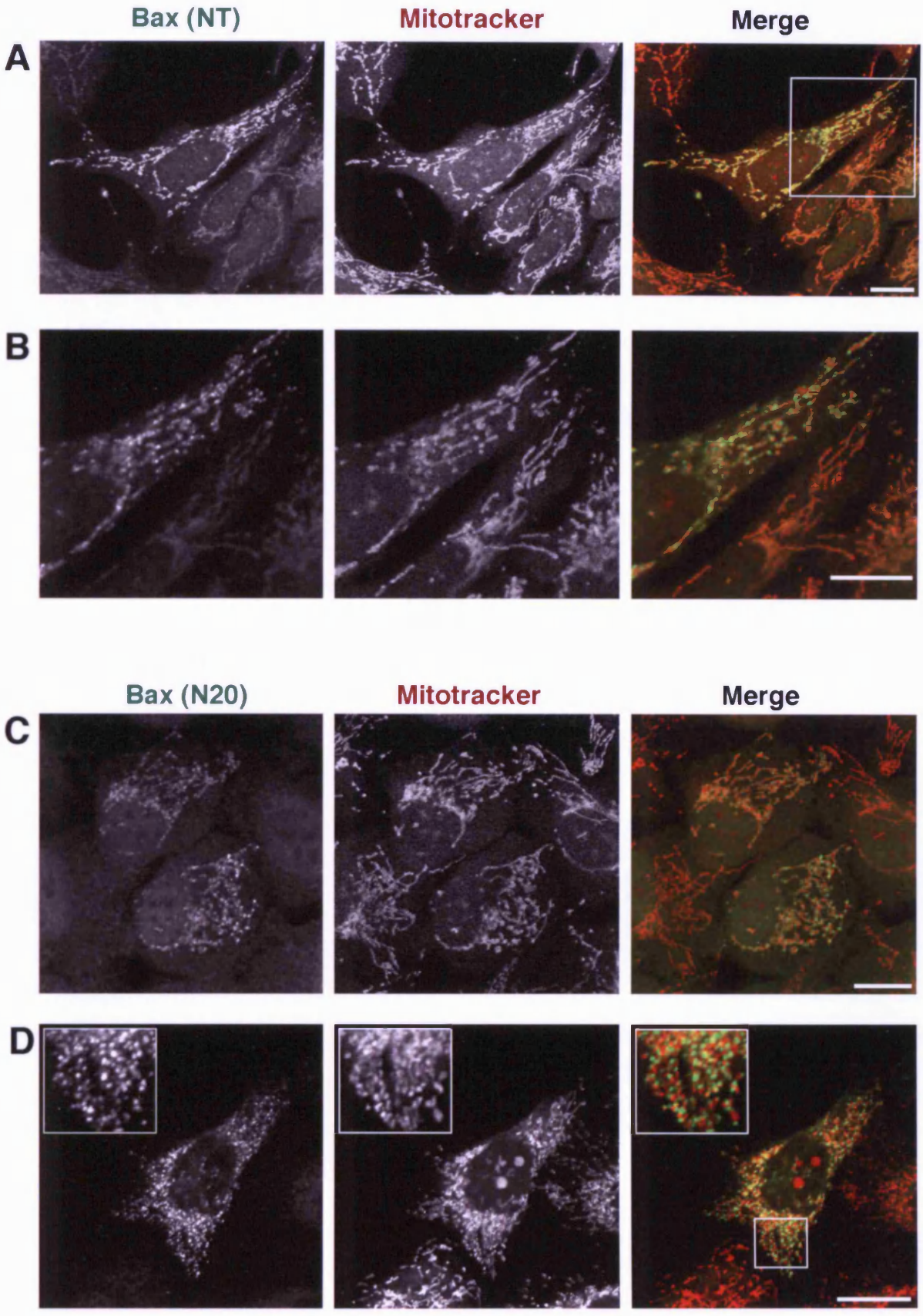
Bax (NT)
Mitotracker
Merge
A
B
Bax (N20)
Mitotracker
Merge
C
D

Figure 3.5 The Bax 43-61 antibody reveals mitochondrially localised Bax in a distribution distinct from the bright Bax foci correlating with Cyt-c release.

The Bax 43-61 antibody reveals Bax evenly distributed on the mitochondrial network in every cell following a gentle stress trigger. **(A)** U2OS cells grown on glass coverslips were treated +/- UV 30 J/m^2 UV irradiation and then re-incubated for a further 18 hrs. Cells were then loaded with 200 nM Mitotracker Orange for 20 mins to reveal the location of mitochondria (red), fixed and immunostained stained using the anti-Bax 43-61 antibody and FITC-linked anti-rabbit IgG (green). Cells were then imaged by confocal microscopy; **(B)** MCF10A cells prepared in an identical manner but treated +/- Fas/CHX for 8 hrs prior to fixation. Cells were then co-immunostained stained using anti-Bax N20 (11-30) antibody and FITC-linked anti-rabbit IgG (green) together with an anti-Cyt-c antibody and Cy3-linked anti-mouse IgG (red). Formation of bright Bax foci correlates with the release of Cyt-c. In all images scale bars represent 20 μm.

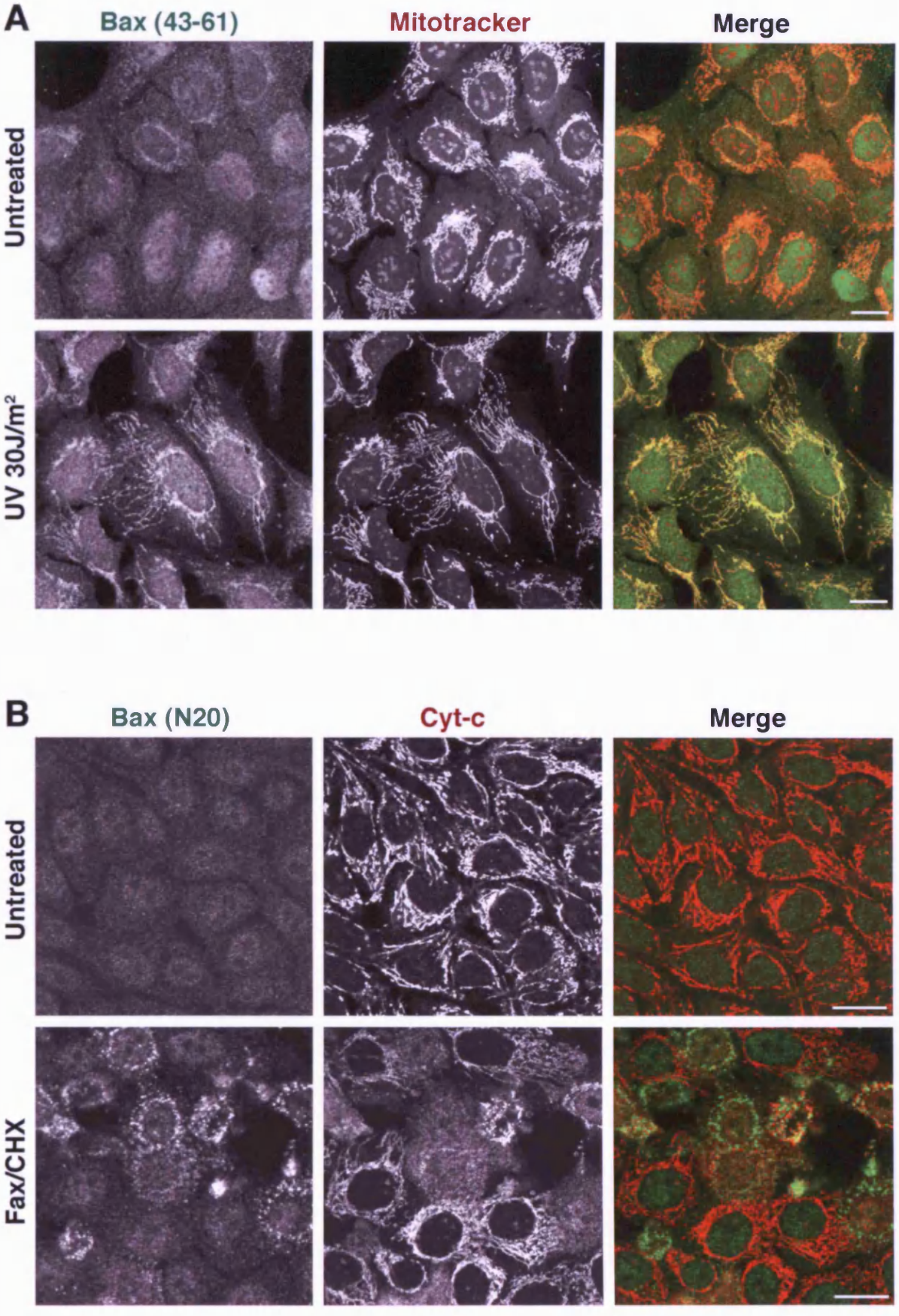
A
Bax (43-61)
Mitotracker
Merge
Untreated
UV 30J/m²
B
Bax (N20)
Cyt-c
Merge
Untreated
Fax/CHX

Figure 3.6 GFP-Bax recapitulates the distributions observed for endogenous Bax.
N-terminally tagged GFP-Bax can be cytoplasmic in healthy cells, enter mitochondrially associated clusters in apoptotic cells or become enriched at mitochondria following a low-dose UV irradiation. **(A)** MCF10A cells were grown on glass coverslips and transfected with GFP-Bax (green). 24 hrs after transfection cells were loaded with 200 nM Mitotracker Orange for 20 mins to reveal the location of mitochondria (red). Cells were then fixed, mounted and imaged by confocal microscopy; **(B)** U2OS cells were prepared identically but treated with 30 J/m^2 UV irradiation 18 hrs prior to fixation in place of Fas/CHX. In all images scale bars represent 20 μm.

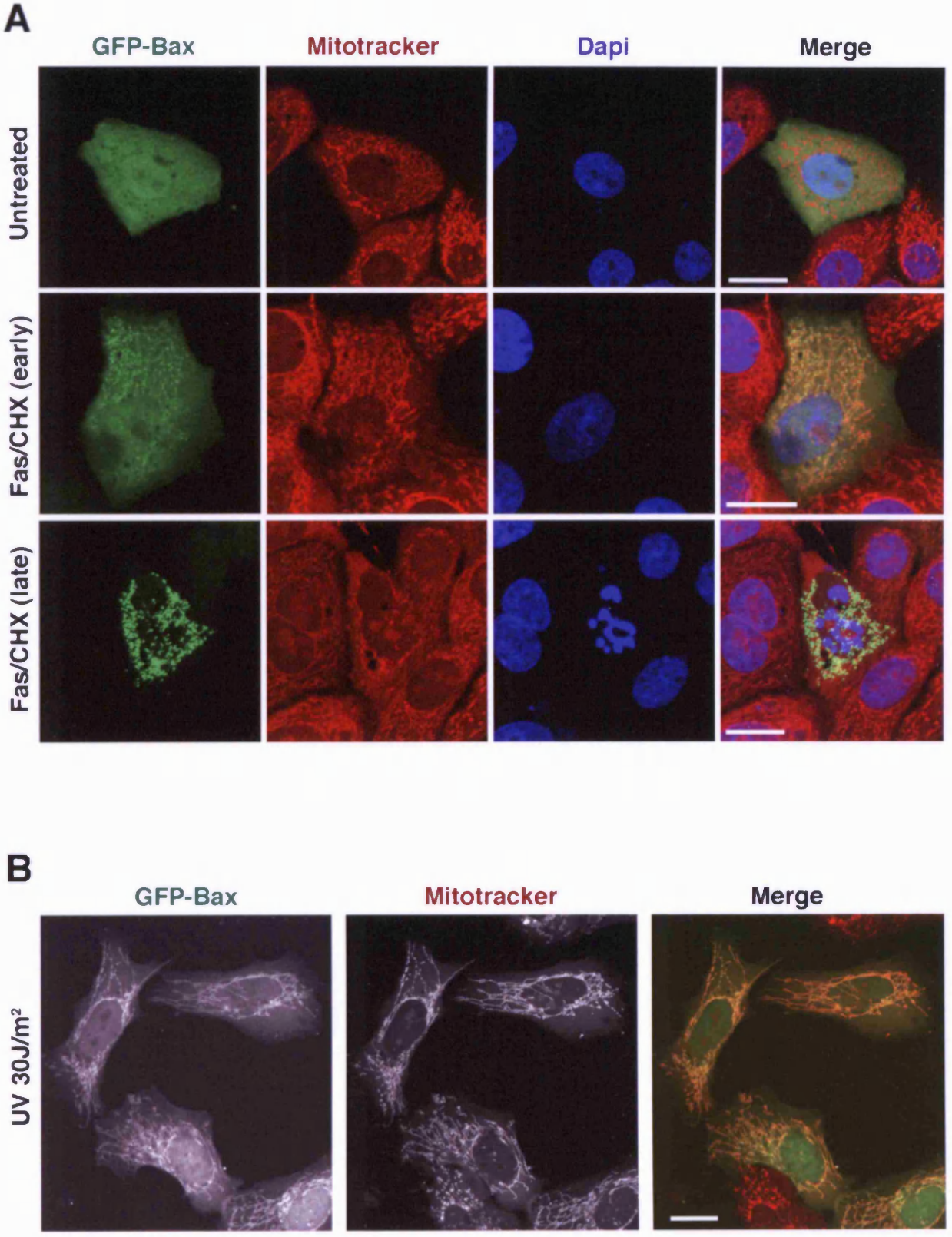
A
GFP-Bax
Mitotracker
Dapi
Merge
Untreated
Fas/CHX (early)
Fas/CHX (late)
B
GFP-Bax
Mitotracker
Merge
UV 30J/m²

Figure 3.7 Initial characterisation of GFP-Bax activation in live cells.

In U2OS and MCF10A cells GFP-Bax rapidly enters bright foci as $\Delta\psi_m$ is lost, shortly after the morphological characteristics of apoptosis are apparent. **(A) Supplementary movie figure M3.1:** Live cell recording of GFP-Bax transfected U2OS cells undergoing apoptosis. U2OS cells were grown in glass-bottomed dishes and transfected with GFP-Bax. 24 hrs later cells were loaded with TMRE to reveal the location of energised mitochondria, then treated with 30 J/m^2 UV irradiation to induce apoptosis and mounted for live cell imaging – for full details of the recording see movie figure legend; **(B) Supplementary movie figure M3.2:** Live cell recording of GFP-Bax transfected MCF10A cells undergoing apoptosis. Cells were treated exactly as described in part (A) – for full details of the recording see movie figure legend; **(C)** Still frames extracted from movie M3.2 showing that the formation of GFP-Bax clusters (green) correlates with loss of mitochondrial membrane potential ($\Delta\psi_m$, orange). Times shown relate to the beginning of this recording and not the time when the UV treatment was administered, which was approximately 15 hrs previously. Scale bars represent 10 μm.

C

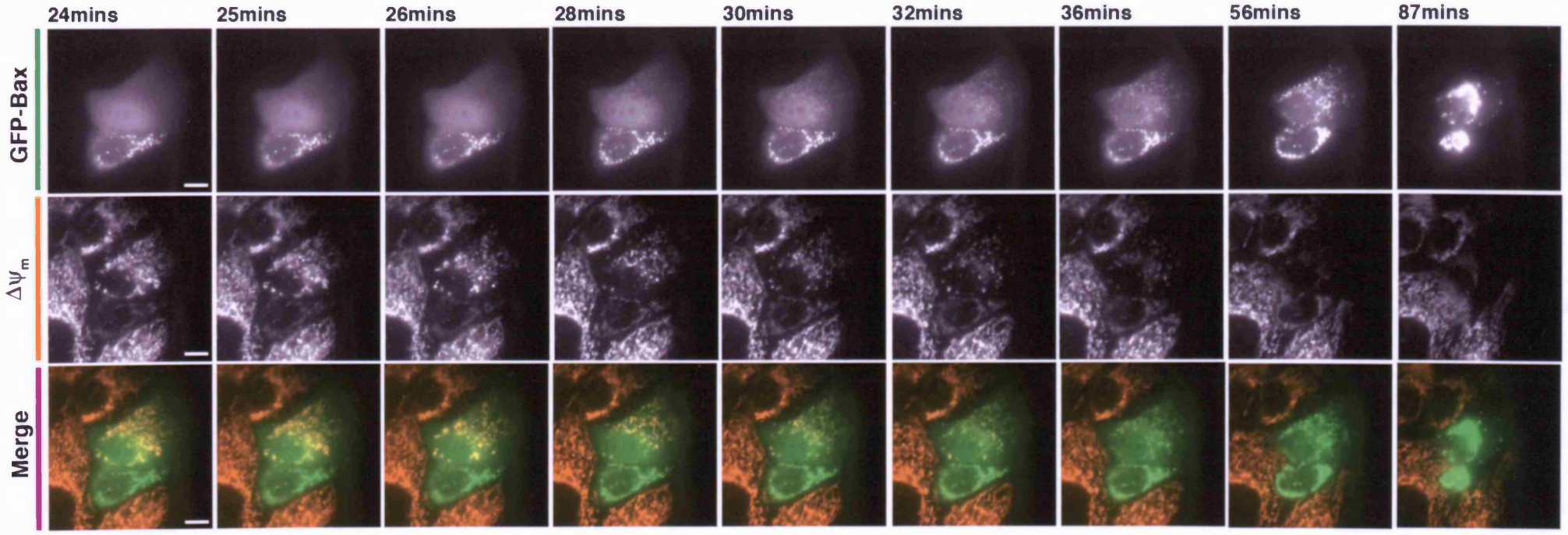
24mins
25mins
26mins
28mins
30mins
32mins
36mins
56mins
87mins
GFP-Bax
$\Delta\psi_m$
Merge

Figure 3.8 Translocation of GFP-Bax into clusters occurs synchronously with $\Delta\psi_m$ loss. Bright foci of GFP-Bax appear exactly as $\Delta\psi_m$ is lost and then increase in size as apoptosis proceeds. **(A) Supplementary movie figure M3.3:** U2OS cells were grown in glass-bottomed dishes and transfected with GFP-Bax. 24hrs later cells were loaded with TMRE to reveal the location of energised mitochondria, then treated with 30 J/m^2 UV irradiation and mounted for live cell imaging – for full details of the recording see movie figure legend; **(B)** Representative still frames taken from the upper cell in movie figure M3.3. Times shown relate to the beginning of this recording and not the time when the UV treatment was administered, which was approximately 18 hrs previously. Scale bars represent 20 μm; **(C)** 3X enlargement of a central portion of the cell shown in part (B). At this magnification some mitochondria clearly show loss of $\Delta\psi_m$ (orange) before others in the same cell. Complete loss of $\Delta\psi_m$ occurs during a window of approximately 5 mins duration. GFP-Bax foci (green) increase in size during this time and continue to enlarge throughout the time course shown.

B

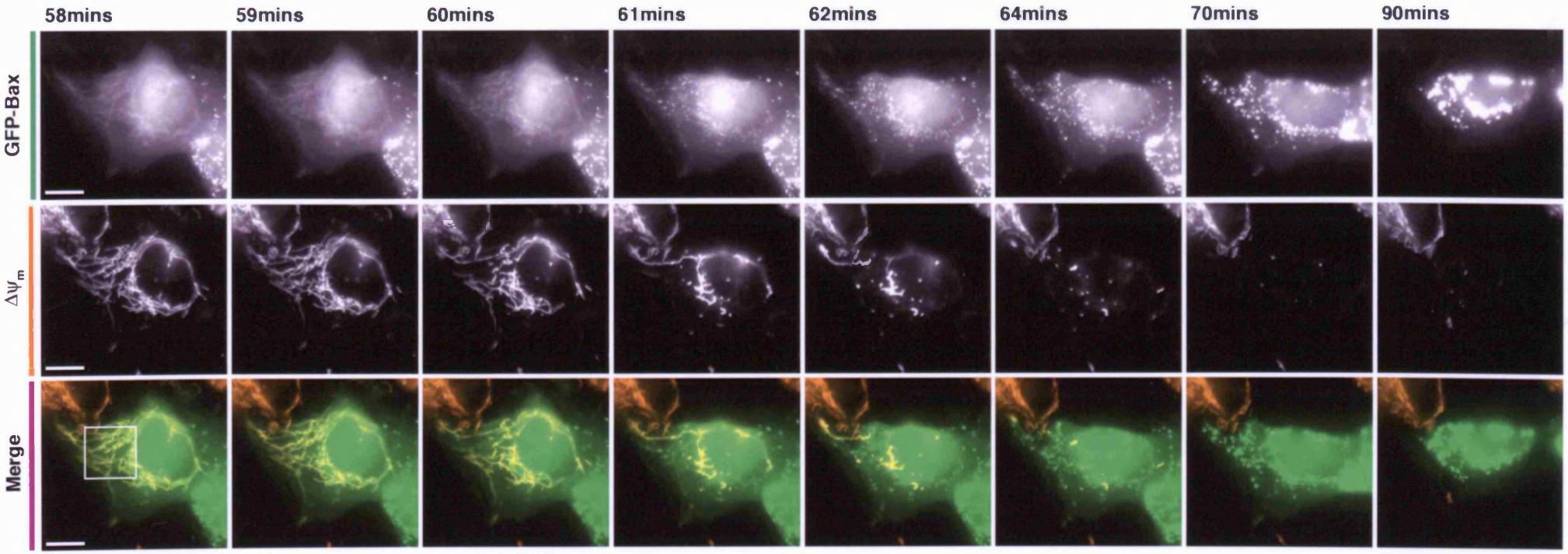
58mins
59mins
60mins
61mins
62mins
64mins
70mins
90mins
GFP-Bax
$\Delta\psi_m$
Merge

Cont.

C

58mins
59mins
60mins
61mins
62mins
64mins
70mins
90mins
GFP-Bax
$\Delta\psi_m$
Merge

Figure 3.9 Local initiation of GFP-Bax activation is followed by spreading loss of $\Delta\psi_m$.
In a more polarised cell the initiation of bright GFP-Bax foci can be seen to initiate in the cell periphery and spread rapidly across the cell body. **(A) Supplementary movie figure M3.4:** The same U2OS cell recording shown in movie figure M3.3 but now played at a slower frame rate to reveal spreading of GFP-Bax activation and corresponding loss of $\Delta\psi_m$ in the lower – for full details of the recording see movie figure legend; **(B)** Representative still frames taken from movie figure M3.4, experimental details therefore as in Figure 3.8. Prior enrichment of GFP-Bax onto the mitochondrial network due to the UV stress trigger can be seen in the first frame (blue arrows). GFP-Bax activation and loss of $\Delta\psi_m$ initiates from the base of the cell and spreads upwards ( ). Complete loss of $\Delta\psi_m$ occurs within approximately 5 min window. t = 0 mins is the first image in the sequence presented and does not relate to the time when the UV dose was administered, which was approximately 18 hrs previously. Scale bars represent 20 μm.

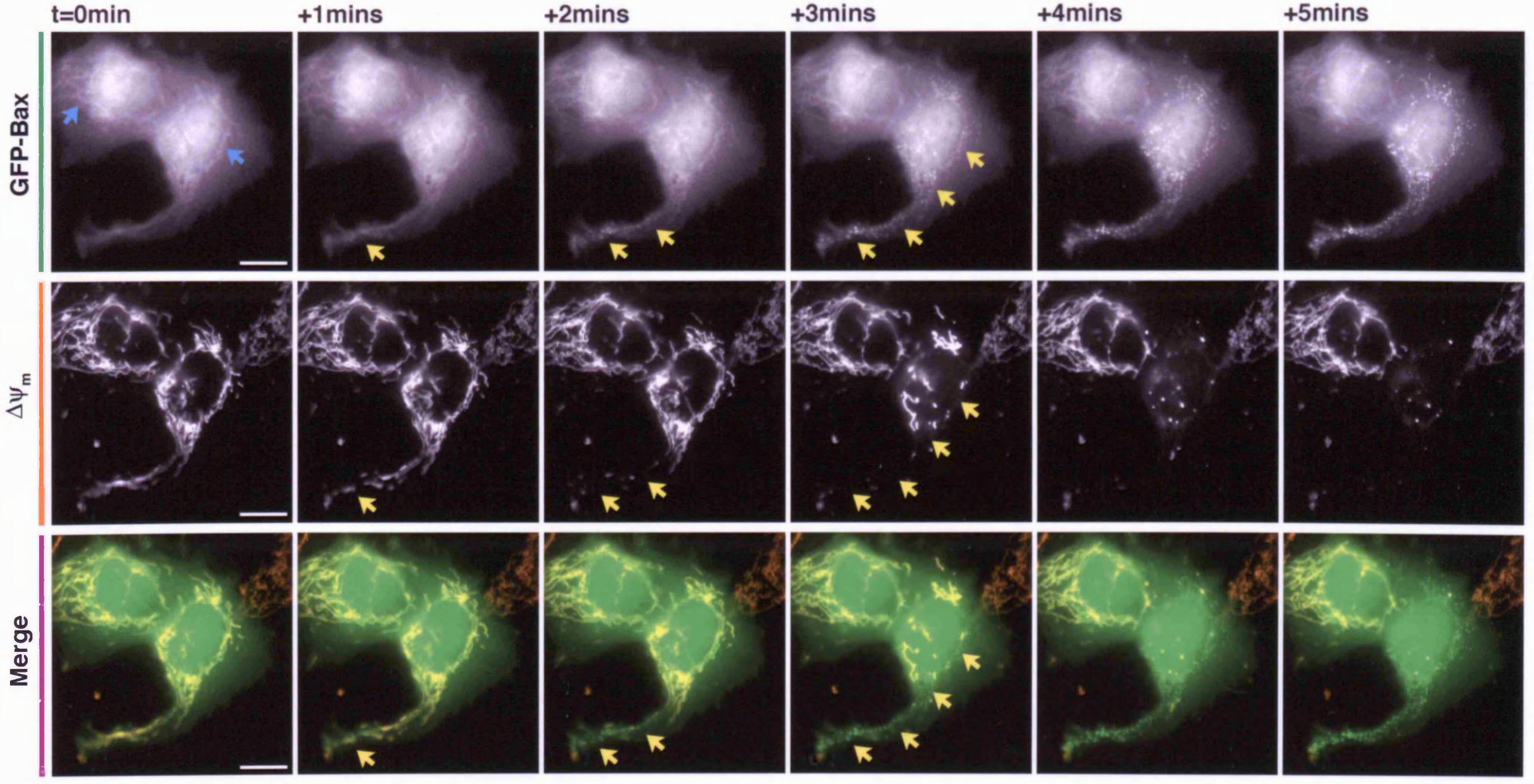
t=0min
+1mins
+2mins
+3mins
+4mins
+5mins
GFP-Bax
$\Delta\psi_m$
Merge

Figure 3.10 Local Bax activation appears to rapidly trigger Bax activation in a neighbouring region.

GFP-Bax becomes active and clustered in the polarised projection of an MCF10A cell and is able to rapidly trigger GFP-Bax activation in the remaining cell body when a narrow cytoplasmic neck is breached. **(A) Supplementary movie figure M3.5:** MCF10A cells were grown in glass-bottomed dishes and transfected with GFP-Bax. 24 hrs after transfection cells were and loaded with TMRE to reveal the location of energised mitochondria, then treated with 30 J/m^2 UV irradiation to induce apoptosis and mounted for live cell imaging – for full details of recording see movie figure legend; **(B) Supplementary movie figure M3.6:** An extended and accelerated version of the recording shown in movie figure M3.5. The phase overlay shows how early changes in the cell shape result in formation of the cytoplasmic projection prior to its retraction towards the cell body; **(C)** Representative still frames taken from movie figure M3.5. GFP-Bax activation, detected as bright foci of GFP-Bax, is first visible in a projection to the right of the cell body (t = 381mins,), which retracts inwards over time. GFP-Bax activation and $\Delta\psi_m$ loss within the main cell body correlates precisely with the breaching of the narrow neck separating this region from the active Bax in the projection (t = 528mins, red arrows). Cell shrinkage and the morphological features of apoptosis rapidly follow from t = 530mins onwards. Times shown indicate relate to the addition of Fas/CHX and start of recording. Scale bars represent 20 μm.

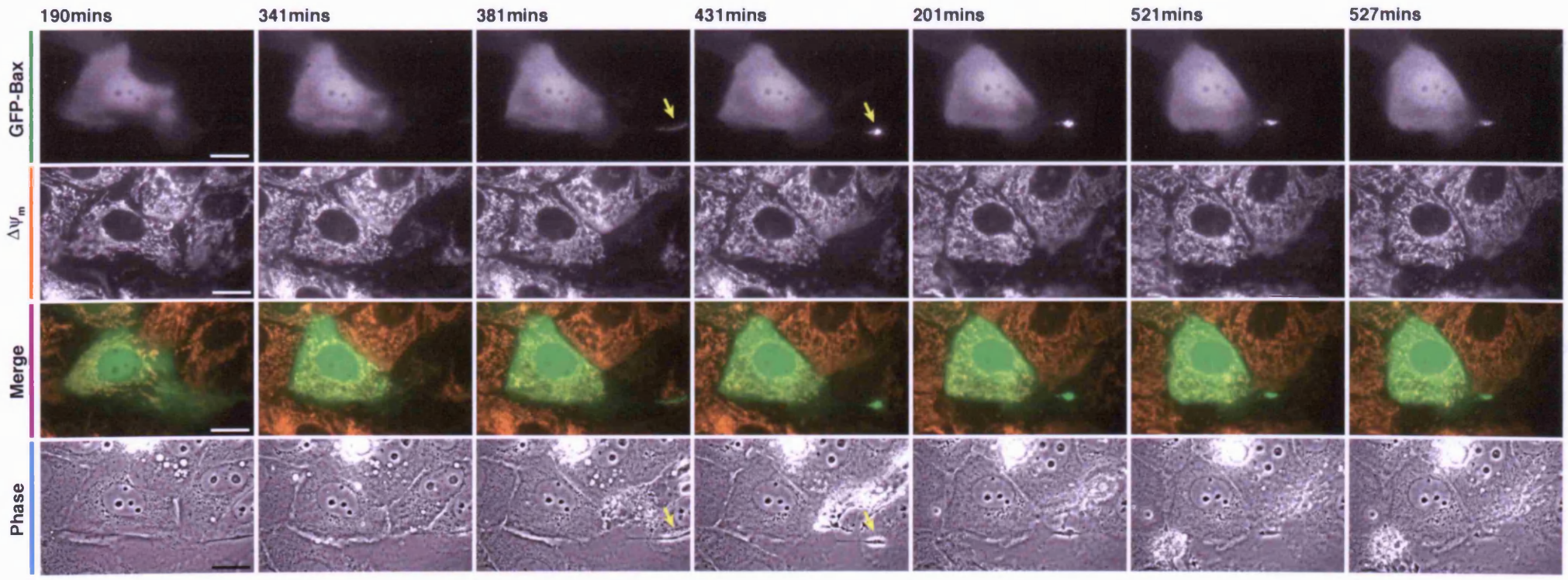
190mins
341mins
381mins
431mins
201mins
521mins
527mins
GFP-Bax
$\Delta\psi_m$
Merge
Phase

Cont.

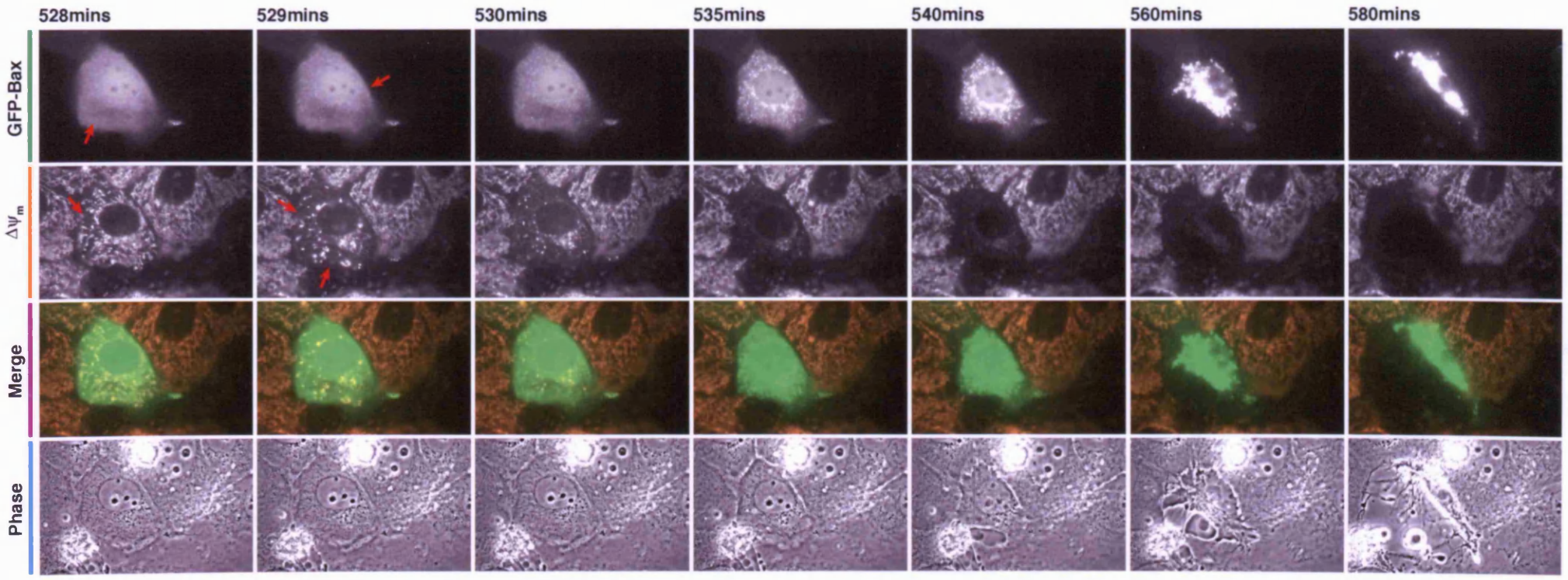
528mins
529mins
530mins
535mins
540mins
560mins
580mins
GFP-Bax
$\Delta\psi_m$
Merge
Phase

Figure 3.11 In low GFP-Bax expressing cells loss of $\Delta\psi_m$ occurs before GFP-Bax foci are detectable.

In cells expressing very low levels of GFP-Bax loss of $\Delta\psi_m$ occurred well before GFP-Bax foci were easily detectable. **(A)** MCF10A cells grown in glass-bottomed dishes and transfected with GFP-Bax. 24 hrs after transfection cells were loaded with TMRE to reveal the location of energised mitochondria, then treated with 30 J/m^2 UV irradiation to induce apoptosis and mounted for live cell imaging. Representative still frames extracted from the resulting recording are shown. Cell A (final panel) expresses very low levels of GFP-Bax, compared to the moderate over-expression in Cell B, (which is the cell recorded in Figure 3.10). The first disruption of the membrane potential is at t = 705mins after administration of the Fas/CHX treatment (orange arrows). GFP-Bax clustering is not detectable for at least a further 2 mins (t = 707 mins, green arrows), and not obvious for a further 5mins (t = 710 mins). Scale bars represent 10 μm; **(B) Supplementary movie M3.7**: The complete image sequence from which still fames shown in part (A) were compiled – for full details of the recording see movie figure legend.

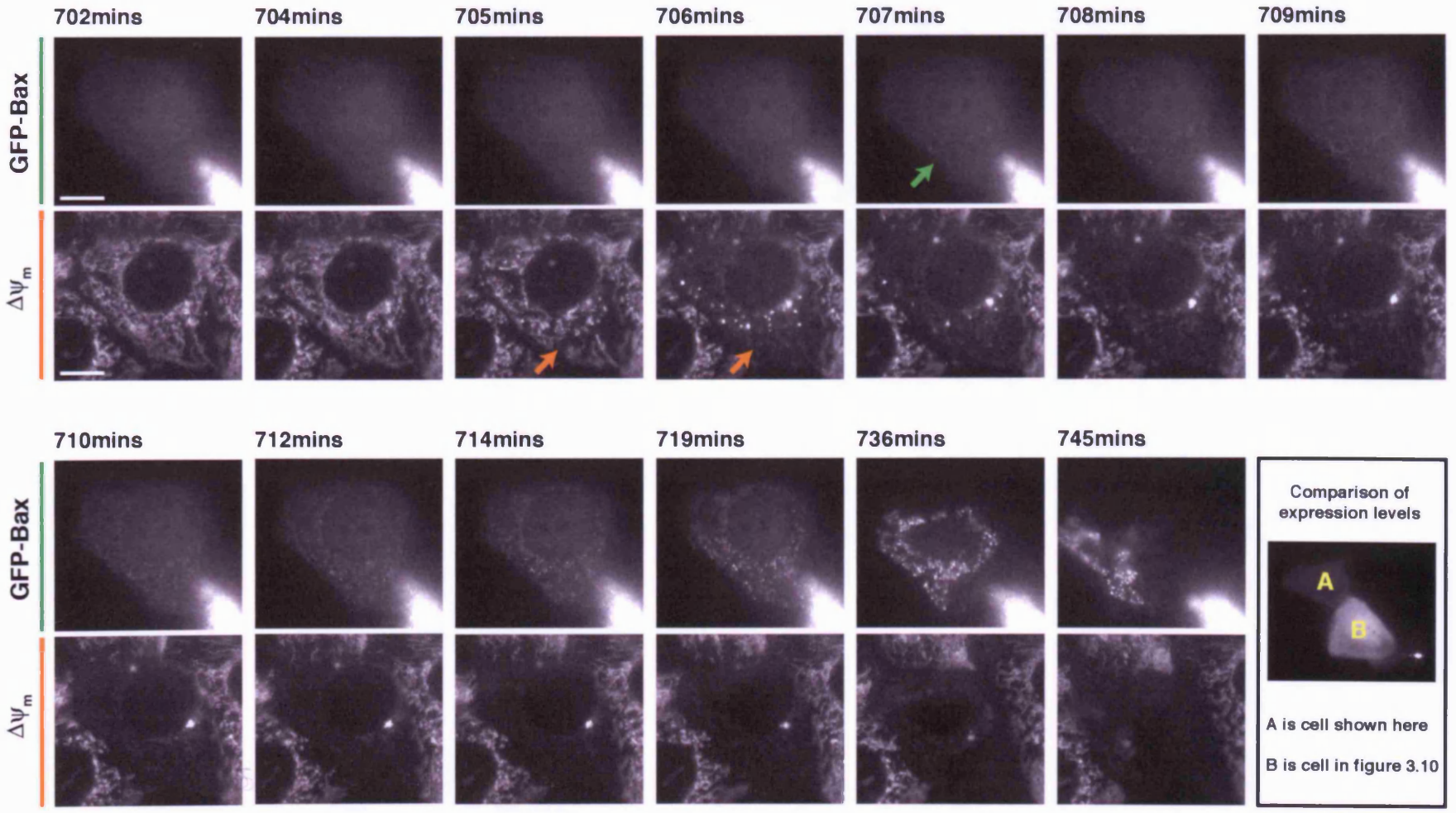
702mins
704mins
705mins
706mins
707mins
708mins
709mins
GFP-Bax
$\Delta\psi_m$
710mins
712mins
714mins
719mins
736mins
745mins
GFP-Bax
$\Delta\psi_m$
Comparison of expression levels
A
B
A is cell shown here
B is cell in figure 3.10

Figure 3.12 Bax activation precedes significant caspase 3/7 activity.

The formation of bright Bax foci precedes significant caspase 3/7 enzymatic activity by 1-2mins. **(A)** MCF10A cells were grown in glass-bottomed dishes and co-transfected the CFP-Bax (green) and YFP based Caspase 3/7 reporter construct (red). 24 hrs after transfection cells were treated with Fas/CHX to induce apoptosis and mounted for live cell imaging. Times indicated relate to the start of this recording and do not relate to the time when the Fas/CHX treatment was administered, which was approximately 4hrs previously. Scale bars represent 10 μM; **(B) Supplementary movie figure M3.10:** The complete image sequence from which the stills shown in part (A) were compiled – for full details of the recording see movie figure legend.

Supplementary material added in support: *Additional parts 3.13 C and 3.13 D can be found in Appendix 1 and represent two further cells recorded in replicate experiments. Experimental details are therefore as part (A) and in both cases CFP-Bax foci formation precedes significant caspase 3/7 enzymatic activity by the same 1-2min interval. The complete image sequence from which these stills were compiled is shown in movie figures M3.11 and M3.12. See movie figure legends for further details of recording.*

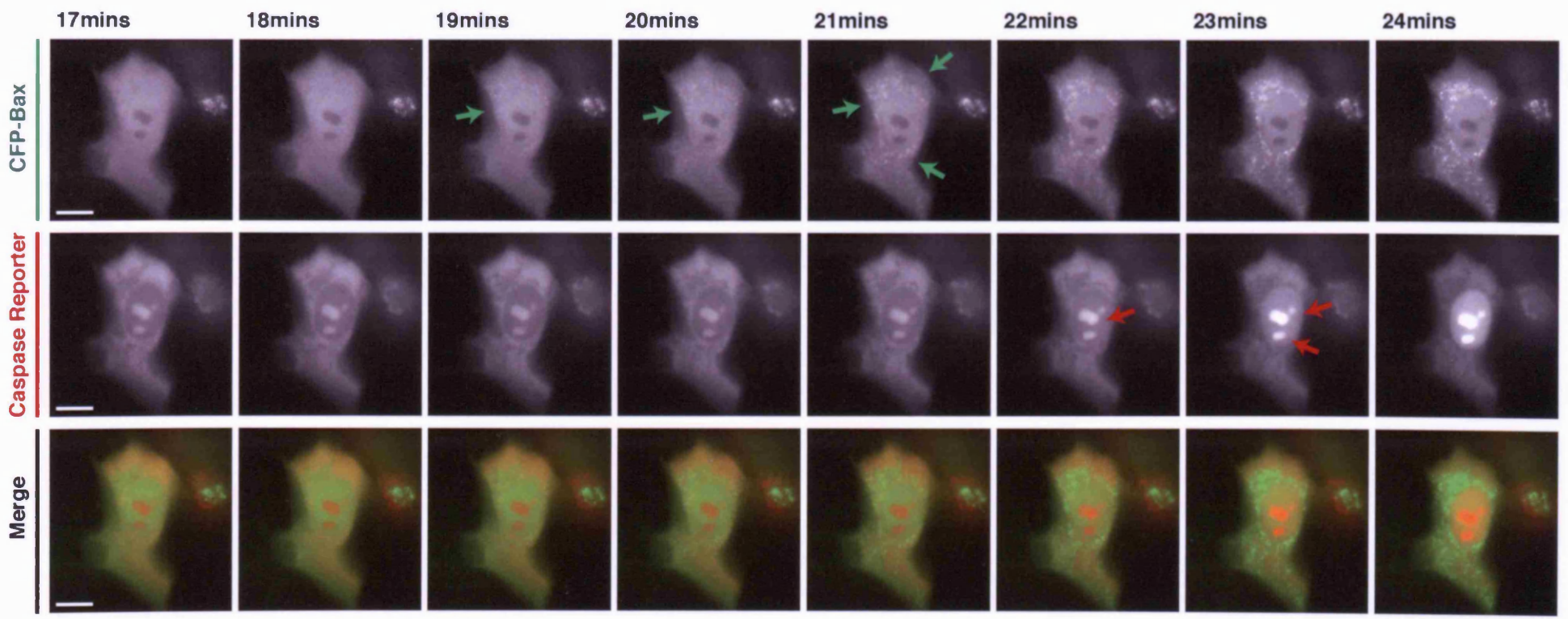
17mins
18mins
19mins
20mins
21mins
22mins
23mins
24mins
CFP-Bax
Caspase Reporter
Merge

Cont.

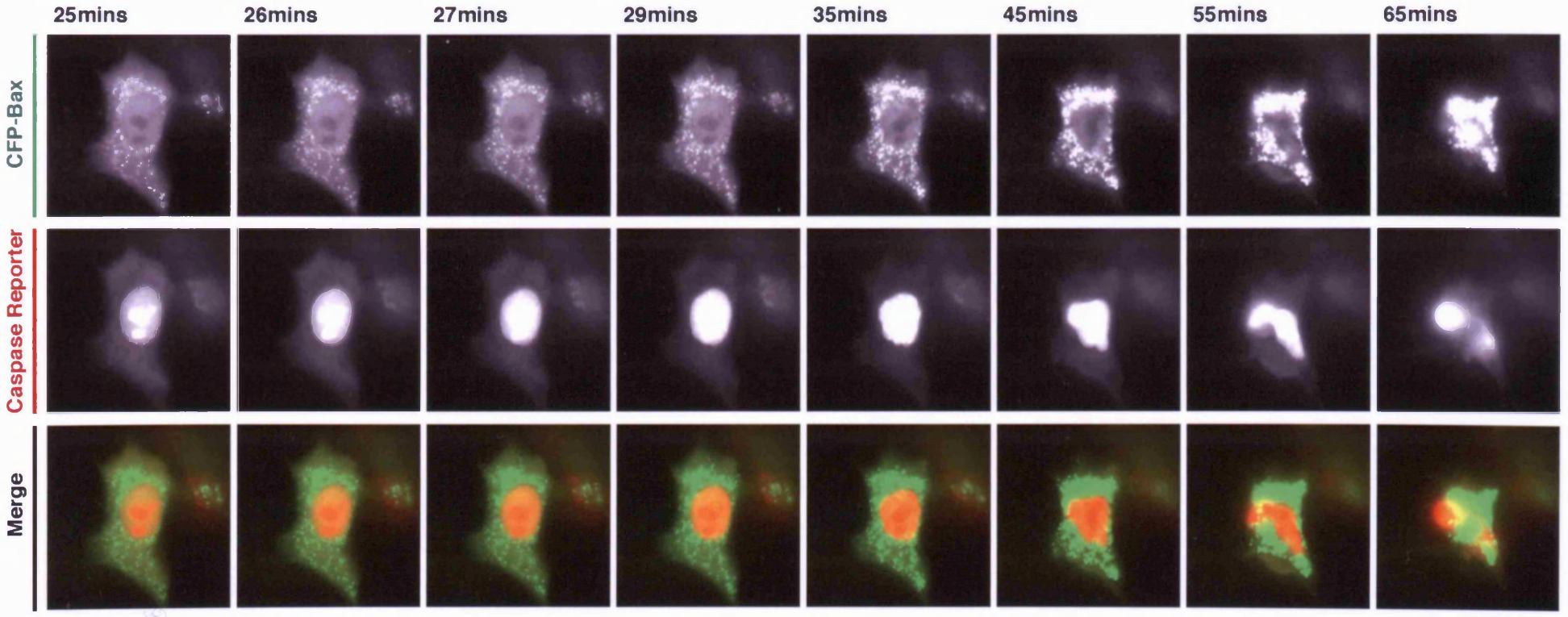
25mins
26mins
27mins
29mins
35mins
45mins
55mins
65mins
CFP-Bax
Caspase Reporter
Merge

Figure 3.13 Flickering of $\Delta\psi_m$ is occasionally observed but does not correlate with the onset of complete $\Delta\psi_m$ loss.

Partial, transient depolarisation of the mitochondrial network was a rare event, and was followed by a rapid and complete recovery of $\Delta\psi_m$, unlike the cell wide depolarisation that accompanied apoptosis. **(A)** Live cell recording from untransfected MCF10A cells grown in glass-bottomed dishes, loaded with TMRE to reveal energised mitochondria and treated with 30 J/m^2 UV irradiation to induce apoptosis. t=0min is the first image in the sequence presented and does not relate to the time when the UV dose was administered, which was approximately 10 hrs previously. The position of a transient depolarisation is marked ( ); **(B)** Live cell recording from U2OS cells showing transient flickers of $\Delta\psi_m$. Cells were prepared as described in part (A). Times indicate duration from the start of recording and do not relate to the time when the UV dose was administered, which was approximately 18 hrs previously. The positions of flickers at t=10mins and t=12mins are marked ( ); **(C)** Two further examples of recordings made from MCF10A cells showing complete loss of $\Delta\psi_m$ during apoptosis. These records are included in quantitation shown in Figure 4.16. In all images scale bars represent 10 μm. **(D) Supplementary movie figure M3.8:** The complete image sequence from which still fames in part (C) were compiled – for full details of the recording see movie figure legend.

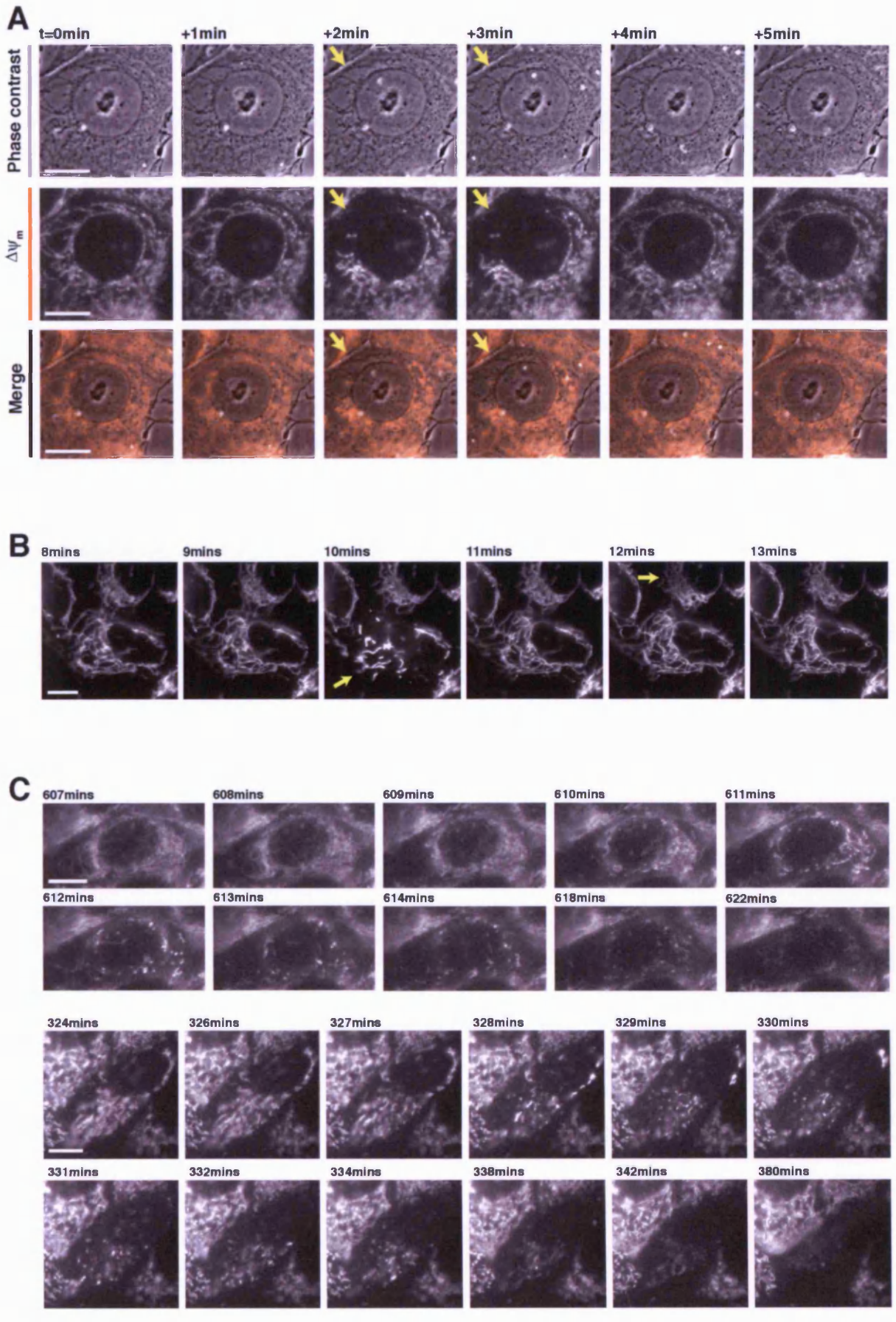
A
t=0min
+1min
+2min
+3min
+4min
+5min
Phase contrast
$\Delta\psi_m$
Merge
B
8mins
9mins
10mins
11mins
12mins
13mins
C
607mins
608mins
609mins
610mins
611mins
612mins
613mins
614mins
618mins
622mins
324mins
326mins
327mins
328mins
329mins
330mins
331mins
332mins
334mins
338mins
342mins
380mins

Figure 3.14 An increase in mitochondrial calcium is detectable prior to Bax activation.
The mitochondrial pericam reporter construct detects increasing levels of Ca^{2+} in the mitochondria of MCF10A cells treated with Fas/CHX, prior to the activation of RFP-Bax. **(A)** MCF10A cells were grown in glass bottom-dishes and co-transfected with RFP-Bax and the mitochondrial pericam. 24 hrs after transfection the cells were treated with Fas/CHX to induce apoptosis and mounted for live recording. Four frames: phase (grey), RFP-Bax (red), pericam excited at 410nm (green), pericam excited at 510nm (blue) were sequentially recorded every 20 seconds throughout the duration of the experiment. The radiometric image was calculated as 510 nm / 410 nm; **(B)** Still frames extracted from the total recording showing the changes in RFP-Bax distribution. Bax activation, as detected by the formation of clusters, is first detectable in frame 585 (195.2mins after the addition of Fas/CHX); **(C)** Integrated mean intensities for Bax (red/pink) and the ratiometric pericam (blue/blue) are plotted over time for two small regions of interest shown in parts (A) and (B) and containing mitochondria.

Supplementary material added in support: *Additional parts 1.14.D and 1.14.E can be found in Appendix 1 and represent two further cells recorded in replicate experiments. Experimental details are therefore as parts (A-C) and in both cases there is an increase in mitochondrial calcium in the period prior to RFP-Bax clustering (green trend line).*

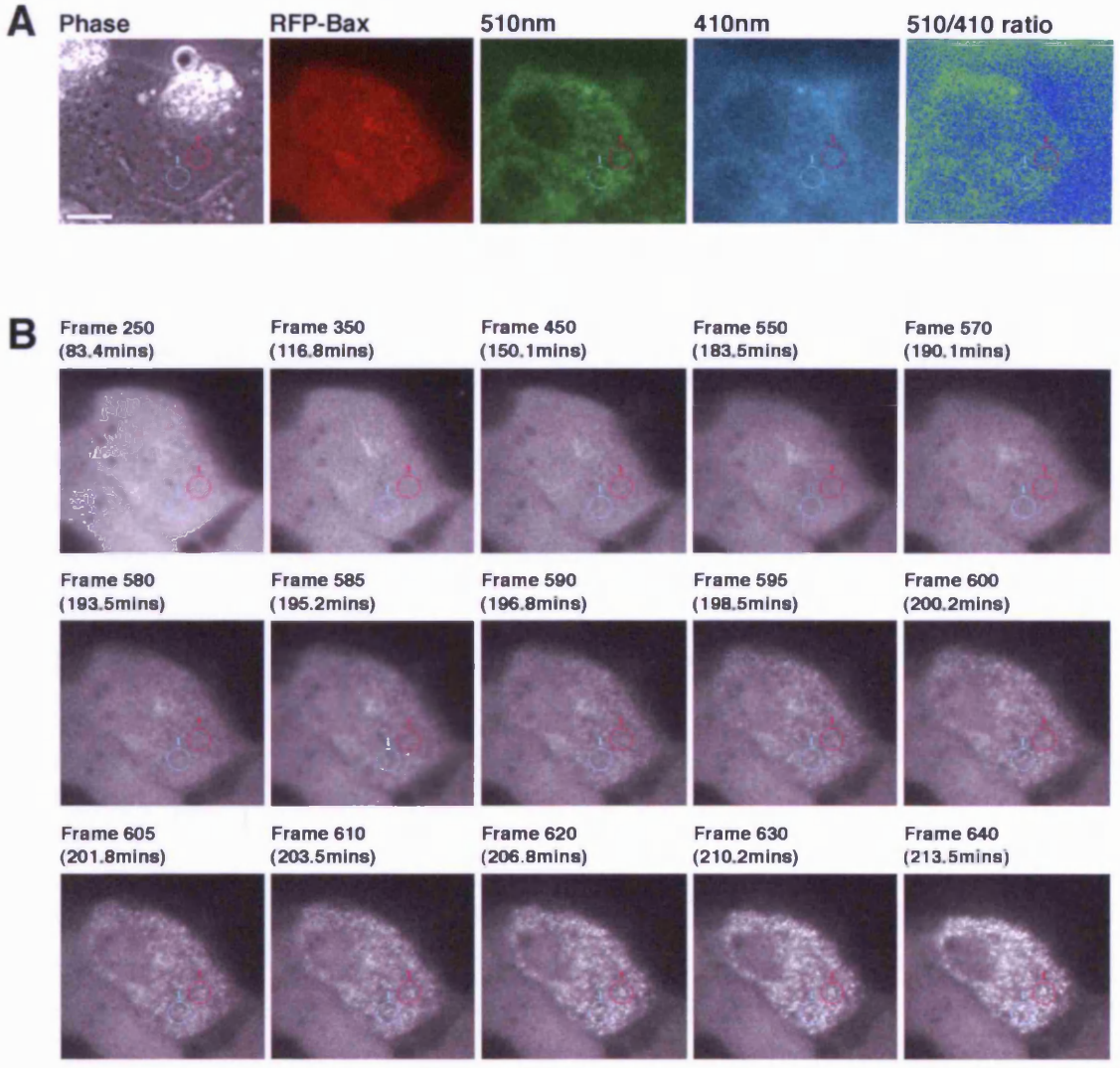
A
Phase
RFP-Bax
510nm
410nm
510/410 ratio
B
Frame 250 (83.4mins)
Frame 350 (116.8mins)
Frame 450 (150.1mins)
Frame 550 (183.5mins)
Fame 570 (190.1mins)
Frame 580 (193.5mins)
Frame 585 (195.2mins)
Frame 590 (196.8mins)
Frame 595 (198.5mins)
Frame 600 (200.2mins)
Frame 605 (201.8mins)
Frame 610 (203.5mins)
Frame 620 (206.8mins)
Frame 630 (210.2mins)
Frame 640 (213.5mins)
C
Mean Bax intensity (arbitrary units)
320
300
280
260
240
220
0.295
0.29
0.285
0.28
0.275
0.27
0.265
0.26
Pericam ratio (510nm/410nm)
33.0
53.0
73.0
93.0
113.0
133.0
153.0
173.0
193.0
213.0
233.0
Time (minutes)

Chapter 4 – Viral pro-survival proteins

4.1 Introduction:

Data presented in the previous chapter indicates that Bax activation is a rapid event that can initiate in a discrete sub-cellular region and then spread rapidly across the cell. These observations suggest the existence of a feed-forward mechanism to ensure the rapid and co-ordinated recruitment of all mitochondria in a cell following commitment to apoptosis. Preliminary evidence also suggests that an increase in mitochondrial calcium levels occurs prior to the onset of Bax activation. There is evidence from the published literature of a calcium wave, propagated by mitochondria, existing around the time of the onset of apoptosis and this is therefore a candidate for such a feed-forward mechanism.

The rapid nature of Bax activation meant that further characterisation, using live cell microscopy was technically challenging and would require much faster rates of image acquisition rates than the 1 frame/minute used in the previous examples. The stochastic nature of the process also means that imaging for several hours is required to guarantee that cell deaths are observed in any given field of cells. In order to address this problem, and in an attempt to learn more about the Bax activation process by perturbing it, the effect of over-expressing pro-survival proteins was investigated.

Historically viral proteins have proved indispensable in aiding our understanding of diverse cellular process. Viruses have co-evolved with their host organisms over millions of years. During this time their relatively small genomes have become highly specialised to contain proteins that target and subvert key cellular processes for the virus's advantage. Understanding which cellular proteins are targeted by viruses has often led to the identification of key steps in the host cell physiology and understanding how the viral proteins function often gives important insights into normal regulation of critical cellular processes. For example, the finding that E1A targets the tumour suppressor, Rb, has led to the paradigm whereby viral oncogenes target tumour suppressor pathways to induce uncontrolled cell proliferation and transformation (Frisch and Mymryk, 2002).

A number of viruses contain proteins that directly target Bax and Bak (Figure 1.1). Some share obvious sequence homology with cellular Bcl-2 proteins, whilst others lack identifiable homology in their primary amino acid sequences but have nevertheless been experimentally demonstrated to block Bax or Bak activation (for further details see section 1.11). This chapter describes experiments using two of these proteins, BHRF1 from Epstein Barr Virus and E1B19k from Adenovirus, that provide further insights into Bax activation.

4.2 Characterisation of cell lines expressing pro-survival proteins:

Four pro-survival proteins were chosen for further analysis of their effect upon Bax activation: two cellular pro-survival proteins, Bcl-2 and Bcl-XL, and two viral proteins, BHRF1 from Epstein Barr Virus, a Bcl-2 sequence homologue, and E1B19k from Adenovirus, which lacks significant sequence homology to the cellular Bcl-2 proteins but still protects against apoptosis. Constructs encoding each protein, or the empty retroviral vector as a control, were introduced into MCF10A cells by retroviral gene transfer. Following infection and drug selection, expression, or over-expression in the case of Bcl-2 and Bcl-XL, was confirmed by western blotting (Figure 4.1). To assess the level of protection conferred by these proteins the stable cell lines were then subjected to a time course of Fas/CHX treatment to induce apoptosis. Cells were harvested every 3 hrs for 15 hrs, fixed and stained for DNA content with propidium iodide. The level of apoptosis was assessed by FACS analysis as the percentage of cells with sub-G1 DNA content (Figure 4.2 A). During the time course the empty vector control line was efficiently killed. Over-expression of the two cellular proteins, Bcl-2 and Bcl-XL, was somewhat able to protect the cells, with around a 5% and 10% reduction in the level of apoptosis, respectively. However, expression of the two viral proteins, E1B19k and BHRF1, conferred a much stronger degree of protection. In both cases the majority of cells remained alive and attached to the culture dishes with normal morphology 15 hrs after the addition of the Fas/CHX (Figure 4.2 B). The E1B19k and BHRF1 cell lines therefore provided a potential source of cellular material in which apoptosis had been strongly triggered for a prolonged period of time but the cells remain alive and amenable to further analysis.

It was next important to establish the level at which apoptotic signalling was blocked in these cell lines. For these experiments, Fas/CHX was again chosen as the apoptotic trigger since events downstream of Fas death receptor activation are well characterised (see section 1.4) and includes cleavage of proteins such as pro-caspase-8 and -3, which can be followed by western blotting. A further time course was therefore conducted during which cells were harvested every 3 hrs and lysates prepared and analysed by western blotting for various components of the cell

death pathway (Figure 4.3). This experiment showed that the processing of proteins located downstream of receptor activation, but upstream of the mitochondria, occurred at the same rate in all cell lines, regardless of whether or not they subsequently underwent a substantial degree of apoptosis. Specifically this was shown to be the case for: the processing of pro-caspase-8, the cleavage of full length Bid and the caspase-8 dependent cleavage of full length caspase-3 (Figure 4.3, labelled pre-mitochondrial events). This contrasted with events known to be downstream of mitochondrial dysfunction, which only occurred in those cell lines where significant apoptosis was observed, ie. the empty vector control, Bcl-2- and Bcl-XL-expressing lines. This was the case for the cleavage of pro-caspase-9, which requires Cyt-c released from mitochondria to active the apoptosome complex. It was also the case for cleavage of the DNA repair enzyme poly (ADP-ribose) polymerase-1 (PARP), a classical marker for the later stages apoptosis. Both of these events were almost completely blocked by expression of E1B19k and BHRF1 (Figure 4.3, labelled post-mitochondrial events). It is also noteworthy that whilst the caspase-8 dependent cleavage of full length caspase-3 was clearly evident in all cell lines, removal of the short pro-domain, converting the caspase-3 from p20 to p17, occurred only in those cell lines where significant cell death was observed and was blocked by expression of both E1B19k and BHRF1. This result indicates that caspase-3 is not yet fully active following the initial caspase-8 dependent cleavage within the linker region. The processing of p20 to p17 is a caspase-9 dependent event and therefore suggests that removal of the short pro-domain represents an additional requirement to generate efficient effector caspase activity *in vivo*. A similar observation has been made in another system (Meergans et al., 2000). Together the data presented in Figure 4.3 suggests that the strong protection from apoptosis conferred by the expression of E1B19k and BHRF1 is due to their abilities to block apoptosis at a level proximal to mitochondria. Under these circumstances events downstream of Fas death receptor activation, but upstream of the mitochondria, proceed unopposed whilst events downstream of mitochondria are efficiently blocked. These results also demonstrate that MCF10A cells, treated with an extrinsic death pathway agonist, appear absolutely dependent on mitochondrial dysfunction to initiate apoptosis and the activation of caspases downstream of death receptor ligation is insufficient to initiate cell death. Such cells are classically described as Type II cells. Since Bax is also critically involved in the regulation of apoptosis at mitochondria, further experiments were conducted to determine the effect of these pro-survival proteins on Bax activation.

4.3 The effect of E1B19k and BHRF1 on Bax (and Bak) activation:

In Chapter 3 it was established that upon activation, both Bax and Bak undergo a dramatic conformational change and antibodies raised against N-terminal epitopes of these proteins only recognise their active conformations. These reagents provide suitable tools with which to assess the effect of the pro-survival proteins upon Bax activation. However, for these experiments the level of protection offered by Bcl-2 and Bcl-XL in the MCF10A cell system was considered too modest to be informative in future analysis and in the subsequent experiments only the E1B19k- and BHRF1-expressing cell lines were pursued.

Initially the Bax N20 (11-30) N-terminal antibody was used to immunoprecipitate active Bax from the empty vector control, E1B19k- and BHRF1-expressing MCF10A cell following the induction of apoptosis by Fas/CHX treatment (Figure 4.4 A). This experiment showed that in the control cells Bax was efficiently activated over the course of 15 hrs of Fas/CHX treatment. At later time points, increasing amounts of Bak could also be observed to co-immunoprecipitate with Bax, indicative of the hetero-oligomerisation of Bax with Bak (Figure 4.4 A, left panel). In contrast Bax activation was almost completely blocked in the BHRF1-expressing cells. In this case, since no active Bax was immunoprecipitated, no further inferences can be made regarding possible Bax / Bak interactions in these cells (Figure 4.4 A, right panel). The surprising result came from the E1B19k-expressing cells. In this case Bax activation was readily detectable, becoming active at a similar rate as in the control cells. There was, however, no significant co-immunoprecipitation of Bak (Figure 4.4 A, middle panel). This result indicates that Bax still undergoes at least the N-terminal conformational change in E1B19k-expressing cells but that subsequent hetero-oligomerisation of Bax and Bak is blocked.

An explanation for these results was suggested when MCF10A cells treated with Fas/CHX for 8 hrs were analysed by confocal microscopy following co-immunostaining with the anti-Bax N20 antibody and anti-Cyt-c (Figure 4.4 B). Under these conditions bright foci characteristic of active Bax were clearly visible in some of the empty vector control cells and this was always correlated with diffuse Cyt-c staining, indicative of its release from mitochondria (Figure 4.4 B, upper panels). As expected from the previous result, no Bax activation was detectable in the BHRF1-expressing cells and Cyt-c retained a distinctive mitochondrial localisation (Figure 4.4 B, lower panels). When E1B19k-expressing cells were examined some were indeed strongly recognised by the Bax N20 antibody. Strikingly, in these N20 positive cells Bax seemed to be evenly distributed over the entire mitochondrial network, co-localising with Cyt-c, which retained a mitochondrial localisation (Figure 4.4 B, middle panels). This distribution was never observed in either the control or BHRF1-expressing cell lines and therefore suggests that

E1B19k is able to block Bax activation at a step subsequent to both its conformational activation and recruitment to mitochondria, but prior to the formation of mitochondrially-associated foci and Cyt-c release. The failure of active Bax to co-immunoprecipitate Bak from Fas/CHX treated MCF10A E1B19k cells (Figure 4.4 A) is therefore explained by the ability of E1B19k to block Bax at a step prior to the formation of the foci where active Bax and Bak would normally co-associate.

The results shown in Figure 4.4 also demonstrate that the rate at which Bax becomes N-terminally active in the E1B19k-expressing and control cells is very similar. For example, the amount of Bax immunoprecipitated from the E1B19k cells was only slightly less than from the control cells (Figure 4.4 A). The failure of Bax to enter oligomers may also explain this small difference, since at later time points co-immunoprecipitation of Bax in the form of homo-dimers and homo-oligomers would act to inflate the amount of Bax immunoprecipitated in the control samples only. In order to confirm this hypothesis MCF10A cells were also fixed and stained with ant-Bax N20 and anti-Cyt-c over a similar time course of Fas/CHX treatment and analysed by confocal microscopy (Figure 4.5). From this experiment it was clear that E1B19k cells did indeed become positive for Bax N20 staining at the same rate as the wild type cells. Also, in both cell types this appeared to be a stochastic, all-or-none event. However, once E1B19k-blocked cells gained conformationally active and mitochondrially localised Bax, they persisted in the culture dish without releasing Cyt-c. This meant that by the later time points, for example the 12 hr time point in Figure 4.5, when many of the control cells had undergone complete apoptosis and become detached, the majority of E1B19k-expressing cells had accumulated positive staining, mitochondrially localised, active Bax. This contrasted with the MCF10A BHRF1 cell line where conformational active Bax and diffuse Cyt-c were only rarely detected even 12 hrs after the application of Fas/CHX.

The results presented in this section go some way towards characterising how E1B19k is able to block Bax activation at a step subsequent to its conformational activation and mitochondrial translocation. They do not, however, address the Bak activation status in these cells. The failure of active Bax to co-immunoprecipitate Bak in E1B19k-expressing cells (Figure 4.4 A) is likely to be explained by a failure of the E1B19k-blocked Bax enter mitochondrially-associated clusters. However, it could however also be explained if these cells were absolutely dependent on Bak activation and if it was this protein which E1B19k was specifically targeting. In addition, in E1B19k-blocked cells, Bax accumulates at mitochondria where Bak is also normally located, so the possibility of an interaction cannot be excluded solely on the grounds that they have not yet entered the same location, namely the mitochondrially-associated clusters. To address these issues, a similar experiment was conducted in which MCF10A cells, following

8 hrs of exposure to Fas/CHX, were co-immunostained with an N-terminal Bak antibody, Bak NT (23-37), together with anti-Cyt-c (Figure 4.6). Under these conditions it was clear that Bak was behaving in an analogous fashion to Bax in all three cell lines. In the control cell line Bak was stochastically activated and formed bright foci correlating with Cyt-c release. Activation of Bak in MCF10A E1B19k cells was clearly visible by an increase in mitochondrial staining intensity by the Bak NT antibody. However, these cells retained mitochondrial Cyt-c staining. No significant activation of Bak in MCF10A BHRF1 cells was detectable under these conditions. Thus E1B19k appears to be able to efficiently block both Bax and Bak activation at a step subsequent to their N-terminal conformational change but before entry into mitochondrial clusters and hetero-dimerisation.

Data presented in Figures 4.4, 4.5 and 4.6 correlates the ability of E1B19k to block the co-immunoprecipitation of Bax and Bak with the lack of detectable mitochondrially-associated foci by immunofluorescence. However, these experiments all rely on the use of N-terminally conformationally sensitive antibodies to Bax and Bak. As discussed in Chapter 3, these reagents are by definition limited to detection of the proteins after they have undergone conformational change. An alternative approach to detecting Bax activation is by gel filtration analysis. This approach has the advantage that the entire cellular pool of Bax can be detected, regardless of the conformational status of the protein. Lysates were prepared from MCF10A E1B19k, BHRF1 and the empty vector cells treated with and without Fas/CHX for 8 hrs to induce apoptosis. Proteins were then separated by gel filtration and the resulting fractions analysed by western blotting for Bax content (Figure 4.7). This data shows that in the control cells, Bax shifts from its monomeric molecular weight of 21 kDa into higher molecular weight fractions following the induction of apoptosis (detectable as Bax dimers at ~43 kDa up to molecular weights greater than 670 kDa), as has been previously described (Antonsson et al., 2001). In both the E1B19k and BHRF1 cells, this change in the Bax elution profile is essentially prevented, with only trace amounts of Bax entering the higher molecular weight range. Importantly, this result shows that the N-terminally active Bax accumulated at the mitochondria of E1B19k-expressing cells truly remains monomeric. Attempts to analyse the gel filtration for Bak were complicated by the protein being distributed over a much broader range of molecular weights even in healthy cells making results difficult to interpret (data not shown). In addition, evidence collected in these experiments suggested that the distribution of E1B19k remained in the low molecular weight range in both treated and untreated cells while BHRF1 was sometimes present at much higher molecular weights (440 - 670 kDa). However, the nature of this higher molecular range of BHRF1 was not investigated although further analysis might provide clues as to the function of the protein.

Finally, two additional pieces of biochemical evidence regarding viral protein blocks are shown in Figure 4.8. In the earlier immunoprecipitation experiment using the Bax N20 antibody (Figure 4.4), the lack of detectable Bax activation in the BHRF1-expressing cells meant that no inferences could be made about Bak activation status or Bax / Bak interactions. To address this issue, a reciprocal co-immunoprecipitation with both anti-Bax N20 and anti-Bak NT was performed from MCF10A control and BHRF1-expressing cells (Figure 4.8 A). This shows that in empty vector control cells, Bax becomes active and co-immunoprecipitates Bak, and that Bak becomes active and co-immunoprecipitates Bax. In the BHRF1 expressing cells activation of Bax is almost completely blocked and no Bak co-immunoprecipitates with Bax, whilst activation of Bak is absolutely blocked and the small amount of protein recognised in untreated cells neither increases, nor co-immunoprecipitates any Bax, following the apoptotic trigger. This confirms that BHRF1 acts as a strong block to Bax and Bak activation, preventing even the earliest sign of their activation, the N-terminal conformational change, and completely preventing co-association of the proteins following an apoptotic trigger.

During the course of this work, several more Bax antibodies characterised in Figure 3.3 where used in immuoprecipitation experiments from E1B19k-expressing cells. Three of these: Bax N20, Bax α7/α8 and Bax 43-61, were used to immunoprecipitate Bax from MCF10A control, E1B19k- and Bcl-2-expressing cells before and after treatment with Fas/CHX (Figure 4.8 B). As expected, Bax 43-61 showed no conformational selectivity and immunoprecipitated Bax equally in all conditions. Also as expected, Bax N20 was highly conformationally sensitive and only immunoprecipitated Bax from the treated cells. In this case no significant protection was detectable by Bcl-2 over-expression, and the small reduction in the amount of Bax immunoprecipitated from E1B19k-expressing cells may be due to lack of Bax oligomerisaiton in these cells, as discussed above. Finally, Bax α7/α8, which is normally conformationally sensitive as shown in the control and Bcl-2 expressing cells, could not immunoprecipitate Bax from treated E1B19k-expressing cells. This result confirms an observation first made following infection with recombinant adenovirus (Sundararajan and White, 2001). It suggests that this region, which corresponds to the Bax BH2 domain, may interact either directly with E1B19k, thereby blocking access to this epitope, or that E1B19k prevents an additional conformational change in this region.

In summary, data presented in this section shows that BHRF1 expression potently prevents cell death by blocking apoptotic signalling at a step proximal to the mitochondria, but before Bax and Bak activation. In contrast to BHRF1, E1B19K appears to block apoptosis by intercepting Bax and Bak activation after the initial N-terminal conformational change has occurred and acts

by preventing only the later stages of their activation, namely the homo- and hetero-oligomerisation of Bax and Bak.

This characterisation was initiated in order to investigate if pro-survival proteins could perturb Bax activation in a way making them suitable for use in live cell experiments. The results obtained suggest that BHRF1 would be of little help, since it entirely prevents Bax activation. However, E1B19k-expressing cells still show evidence of Bax translocation to mitochondria and N-terminal conformational activation, and importantly this occurs at the same rate as in wild type cells. This result indicates that the apoptotic signalling events that lead to these initial steps in Bax activation remain unopposed in the E1B19k cells. Rather, the block to cell death acts at a later step, by preventing subsequent oligomerisation of the protein. Since Bax activation is a very rapid event, this ability of E1B19k to separate the initial from the subsequent steps in this process and thereby keep the cells alive, would be interesting to investigate in real time. However, to use E1B19k to manipulate Bax activation in live cell experiments it is first important to determine that over-expressed GFP-Bax can be blocked in an analogous manner to the endogenous protein.

4.4 Activation of GFP-Bax can also be blocked by E1B19k:

In order to determine whether E1B19k could also block GFP-Bax activation, MCF10A E1B19k cells were transfected with GFP-Bax and treated with Fas/CHX to induce apoptosis. The cells were then fixed and stained with anti-Bax N20, to monitor Bax activation status, and anti-Cyt-c, to monitor mitochondrial dysfunction. Examination of these cells by confocal microscopy showed that the majority of the transfected cells either retained cytoplasmic GFP-Bax, indicating the protein was not active, or had already progressed into full apoptosis with cells present at various stages of death containing the characteristic bright punctate foci of fully active Bax (data not shown). This result was a likely reflection of the total level of Bax in the transfected cells simply overwhelming the ability of E1B19k to provide an efficient block to Bax activation. There were, however, a few cells in which over-expressed GFP-Bax appeared to become blocked in an analogous fashion to the endogenous protein, representative examples of the situations observed are shown in Figure 4.9: following 8 hrs of exposure to Fas/CHX many of the untransfected cells stained positively for Bax N20 (Figure 4.9 A, label a), indicating the initial N-terminal conformational activation of Bax had taken place. These cells show the characteristic even distribution of Bax at mitochondria, without Cyt-c release, characteristic of E1B19k-blocked cells, as described in the pervious section. A few cells had yet to initiate Bax activation, and did not stain with Bax N20 (Figure 4.9 A, label b). In cases where these cells are

also transfected with GFP-Bax, the tagged Bax also remains cytoplasmic (Figure 4.9 A, label c). In a few cells, GFP-Bax appeared to have become highly enriched at the mitochondria. These cells also showed strong mitochondrially localised anti-Bax N20 staining and mitochondrial Cyt-c (Figure 4.9 A, label d). In these cells the exogenous GFP-Bax appeared to have been blocked in a similar fashion to endogenous Bax was being blocked in the majority of surrounding untransfected cells.

In some cells additional distributions could also be observed. Sometimes the E1B19k block to GFP-Bax activation appeared to have formed but subsequently breached, resulting in the release of Cyt-c. This is shown in Figure 4.9 B, compare cell a, in which the block is fully formed with complete depletion of GFP-Bax from the cytoplasm onto the mitochondria, with cell b, where the block appears to have formed and subsequently breached, resulting in the partial release of Cyt-c. There were also occasional examples where the block appeared to be partially or incompletely formed. This is shown in Figure 4.11 C: compare cell a, in which the block appears to be incompletely formed with only partial depletion of cytoplasmic GFP-Bax onto the mitochondria, with cell b, where the block appears to have been beached with bright foci of GFP-Bax visible and Cyt-c full released.

This experiment confirmed that, following the induction of apoptosis, E1B19k could block GFP-Bax at mitochondria in an analogous manner to the endogenous Bax protein. From data presented in Figure 4.6 and 4.7, characterising this block using a Bax conformationally sensitive antibody, it was not possible to know what fraction of the total cellular pool of Bax had become active and translocated to mitochondria. The use of GFP-Bax reports on that entire cellular pool and demonstrates that in a cell where the E1B19k block to Bax activation has stably formed there is almost complete depletion of the cytoplasmic pool of GFP-Bax to mitochondria. This distribution therefore clearly differs from partial mitochondrial enrichment of GFP-Bax seen in wild type cells following a UV stress trigger (Figure 3.6). It was next important to characterise how this block arose.

4.5 Characterisation of the E1B19k block to GFP-Bax activation in live cells:

The formation of a complete and stable block to GFP-Bax activation is E1B19k-expressing cells was not a common event. In Fas/CHX treated cells it occurred in about 1 in 30 transfected cells examined. However, this was deemed sufficiently frequent to attempt to record the block forming in live cells and thereby determine how the kinetics compared to that of full GFP-Bax activation in wild type cells. To this end, live cell microscopy recordings were made of GFP-

Bax transfected MCF10A E1B19k cells, loaded with TMRE to reveal the location of energised mitochondria and treated with Fas/CHX to induce apoptosis. Figure 4.10 and Supplementary Movie Figures M4.1 (short record) and M4.2 (full record) show a cell in which the formation of the E1B19k block was successfully captured. In this example GFP-Bax is initially cytoplasmic as expected. Increased levels of GFP-Bax at mitochondria are first detectable at ~220 mins and complete at ~320 mins, giving a total duration of ~100 mins. The E1B19k-expressing cell shown in Figure 4.10 remained alive, with intact $\Delta\psi_m$, until the end of the recording, more than 11 hrs after GFP-Bax had become fully loaded onto the mitochondria (Figure 4.10 and Movie Figure M4.2). The cell shown in Figure 4.10 was one of six recorded in which GFP-Bax became fully blocked by E1B19k. Together they showed a mean duration for the complete translocation of GFP-Bax to mitochondria of 64 mins (standard deviation 26 mins). In each of these E1B19k-expressing cells the block remained intact for at least 2 hrs or until the end of recording. This rate of accumulation is substantially slower than the rate at which GFP-Bax enters the bright foci in wild type cells (compare figure 4.10 / M4.1 with Figures 3.7, 3.10 and 3.13 and their accompanying movies). In wild type cells, the bright foci of active GFP-Bax rapidly increase in size following their initial appearance, and the majority of cytoplasmic GFP-Bax appears to have entered them within 20 mins. However, exact quantitation of this process is not possible due to cell shrinkage and shape changes as apoptosis proceeds. Nevertheless, from these initial recording, it is apparent that the E1B19k block observed in fixed cells (Figure 4.9 A) is the result of a gradual enrichment of GFP-Bax at mitochondria over the course of around an hour.

As mentioned previously, GFP-Bax activation was only fully blocked at mitochondria in a low proportion of E1B19k-expressing cells; in the majority the protein became fully active. This is likely to be explained, at least in part, by the change in Bax to E1B19k stoichiometry caused by transfection. It appears that in the MCF10A E1B19k cell line there is sufficient E1B19k expressed to block activation of endogenous Bax in vast the majority of cells (Figure 4.5). It is likely that when GFP-Bax is over-expressed this is no longer the case, and the increased amount of total Bax in the cell overwhelms the ability of E1B19k to prevent its full activation. A further recording, shown in Figure 4.11 B and Supplementary Movie Figure M4.3, goes some way to confirm this hypothesis. The experimental set-up was exactly as described for Figure 4.10, however the field recorded in Figure 4.11 shows 3 transfected cells. Cell A expresses very low levels of GFP-Bax. Early in the recording GFP-Bax translocates to the mitochondria over a period of ~55 mins (frames from 230 - 285 mins), where it becomes blocked. GFP-Bax is retained in this distribution for the duration of the recording (> 6.5 hrs) with no evidence of full GFP-Bax activation or loss of $\Delta\psi_m$. Cell B expresses intermediate levels of GFP-Bax which begins to accumulate at mitochondria for ~15 mins (frames from 270 - 285 mins). At this point

the E1B19k block is becomes breached, resulting in loss of $\Delta\psi_m$, GFP-Bax entry into bright foci and apoptosis. Additional frames showing these events in more detail are included as supplementary part 4.13 C in Appendix 1. Cell C expresses the highest levels of GFP-Bax. In this case the protein immediately clusters at ~320 mins with an associated loss of $\Delta\psi_m$; there is no evidence of E1B19k retarding activation of GFP-Bax. This recording therefore supports the hypothesis that the level of GFP-Bax expression is a major determinant the ability of E1B19k to block complete Bax activation.

Further examples of GFP-Bax becoming transiently blocked in E1B19k-expressing cells, followed by the block being breached are included in Figure 4.12 and Supplementary Movie Figure M4.4. Cells were prepared and treated exactly as in Figure 4.11. In this recording Cell A forms the block for ~23 mins (frames from 221 - 244 mins) and Cell B forms the block for ~12 mins (frames from 242 - 254 mins). In each case the breaching of the block can be clearly detected by the loss of $\Delta\psi_m$ and the appearance of bright foci of GFP-Bax. Interestingly, although Cell A continues to shrink until the end of the recording, the intracellular movement of GFP-Bax loaded mitochondria freezes at ~280 mins, just as the first GFP-Bax foci first become clearly visible. This is a further indication that it is Bax oligomerisation that marks the key point at which the cell undergoes a bioenergetic death. In total, 8 cells were recorded in which the E1B19k block partially formed and was then breached. The period of GFP-Bax accumulation at the mitochondria, prior to the formation of bright clusters and loss $\Delta\psi_m$, had a mean duration of 16 mins (standard deviation 3 mins), substantially less than the ~64 mins taken for the complete block to form stably.

Examination of fixed cells had previously indicated that E1B19k could occasionally block activation of over-expressed GFP-Bax and that this resulted in its complete and stable redistribution to mitochondria. Data presented in this section demonstrates that this does indeed occur, and the distribution observed in the fixed cells is the result of steady accumulation of GFP-Bax at mitochondria over a prolonged period of time, without entry into bright foci or loss of $\Delta\psi_m$. Images from fixed samples had also suggested that sometimes the E1B19k block may partially form and then become breached (Figures 4.9 B and C). The live cell experiments presented here also confirm that this is indeed the case. In these cells in which the E1B19k block is breached there is a period during which GFP-Bax initially translocates and accumulates at mitochondria. However, before complete translocation of the protein has occurred, GFP-Bax can be seen to enter bright foci and there is a corresponding loss of $\Delta\psi_m$, indicating that the block is breached. After observing many of these recordings it became apparent that there were additional changes in the $\Delta\psi_m$ of E1B19k-expressing cells induced to undergo apoptosis that have not previously been described. These are characterised in the next section.

4.6 Spreading loss and partial recovery of $\Delta\psi_m$ in E1B19k-expressing cells:

After observing many E1B19k-expressing cells in which GFP-Bax activation was only transiently blocked, it became apparent that the breaching of this block was often accompanied by a progressive loss of $\Delta\psi_m$. Representative recordings are shown in Figure 4.13 and Supplementary Movie Figures M4.5 to M4.7. These recordings show E1B19k-expressing cells, transfected with GFP-Bax and loaded with TMRE to reveal the mitochondria. As before, the cells were treated with Fas/CHX to induce apoptosis. Both cells shown in Figure 4.13 B exhibit a partial formation of the GFP-Bax block, Cell A for ~6 mins (frames from 198 - 204 mins) and Cell B for ~14 mins (frames from 198 - 212 mins). The partially formed block is then breached and this correlates with a wave of mitochondrial depolarisation. In both cells this starts at one extremity and then progresses across the cell body. Strikingly, this is followed by a partial recovery of $\Delta\psi_m$, such that as the cells round up and detach they exhibit bright TMRE fluorescence. Additional live cell records in Supplementary Movie Figures M4.6 and M4.7 show further examples of both this spreading loss and partial recovery of $\Delta\psi_m$. In total of 52 out of 78 (67%) E1B19k-expressing cells observed (both GFP-Bax transfected and untransfected) showed evidence of $\Delta\psi_m$ recovery as described, and retained bright TMRE fluorescence as they rounded up and detached. This was never seen in wild type MCF10A cells (n = 30). A graphical representation of this phenotype is shown in Figure 4.14 A. In each case the mean integrated intensity of TMRE fluorescence was calculated for a region of interest (ROI) defined by the cell perimeter exactly at the point when GFP-Bax foci and $\Delta\psi_m$ loss were first detected (indicated by *). Due to the rapid movement of cells into and out of this ROI the traces are only accurate for a limited temporal window. Nevertheless, they show that in both wild type MCF10A (Figure 4.14 C panel i) and U20S (Figure 4.14 C panel ii) cells, the loss of $\Delta\psi_m$ was both rapid and complete. Five traces from MCF10A E1B19k cells are shown in which the initial decrease in $\Delta\psi_m$ (indicated by *) was followed by a partial recovery phase (Figure 4.14 C panel iii). Finally, in some MCF10A E1B19k cells were seen to exhibit dramatically increased rates of $\Delta\psi_m$ flickering, for example see Supplementary movie figures M4.1, M4.5 and M4.8. A particularly striking example is shown in M4.8 (panel A), with representative frames shown in Figure 4.14 B. Although dramatic, this flickering is transient and localised making it clearly distinguishable from the cell-wide loss of $\Delta\psi_m$ that accompanies apoptosis (Figure 4.14 C). As mentioned in Chapter 3, flickering of $\Delta\psi_m$ is a physiologically normal event (O'Reilly et al., 2003), although it was rarely seen in recordings made from wild type cells with an image acquisition rate of 1 frame/minute (Figure 3.12). Although flickering was easily detected in MCF10A E1B19k cells it should be noted that it was not predictive of either the initial translocation of GFP-Bax to mitochondria or its full activation (see M4.5 for example). Together the data presented in this section demonstrates that, when induced to undergo apoptosis, MCF10A E1B19k cells have

significantly different $\Delta\psi_m$ characteristics to their wild type counterparts. They show increased local $\Delta\psi_m$ flickering, a spreading loss of $\Delta\psi_m$ when cell-wide depolarisation occurs and, in two thirds of cells, there is a partial recovery of $\Delta\psi_m$ after the initial loss.

4.7 Mitochondrial ultrastructural analysis in protected MCF10A cells:

This study was initiated in order to learn more about Bax regulation by observing its activation at high temporal and spatial resolution. Data presented here (Figures 3.5 and 3.6) and elsewhere (Annis et al., 2005; Valentijn et al., 2003) demonstrate that Bax can, under certain circumstances, partially translocate to mitochondria prior to its full activation. Therefore translocation alone cannot explain activation. Data from live cell imaging experiments also demonstrated that full Bax activation could initiate in a local subcellular region and then propagate across the cell (Figure 3.9 and 3.10). This may be more easily detectable in E1B19k expressing cells when a spreading loss of $\Delta\psi_m$ was frequently observed (for examples see Figure 4.13). In addition, cells protected from apoptosis by the expression of E1B19k showed increased rates of $\Delta\psi_m$ flickering, relative to wild type controls, indicating that there may be perturbations in their mitochondrial physiology prior to Bax activation (Figure 4.14). The formation of oligomeric clusters of Bax and Bak is temporally indistinguishable from the initiation of mitochondrial dysfunction and the release of inter-membrane space proteins (Korsmeyer et al., 2000). However, taken together the observations presented above suggest that mitochondria may not function solely as passive bystanders in the apoptotic program up until the moment Bax (and Bak) become fully active and oligomerised. Instead, these data raise the possibility that Bax activation may, in fact, be influenced by the physiology or local environment of the mitochondria at which the protein becomes active.

The precise mechanism of mitochondrial dysfunction and the release of inter-membrane space proteins is still a matter of uncertainty. Swelling and rupture of the MOM has sometimes been observed in apoptotic and necrotic cell deaths (Lemasters et al., 1998; Vander Heiden et al., 1997), but the physiological relevance of this as a release mechanism has been questioned (Kluck et al., 1999). There are, however, long-standing observations that changes in mitochondrial ultrastructure occur during apoptosis (Sheridan et al., 1981). Mitochondria are highly organised organelles consisting of an outer membrane and inner membrane. The inner membrane can be categorised as either that directly facing the outer membrane, the inner boundary membrane, or the membrane that folds inwards to enclose the matrix and form cristae, the cristae membranes. A rigid baffle model of cristae structure was held in favour for many years, but recently the advent of electron microscope tomography has challenged this view and

suggests that cristae structure can be more varied (Frey and Mannella, 2000). It has also recently been suggested that ultrastructural changes in cristae morphology are required for complete and efficient release of Cyt-c (Scorrano et al., 2002). Such a mechanism is thought to be necessary since only 15-20% of Cyt-c is estimated to be in the inter-membrane space, between the mitochondrial outer and inner boundary membranes (Frey and Mannella, 2000), with the remainder sequestered in the cristae folds, which are also the principal site for oxidative phosphorylation (Gilkerson et al., 2003). Cristae junctions, where the involuted cristae membranes meet the inner boundary membrane, are suggested have a diameter of only ~28nm (Frey and Mannella, 2000). This represents a diffusion barrier effectively subcompartmentalising the cristae space from the intermembrane space (Mannella et al., 2001). High voltage electron microscopic tomography and transmission electron microscopy have been used to demonstrate that remodelling of the cristae membranes of purified mitochondria in response to recombinant tBid (Scorrano et al., 2002). These experiments were performed in mitochondria purified from Bak deficient animals, the implication being that Bax would also be absent from the mitochondria as it would been lost, along with other cytosolic proteins, during purification, although this was not explicitly demonstrated. The analysis was also performed in whole cells from Bax/Bak doubly deficient animals. In both cases this was necessary to separate a remodelling function of tBid from its role as a BH3-only protein in promoting Bax and Bak activation. The MCF10A cell system characterised in this chapter offers an alternative way to address the question of when mitochondrial ultrastructure perturbations occur in response to the induction of apoptosis, since the viral proteins E1B19k and BHRF1 potently block apoptotic signalling at different steps. Expression of E1B19k allows the initial stages of Bax and Bak activation to occur unopposed, namely mitochondrial translocation for Bax and N-terminal conformational change for both. Only the later steps involving full activation and oligomerisation are prevented. In contrast, BHRF1 expression blocks all detectable signs of Bax and Bak activation. In both of the protected cell lines, some upstream apoptotic signalling events, including the processing of full length Bid, still occur (Figure 4.3). The advantage of using viral proteins to block Bax and Bak at different steps is that the analysis can be performed in whole cells in which the Bax and Bak proteins are still present. If ultrastructural changes are a result of the Bax/Bak-mediated terminal stages of mitochondrial dysfunction they should only occur in the wild type cells. If they are related to the first activation of Bax and Bak they may also occur in E1B19k cells. However, if they are dependent on more upstream responses to the induction of apoptosis, which could include the activation of Bid, they will also occur in BHRF1-expressing cells.

To test these hypotheses, E1B19k- and BHRF1-expressing MCF10A cells, as well as the empty vector control cells, were treated with or without Fas/CHX for 12.5 hrs to induce apoptosis.

This was sufficient time to cause the initial activation of Bax and Bak in the majority of E1B19k-expressing cells (Figure 4.5), yet there were still sufficient control cells remaining adherent to make the analysis feasible (Figure 4.2). The cells were then fixed and prepared for transmission electron microscopy. After viewing mitochondria from both treated and untreated control cells, a number of structural changes in the cristae were observed following the induction of apoptosis (Figure 4.5). Mitochondria from untreated samples displayed wide mitochondria with low matrix contrast and cristae membranes forming tight parallel lines. (Figure 4.15 A, panel i). In cells treated with Fas/CHX, both moderate (Figure 4.15 A, panel ii) and severe (figure 4.15 A, panel ii) changes were observed. These were characterised by increased density of the mitochondrial matrix and ballooning of cristae membranes to create electron-transparent spaces. Occasionally, a distinctive phenotype was seen in Fas/CHX-treated E1B19k cells, which appeared to be disruption of cristae membranes, in some cases resulting in their circularisation, but without the increases in matrix contrast or ballooning described above (Figure 4.15 A, panel iv). Additionally, in necrotic cell patches, which occasionally form in over-confluent MCF10A cell culture, mitochondria were observed with a much more extreme ballooning of their cristae (Figure 4.15 A, panel v). These last two phenotypes were not investigated further since they occurred very infrequently.

An additional striking feature of the electron micrographs from the treated samples was the appearance of electron dense granules in the mitochondrial matrix, referred here as mitochondrial spots (Figures 4.15 A, panels ii and iii). It is likely these spots represent precipitates of calcium phosphate. In healthy cells, free Ca^{2+} in the matrix is substantially buffered by binding to proteins and phospholipids as in the cytoplasm, resulting in a total/free ratio of around 100. However, in the alkaline conditions of the matrix compartment (around pH 8), an additional buffering system is able to operate whereby calcium can precipitate as insoluble calcium phosphate if the concentration exceeds a few tens of micromolar (Rizzuto et al., 2004). Such precipitates have been observed in heavily damaged neuronal cells (David, 1999) but are also detectable in quickly frozen neuronal samples following brief periods of stimulation (Pivovarova et al., 1999). The existence of these precipitates is also consistent with long-standing observations that the total concentration of mitochondrial phosphate increases with Ca^{2+} uptake (Greenawalt et al., 1964) and that uptake of Ca^{2+} by isolated mitochondria is greatly increased by the presence of phosphate (Mela and Hess, 1982).

In a previous publication, describing ultrastructural remodelling of mitochondria in response to tBid, a series of categories were devised in order to classify the morphological changes (Scorrano et al., 2002). These were based on the response of purified mitochondria to recombinant tBid as visualised by high voltage electron microscopic tomography. Nevertheless,

the essential features of these categories were applicable to changes observed in fixed cells visualised by transmission electron microscopy. A similar categorisation was therefore devised based on the changes observed in Fas/CHX treated MCF10A cells. A schematic of micrographs (Figure 4.15 B) and cartoons (figure 4.15 C) illustrating the key features the Type I - Type IV categories are shown. Type I represents the distinctive pattern of tight parallel cristae membranes observed in healthy cells. The Type II category, as defined by Scorrano et. al, was further subdivided into moderate (Type IIa) and more severe (Type IIb) cristae remodelling, ballooning of crisae membranes and increased matrix density. Type III and Type IV mitochondria were those with the most severe morphological alterations, in agreement with the previous publication, such mitochondria were rarely observed. These classifications were then used to score a minimum of 40 images, each containing a different cell, from MCF10A control, E1B19k and BHRF1 cells, treated with and without Fas/CHX (Figure 4.16 A). This analysis shows that Type I cristae predominated in all the untreated samples. As expected, following Fas/CHX treatment there was substantial remodelling of the cristae structure of control cells with Type I mitochondria being largely replaced with Type IIa and Type IIb morphologies. Strikingly, in both the E1B19k and BHRF1 treated samples substantial cristae remodelling was also observed, despite the fact these cells are potentially protected from cell death. The remodelling was consistently less severe in the E1B19k cells than in the BHRF1 cells, meaning that there was a lower proportion of Type IIb in favour of Type IIa morphologies. Additionally, analysis of the median number of electron dense granules, or spots, appearing in the mitochondria of these samples was assessed (Figure 4.16 B). This showed that in all untreated samples spots were virtually absent from the mitochondrial matrix. However, following treatment with Fas/CHX they become common in all samples, with a median frequency of around 1.5 spots per mitochondrion. Data from two further replicates of this experiment were similarly quantified and showed the same results (Supplementary figures 4.16 C – E in Appendix 1).

Taken together, these results show that E1B19k and BHRF1, which potently protect against Bax and Bak activation, albeit at different steps, do not prevent the changes in mitochondrial ultrasturcture or the appearance of electron dense granules, presumed to be Ca^{2+} deposits, following the induction of apoptosis with Fas/CHX. The data is consistent with the earlier report that tBid is responsible for mitochondrial cristae remodelling since this protein is generated in response to the Fas/CHX trigger in all three of the cells lines tested (Figure 4.3). However, the additional finding that areas thought to be Ca^{2+} deposits have also increased in the treated samples indicates that the mitochondria have also responded to the induction of apoptosis by accumulating substantially increased levels of matrix Ca^{2+}. In light of these findings, it is highly

unlikely that changes in mitochondrial ultrastructure are the result of Bax and Bak activation, and are instead driven by earlier events in the apoptotic pathway.

4.8 Discussion:

The results presented in Chapter 3 indicated that Bax activation might not be a cell-wide process but instead initiate in discrete subcellular locations. Live cell recordings suggested the existence of a feed-forward mechanism whereby, Bax activation in a single location, could rapidly initiate Bax activation in adjacent subcellular regions. Preliminary experiments also indicated that there may be a gradual increase in mitochondrial Ca^{2+} in the period following the application of an apoptotic trigger, but before Bax activation. However, the extremely rapid nature and unpredictable timing of these events confounded further in-depth investigation of these findings. In order to analyse these events in more detail, an alternative approach was sought.

Bcl-2 pro-survival homologues are known to block Bax activation (Cory et al., 2003). It was therefore possible that imaging cells in which Bax activation had been blocked or perturbed might reveal more about the underlying mechanism involved in the normal activation of this protein. Four pro-survival proteins were selected for this analysis: Bcl-2, Bcl-XL, E1B19k and BHRF1. Over-expression of the two cellular proteins, Bcl-2 and Bcl-XL, offered only modest levels of protection to Fas/CHX treated MCF10A cells and were therefore not pursued further. Both viral proteins, E1B19k and BHRF1, strongly protected MCF10A cells from Fas/CHX induced apoptosis. Fas/CHX was chosen as the apoptotic trigger since it is relatively acutely acting, with the majority of control cells undergoing apoptosis within 8 - 15 hrs after its addition (Figure 4.2). In addition, as it is a trigger for the extrinsic cell death pathway, Fas has physiological relevance in respect of the protection conferred by viral pro-survival proteins since immune surveillance mechanisms in a host organism include the attack of infected cells with secreted death ligands, such as Fas, TNF-α and TRAIL. Viral Bcl-2 homologues are one line of defence employed by viruses to block death of the infected cell due to pro-apoptotic cytokines released by the host immune system. In other cellular systems, both BHRF1 and E1B19k have previously been reported to protect against activation of the extrinsic death pathway (Kawanishi, 1997; Sundararajan et al., 2001). In addition, early signalling events downstream of Fas death receptor activation are well characterised and include the processing of full length forms of caspase-8, caspase-3 and Bid which can be followed by western blotting. Strikingly, these events were unperturbed by expression of either E1B19k or BHRF1 (Figure

4.3), indicating the viral proteins intercept the apoptotic signal further downstream, at a level proximal to mitochondrial dysfunction.

Further investigation revealed that expression of BHRF1 almost completely prevented both Bax and Bak activation, as assessed by a lack of both N-terminal conformational change and oligomerisation of the proteins (Figures 4.4 to 4.8). The nature of protection conferred by BHRF1 is not currently understood. As predicted from sequence homology, the structure of BHRF1 has the same central helical pair surrounded by several amphipathic helices seen in other Bcl-2 proteins (Huang et al., 2003). However, the protein does not contain a prominent BH3-binding groove seen in the other family members and, consistent with this, is not able to efficiently bind BH3 peptides from Bax, Bak, Bad and Bid (Huang et al., 2003). In this respect BHRF1 is more similar to Bid, which also lacks a deep hydrophobic cleft (McDonnell et al., 1999). It may be that peptide-binding studies do not reflect the interactions formed by BHRF1 *in vivo*, or that BHRF1 interacts with cellular Bcl-2 by a different mechanism. For example the C-terminal sequence, not included in the published structure, may occupy the hydrophobic binding cleft of other family members. Nevertheless, BHRF1 may also have a distinct anti-apoptotic function, independent of its binding to other BH3-containing proteins. On the basis of mutational studies such a role has also been proposed for Bcl-XL (Minn et al., 1999). In this respect, it was interesting that BHRF1 was also seen in high molecular weight fractions of ~670 kDa by gel filtration (data not shown), as has been observed previously for Bcl-XL (Antonsson et al., 2001). Determining the composition of such complexes could provide important insights into the pro-survival mechanisms of Bcl-2 family proteins.

Like BHRF1, expression of E1B19k also potently protected MCF10A cells from Fas/CHX induced apoptosis. However, further analysis revealed that in these cells the N-terminal activation of both Bax and Bak, and the translocation of Bax to mitochondria, still occurred (Figures 4.4 to 4.9). Strikingly, at the population level, these events took place at the same rate as in the control cells (Figures 4.4 and 4.5), indicating upstream apoptotic signalling events were reaching Bax and Bak unopposed. At the single cell level, Bax and Bak N-terminal activation still appeared to be an all-or-none event, similar to control cells (Figure 4.5 and 4.6). However, in contrast to control cells, the conformational change in Bax and Bak did not result in the detectable formation of Bax and Bak foci by immunofluorescence (Figure 4.4 B and 4.6). Under these circumstances, N-terminally active Bax and Bak accumulated with an even distribution along the mitochondrial network, suggesting that oligomerisation of the proteins was blocked by E1B19k. This result was confirmed by the lack of Bax in high molecular weight fractions by gel filtration (Figure 4.7) and the failure of Bak to co-immunoprecipitate with Bax (Figure 4.4 A). Together these results support earlier data that showed that E1B19k blocked

Bax-Bak interactions following the infection of HeLa cells with recombinant adenoviruses (Sundararajan and White, 2001). It therefore seems likely that E1B19k has evolved to be a highly specialised inhibitor of a key checkpoint in the apoptotic pathway. Oligomerisation is likely to be the irreversible step in Bax activation, since enforced dimerisation has been shown to result in immediate mitochondrial translocation and mitochondrial dysfunction, which cannot be prevented by Bcl-XL (Gross et al., 1998). By preventing the oligomerisation of both Bax and Bak, even after their initial conformational activation, it is likely that E1B19k is targeting both the key players at the last possible step before mitochondrial dysfunction ensues. This is a powerful strategy for a viral protein in order to intercept the widest possible variety of apoptotic stimuli.

Direct interaction of Bax and E1B19k has previously been shown by yeast two-hybrid, *in vitro* binding and immunoprecipitation assays (Han et al., 1998; Han et al., 1996) and has been shown to be specific for conformationally active Bax (Perez and White, 2000). It is also known to involve the Bax BH3 domain (Han et al., 1996). The finding that E1B19k blocked recognition of Bax by an antibody spanning the Bax BH2 domain, following an apoptotic trigger, (Figure 4.8) supports an earlier finding made following the infection of HeLa cells with recombinant adenoviruses (Sundararajan and White, 2001). It could be that E1B19k also interacts directly with active Bax in this region, thereby blocking access to the antibody. Alternatively, this may indicate that the BH2 epitope only becomes exposed upon full activation. At present these two possibilities cannot be distinguished.

The finding that over-expressed GFP-Bax could also become blocked at the mitochondria in MCF10A cells expressing E1B19k (Figure 4.9) allowed a range of further experiments to be attempted. Unlike the conformationally sensitive antibodies, the use of GFP-Bax allows visualisation of the entire pool of exogenously expressed Bax, not just the fraction that had undergone a conformational change. In fixed cells, the use of GFP-Bax demonstrated that, when a stable block formed, it was the result of almost complete relocalisation of cytoplasmic GFP-Bax to the mitochondria (Figure 4.9 A). GFP-Bax also allowed the formation of the E1B19k block to be followed in live cells. This showed that the block was the result of a gradual accumulation of GFP-Bax at the mitochondria, over a substantially longer period than it took to enter the bright foci in wild type cells (Figure 4.10). However, the complete and stable accumulation of GFP-Bax at mitochondria was rarely observed; usually the block was partially formed and then breached, as indicated by a spreading loss of $\Delta\psi_m$ that was frequently observed (Figures 4.11 to 4.13).

The spreading of GFP-Bax activation and $\Delta\psi_m$ loss had been observed previously in wild type cells (Figures 3.9 and 3.10), and suggested a model by which Bax activation is propagated by a feed-forward mechanism. This would consist of the protein first becoming active in a discrete subcellular region (local activation). The first pool of active Bax then triggers Bax activation in neighbouring sub-cellular regions, thereby resulting in the rapid propagation across the cell (cell-wide or global activation). Such a mechanism would have advantages, particularly in large cells, by co-ordinating efficient recruitment of all mitochondria into the apoptotic program. However, the propagation of Bax activation, and a corresponding loss of $\Delta\psi_m$, were only observed in particularly highly polarised wild type cells and could not be demonstrated to be more generally applicable. Observations made from E1B19k-expressing cells presented above suggest that the feed-forward spreading of Bax activation and $\Delta\psi_m$ loss may, in fact, be a more generally applicable phenomenon. It could be that this process it too rapid to be reproducibly captured in wild type cells using an image acquisition rate of 1 frame/minute, except in more polarised cells where it propagates over larger distances and therefore has a longer duration. Since E1B19k is able to block GFP-Bax activation at a step subsequent to mitochondrial translocation it must provide a barrier to Bax activation at the mitochondria. If Bax becomes fully active in a local region, breaching the E1B19k block and initiating feed-forward activation, it is likely that there will be additional resistance to further Bax activation created by E1B19k at each successive mitochondrion. Whilst this might not prevent the propagation of full Bax activation once initiated, it may well act to retard it; bringing the feed-forward propagation into a temporal range more easily detected at a 1 frame/minute image acquisition rate. Direct visualisation of spreading GFP-Bax activation in E1B19k cells was complicated by the initial formation of the block during which GFP-Bax accumulates at mitochondria. This initial enrichment prevented detection of the first crucial bright foci of GFP-Bax, because they were superimposed on a background of already elevated GFP-Bax intensity. However, it was demonstrated in Chapter 3 that, in MCF10A cells expressing moderate levels of GFP-Bax, the loss of $\Delta\psi_m$ was synchronous with Bax activation (Figures 3.7 and 3.10). Therefore, detection of a spreading loss of $\Delta\psi_m$ can be considered as an indirect readout for spreading GFP-Bax activation, and thereby provides additional support for the feed-forward model of Bax activation and spreading of the apoptotic signal from a local site of initiation.

Mitochondria are known to participate in Ca^{2+} signalling (Ichas et al., 1997) and apoptotic Ca^{2+} waves have been previously reported in myocardial myotubes (Pacher and Hajnoczky, 2001). Therefore, a possible mechanism for the feed-forward propagation of Bax activation is a Ca^{2+} signal that originates from the mitochondria where Bax first becomes active and then triggers Bax activation at neighbouring mitochondria. In support of such a model, Ca^{2+} overload of mitochondria is known to promote outer membrane permeabilisation and apoptosis (Bernardi,

1999). Bax activation has also been shown to result in mitochondrial Ca^{2+} release in permeabilised cells (Carvalho et al., 2004) and, following partial irradiation, Ca^{2+} release has been observed from damaged mitochondria that is then taken up by non-irradiated mitochondria (Lum and Nagley, 2003). Although it has not been demonstrated in the present study, the MCF10A E1B19k cell system may provide a useful background in which to attempt to demonstrate the existence of a Ca^{2+} wave at the time when loss of $\Delta\psi_m$ and GFP-Bax activation propagate across the cell.

Finally, the potent ability of E1B19k and BHRF1 to block Bax and Bak at different steps was exploited to examine whether changes in mitochondrial ultrastructure that occur during apoptosis (Sheridan et al., 1981) (Figure 4.15 A) were likely to be downstream consequences of Bax/Bak mediated mitochondrial dysfunction. Electron microscopy analysis revealed that remodelling of mitochondrial ultrastructure occurred in response to treatment of the cells with Fas/CHX, independently of both Bax and Bak activation, since it was not prevented by either E1B19k or BHRF1 (Figure 4.16). This places changes in mitochondria ultrastructure in an upstream or parallel pathway to Bax and Bak activation. This result was in good agreement with a previous study showing that tBid can induce mitochondrial remodelling in a system where Bax and Bak were absent (Scorrano et al., 2002) as in the MCF10A E1B19k- and BHRF1-expressing cells, used in the present study, tBid was still generated downstream of Fas death receptor activation (Figure 4.3).

It has been shown that tBid is able promote Ca^{2+} uptake by increasing the Ca^{2+} permeability of the MOM, and may therefore accelerate progression towards Ca^{2+} overload (Csordas et al., 2002). Strikingly, the electron microscopy analysis also revealed the presence of electron dense granules appearing throughout the mitochondrial matrix in cells treated with Fas/CHX, indicative of Ca^{2+} accumulation and precipitation of insoluble Ca^{2+} phosphate salts (section 4.7). The significance of this Ca^{2+} accumulation will be discussed in more detail in Chapter 7, in relation to the findings presented in Chapter 6. For now, it is necessary to mention that these precipitates are thought to be rapidly reversible (Pivovarova et al., 1999), and therefore a prolonged period of Ca^{2+} accumulation prior to Bax activation suggests mitochondria are potentially able to release large amounts of Ca^{2+}, in the form of a propagating apoptotic wave, than would normally be the case, as mitochondria contain negligibly low levels of Ca^{2+} in healthy cells (Somlyo et al., 1979).

In summary, the data presented in this chapter supports the model of Bax activation shown in Figure 4.17. Following the induction of apoptosis by Fas/CHX, BHRF1, and by extension other Bcl-2 sequence homologues, can act to block the earliest detectable signs of Bax activation,

namely the N-terminal conformational change and mitochondrial translocation of the protein. E1B19k, however, blocks at a later step, allowing these initial changes to proceed unopposed by preventing Bax oligomerisation and ensuing mitochondrial dysfunction. Neither protein is able to block changes in mitochondrial ultrastructure or the apparent accumulation of mitochondrial Ca^{2+} following exposure to Fas/CHX. This places the mitochondrial changes in either an upstream or parallel pathway to Bax activation. Furthermore, when Bax activation does occur, it can be seen to initiate locally in a discrete subcellular region. Since Bax activation likely takes place in the plane of a membrane (Annis et al., 2005) prior changes in mitochondrial physiology are well placed to influence or even explain the initiation of Bax activation. The remainder of this thesis describes attempts made to interrogate the mitochondrial stages of Bax activation.

Figure 4.1 Generation of stable MCF10A cell lines expressing pro-survival proteins.
Pro-survival proteins: Bcl-2, Bcl-XL, E1B19k and BHRF1, or an empty vector control, were introduced into MCF10A cells by retroviral transduction. Following selection, stable expression was confirmed by analysing 1% CHAPS total cell lysates by SDS-PAGE and western blotting using antibodies to the proteins indicated. Relative levels of over-expression of the two cellular proteins, Bcl-2 and Bcl-XL, can be seen relative to their endogenous levels. Bax, Bak, Bid and Actin are shown as controls.

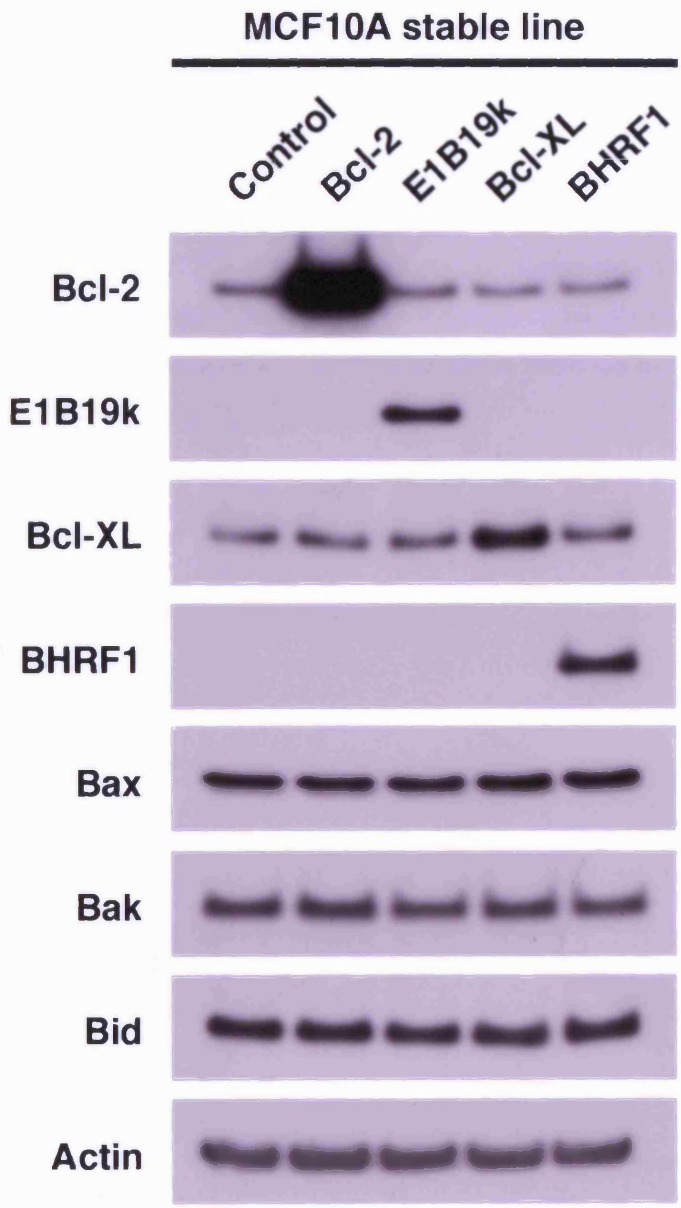
MCF10A stable line
Control
Bcl-2
E1B19k
Bcl-XL
BHRF1
Bcl-2
E1B19k
Bcl-XL
BHRF1
Bax
Bak
Bid
Actin

Figure 4.2 E1B19k and BHRF1 strongly protect against Fas/CHX induced apoptosis.
MCF10A cells over-expressing the cellular proteins Bcl-2 and Bcl-XL have modest protection against Fas/CHX induced apoptosis, but expression of the viral proteins E1B19k and BHRF1 provides a much greater level of protection. **(A)** MCF10A cells were grown in 6 cm dishes and treated in triplicate with Fas/CHX for the indicated times. To quantify the amount of apoptosis both adherent and floating cells were harvested, fixed, stained for DNA content with propidium iodide and analysed by FACS. The proportion of cells containing sub-G1 DNA content is shown. Error bars represent ± 1 standard deviation from the mean, calculated from triplicate samples; **(B)** Phase contrast images taken showing representative fields containing the cells harvested and used for the FACS analysis described in part (A).

A

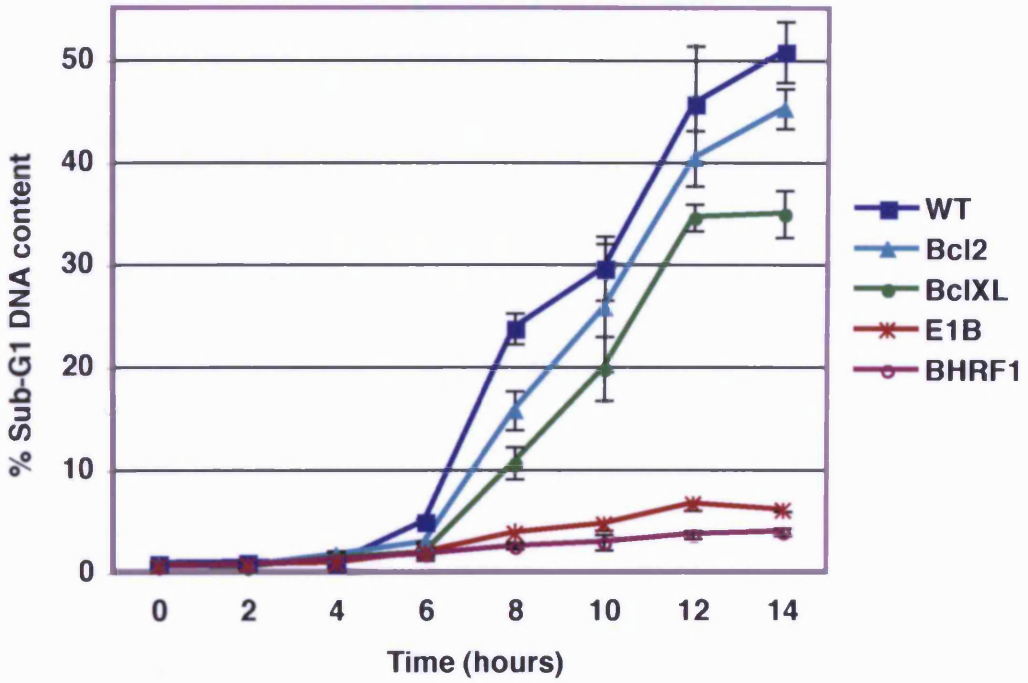
% Sub-G1 DNA content
50
40
30
20
10
0
0
2
4
6
8
10
12
14
Time (hours)
WT
Bcl2
BclXL
E1B
BHRF1

B

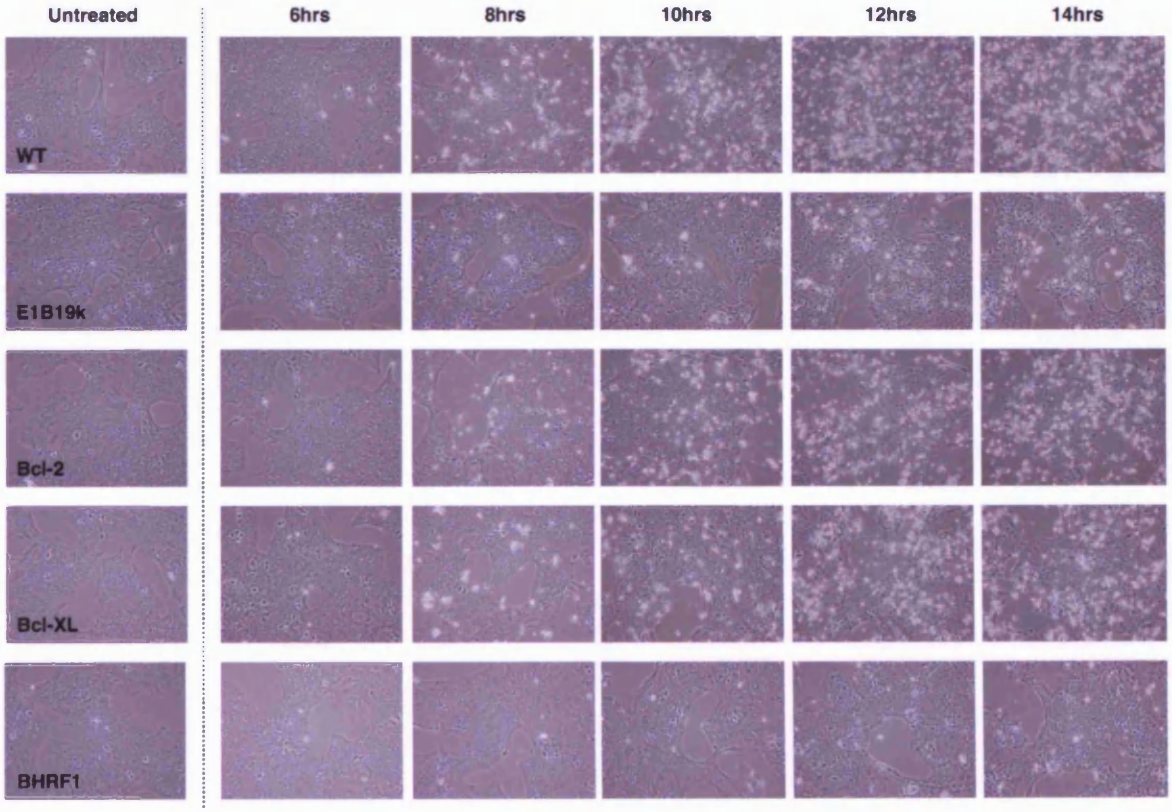
Untreated
6hrs
8hrs
10hrs
12hrs
14hrs
WT
E1B19k
Bcl-2
Bcl-XL
BHRF1

Figure 4.3 Pre-mitochondrial events occur in all cell lines whereas post-mitochondrial events are effectively blocked in the most strongly protected lines.

Western blotting analysis of well characterised signalling events in the extrinsic pathway shows E1B19k and BHRF1 effectively block events downstream of mitochondria. MCF10A cells were grown in 6 cm dishes and treated with Fas/CHX for the indicated times (0-15 hrs). Whole cell lysates were then prepared in 1% CHAPS buffer. For each time point 15 μg of total protein was analysed by SDS-PAGE followed by western blotting for the proteins indicated.

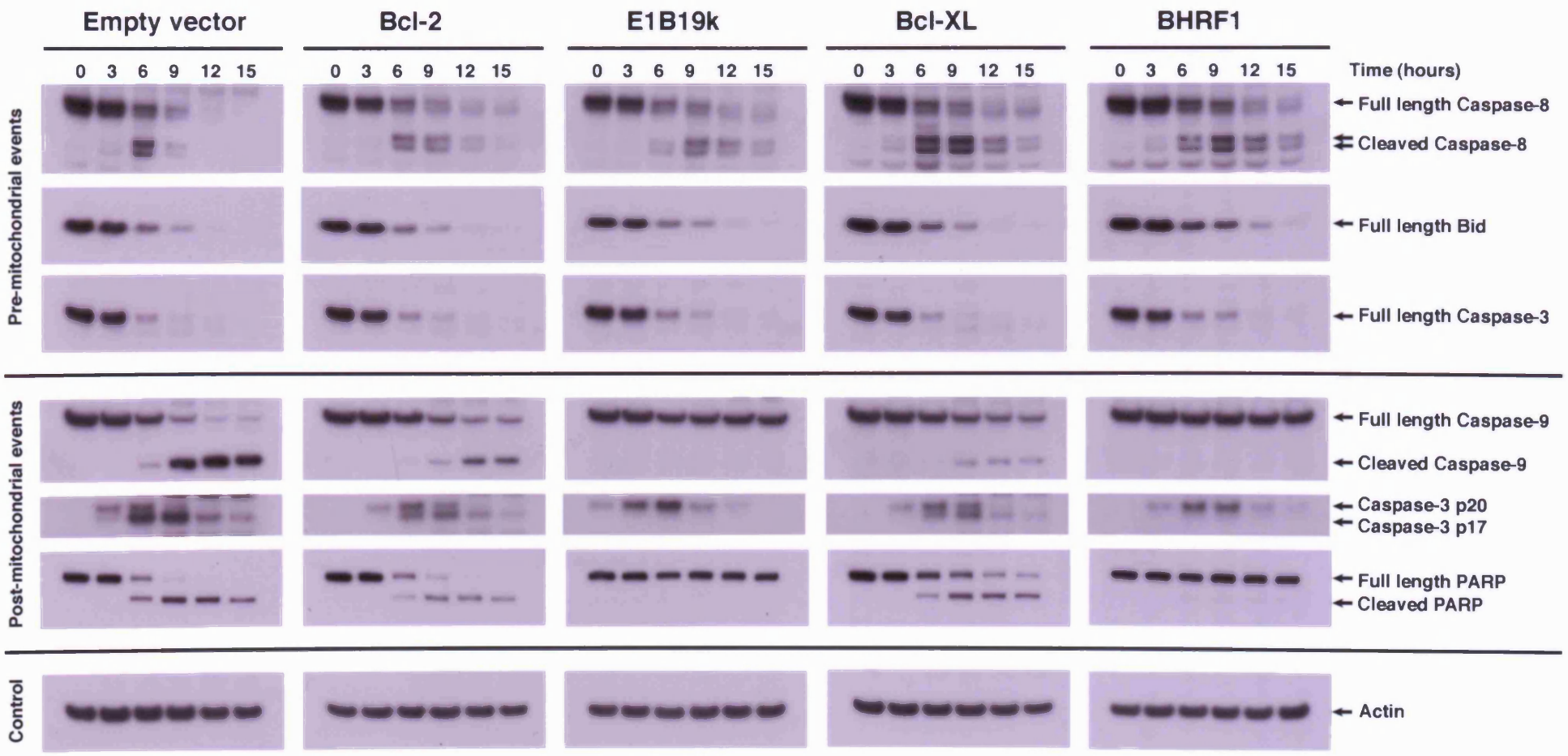
Empty vector
Bcl-2
E1B19k
Bcl-XL
BHRF1
0 3 6 9 12 15
Time (hours)
Pre-mitochondrial events
Full length Caspase-8
Cleaved Caspase-8
Full length Bid
Full length Caspase-3
Post-mitochondrial events
Full length Caspase-9
Cleaved Caspase-9
Caspase-3 p20
Caspase-3 p17
Full length PARP
Cleaved PARP
Control
Actin

Figure 4.4 E1B19k and BHRF1 differ in their ability to block Bax and Bak activation.
BHRF1 effectively blocks Bax conformational change whilst E1B19k allows Bax the N-terminal change to take place but prevents oligomerisation. **(A)** The remainder of the MCF10A whole cell lysates prepared from the experiment shown in Figure 1.5 were used in immunoprecipitation assays with agarose-coupled anti-Bax N20 (11-30) antibody. Equal fractions of the final elutate were analysed by western blotting with anti-Bax (2D2) and anti-Bak (NT); **(B)** In a parallel experiment MCF10A were grown on glass coversliips and treated with Fas/CHX for 8 hrs. Cells were then fixed and co-immunostained with anti-Bax N20 (11-30) and FITC-coupled anti-rabbit IgG (green) together with anti-Cyt-c and Cy3-coupled anti-mouse IgG (red). Cells were then imaged by confocal microscopy and representative frames are shown. Scale bars represent 10 μm.

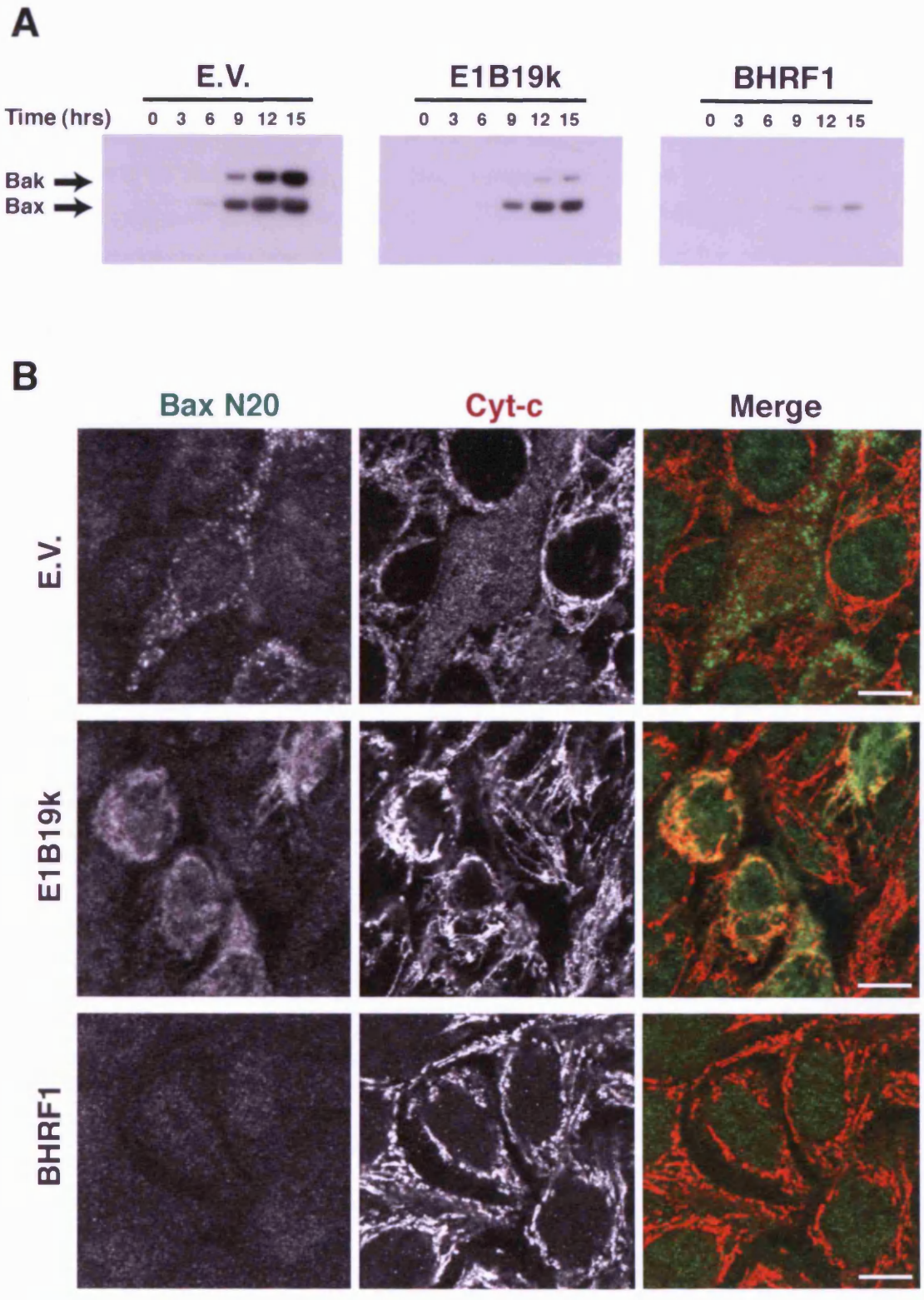
A
E.V.
E1B19k
BHRF1
Time (hrs)
0 3 6 9 12 15
0 3 6 9 12 15
0 3 6 9 12 15
Bak
Bax
B
Bax N20
Cyt-c
Merge
E.V.
E1B19k
BHRF1

Figure 4.5 The Bax conformational change takes place at the same rate in E1B19k and E.V. control cells.

E1B19k-expressing and empty vector control MCF10A cells become positive for Bax N20 (11-30) staining at the same rate, while this change is prevented in BHRF1-expressing cells. MCF10A cells were grown on coverslips and treated with Fas/CHX over a 15 hr time course. At the indicated times cells were fixed and co-immunostained with anti-Bax N20 (11-30) and FITC-coupled anti-rabbit IgG (green) together with anti-Cyt-c and Cy3-coupled anti-mouse IgG (red) before imaging by confocal microscopy. Representative frames from the 6, 9 and 12 hr time points are shown with a 3X enlargement of the indicated area from the 9 hr time point. Scale bars represent 20 μm.

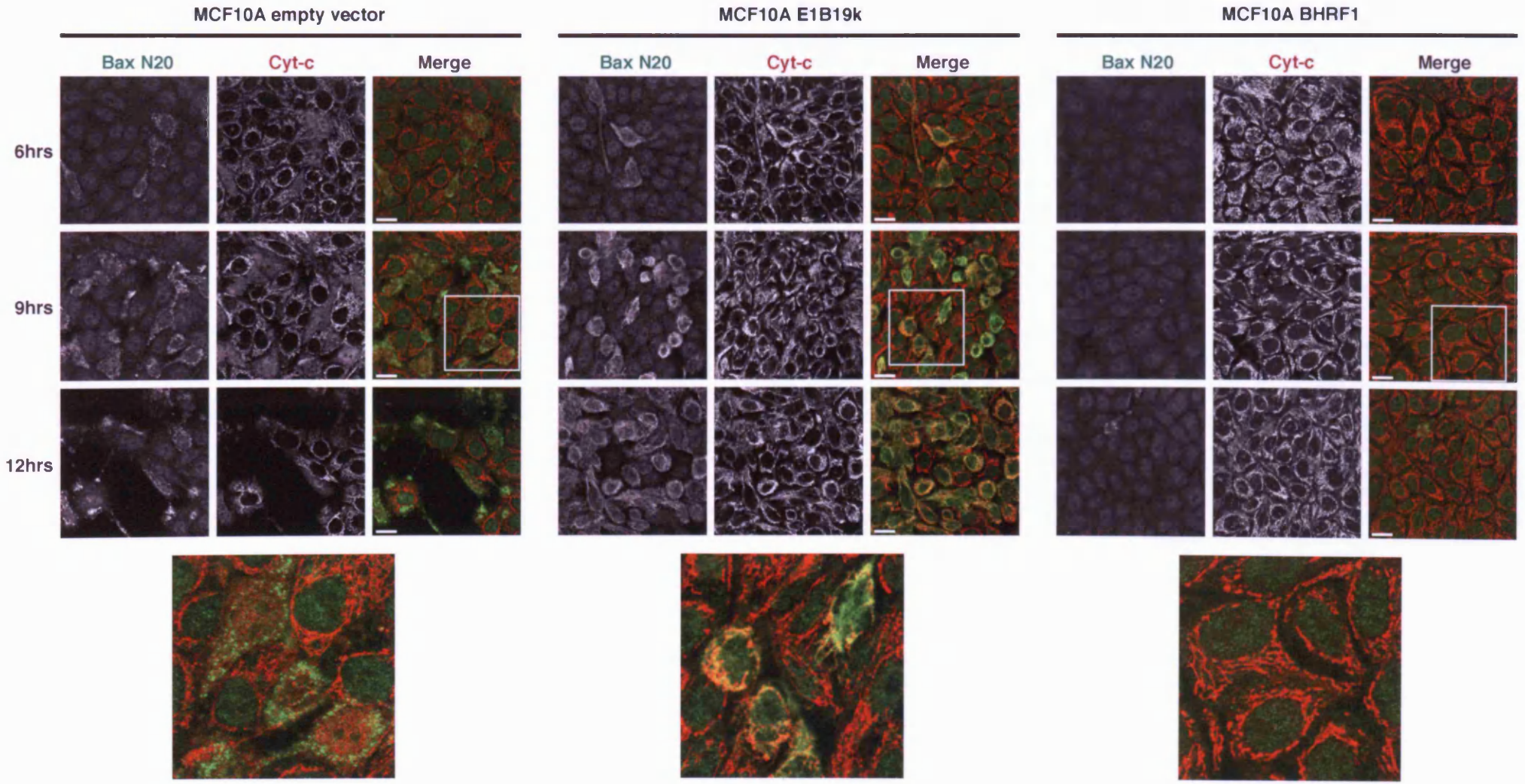
MCF10A empty vector
MCF10A E1B19k
MCF10A BHRF1
Bax N20
Cyt-c
Merge
6hrs
9hrs
12hrs

Figure 4.6 Bak conformational change is also blocked in BHRF1-, but not in E1B19k-expressing cells.

MCF10A E1B19k cells also became positive for N-terminal Bak antibody staining but showed no evidence of bright foci formation or release of Cyt-c whilst the Bak conformation change was prevented in MCF10A BHRF1 cells. MCF10A cells were grown on coverslips and treated with Fas/CHX for 8 hrs. Cells were then fixed and co-immunostained with anti-Bak NT (23-37) and FITC-coupled anti-rabbit IgG (green) together with anti-Cyt-c and Cy3-coupled anti-mouse IgG (red) and imaged by confocal microscopy. The final panel shows a 3X enlargement of the area indicated in the merged panels. Scale bars represent 20 μm.

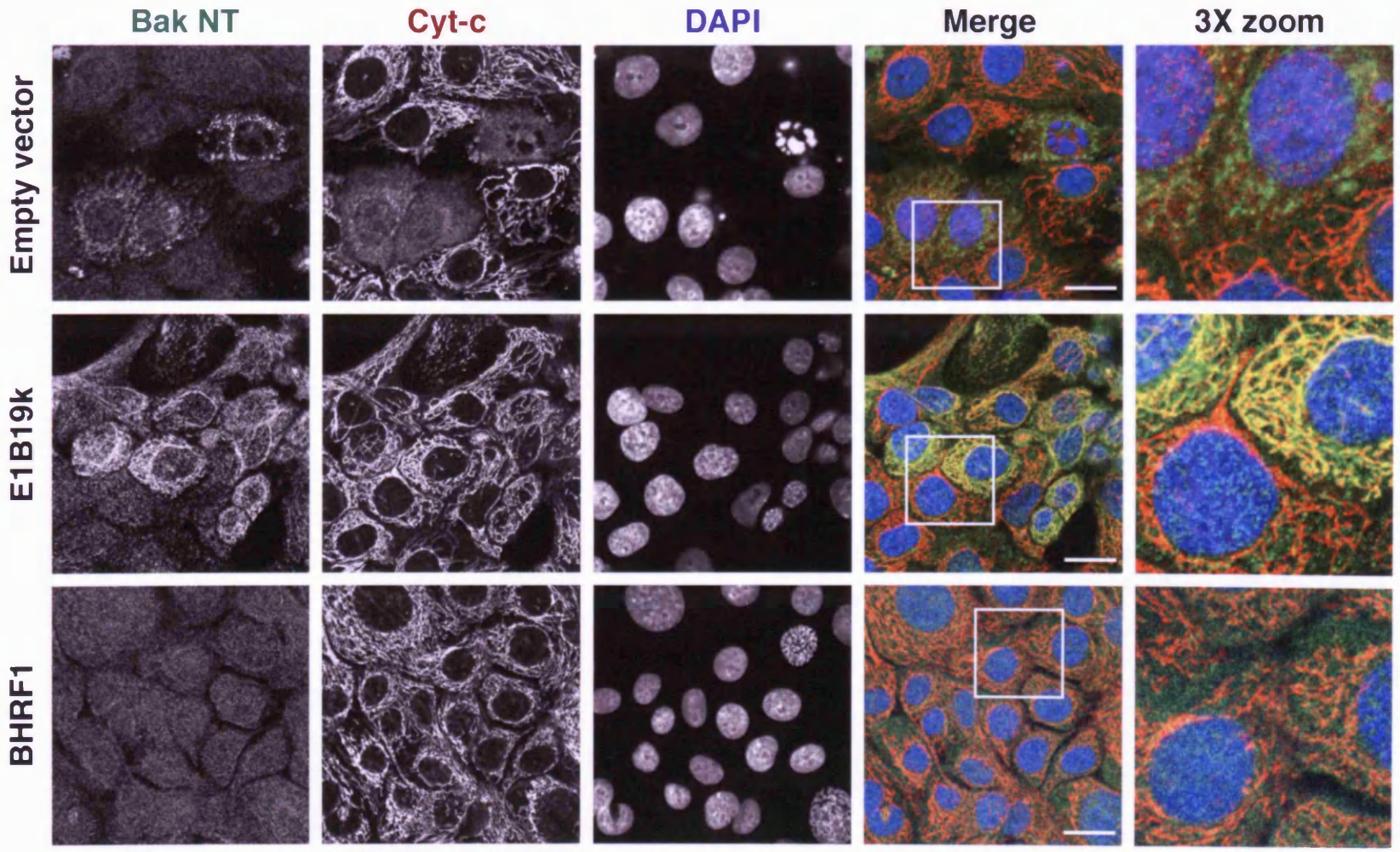
Bak NT
Cyt-c
DAPI
Merge
3X zoom
Empty vector
E1B19k
BHRF1

Figure 4.7 Gel filtration confirms E1B19k and BHRF1 block Bax oligomerisation.

Both E1B19k and BHRF1 block the shift of Bax into higher molecular weight fractions following the addition of an apoptotic trigger. MCF10A cells (empty vector control (E.V.), E1B19k- and BHRF1-expressing) were treated +/- Fas/CHX for 8 hrs and then lysed in an equal volume of 2% CHAPS lysis buffer. Samples were analysed by gel filtration followed by SDS PAGE and western blotting with anti-Bax (2D2).

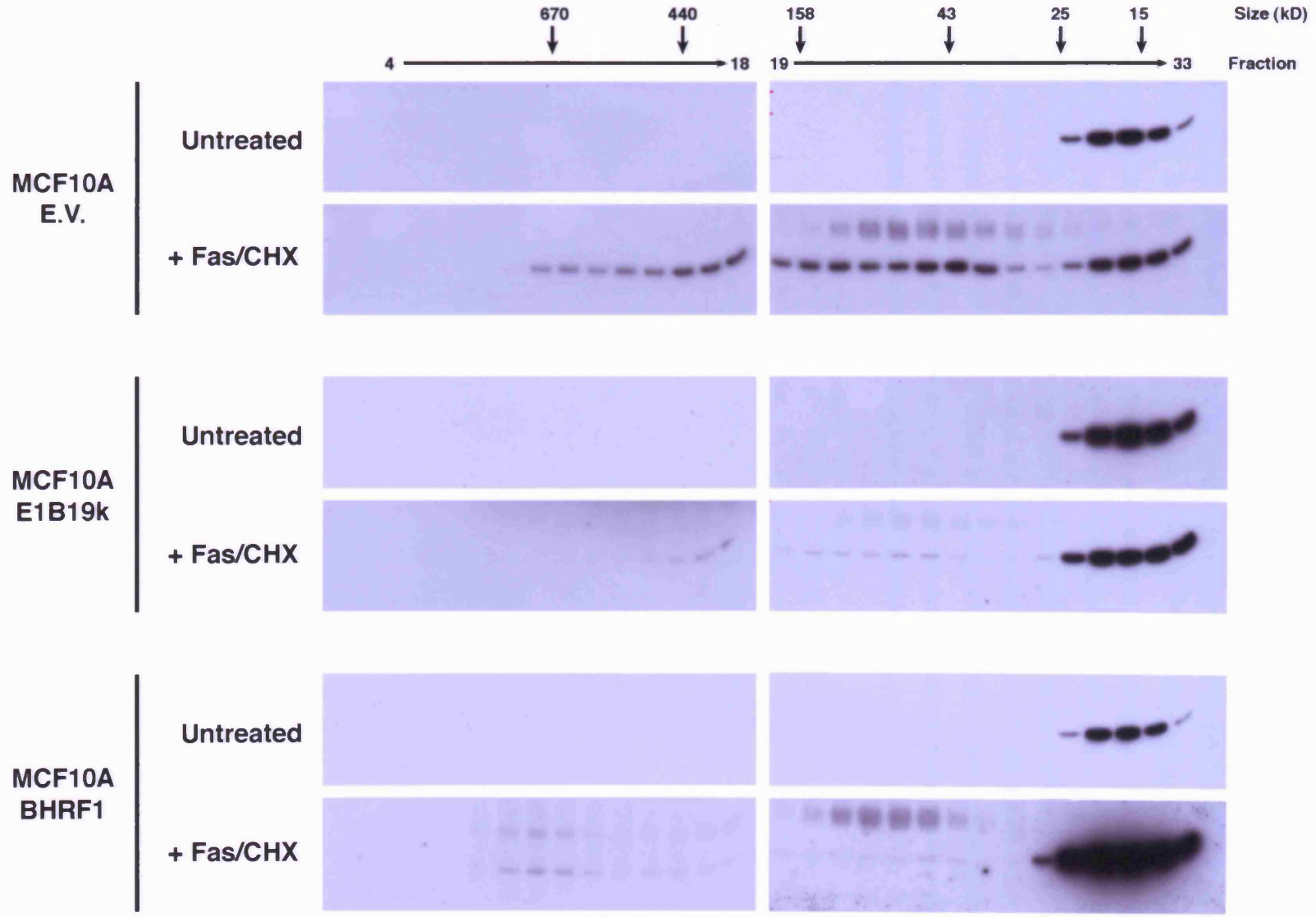
670
440
158
43
25
15
Size (kD)
4
18
19
33
Fraction
MCF10A
E.V.
Untreated
+ Fas/CHX
MCF10A
E1B19k
Untreated
+ Fas/CHX
MCF10A
BHRF1
Untreated
+ Fas/CHX

Figure 4.8 Additional biochemical characterisation of the action of BHRF1 and E1B19k.
(A) Co-immunoprecipitations using N-terminal anti-Bax and -Bak antibodies confirms neither protein is significantly activated in MCF10A BHRF1 cells following Fas/CHX treatment. MCF10A cells (BHRF1-expressing and empty vector controls) were grown in 10 cm dishes and treated + / - Fas/CHX for 9 hrs. Cells were then lysed in 1% CHAPS buffer and used in immunoprecipitation assays with anti-Bax N20 and anti-Bak NT antibodies. Equal fractions of the final eluate were analysed by western blotting with anti-Bax (2D2) and anti-Bak (NT); **(B)** MCF10A E1B19k, Bcl-2 and empty vector control cells were treated as described in part (A) and lysates used for immunoprecipitation assays with the indicated anti-Bax antibodies (N20, a7/a8 and 43-61). Equal fractions of the final eluate were analysed by western blotting with anti-Bax (2D2) and anti-E1B19k (for the N20 IP only). Lanes in the upper panel were digitally re-ordered for ease of understanding only and without further manipulation.

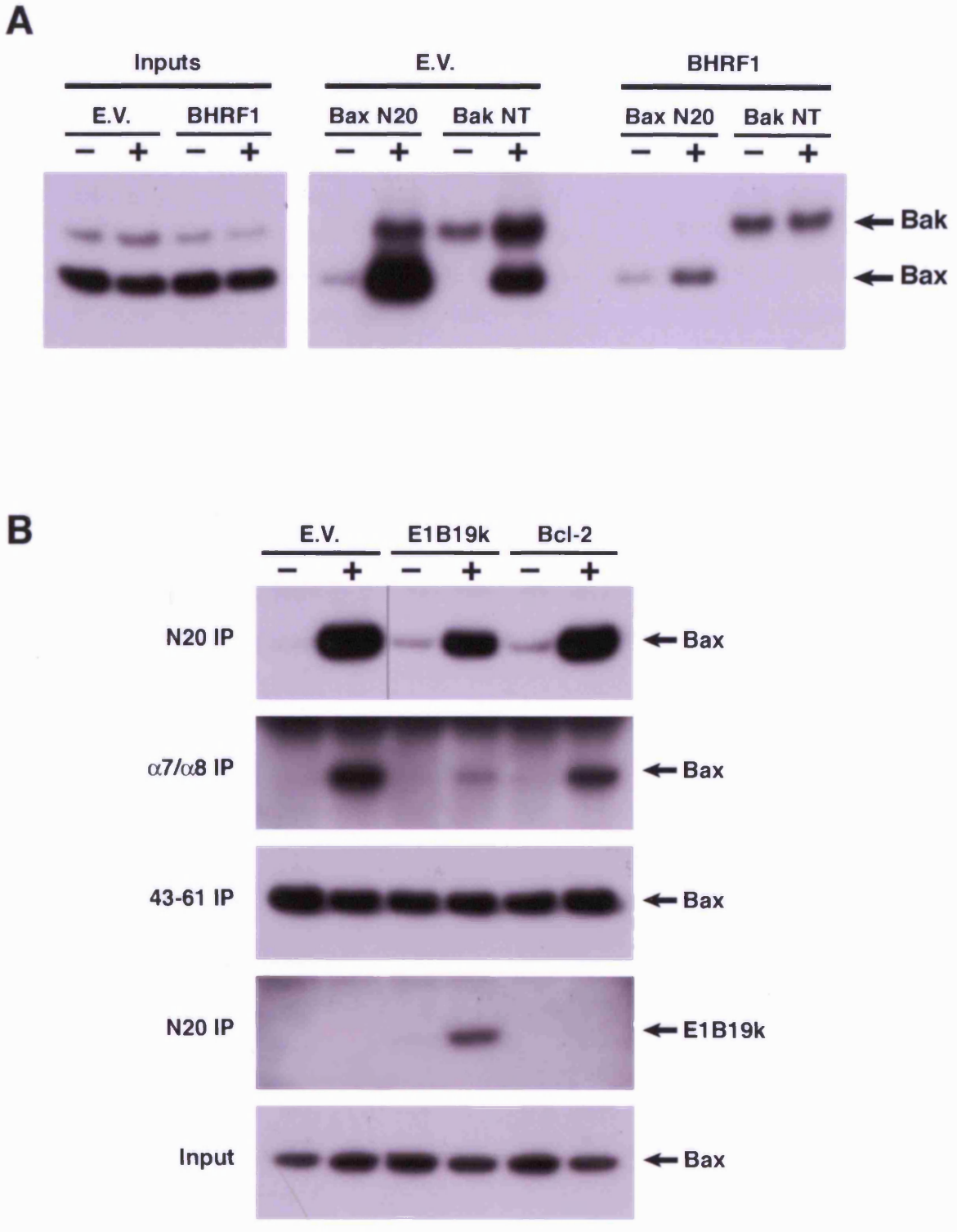
A
Inputs
E.V.
BHRF1
E.V.
Bax N20
Bak NT
BHRF1
Bax N20
Bak NT
– + – + – + – + – + – +
Bak
Bax
B
E.V.
E1B19k
Bcl-2
– + – + – +
N20 IP
Bax
α7/α8 IP
Bax
43-61 IP
Bax
N20 IP
E1B19k
Input
Bax

Figure 4.9 GFP-Bax is also blocked at mitochondria in E1B19k-expressing cells.
E1B19k can block GFP-Bax at mitochondria in the same way that endogenous Bax becomes blocked in surrounding untransfected cells. MCF10A cells were grown on glass coverslips and transfected with GFP-Bax. 24 hrs later cells were treated with Fas/CHX for a further 8 hrs. Cells were then fixed and co-immunostained with: anti-Bax N20 (11-30) and Cy3-coupled anti-rabbit IgG together with anti-Cyt-c and Cy5-coupled anti-mouse IgG. Cells were imaged by confocal microscopy. Scale bars represent 10 μm. **(A)** E1B19k can fully block GFP-Bax at mitochondria. Labels show: (a) untransfected cell with active enendogenous Bax, (b) untransfected cell without active endogenous Bax, (c) GFP-Bax transfected cell without active Bax, (d) GFP-Bax transfected cells with active Bax blocked at mitochondria; **(B)** Some cells show Cyt-c release indicating the block afforded by E1B19k has been breached. Labels show: (a) GFP-Bax transfected cell with active Bax blocked at mitochondria; (b) cell with active Bax and complete depletion of GFP-Bax from the cytoplasm to mitochondria, but also partial release of Cyt-c; **(C)** In some cells the GFP-Bax block appeared to be partially formed while in others the appearance of bright Bax foci correlated with complete Cyt-c release. Labels show: (a) GFP-Bax partially localised at mitochondria in a cell with active Bax, (b) cell with bright punctate Bax distribution and completely diffuse Cyt-c, (c) untransfected cell with active enendogenous Bax, (d) untransfected cell without active endogenous Bax.

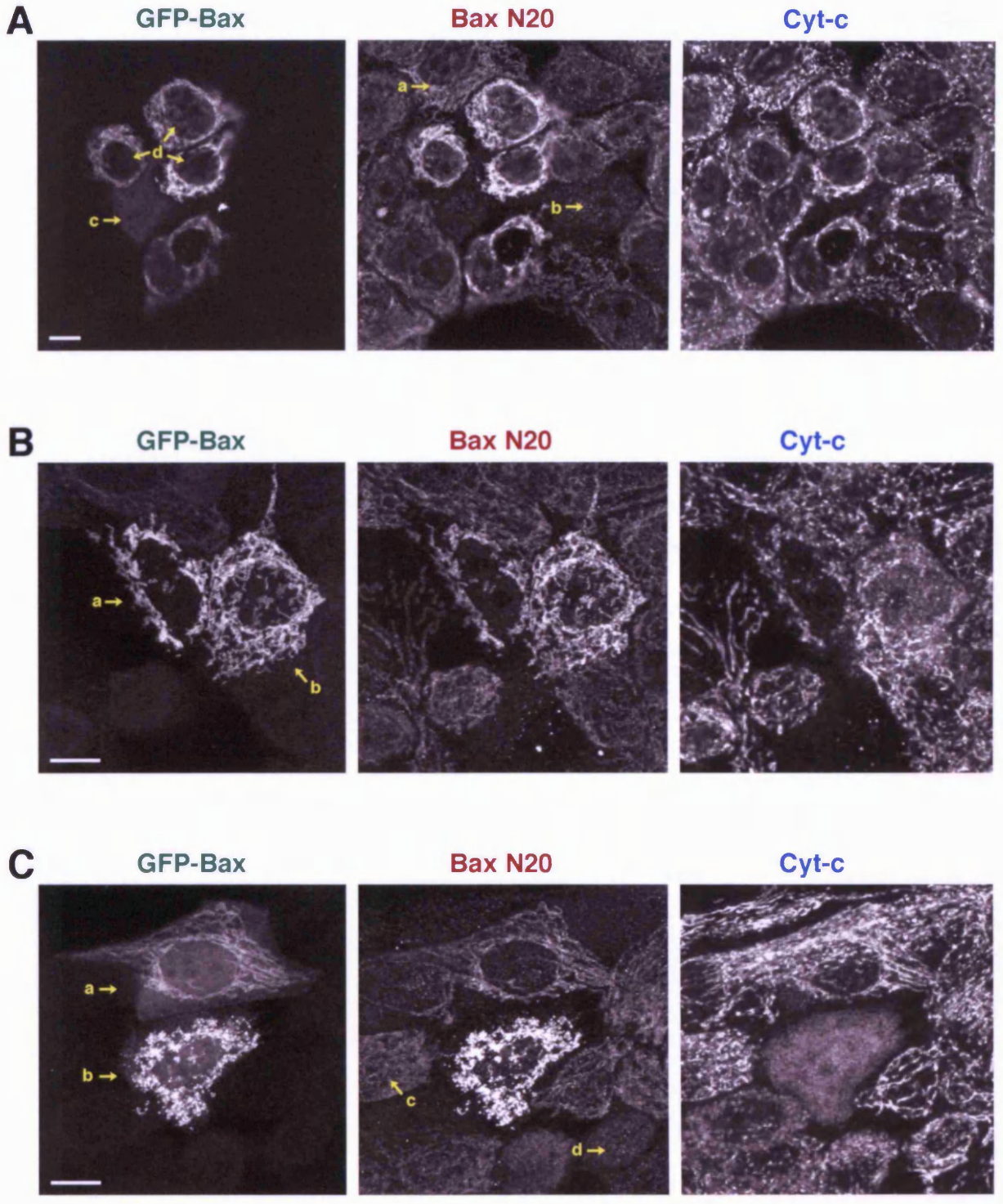
A
GFP-Bax
Bax N20
Cyt-c
a
b
c
d
B
GFP-Bax
Bax N20
Cyt-c
a
b
C
GFP-Bax
Bax N20
Cyt-c
a
b
c
d

Figure 4.10 GFP-Bax steadily accumulates at mitochondria of E1B19k-expressing cells.

In MCF10A E1B19k cells the block to full GFP-Bax activation results in a steady depletion of cytoplasmic GFP-Bax and accumulation onto the mitochondria over a much longer time frame than 5min window observed in control cells. **(A)** Live cell recording of MCF10A E1B19k cells grown in glass-bottomed dishes and transfected with GFP-Bax. 24 hrs after transfection cells were loaded with TMRE to reveal the location of energised mitochondria and then treated with Fas/CHX before being mounted for live cell recording. The image sequence presented shows representative frames extracted from the total recording. Times relate to the addition of the Fas/CHX at the start of recording. Scale bars represent 10 μm. **(B) Supplementary movie figure M4.1:** The complete image sequence from which the still frames shown in part (A) were extracted – for full details of recording see the movie figure legend. **(C) Supplementary movie figure M4.2:** An accelerated version of the recording shown in figure M4.1 documenting the persistence of the E1B19k block to GFP-Bax activation and loss for $\Delta\psi_m$ for a further 11.3 hrs until recording was ended – for full details of the recording see movie figure legend.

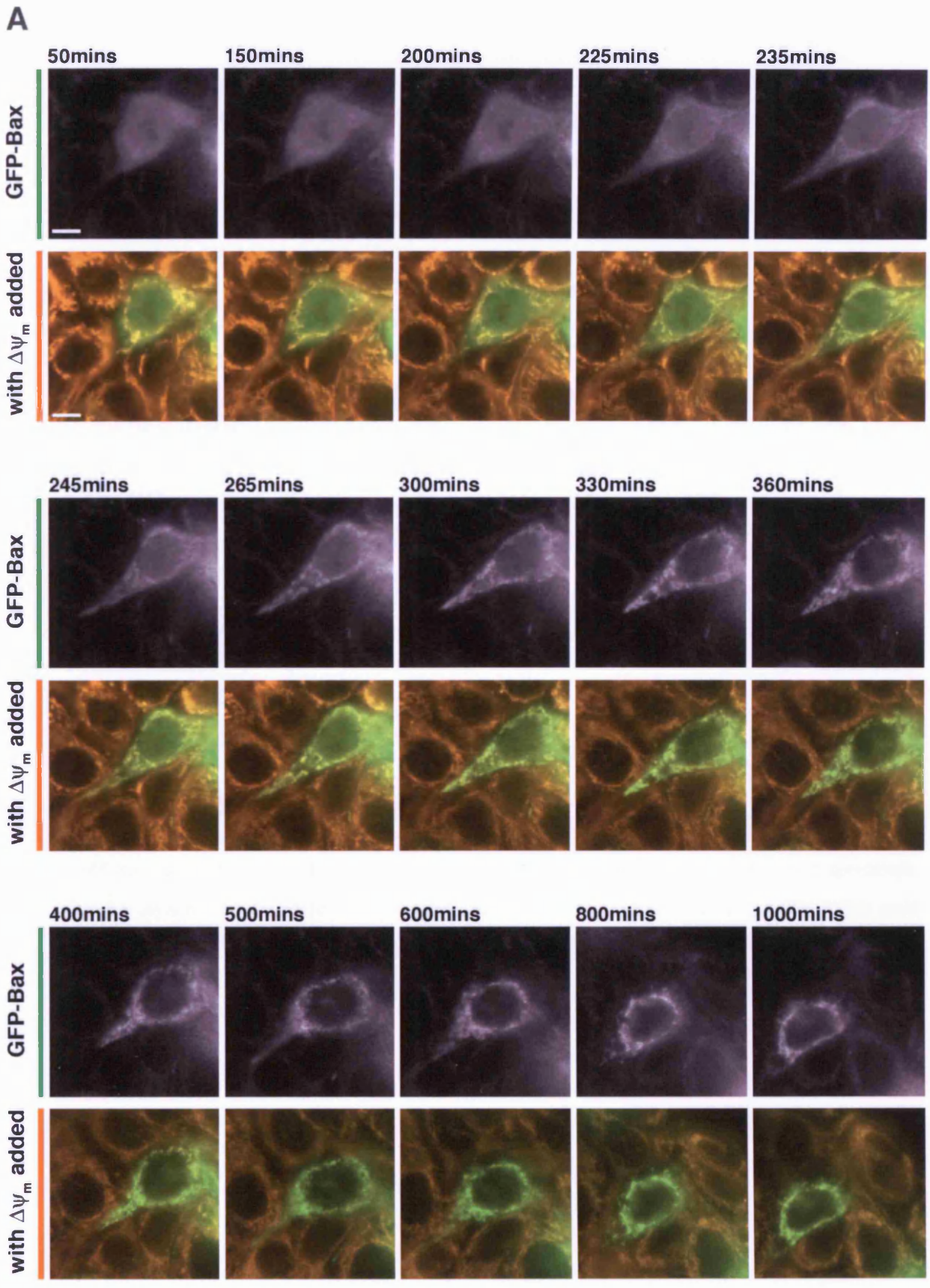
A
50mins
150mins
200mins
225mins
235mins
GFP-Bax
with $\Delta\psi_m$ added
245mins
265mins
300mins
330mins
360mins
GFP-Bax
with $\Delta\psi_m$ added
400mins
500mins
600mins
800mins
1000mins
GFP-Bax
with $\Delta\psi_m$ added

Figure 4.11 The ability of E1B19k to block Bax activation is dependent upon expression level of GFP-Bax.

The level of GFP-Bax over-expression is a major determinant as to whether the EB19k block forms successfully. **(A) Supplementary movie figure M4.3:** MCF10A E1B19k cells were grown in glass bottomed dishes and transfected with GFP-Bax. 24 hrs after transfection cells were loaded with TMRE to reveal the location of energised mitochondria and treated with Fas/CHX to induce apoptosis. Cells were then mounted for live cell recording – for full details of the recording see movie figure legend. **(B)** Representative still frames extracted from movie figure M4.3. Cell A expresses low levels of GFP-Bax and orange arrows indicate formation of the full block. Cell B is expresses intermediate levels of GFP-Bax and blue arrows indicate when the partially formed block is breached with loss of $\Delta\psi_m$. Cell C expresses the highest levels of GFP-Bax and purple arrows indicate GFP-Bax immediately entering bright foci with the corresponding loss of $\Delta\psi_m$. Times shown relate to the addition of the Fas/CHX at the start of recording. Scale bars represent 10 μm.

Supplementary material added in support: *Part 4.13 C can be found in Appendix 1 and contains additional still frames to more clearly document the partial formation and subsequent breach of the E1B19k block in cell B.*

Supplementary figure 4.13 C: *Additional still frames documenting the partial formation of the block in cell B from figure 4.13 B. Recruitment of GFP-Bax onto the mitochondria occurs from ~270 mins at ~285 mins the E1B19k block is breached, resulting in loss of $\Delta\psi_m$ and apoptosis. For full details of the recording see Figure 4.13 main legend. Additional labels in this part: Orange arrows: the E1B19k block to GFP-Bax activation beginning to form. Blue arrows: the first signs of $\Delta\psi_m$ loss and breach of the block. Green arrows: soon after bright foci of GFP-Bax become visible. Scale bars represent 10 μm.*

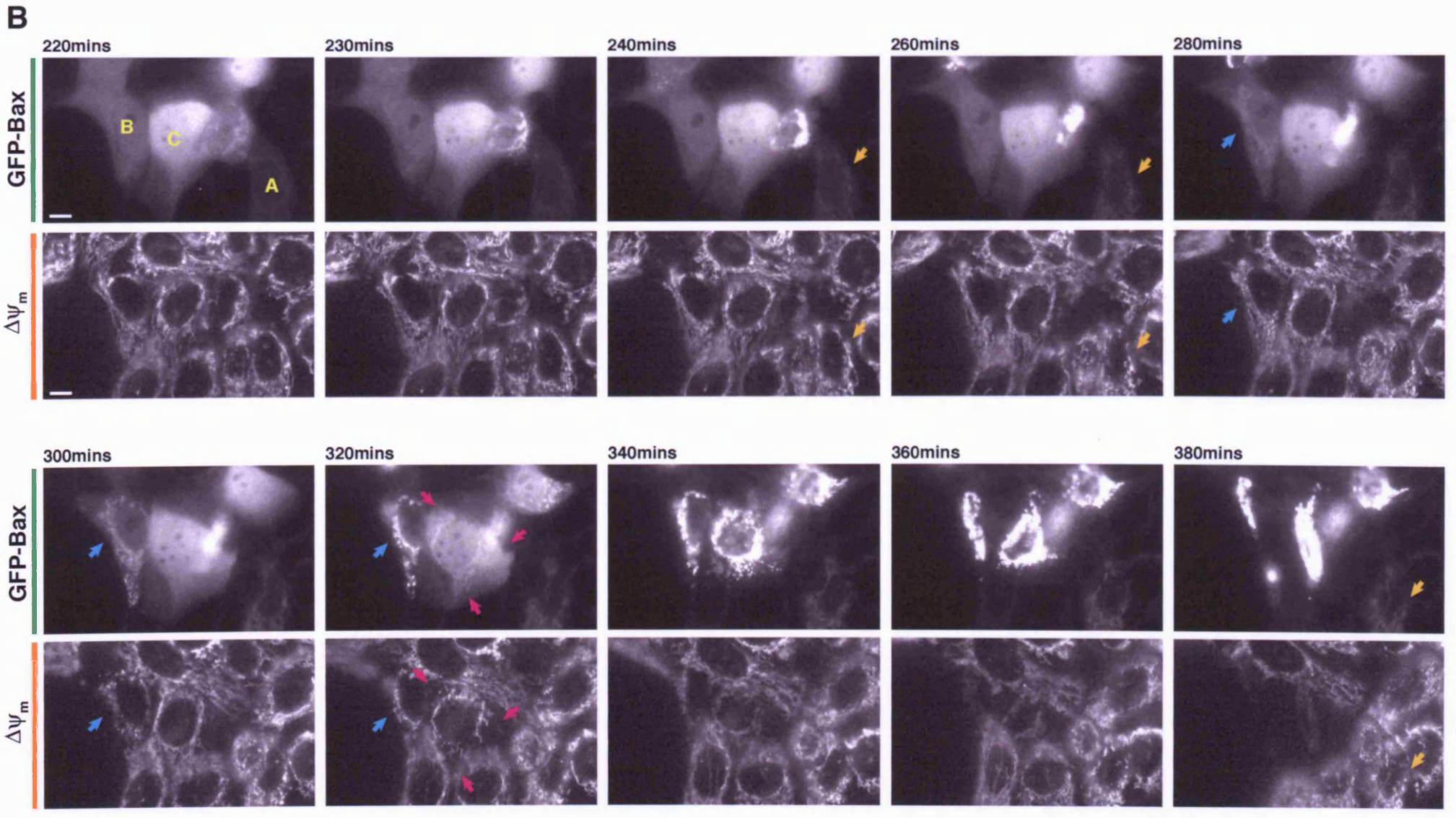
B
220mins
230mins
240mins
260mins
280mins
GFP-Bax
$\Delta\psi_m$
B
C
A
300mins
320mins
340mins
360mins
380mins
GFP-Bax
$\Delta\psi_m$

Figure 4.12 Further characterisation of E1B19k block forming and being breached.
In E1B19k-expressing cells the slow initial recruitment of GFP-Bax onto mitochondria can rapidly convert into the formation of bright foci and onset of $\Delta\psi_m$ loss. **(A) Supplementary movie figure M4.4:** Live cell recording made from MCF10A E1B19k cells grown in glass bottomed dishes and transfected with GFP-Bax. 24 hrs after transfection cells were loaded with TMRE to reveal the location of energised mitochondria. Cells were then treated with Fas/CHX and mounted for live cell imaging – for full details of the recording see movie figure legend. **(B)** Representative still frames extracted from movie figure M4.4. The E1B19k block to GFP-Bax activation first begins to form in cell A (arrow) but is subsequently breached with loss of $\Delta\psi_m$ loss from 245 mins (blue arrow). At around 280 mins bright foci of GFP-Bax become clearly visible and internal movement of structures within the cell stops (purple arrow). In cell B the first loss of $\Delta\psi_m$ at 255 mins occurs shortly after recruitment of GFP Bax to the mitochondria has begun (green arrow), and by 260 mins bright GFP-Bax foci are visible (red arrow). The times shown relate to the addition of the Fas/CHX at the start of recording. Scale bars represent 10 μm.

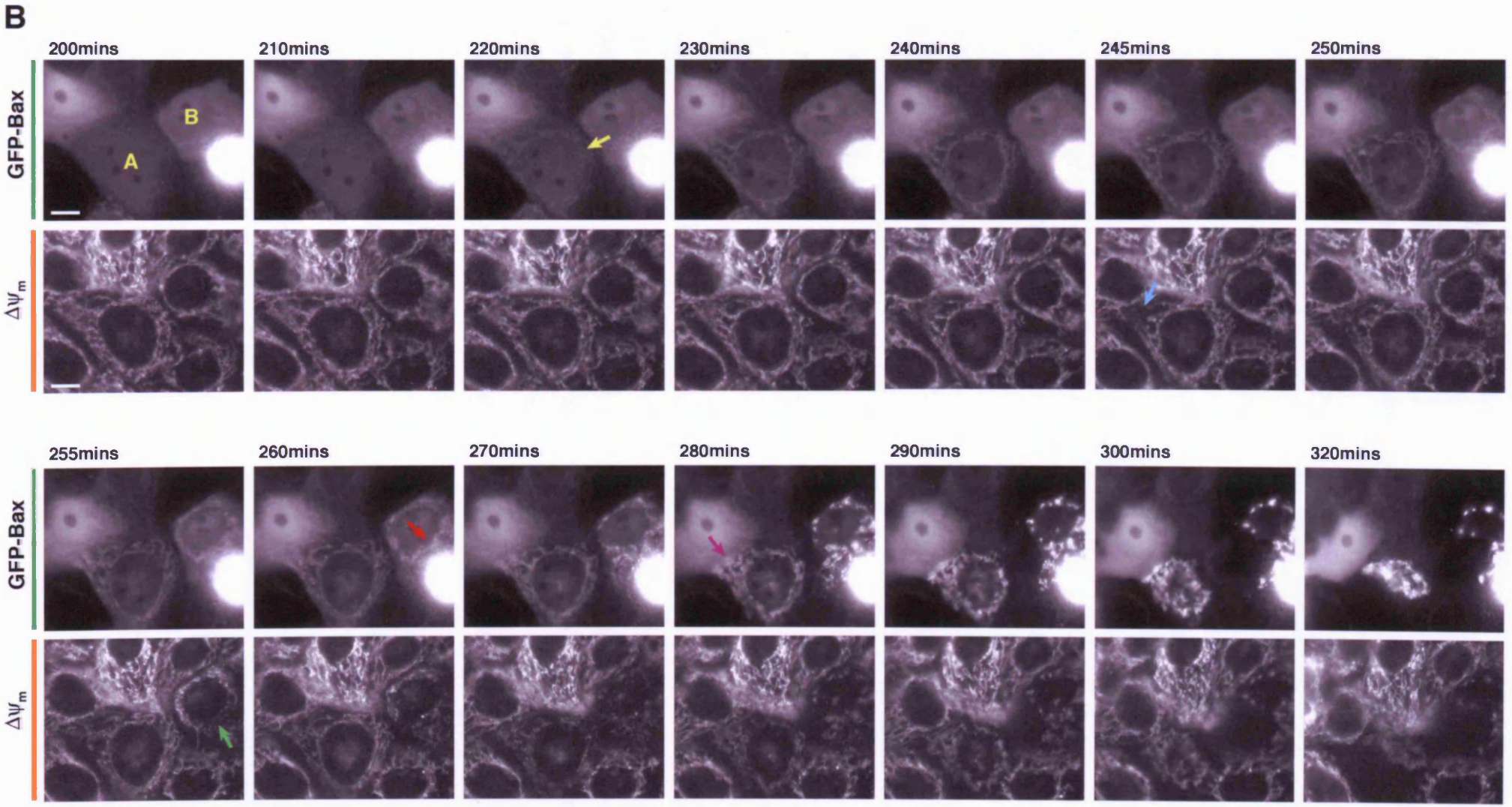
B
200mins
210mins
220mins
230mins
240mins
245mins
250mins
GFP-Bax
$\Delta\psi_m$
A
B
255mins
260mins
270mins
280mins
290mins
300mins
320mins
GFP-Bax
$\Delta\psi_m$

Figure 4.13 E1B19k-expressing cells exhibit a spreading loss followed by partial recovery of $\Delta\psi_m$.

The breaching of the block to GFP-Bax activation in MCF10A E1B19k cells often results in a progressive loss of $\Delta\psi_m$ spreading across the cell; this is sometimes followed by a partial recovery. **(A) Supplementary movie figure M4.5:** Live cell recording made from MCF10A E1B19k cells grown in glass bottomed dishes and transfected with GFP-Bax. 24hrs after transfection cells were loaded with TMRE to reveal the location of energised mitochondria. Cells were then treated with Fas/CHX and mounted for live cell imaging – for full details of the recording see movie figure legend. **(B)** Representative still frames extracted from movie figure M4.5. Cell A: GFP-Bax begins to accumulate at mitochondria (green arrow), but disruption of $\Delta\psi_m$ soon follows at ~206 mins (orange arrow) and then spreads rapidly across the cell. Cell B: disruption of $\Delta\psi_m$ begins at ~214 mins (blue arrow) and also spreads across the cell. In both cells there is a subsequent partial recovery of $\Delta\psi_m$ (for example purple arrow at 240 mins in cell B); this leads to both cells rounding up and forming corpses that retain strong TMRE staining (red arrows). The times shown relate to the addition of the Fas/CHX at the start of recording. Scale bars represent 10 μm.

Supplementary material added in support: *Movie figures M4.6 and M4.7 contain additional examples of the loss and partial recovery of $\Delta\psi_m$ in MCF10A E1B19k cells. Experimental setup was exactly as described in Figure 4.15 A.*

Movie figure M4.6: *Cell A shows cell-wide flickering (usually associated with complete loss of $\Delta\psi_m$) followed by a clear recovery which results in the dying corpse retaining bright TMRE staining; Cell B clearly shows loss of $\Delta\psi_m$ spreading across the cell – in this case there is no significant recovery after the initial loss. Parts 4.15 C and D can be found in Appendix 1 and contain representative still frames extracted from Movie figure M4.6.*

Movie figure M4.7: *Four GFP-Bax transfected MCF10A E1B19k cells illustrating several of the scenarios commonly observed: Cell A shows immediate loss of $\Delta\psi_m$ followed by a partial recovery; Cell B shows a partial block forming, followed by spreading loss of $\Delta\psi_m$ with recovery; Cell C undergoes a mitosis and then both daughter cells show loss and partial recovery of $\Delta\psi_m$; Cell D shows a spreading loss of $\Delta\psi_m$. This movie figure is not accompanied by still frames.*

Supplementary figure 4.13 C and D*: Representative still frames extracted from Movie figure M4.6.* ***(C)*** *GFP-Bax transfected MCF10A E1B19k cell exhibits whole-cell flickering of $\Delta\psi_m$ (normally associated with complete loss of TMRE staining) but then goes on to show a partial recovery.* ***(D)*** *GFP-Bax transfected MCF10A E1B19k shows a spreading loss of $\Delta\psi_m$. Times are measured from the start of the recording and do not relate to the time when Fas/CHX was added. Scale bars represent 10 μm.*

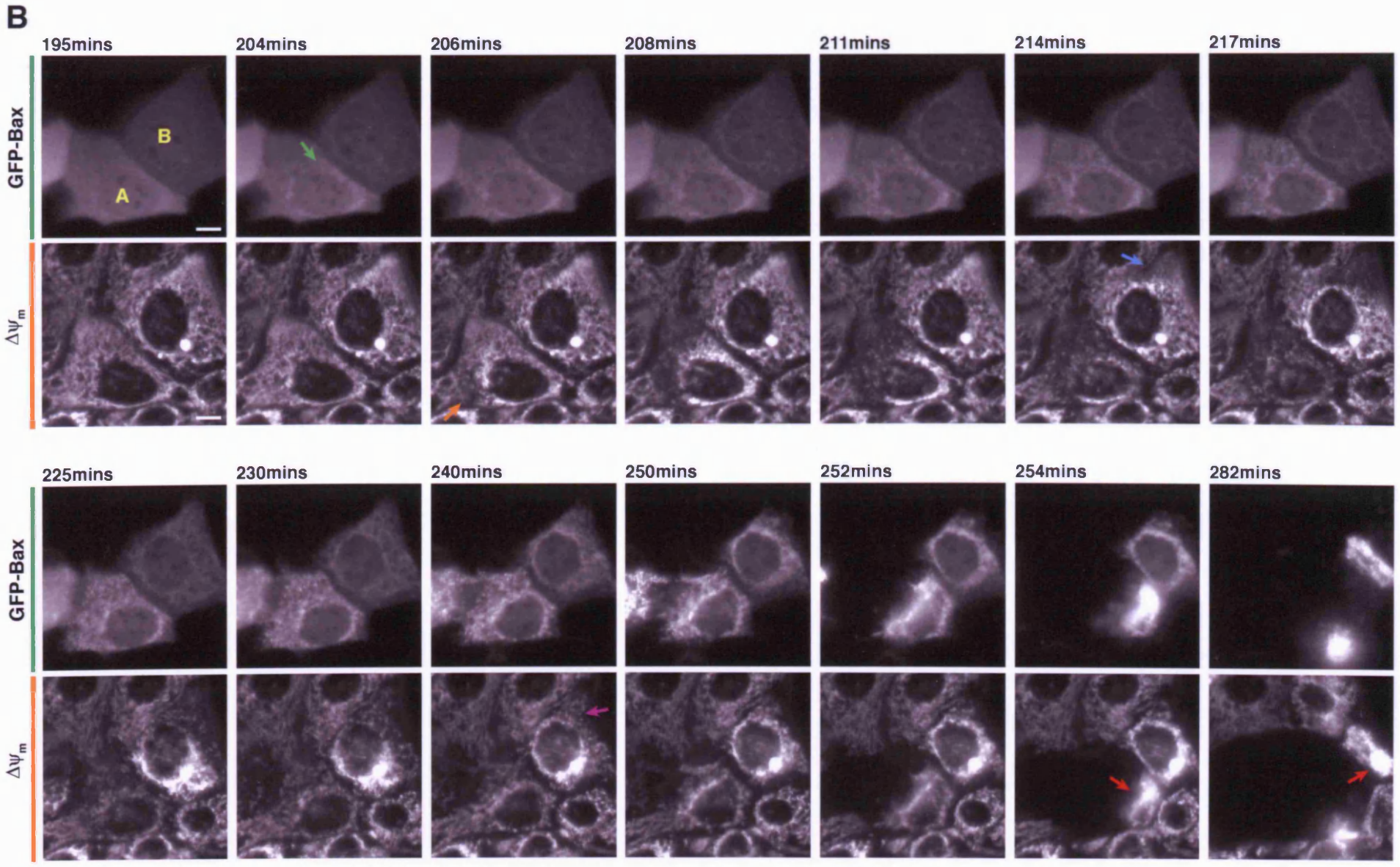
B
195mins
204mins
206mins
208mins
211mins
214mins
217mins
GFP-Bax
$\Delta\psi_m$
B
A
225mins
230mins
240mins
250mins
252mins
254mins
282mins
GFP-Bax
$\Delta\psi_m$

Figure 4.14 E1B19k-expressing cells exhibit rapid flickering and incomplete loss of $\Delta\psi_m$. MCF10A E1B19k cells, treated to induce apoptosis, show increased flickering of $\Delta\psi_m$; cell-wide loss $\Delta\psi_m$ is sometimes followed by a recovery phase. **(A)** Graphical compilation of $\Delta\psi_m$ recordings. Each trace represents the mean integrated TMRE intensity calculated from a ROI defined as the cell shape at the time $\Delta\psi_m$ loss was first detectable (indicated by *), (i) $\Delta\psi_m$ recordings from MCF10A wild type cells, (ii) $\Delta\psi_m$ recordings from U20S wild type cells, (iii) four examples of $\Delta\psi_m$ recordings from MCF10A E1B19k cells where the initial loss of $\Delta\psi_m$ was followed by a recovery. If cells have featured in previous figures in this study the figure numbers are indicated. The x-axis shows the time in minutes since the start of each recording and is scaled equally in all three graphs. **(B)** MCF10A E1B19k cells were loaded with TMRE to reveal the location of energised mitochondria, then treated with Fas/CHX to induce apoptosis and mounted for live cell recording. Representative still frames extracted from Movie Figure M4.8 (panel A) are shown as an example of the localised flickering of $\Delta\psi_m$ observed. Red arrows indicate areas where $\Delta\psi_m$ is transiently lost, green arrows indicate partial recovery. The times shown relate to the addition of Fas/CHX and start of recording. Scale bar represents 10 μm. **(C)** The same cell shown in part (B) but at later time points when complete loss of $\Delta\psi_m$ occurred. **(D) Supplementary movie figure M4.8:** The complete sequence of images from which those shown in parts (B) and (C) were extracted. The movie shows a $\Delta\psi_m$ recording from a single MCF10A E1B19k cell treated with Fas/CHX to induce apoptosis – for full detail of the recordings see movie figure legend.

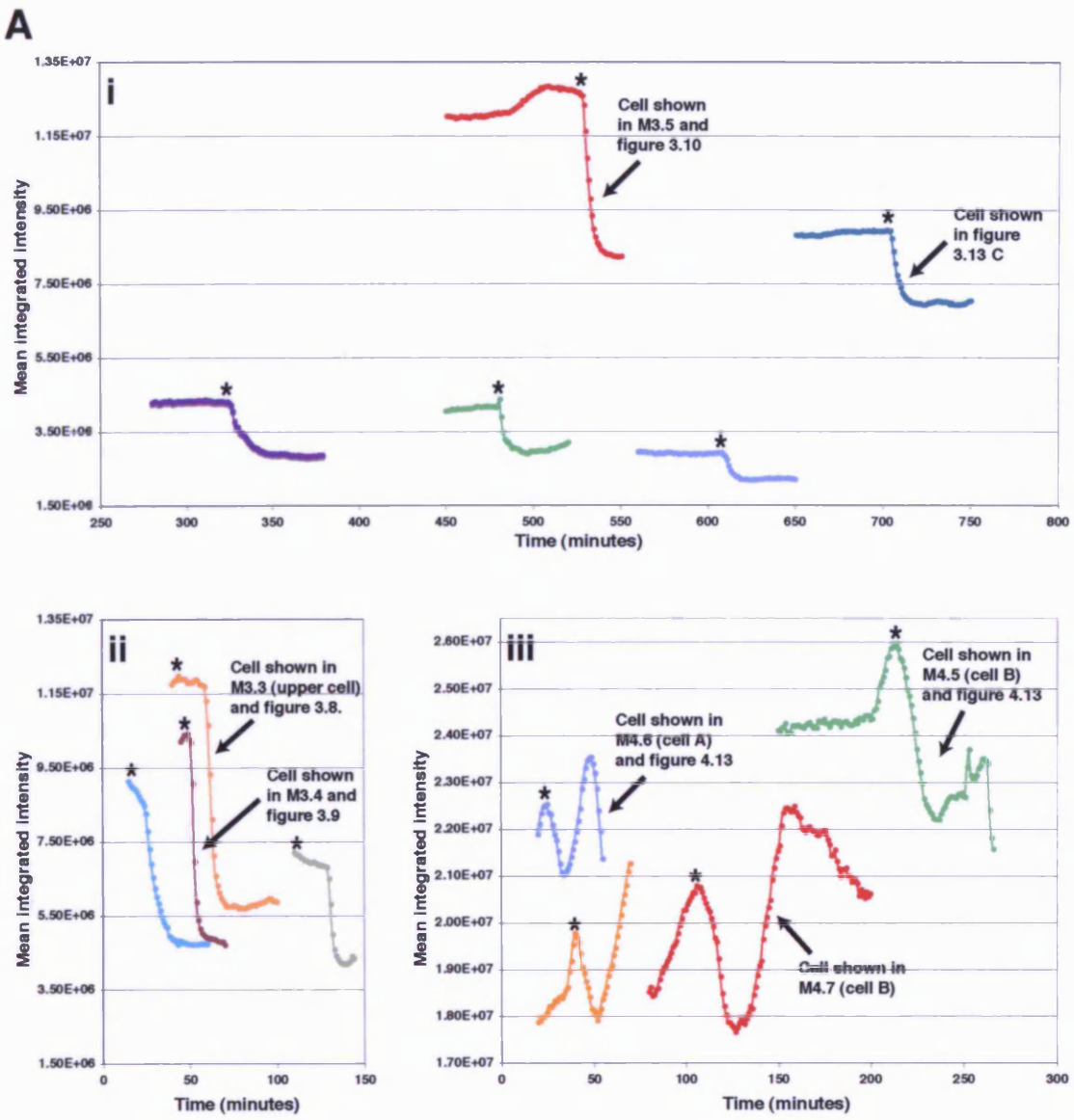
A
i
Cell shown in M3.5 and figure 3.10
Cell shown in figure 3.13 C
Mean integrated intensity
Time (minutes)
ii
Cell shown in M3.3 (upper cell) and figure 3.8.
Cell shown in M3.4 and figure 3.9
iii
Cell shown in M4.5 (cell B) and figure 4.13
Cell shown in M4.6 (cell A) and figure 4.13
Cell shown in M4.7 (cell B)
B
163mins
164mins
165mins
166mins
167mins
170mins
C
411mins
412mins
413mins
414mins
419mins
428mins

Figure 4.15 Characterisation of the changes in mitochondrial ultrastructure occurring following the induction of apoptosis.

MCF10A cells were grown on plastic coverslips and treated + / - 250 ng/ml anti-Fas IgM and 2 μg/ml CHX, in minimal media, for 12.5 hrs to induce apoptosis. Cells were then fixed and processed for electron microscopy. Representative images documenting the changes observed are shown in this figure. **(A)** Representative micrographs showing mitochondrial and cristae morphology in: (i) healthy, untreated cells; (ii) moderate morphological changes in cells induced to undergo apoptosis; (iii) more severe morphological changes in some cells induced to undergo apoptosis; (iv) an unusual morphology occasionally observed in MCF10A E1B19k cells. The mitochondrial outer membrane seems discontinuous in the plane of the image, cristae membranes remain tightly associated but become disordered and some are circularised; (v) a distinctive cristae morphology seen in patches of necrotic cells if MCF10A cells were allowed to become over-confluent; **(B)** The various morphologies seen in electron micrographs were categorised into Type I (healthy) through to Type IV (terminally disrupted). This scheme was subsequently used as the basis for the quantification of morphological changes. The scheme is based on criteria established in a previous publication (Scorrano et. al., 2002), however the Type II category is further sub-divided into IIa and IIb to reflect minor and more severe ultrastructural changes respectively; **(C)** Cartoon representations of the morphological phenotypes observed highlighting of the key features upon which each classification was based. In all electron micrographs scale bars represent 0.5 μm.

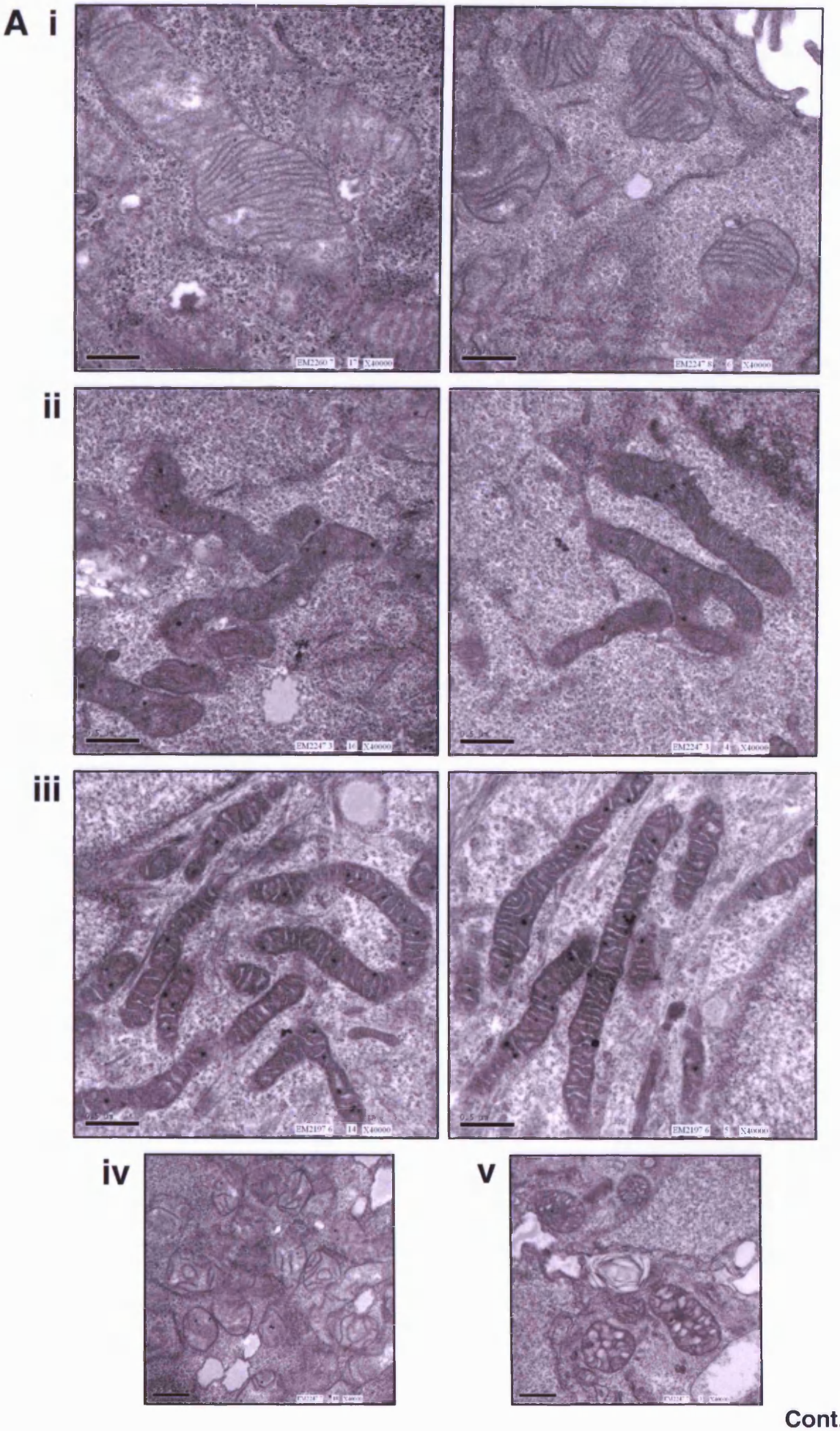

Cont.

B

Type I Normal cristae morphology in untreated cells: cristae forming tight parallel lines. No evidence of ballooning or electron dense granules.

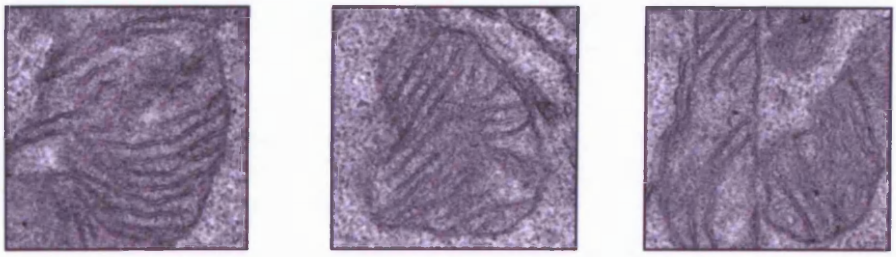

Type IIa Moderate disruption of cristae from Type I: this could be partial ballooning, disruption of regular stacking or less cristae per mitochondria. Decrease in mitochondrial width with densely staining matrix and electron dense granules.

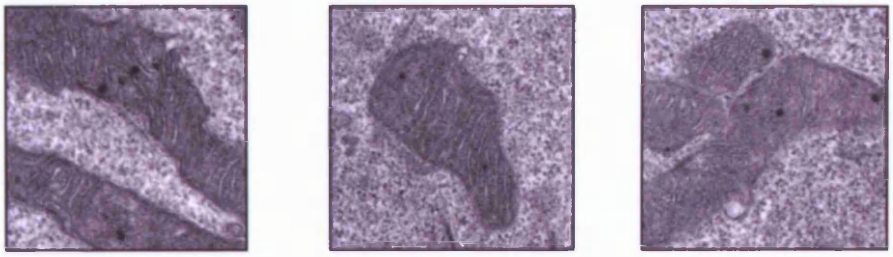

Type IIb Cristae fully remodelled. Outer membrane is still inact but internal membranes are reticularised or with completely ballooned cristae and some with open cristae necks. Matrix is densely staining with electron dense granules.

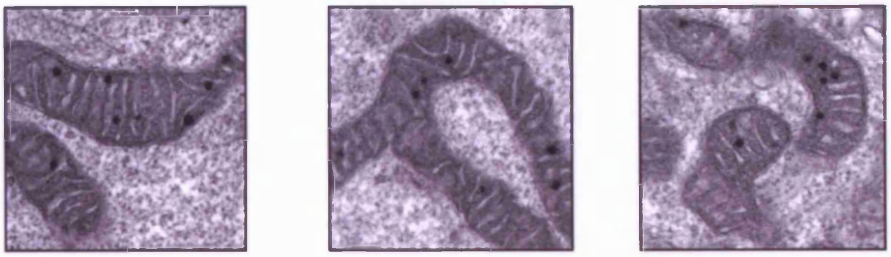

Type III Every cristae is completely ballooned with asymetric swelling.

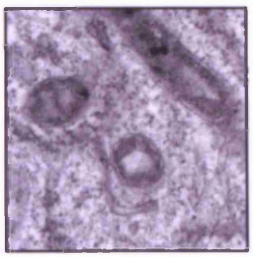

Type IV Terminal. No discernable cristae structure.

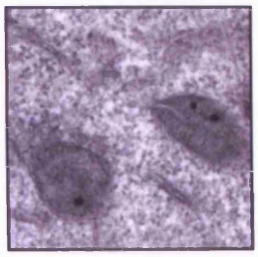

0.5μm

Cont.

C

Type I Cristae tight and parallel

Membranes slightly spaced but no evidence of ballooning

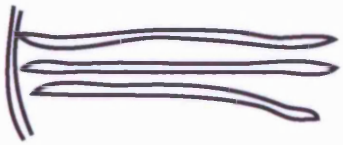

Type IIa Partial ballooning of cristae

Cristae expanded but aligned

Irregular widening

Type IIb Completely ballooned cristae

Open cristae necks

Fused & reticularised cristae

Type III Every cristae is completely ballooned

Type IV No discernable cristae structure

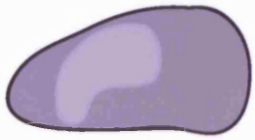

Figure 4.16 Neither E1B19k nor BHRF1 prevent changes in mitochondrial ultrastructure. Even though MCF10A E1B19k and BHRF1 cells are strongly protected from apoptosis the changes in mitochondrial ultrastructure characteristic of apoptotic cells still occur. **(A)** MCF10A cells (empty vector control, E1B19- and BHRF1-expressing) were grown on plastic coverslips and treated + / - 250 ng/ml anti-Fas IgM and 2 μg/ml CHX, in minimal media, for 12.5 hrs to induce apoptosis. Cells were then fixed and processed for electron microscopy. For example, sample 40 images were collected each representing a different cell. Changes in mitochondrial ultrastructure were quantified by classifying the mitochondria in each image according to the scheme show in Figure 1.17 B and C. The graph shows the percentage of mitochondria of each morphological class expressed as a percentage of the total number of mitochondria scored. **(B)** In addition to changes in mitochondrial morphology electron dense granules or spots appeared in the matrix of cells induced to undergo apoptosis. For each of the image sets quantified in part (A), the median number of spots per mitochondria was also calculated.

Supplementary material added in support: *Two additional data sets from replicate experiments were quantified in a similar manner and the results are included as Part 4.14 C-E and can be found in Appendix 1.*

Supplementary figure 4.14 C-E: *MCF10A cells were prepared and treated exactly as described in part (A).* ***(C)*** *and* ***(E)*** *show a similar quantification of the changes in mitochondrial ultrastructure observed in these additional data sets.* ***(D)*** *shows quantification electron dense spots appearing in the images used in (C).*

A

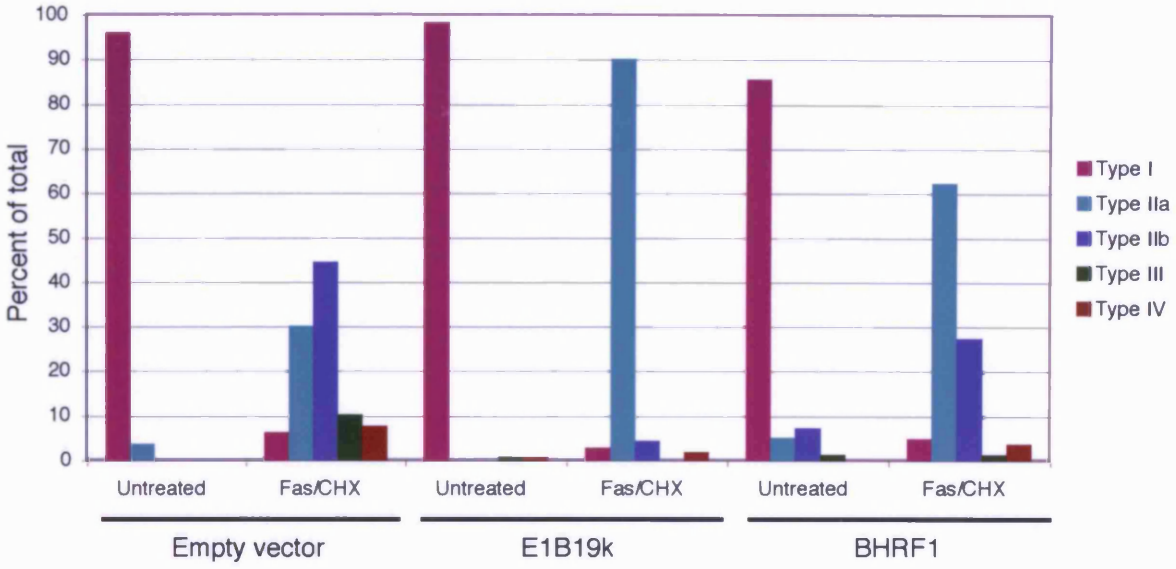
Percent of total
100
90
80
70
60
50
40
30
20
10
0
Untreated
Fas/CHX
Untreated
Fas/CHX
Untreated
Fas/CHX
Empty vector
E1B19k
BHRF1
Type I
Type IIa
Type IIb
Type III
Type IV

B

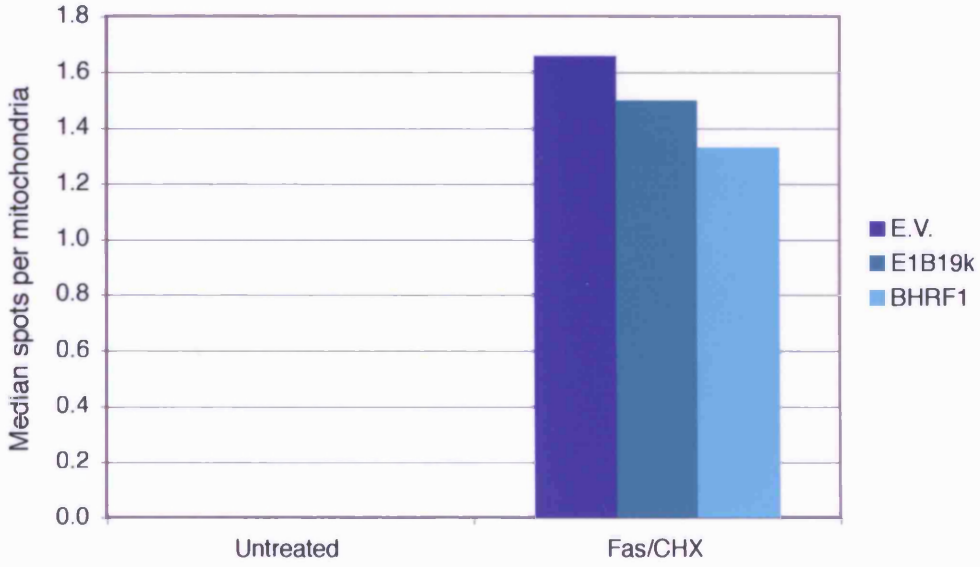
Median spots per mitochondria
1.8
1.6
1.4
1.2
1.0
0.8
0.6
0.4
0.2
0.0
Untreated
Fas/CHX
E.V.
E1B19k
BHRF1

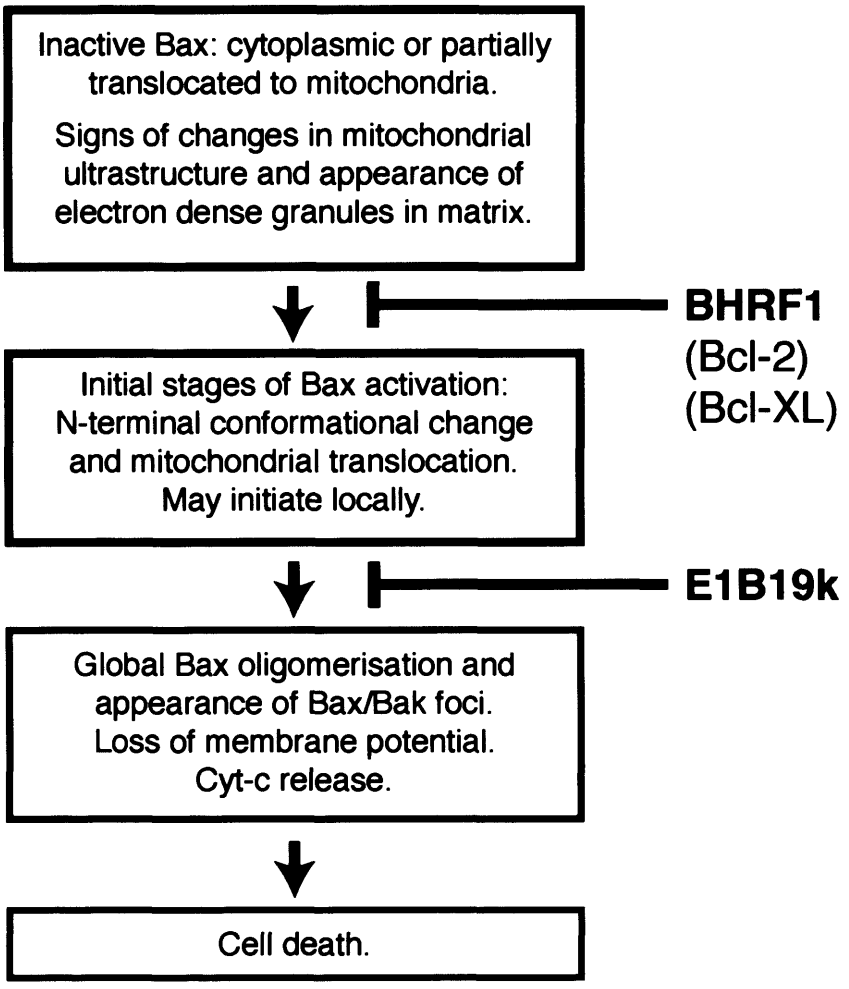
Inactive Bax: cytoplasmic or partially translocated to mitochondria.
Signs of changes in mitochondrial ultrastructure and appearance of electron dense granules in matrix.
BHRF1
(Bcl-2)
(Bcl-XL)
Initial stages of Bax activation:
N-terminal conformational change and mitochondrial translocation.
May initiate locally.
E1B19k
Global Bax oligomerisation and appearance of Bax/Bak foci.
Loss of membrane potential.
Cyt-c release.
Cell death.

Chapter 5 – Bax structure function analysis

5.1 Introduction:

Data presented in the previous chapter identifies E1B19k as a potentially useful tool with which to stabilise cells that have undergone the initial stages of Bax activation, as such cells would otherwise be rapidly lost by apoptosis. Using E1B19k to accumulate cells with active Bax may provide an entry point into a biochemical analysis of Bax at a critical step in its activation. However, before undertaking such an analysis a further problem exists: how to activate Bax rapidly and in as many cells as possible? Previous experiments in this study have, for the most part, relied upon Fas/CHX as an acutely acting and reproducible cell death stimulus; the majority of cells were induced to initiate Bax activation within 8 - 12 hrs of Fas/CHX addition. However, this was due to activation of endogenous Bax. A biochemical strategy to purify Bax without the use of multiple chromatography columns would require the expression of exogenous tagged Bax and would therefore be more analogous to the experiments using over-expressed GFP-Bax. As described in chapter 4, E1B19k only rarely blocked over-expressed GFP-Bax for a sustained period of time. In addition, the use of Fas/CHX was considered economically unfeasible for treating the large number of cells required for biochemical purifications. A number of other potential apoptotic triggers were investigated, including H_2O_2 and UV irradiation, but all proved much less efficient at reproducibly inducing rapid cell death in large-scale cultures. An alternative approach was therefore investigated relying on the use of constitutively active Bax mutants. If such mutants could be developed and placed under control of an inducible promoter system this would allow the synchronous expression of activated Bax in all cells in the culture. To this end a structure / function analysis of Bax was conducted to determine the effect of mutating key regions of the protein.

5.2 Selection of Bax mutations:

Previously systematic deletion and mutational analysis of the Bax C-terminus identified Serine 184 (S184) as critical for regulating Bax subcellular localisation (Nechushtan et al., 1999). Mutation of this residue to a more hydrophobic residue such as alanine (S184A) or valine

(S184V), or deleting it entirely (ΔS-184), has previously been shown to result in constitutive mitochondrial localisation of a GFP-Bax reporter (Nechushtan et al., 1999). This may be partly explained by these mutations increasing the overall hydrophobicity, thereby promoting membrane insertion. However, elucidation of the Bax structure also revealed that S184 is orientated into the BH3-binding cleft of Bax (Suzuki et al., 2000). This provides the alternative explanation that substitution of S184 may disrupt a salt bridge that normally helps to retain the C-terminus folded back across the core of the Bax protein (Suzuki et al., 2000), and that this causes the C-terminus to disengage from the core of the protein and constitutively insert into mitochondrial membranes. Surprisingly however, the mitochondrial localisation of Bax caused by the S184V substitution was not associated with a large increase in Bax toxicity, and the N-terminal 6A7 epitope was reported to be still hidden (Nechushtan et al., 1999). These results further support the hypothesis developed in Chapter 3 that mitochondrial localisation is not sufficient to cause Bax activation and a further change is likely to be necessary to cause full activation. To this end other residues in the conformationally sensitive N-terminus and the α5/α6 helical hairpin were identified for mutation in an attempt to increase Bax toxicity and cause constitutive activation of the protein.

The N-terminus of Bax clearly plays an important role its activation (see Figures 3.1 and 3.3). The Bax N-terminus consists of an unstructured and flexible region (residues 1 to 15) followed by helix α1 (hα1; residues 16 to 35) (Suzuki et al., 2000). The conformational change associated with Bax activation is likely to include the disengaging of hα1 from the core of the protein and Bax mutants lacking the N-terminus have increased toxicity (Cartron et al., 2003). For a proteomic study it is preferable to keep the complete protein intact so a mutation, rather than deletion, which might mimic the effect of loss of the N-terminus was considered. Hence, the second mutation considered targeted a central residue in hα1, leucine 25, and replaced it with a helically disrupting proline residue (L25P). It was hoped that this mutation would disrupt hα1 and destabilise the inactive form of the protein, thereby promoting Bax activation.

The central pair of amphipathic alpha helices in Bax, hα5 and hα6, are structurally conserved in both the cellular and viral Bcl-2 proteins. They are also key features of the pore forming domains of bacterial toxins such as Diphtheria toxin (Lazebnik, 2001). It is well established that the equivalent pair of helices from the toxin proteins insert into cellular membranes (Rosconi and London, 2002). For the Bcl-2 proteins the α5/α6 region has been shown to be required for their function (Matsuyama et al., 1998), and recent evidence reveals that this region also inserts into mitochondrial membranes during apoptosis (Annis et al., 2005; Kim et al., 2004a). It is possible that membrane insertion of this region represents a key step in Bax activation. Therefore, the final two mutations were selected to target this region.

A long standing observation, and one of the few major differences at the primary amino acid sequence level between pro-apoptotic and pro-survival Bcl-2 proteins, concerns the distribution of charged resides within the α5/α6 region (Schlesinger et al., 1997). In Bax there is a predominance of positively charged residues, whilst in Bcl-2 negatively charged residues occur in the equivalent positions (Figure 5.2 A). Based on an alignment of the primary sequence of Bcl-2, Bcl-XL, Bax and Bak in this region, three lysine (K) residues near the apex of the Bax α5/α6 hairpin were chosen for mutation (Figure 5.2 B). The first of these, Bax K119, is positively charged in both Bax and Bak but the equivalent reside in Bcl-2 and Bcl-XL is small and hydrophobic. The second position, Bax K123, is positively charged in both Bax and Bak but the equivalent position is negatively charged, a glutamic acid, in both Bcl-2 and Bcl-XL. Finally, Bax K128 carries a positive in Bax, but not Bak, with the equivalent residue being negatively charged in Bcl-2 and Bcl-XL.

To alter the characteristics of this region alanine (A) and aspartic acid (E) residues were introduced. The first of two substitution mutations chosen was K119A, K123E, K128E, referred to as AEE throughout this study. This mutation was selected to be a 'charge reversal' mutation, making the apex of the Bax α5/α6 hairpin resemble that of the pro-survival proteins Bcl-2 and Bcl-XL. The other mutation was a triple alanine substitution: K119A, K123A, K128A, referred to as AAA throughout this study. This mutation was selected to make the α5/α6 more closely mirror the hydrophobic nature of this region in the bacterial toxins such as Diphtheria toxin, which is known to insert constitutively into the membrane (Rosconi and London, 2002). Multiple alanine substitutions of the Bax α5/α6 have been previously reported to confer a gain-of-function phenotype, enhancing Bax toxicity, but detailed localisation data has not been reported (Nouraini et al., 2000).

This approach resulted in the generation of a series of five Bax constructs: (i) wild type Bax, (ii) the previously described S184V mutant, (iii) the L25P mutation selected to destabilise the cytoplasmic form of Bax, (iv) the triple alanine mutant (AAA) selected to enhance membrane insertion and (v) the charge reversal mutant (AEE) selected to mimic pro-survival proteins. The position of these mutations in relation to the Bax structure is shown in Figures 5.1 C and 5.1 D.

5.3 Analysis of the effect of Bax mutations on protein localisation:

To assess the effect of these mutations on Bax protein localisation they were introduced into wild type GFP-Bax and transfected into MCF10A cells. In all cases, some cells, usually those

expressing the highest levels of the GFP-Bax proteins, could be seen to exhibit the bright punctate GFP-Bax pattern characteristic of full activation. Often these cells failed to stain with Mitotracker and showed signs of nuclear condensation, indicating progression into apoptosis. This indicated that all the GFP-Bax mutants were functional and induced apoptosis when expressed at high levels. The basal location of each GFP mutants in moderately expressing cells prior to the onset of apoptosis was recorded. MCF10 empty vector control cells together with the E1B19k- and BHRF1-expressing lines were included in the analysis (Figure 5.2). The presence of E1B19k and BHRF1 had no effect on the localisation of the GFP-Bax mutants, although they did appear to increase the level of GFP expression and number of surviving cells 24 hrs after transfection. This is presumably because higher expressing cells survived for longer in the presence of viral pro-survival proteins (data not shown).

As expected, wild type GFP-Bax was cytoplasmic (Figure 5.2 A) and the S184V mutation caused constitutive localisation to the mitochondria (Figure 5.2 B) as reported previously (Nechushtan et al., 1999). The stable mitochondrial distribution of the S184V construct provides further evidence that mitochondrial localisation of Bax alone is not sufficient to guarantee activation, and further changes, which may occur at the mitochondria, are necessary. The L25P mutation however did promote activation of the protein: this construct has a reduced cytoplasmic distribution, showed enrichment at mitochondria and frequently entered small foci characteristic of active Bax (Figure 5.2 C). Mutations in the $\alpha5/\alpha6$ region also changed the protein localisation: the AAA mutation appeared to be the most toxic of the mutant constructs, fewer transfected cells were visible 24hrs after transfection and those that remained expressed low levels of GFP. Small mitochondrial associated clusters were visible in these cells (Figure 5.2 D). Finally, the AEE mutation expressed at much higher levels and the AA mutant had an intermediate distribution: a large proportion of the protein remains in the cytoplasm but a clear enrichment at mitochondria could also be seen (Figure 5.2 E).

When this work was begun it was already established that the Bax N-terminus was conformationally sensitive. It was therefore a particular concern that adding a large protein tag (GFP is 27 kDa, compared with Bax at 21 kDa) to the Bax N-terminus may interfere with its regulation. This could be important if such a construct were then to be used as the basis for a proteomic analysis. Work presented in Chapters 3 and 4 clearly validates the use of GFP-Bax as a reporter to monitor Bax activation in live cells. This does not however confirm that GFP-Bax is truly regulated in the same manner as the endogenous protein. For example, GFP-Bax may faithfully report on the location of the endogenous protein, being rapidly recruited into foci upon activation along with endogenous Bax molecules, but not actually participate in the initial activation event itself. The observation that high level GFP-Bax over-expression can override

endogenous controls and promotes the induction of apoptosis (Rosse et al., 1998; Xiang et al., 1996), argues that the N-terminally tagged protein may indeed retain full functionality. However, in an attempt to address these concerns, the behaviour of Bax tagged at the carboxy-terminus (Bax-GFP) was also investigated.

Figure 5.3 shows that Bax-GFP was cytoplasmic in wild type MCF10A cells, similar to GFP-Bax. Strikingly, the C-terminal GFP tag prevented three of the Bax mutants, S184V, L25P and AEE, from altering the protein localisation; all three accumulated in the cytoplasm and were indistinguishable from wild type Bax-GFP (Figure 5.3). Occasionally cells were still seen in which full Bax activation had occurred and the Bax-GFP constructs entered mitochondrial foci, but these were extremely rare in comparison with that seen with the GFP-Bax (data not shown). The exception was Bax-GFP AAA, which was still able to form small mitochondrially associated foci and expressed at noticeably lower levels than the other C-terminally tagged constructs. Together, these results indicate that a C-terminal GFP tag significantly impairs the function of the Bax protein and prevents its localisation to mitochondria. The ability of the Bax-GFP AAA construct to by-pass the inhibition imposed by the C-terminal tag is an indication that this protein retains a gain-of-function phenotype originally reported in an N-terminal HA tagged version of this mutant (Nouraini et al., 2000), and shown here with an N-terminal GFP tag (Figure 5.2 D).

The effect of E1B19k and BHRF expression on the localisation of the Bax-GFP constructs was also investigated. As with the GFP-Bax mutants, the addition of BHRF1 had no effect on the localisation of any of the Bax-GFP mutants (data not shown). The N-terminally tagged GFP-Bax mutants were also unaffected by expression of E1B19k. However, localisation of two of the C-terminal Bax-GFP mutants, Bax-GFP L25P and Bax-GFP AAA, was dramatically altered by the presence of E1B19k (Figure 5.4). Bax-GFP L25P, which was strongly cytoplasmic in control cells, could be seen to enter small mitochondrially associated foci in MCF10A E1B19k cells (Figure 5.4, upper panels). Bax-GFP AAA formed small mitochondrial clusters and expressed at low levels in control cells. In E1B19k cells, however, this mutant expressed at higher levels and formed a mesh-like network throughout the cytoplasm with strong straining around the nucleus; such a distribution is the signature of ER localisation. A potential model to explain this shift in distribution is discussed below.

[Data added in support: Supplementary Figure 5.7 in Appendix 1 shows a comparison of the ER-like distribution of Bax-GFP AAA in MCF10A E1B19k cells with that of a resident ER protein marker and with E1B19k, which predominantly localises to nuclear and ER membranes (White et al., 1984).]

5.4 The toxicity of Bax mutations correlates with their localisation:

To asses the relative toxicity of the GFP Bax mutants a classical Annexin V / PI apoptosis assay was used (Koopman et al., 1994). The GFP Bax constructs were transfected into MCF10A control and E1B19k-expressing cells, and 24 hrs later the cells were subjected to FACS analysis: first to sort the GFP-expressing cells and then to asses the degree of apoptosis by measuring their ability to bind Annexin V. Apoptotic cells were considered as those staining positively for Annexin V, indicating externalisation of the membrane lipid phosphatidylserine (PS) and a marker for apoptotic cell death (Koopman et al., 1994), but negatively for the cell impermeant DNA stain propidium iodide (PI), thereby excluding cells with ruptured plasma membranes. The results of this analysis are shown in Figure 5.6 A. As expected from the localisation study, the C-terminally tagged Bax-GFP constructs, being predominantly cytoplasmic, are considerably less toxic than the N-terminally tagged GFP-Bax variants. Untagged constructs, which were co-transfected with a GFP marker, show an intermediate level of toxicity. In most cases the presence of E1B19k had only a marginal effect in reducing the overall level of apoptosis, although this effect becomes more obvious the more toxic the construct. For example, the level of apoptosis induced by GFP-Bax L25P and GFP-Bax AAA is considerably reduced in the presence of E1B19k (Figure 5.6 A).

Considering the individual mutations in the context of GFP-Bax: whilst over-expression of the wild type protein causes a modest increase in apoptosis relative to the GFP empty vector control, this level is increased by the constitutive localisation of Bax to mitochondria (S184V) and increased further by promoting entry into mitochondrially associated foci (L25P). Mutations in the α5/α6 also influence GFP-Bax toxicity with the AAA construct, which constitutively enters mitochondrially-associated foci, being more toxic than S184V and approaching levels seen with L25P. This contrasts with the AEE mutation, which only partially localises to mitochondria, does not form foci, and shows levels of toxicity similar to S184V. This trend described for the GFP-Bax mutants is suppressed, but still present, in the untagged Bax mutant series. Interestingly, it is also still present in the C-terminally tagged Bax-GFP set, albeit with much decreased overall levels of toxicity (Figure 5.6 A). Together these results show that, in general, there is a strong correlation between the ability of Bax mutations to promote mitochondrial localisation and their increased levels of toxicity, with those promoting entry into mitochondrially-associated foci being the most toxic of all. A notable exception to this rule was the Bax-GFP L25P construct, which, in the presence of E1B19k, did enter very small mitochondrial foci (Figure 5.4), yet still displayed very low levels of toxicity (Figure 5.6 A). This situation is particularly interesting, as it appears to stabilise a distribution of Bas normally

associated with much higher levels of toxicity. It could therefore be a useful entry point for the biochemical analysis of Bax located at mitochondria.

Finally, this assay showed no significant change in the toxicity of GFP-Bax AAA with and without the presence of E1B19k. This is surprising since the E1B19k causes a dramatic shift in the localisation of this protein away from mitochondria into an ER-like distribution (Figure 5.4), and could therefore be expected to lower the protein's toxicity. It is also surprising that, in the absence of E1B19k, Bax-GFP AAA displays lower toxicity than Bax-GFP L25P despite being constitutively localised to mitochondrial clusters while Bax-GFP L25P is predominantly cytoplasmic (Figure 5.5). A possible explanation for this was gained by analysing the median GFP fluorescence intensity for each sample, as an indicator of their relative expression levels (Figure 5.6 B). These data reveals that Bax-GFP AAA expresses at much lower levels than the other C-terminally tagged mutants. It is possible that cells expressing extremely low levels of GFP fluorescence may not have been detectable by FACS, and therefore inappropriately excluded from the subsequent Annexin / PI analysis. This interpretation supports the qualitative observation that the AAA variant induced apoptosis in the majority of transfected cells even at very low levels of expression (Figure 5.5) and implies the toxicity of the AAA mutation may have been under-represented in this FACS based assay. In general, the wide variation in expression level seen using these GFP-tagged Bax constructs (Figure 5.6 B) highlights the inherent difficulties in assessing the relative toxicity of mutant proteins at a single time point. Nevertheless the results obtained are in broad agreement with the conclusions gained from the localisation studies (Figure 5.5).

5.5 Discussion:

The objective of the work presented in this chapter was to conduct a structure / function analysis of key regions in the Bax protein in order to identify mutations which would constitutively activate Bax. The four mutations: S184V, L25P, AAA and AEE were examined. In addition, the effect of tagging these mutants with GFP at their N- or C- termini, and the effect of co-expression of E1B19k was also considered.

N-terminally tagged GFP-Bax is cytosolic in the majority of cells (Wolter et al., 1997) and each mutation altered this localisation. The S184V mutation resulted in a constitutive mitochondrial localisation with GFP-Bax S184V accumulating evenly along the mitochondrial network, as has been previously described (Nechushtan et al., 1999). In contrast to the previous report this mutant did show increased toxicity relative to wild type GFP-Bax (Figure 5.6 A), but

considering GFP-Bax was entirely loaded into the mitochondria (Figure 5.2 B), the associated increase in toxicity was modest. These data further confirms that mitochondrial localisation alone is insufficient to trigger GFP-Bax activation and suggests additional steps, such as dimerisation or oligomerisation are necessary for its full activation (Gross et al., 1998). Whilst these properties make the S184V mutation potentially useful in isolating Bax forced into a mitochondrial localisation it does not appear to significantly promote activation of the protein.

The L25P mutation was selected based on the premise that disrupting hα1 in conformationally sensitive N-terminus of Bax might promote activation of the protein. The results presented show the L25P mutation did significantly enhance both toxicity (Figure 5.6 A) and entry into bright mitochondrially-associated toxicity foci (Figure 5.2 C). It is possible that constitutive localisation into the foci characteristic of fully active Bax may mean this protein completely bypasses earlier steps in the protein's normal activation, and the point at which E1B19k blocks this. If true these properties would make the L25P mutation unsuitable for use in biochemical purifications designed to interrogate these earlier steps. However, this appears not to be the case as, in a few cells, the protein could also be seen to be either partially cytoplasmic or co-localised with mitochondria and not in foci (data not shown). Additionally, the toxicity of GFP-Bax L25P mutation could be reduced by the presence of E1B19k. Together the data presented supports an interpretation that the L25P mutation does indeed act to promote Bax activation by destabilising the inactive conformation of the protein. Recently, a similar mutation in Bax hα1, a glycine (G) substitution for leucine 26 (L26G) has been reported (Cartron et al., 2003). In this case it was shown to have decreased mitochondrial targeting activity *in vitro* and decreased toxicity in transfection assays, although it retained Cyt-c releasing activity when expressed in yeast (Cartron et al., 2003). This is surprising since complete deletion of the Bax N-terminus has been reported to enhance Bax toxicity (Goping et al., 1998). At present the reasons for discrepancies in these data cannot be explained.

It is likely that the insertion of charged residues within the α5/α6 region into the mitochondrial membrane represents a significant energetic barrier to Bax activation. Membrane insertion of the Bax α5/α6 region during apoptosis has recently been explicitly demonstrated using a chemical labelling technique (Annis et al., 2005). The insertion of the equivalent region of Bcl-2 into both mitochondrial and ER membranes upon receipt of an apoptotic trigger has also been demonstrated (Kim et al., 2004a). Localisation data obtained using the charge neutralisation mutation, AAA, and the substitution mutant, AEE, within the Bax α5/α6 helical hairpin region supports the hypothesis that this region has important roles in regulating both the membrane targeting and bioactivity of Bax. The AAA mutation in Bax was selected to mimic hydrophobicity observed in the analogous region of structurally similar bacterial toxins such as

Diphtheria toxin. In the toxin protein, this has been shown to insert constitutively into cellular membranes (Rosconi and London, 2002). It was hypothesised that increasing α5/α6 hyrdophobicity may also increase Bax insertion into mitochondria and thereby enhance Bax toxicity. In support of this hypothesis a range of alanine substitution mutations into this region of Bax have been reported to confer a gain-of-function phenotype in both yeast and mammalian cells (Nouraini et al., 2000). In the context of GFP-tagged proteins transfected into MCF10A cells the AAA mutation showed enhanced toxicity, even at low-level expression (Figure 5.6), and was constitutively localised to small mitochondrially-associated foci in wild type cells (Figure 5.5). Interestingly, this change in localisation was unique amongst the mutations investigated in that it also occurred when the GFP tag was placed at the C-terminus of Bax (Figure 5.5). A possible explanation for these results is that by increasing the hydrophobic nature of the α5/α6 region the energetic barrier of insertion of the charged residues in this region into the mitochondrial membrane is removed, resulting in constitutive insertion. If true, it would be interesting to know why it is still mitochondrial membranes that are the preferred target for Bax AAA as this may reflect additional protein or lipid requirements necessary for Bax action unique to that environment.

A striking feature of the Bcl-2 family proteins is that members with significant sequence homology can have opposing cellular function. One of the few clear differences between pro- and anti-apoptotic family members is a predominance of positively charged residues within the α5/α6 region of pro-apoptotic members, while negative charged residues predominate in the pro-survival members (Nouraini et al., 2000). The AEE mutation was selected to change the characteristics of the Bax α5/α6 region to more closely resemble that of Bcl-2 and Bcl-XL. Whilst the AEE mutation did not turn Bax into a pro-survival protein, it did alter the localisation of the protein, resulting in a partial mitochondrial enrichment (Figure 5.2 E), further supporting the hypothesis that characteristics of the α5/α6 region contribute to determining the location of Bcl-2 family proteins. It is interesting to note that the partial cytoplasmic and mitochondrial distribution observed with GFP-Bax AEE closely mimics that described for Bcl-XL (Jeong et al., 2004).

Finally, the presence of E1B19k on the localisation of Bax mutants was also investigated. In general this had little effect, beyond a modest reduction in their toxicity (Figure 5.6). It is likely this reflects the ability of E1B19k to stall Bax activation described in detail in the previous chapter. However, the localisation of two of the C-terminally tagged mutants was dramatically altered: Bax-GFP L25P moved from being a cytoplasmic protein into small mitochondrially-associated foci, and Bax-GFP AAA moved from small mitochondrial foci to an ER-like distribution. In healthy cells, E1B19k predominantly localises to the nuclear lamina,

endoplasmic reticulum and nuclear membranes (White et al., 1984). Although the protein can partially redistribute to mitochondria in the presence of over-expressed Bax (Han et al., 1998) and upon the activation of Bax by the expression of tBid (Perez and White, 2000), in which cases E1B19k is thought to directly bind the N-terminally active conformation of Bax (Sundararajan and White, 2001). The ability of E1B19k to interact with conformationally altered Bax with high affinity may explain the shift in localisation of the Bax-GFP constructs. In the presence of N-terminal GFP, the L25P mutation promoted Bax activation as discussed above, it is therefore likely the same mutation would also destabilise the inactive conformation of Bax when the GFP tag is placed at the C-terminus. In the absence of E1B19k this effect may not be detected due to the inhibition on mitochondrial localisation generally conferred by the C-terminal tag (Figure 5.3). However, when E1B19k is co-expressed the combined effect of a high affinity of the destabilised protein for E1B19k may override this effect, causing Bax, and bound E1B19k, to enter a mitochondrial distribution where the interaction between these proteins normally occurs. A similar argument can be used to explain the change in localisation of the Bax-GFP AAA protein. In this case, it can be imagined that the protein is so destabilised and prone to activation that rather than E1B19k translocating to bind it at the mitochondria, it is recruited to the normal location of E1B19k, namely the ER. If correct, one prediction from this model would be that Bax-GFP L25P and AAA would both bind avidly to E1B19k. This is shown to be the case in data presented in Chapter 6 (Figure 6.7).

The work presented in this chapter was initiated in order to identify mutations in the Bax protein that might promote constitutive activation of the molecule to be exploited in biochemical purifications. From the data presented both disruption of the conformationally sensitive N-terminal hα1 by the L25P mutation and charge neutralisation within the α5/α6 region can act to promote activation of the protein. It was also discovered that whilst a C-terminal tag is generally inhibitory to Bax function, in combination with the L25P mutation and co-expression of E1B19k, Bax appears to become 'frozen' in multiple small mitochondrially-associated foci but without the associated increase in toxicity usually observed. This combination may be particularly interesting to pursue for a biochemical analysis since this distribution is highly reminiscent of that of Bax just at the point of its activation in wild type cells treated with an apoptotic stimulus.

Figure 5.1 Schematics showing the positions of Bax mutations characterised in this study.

(A) Comparison of charged amino acids in the membrane-penetrating α5 and α6 helices of Bax and Bcl-2. This region has a net positive charge (blue) in Bax, while the corresponding region carries a net negative charge (red) in Bcl-2. Figure adapted from Nouraini et. al., 1997; **(B)** Alignment of the α5/α6 region from four cellular Bcl-2 proteins. The position of the Bax lysine residues K119, K123 and K128 targeted for mutation are highlighted. Positively charged residues are in , negatively charged residues in blue, and the hydrophobic resides in pro-survival proteins in place of Bax K119 in ; **(C)** Cartoon of the Bax protein structure indicating the positions of hα1 (green) and the a6/a6 region (blue). The position of the L25P mutation is shown (red); **(D)** An alternative view of Bax showing the location of hα9 ( ) and the S184V mutation ( ). The position of the three lysines targeted in the a5/a6 region (orange). Images were produced using the Protein Structural Database (PDB) record for Bax and RasMol software.

A

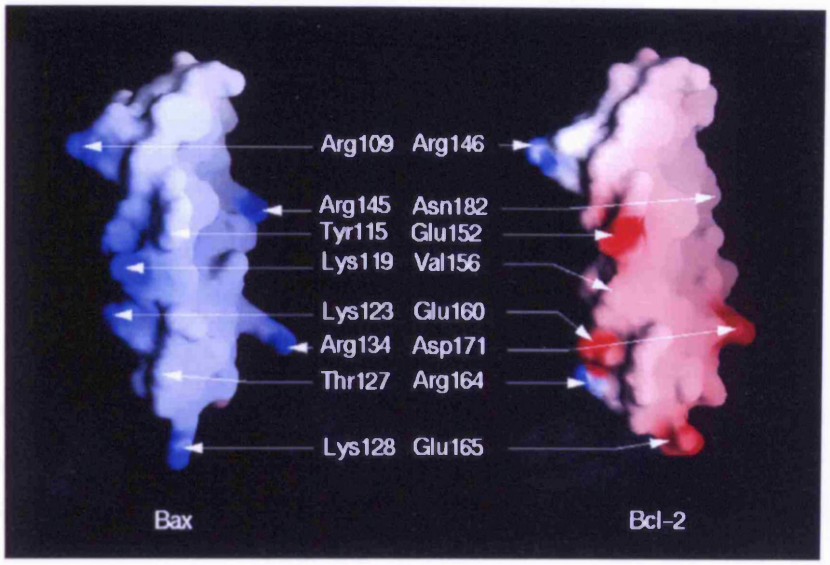
Arg109 Arg146
Arg145 Asn182
Tyr115 Glu152
Lys119 Val156
Lys123 Glu160
Arg134 Asp171
Thr127 Arg164
Lys128 Glu165
Bax
Bcl-2

B

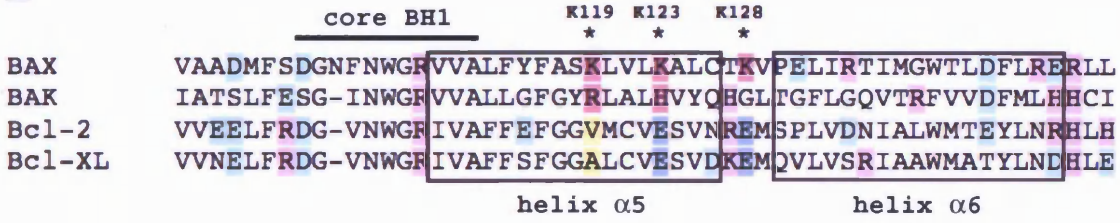
core BH1
K119
K123
K128
BAX VAADMFSDGNFNWGRVVALFYFASKLVLKALCTKVPELIRTIMGWTLDFLRERLL
BAK IATSLFESG-INWGFVVALLGFGYRLALHVYQHGLTGFLGQVTRFVVDFMLHHCI
Bcl-2 VVEELFRDG-VNWGFIVAFFEFGGVMCVESVNREMSPLVDNIALWMTEYLNRHLH
Bcl-XL VVNELFRDG-VNWGFIVAFFSFGGALCVESVDKEMQVLVSRIAAWMATYLNDHLE
helix α5
helix α6

C

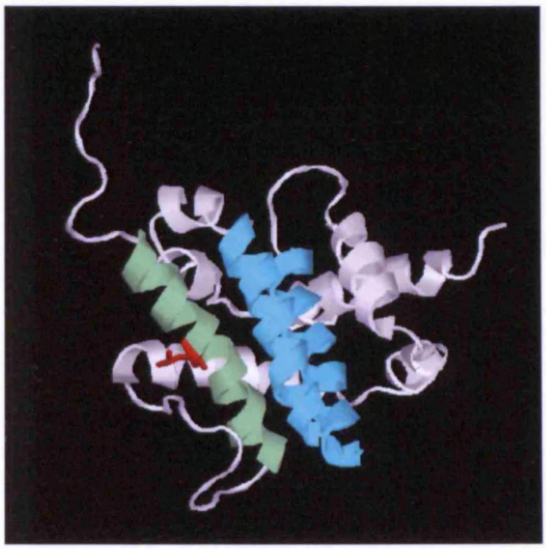

D

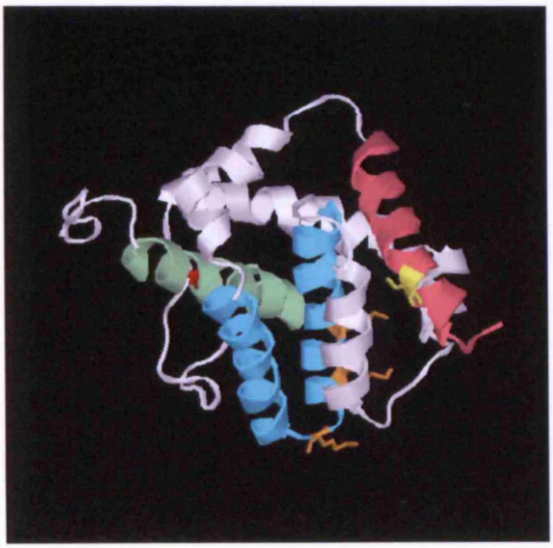

Figure 5.2 Analysis of the effect of mutations on N-terminal GFP-Bax localisation.

MCF10A empty vector control, E1B19k- and BHRF1-expressing cells were grown on glass coverslips and transfected with either wild type or the indicated GFP-Bax mutant. 24 hrs after transfection cells were loaded with 200 nM Mitotracker Orange for 20 mins to reveal the location of energised mitochondria. Cells were then fixed, mounted and imaged by confocal microscopy. For each mutant two representative fields are shown to illustrate the basal distribution of the transfected protein in the majority of moderately expressing cells. **(A)** GFP-Bax wild type control is predominantly cytoplasmic, **(B)** GFP-Bax S184V is constitutively localised to mitochondria; **(C)** GFP-Bax L25P enters into small mitochondrially associated foci; **(D)** GFP-Bax AAA is toxic at low levels and shows small mitochondrial foci; **(E)** GFP-Bax AEE is largely cytoplasmic but shows an enrichment at mitochondria. The presence of E1B19k and BHRF1 does not alter the behaviour of the N-terminally tagged GFP-Bax mutants. In all images scale bars represent 10 μm.

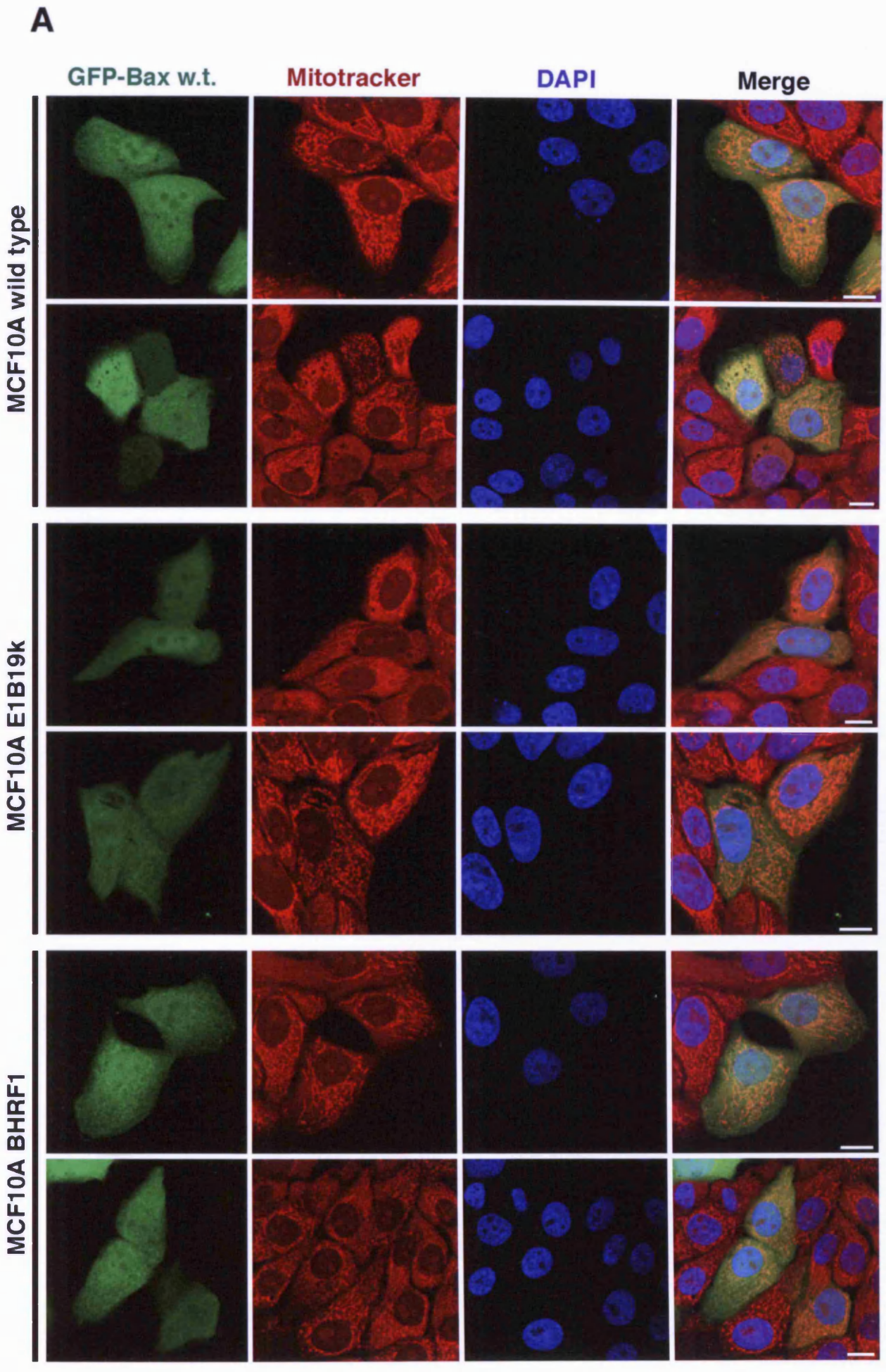
A
GFP-Bax w.t.
Mitotracker
DAPI
Merge
MCF10A wild type
MCF10A E1B19k
MCF10A BHRF1

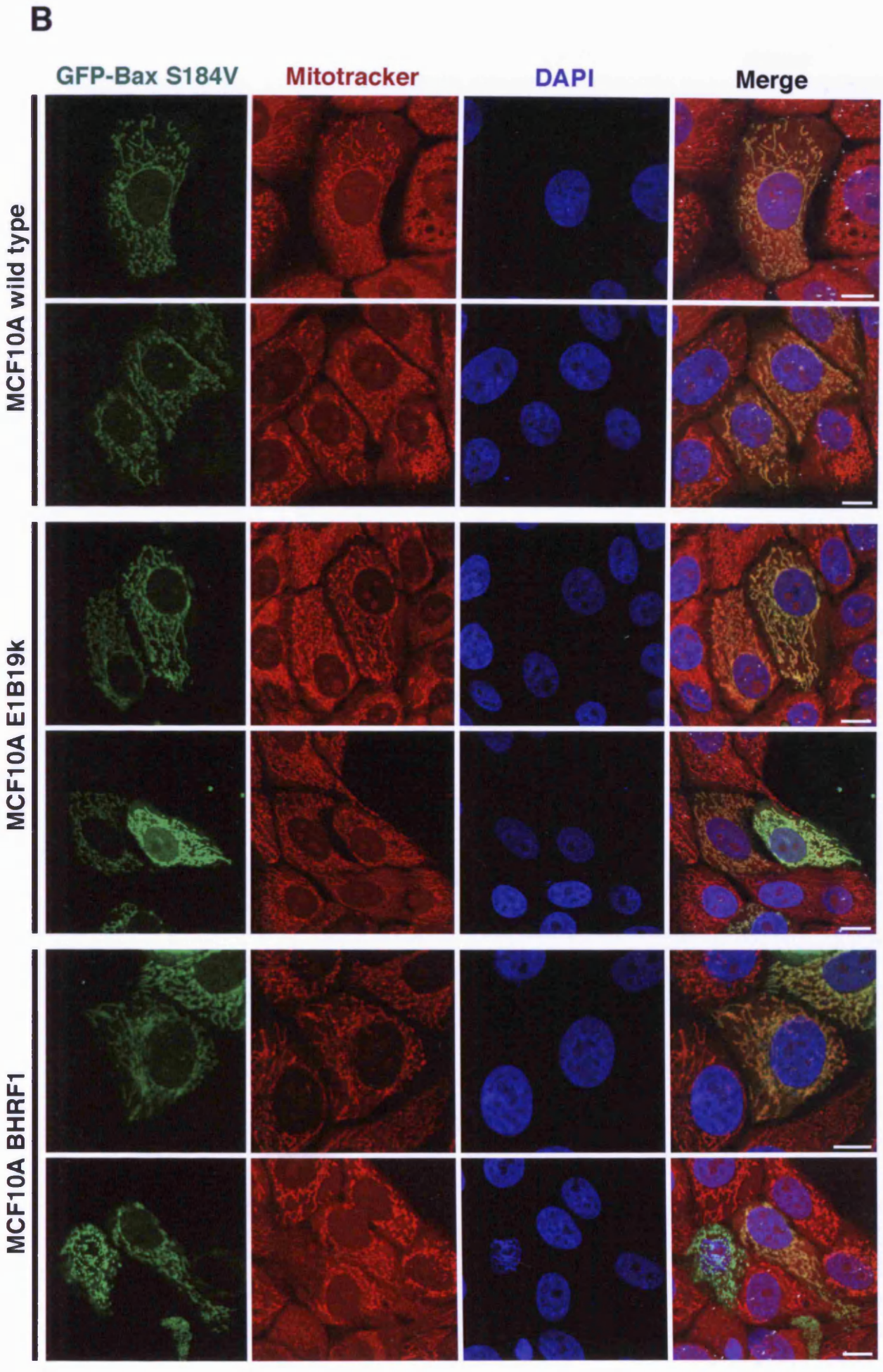
B
GFP-Bax S184V
Mitotracker
DAPI
Merge
MCF10A wild type
MCF10A E1B19k
MCF10A BHRF1

C

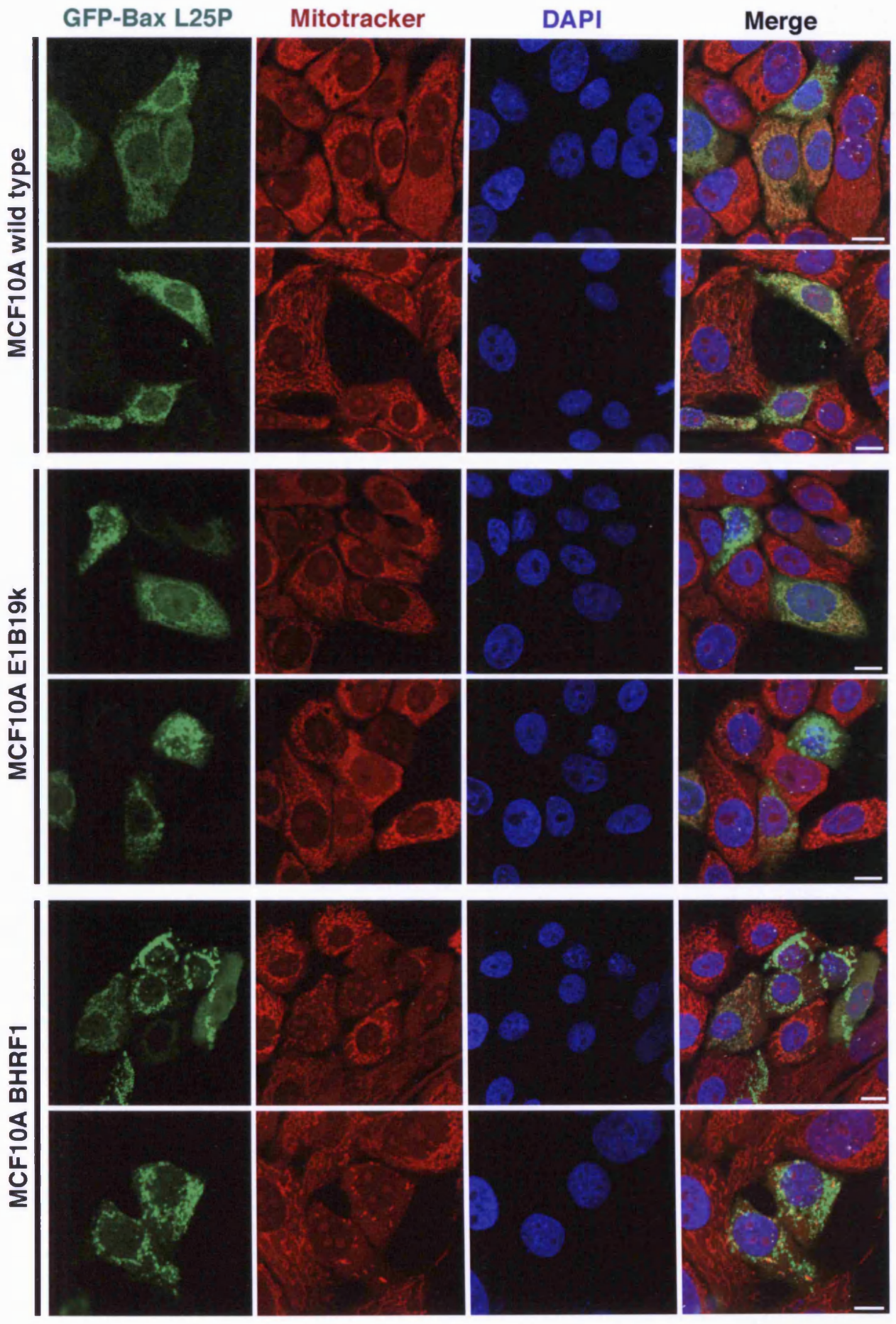
GFP-Bax L25P
Mitotracker
DAPI
Merge
MCF10A wild type
MCF10A E1B19k
MCF10A BHRF1

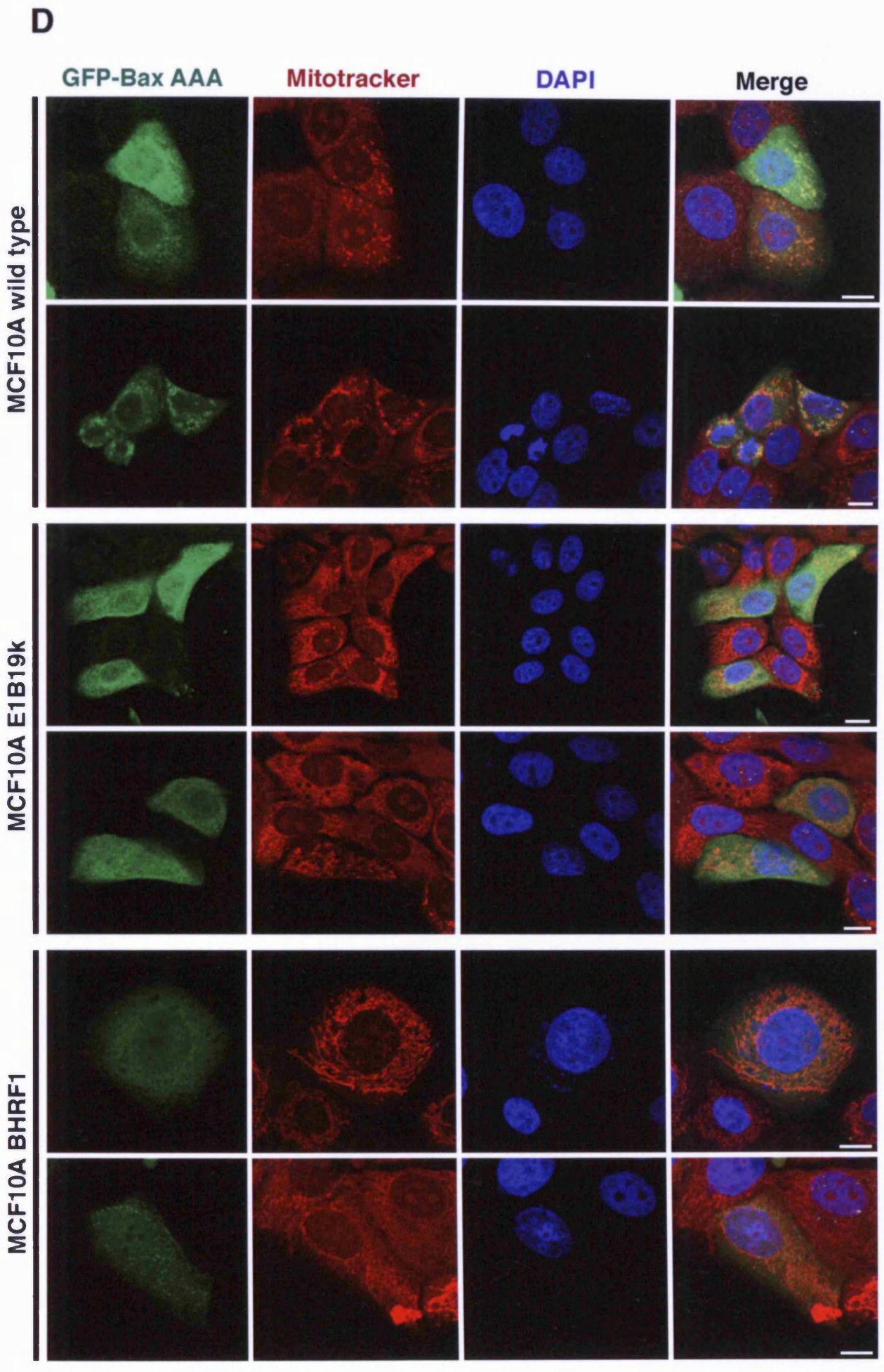
D
GFP-Bax AAA
Mitotracker
DAPI
Merge
MCF10A wild type
MCF10A E1B19k
MCF10A BHRF1

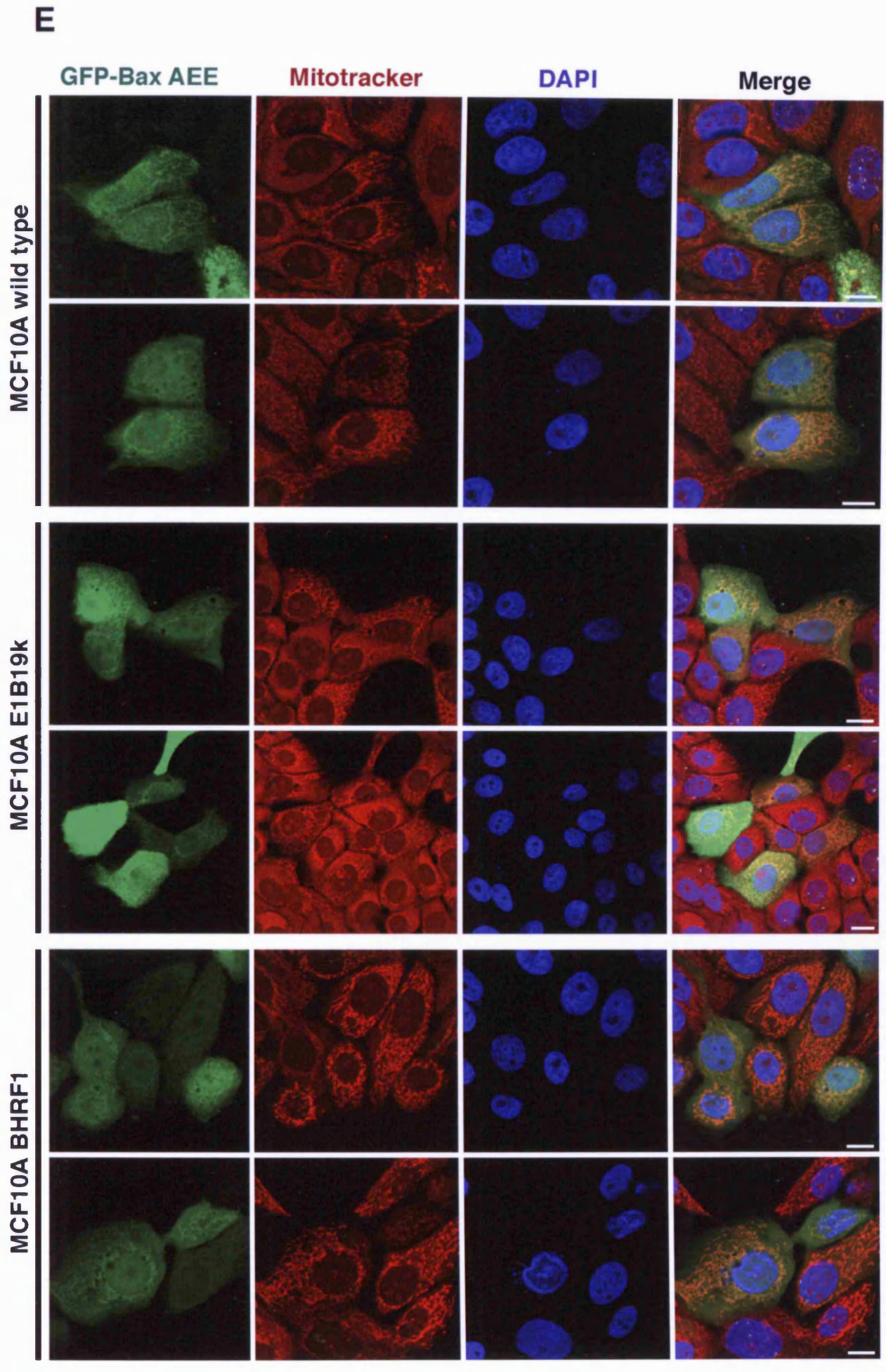
E
GFP-Bax AEE
Mitotracker
DAPI
Merge
MCF10A wild type
MCF10A E1B19k
MCF10A BHRF1

Figure 5.3 C-terminally tagged GFP-Bax mutants are predominantly cytoplasmic.

MCF10A wild type cells were grown on glass coverslips and transfected with the indicated GFP-Bax construct. 24 hrs after transfection cells were loaded with 200 nM Mitotracker Orange for 20 mins to reveal the location of energised mitochondria. Cells were then fixed, mounted and imaged by confocal microscopy. The cells shown are representative of the basal distribution of the transfected protein in the majority of moderately expressing cells. In all images scale bars represent 10 μm.

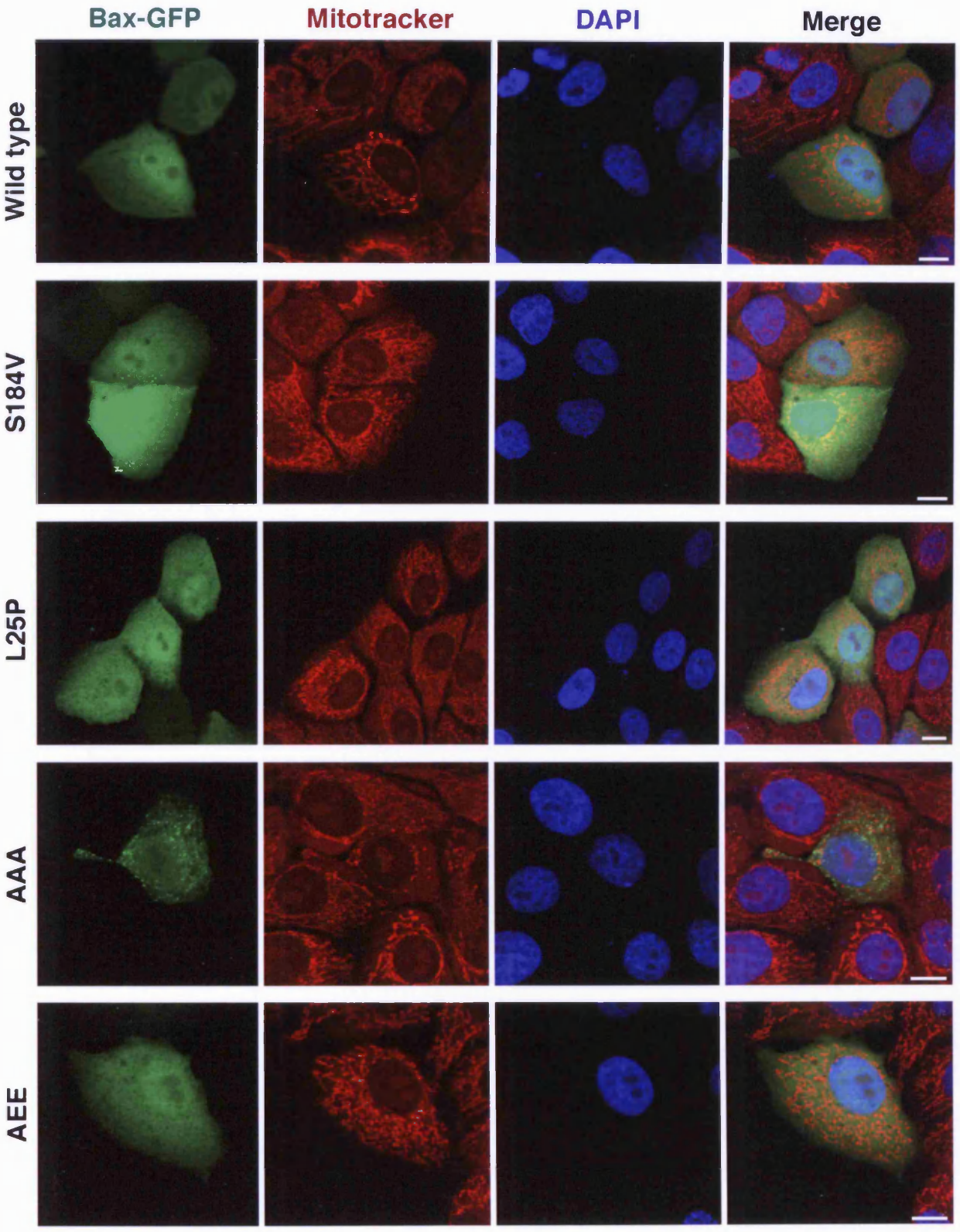
Bax-GFP
Mitotracker
DAPI
Merge
Wild type
S184V
L25P
AAA
AEE

Figure 5.4 Bax-GFP L25P and Bax-GFP AAA show altered distributions in MCF10A E1B19k cells.

MCF10A E1B19k cells were grown on glass coverslips and transfected with the indicated GFP-Bax construct. 24 hrs after transfection cells were loaded with 200 nM Mitotracker Orange for 20 mins to reveal the location of energised mitochondria. Cells were then fixed, mounted and imaged by confocal microscopy. The cells shown are representative of the basal distribution of the transfected protein in the majority of moderately expressing cells. In all images scale bars represent 10 μm.

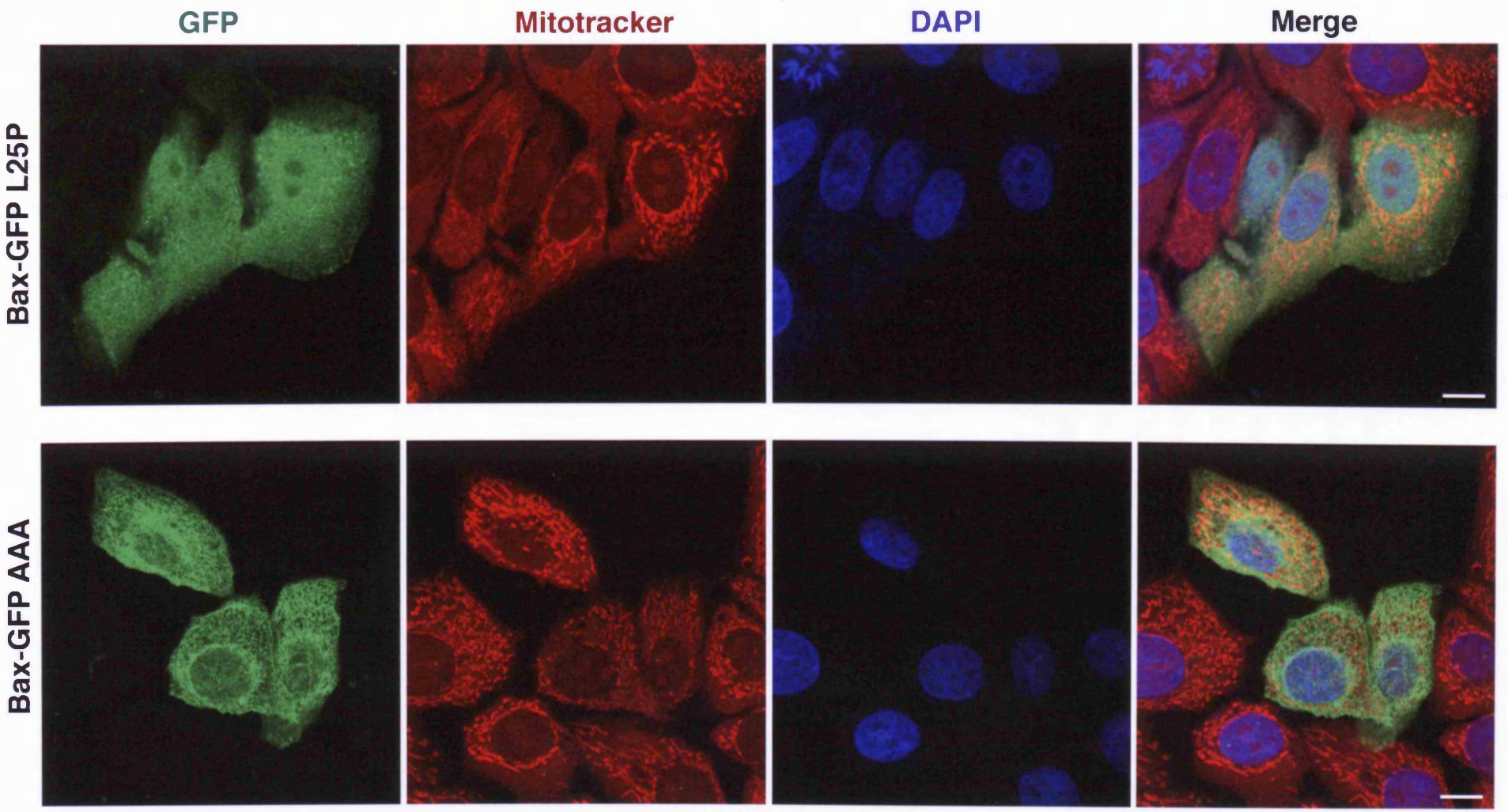
GFP
Mitotracker
DAPI
Merge
Bax-GFP L25P
Bax-GFP AAA

Figure 5.5 Summary of the localisation of the GFP Bax constructs analysed in this study. Images compiled from the experiments described in figures 5.2, 5.3 and 5.4 to summarise the effect of Bax localisation of the Bax mutants. Each of the four mutations tested: S184V, L25P, AAA and AEE alters the distribution of the N-terminally tagged GFP-Bax. These changes are not seen with Bax-GFP, which is constitutively cytoplasmic, except for the Bax-GFP AAA mutant which enters small mitochondrially associated foci regardless of the location of the GFP tag. The distributions of two of the constructs: Bax-GFP L25P and Bax-GFP AAA were strikingly altered in MCF10A E1B19k-expressing cells, Bax-GFP L25P entering mitochondrial clusters and Bax-GFP AAA showing a characteristic ER distribution.

Bax mutation	WT	S184V	L25P	AAA	AEE
GFP-Bax	Cytoplasmic	Mitochondrial not clustered	Mitochondrial clustered	Low expression clustered	Cytoplasmic and mitochondrial
	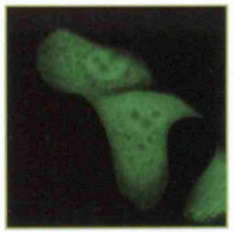	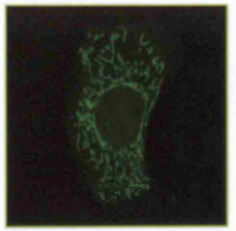	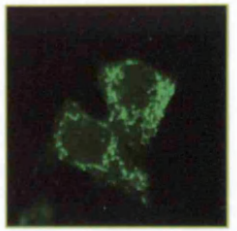	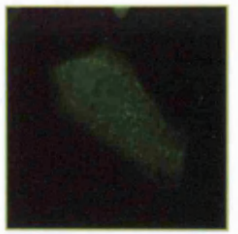	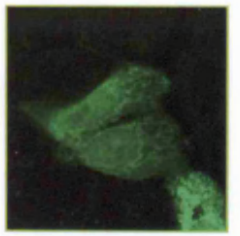
Bax-GFP	Cytoplasmic	Cytoplasmic	Cytoplasmic	Cytoplasmic and small clusters	Cytoplasmic
	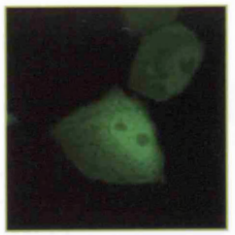	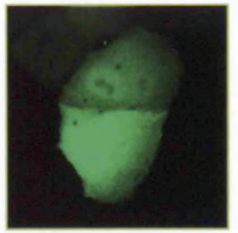	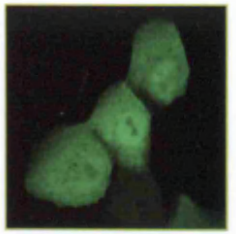	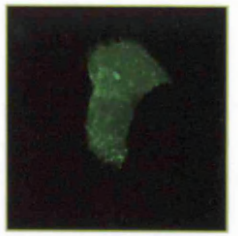	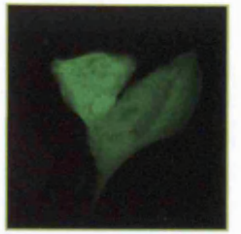
			↓	↓	
			Small clusters	ER distribution	
Add E1B19k:			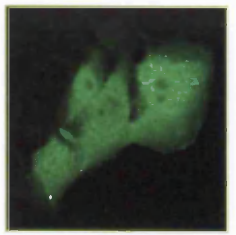	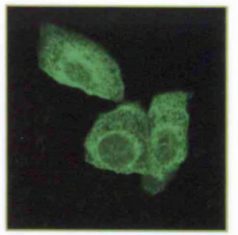	

Figure 5.6 Analysis of the toxicity of GFP Bax mutants.

MCF10A empty vector control and E1B19k-expressing cell lines were grown in 6-well dishes and transfected with the indicated GFP-Bax (N-terminally tagged) and Bax-GFP (C-terminally tagged) proteins. Untagged Bax constructs were also transfected, together with a GFP empty vector marker in a ratio of 10:1 (Untagged). 24 hrs after transfection cells were harvested and stained with Annexin V / PI and immediately analysed by FACS. For each data set: EV is the GFP empty vector transfected as a control and WT is the wild type Bax construct. **(A)** The proportion of apoptotic (Annexin V positive / PI negative) GFP positive cells in each sample, expressed as a percentage of the total number of GFP positive cells; **(B)** The median GFP fluorescence intensity for each sample as an indicator of the relative expression levels of the GFP constructs. In both samples error bars represent ± 1 standard deviation from the mean calculated from triplicate samples.

A

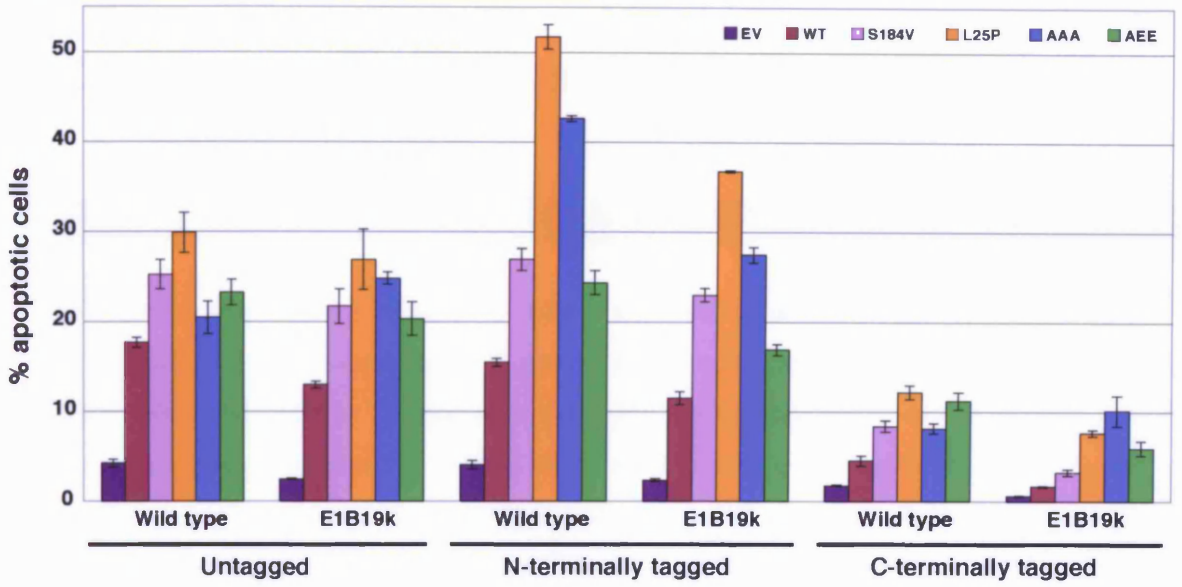
EV
WT
S184V
L25P
AAA
AEE
% apoptotic cells
0
10
20
30
40
50
Wild type
E1B19k
Wild type
E1B19k
Wild type
E1B19k
Untagged
N-terminally tagged
C-terminally tagged

B

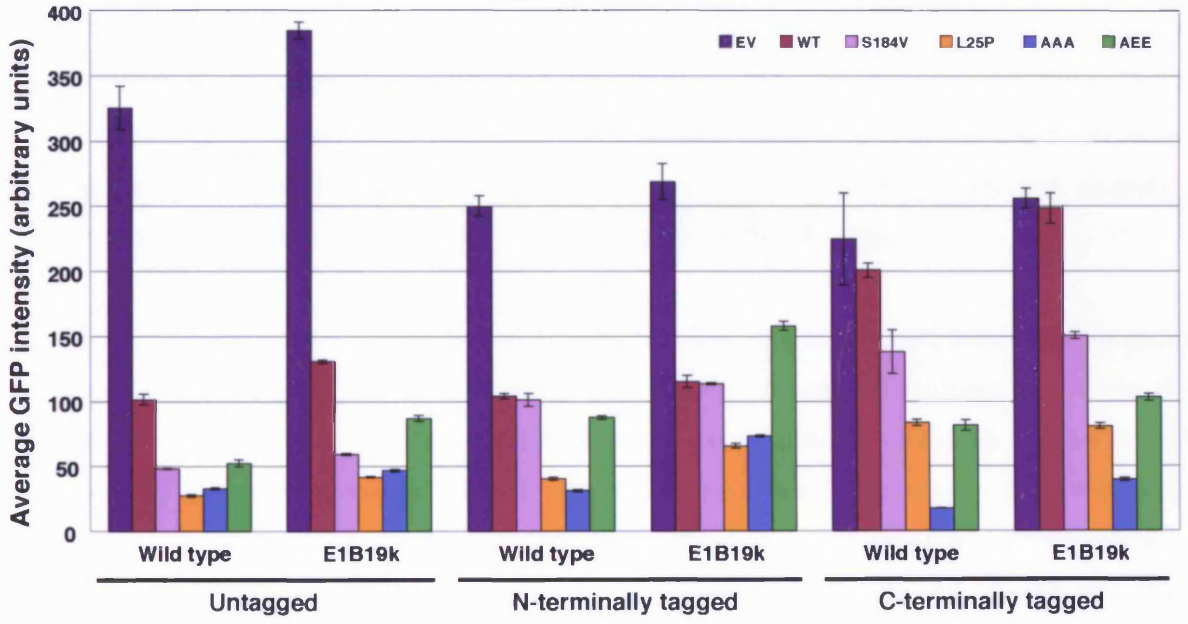
EV
WT
S184V
L25P
AAA
AEE
Average GFP intensity (arbitrary units)
0
50
100
150
200
250
300
350
400
Wild type
E1B19k
Wild type
E1B19k
Wild type
E1B19k
Untagged
N-terminally tagged
C-terminally tagged

Chapter 6 – Bax interacting proteins

6.1 Introduction:

The pro-apoptotic Bcl-2 family members Bax and Bak are required for the onset of mitochondrial dysfunction and cell death following a diverse range of stimuli (Lindsten et al., 2000; Wei et al., 2001). Yet, despite intensive investigations the nature of the Bax and Bak activation mechanism remains an area of uncertainty and great debate. Once active, Bax and Bak form oliogomers that are associated with the loss of $\Delta\psi_m$ and release of Cyt-c and other mitochondrial inter-membrane space proteins. These events are widely accepted to represent the commitment point in the apoptotic program from which cells can no longer recover. Thus, understanding the nature of the Bax/Bak activating events goes to the heart of our understanding of how apoptosis is initiated in mammalian cells.

As demonstrated in Chapter 3, Bax activation is a sudden and rapid event occurring stochastically throughout a population of cells, often many hours after they have been exposed to a cytotoxic stress to induce cell death. Once initiated the loss of $\Delta\psi_m$ and translocation of a large proportion of the cytoplasmic pool of Bax into mitochondrially-associated clusters is complete within a five-minute period. Within an hour the cell is a dead.

Further insights into the mechanism and regulation Bax activation could potentially be gained from identifying any proteins interacting with Bax at the critical moments when the first molecules become active within the cell. However, the stochastic, transient and irreversible nature of this process means that only a small proportion of cells within a population are undergoing these events at any one time. Furthermore, data presented in Chapters 3 and 4 suggests Bax activation may initiate within a localised region of the cell, maybe at a single mitochondrion, with other mitochondria being recruited into the apoptotic program by a means of a rapidly acting feed-forward mechanism. These characteristics have made the question of Bax activation *in vivo* particularly intractable to biochemical analysis, which is optimally performed using large numbers of cells behaving synchronously. For this reason, current models for Bax activation are based largely on evidence gained from *in vitro* reconstitution systems using purified mitochondria.

Some candidate proteins and lipids, have been suggested to be involved in Bax activation, including: the DNA repair protein Ku70 and as well as two 14-3-3 proteins, theta and sigma, have been suggested to function as cytoplasmic anchors for Bax (Nomura et al., 2003; Samuel et al., 2001; Sawada et al., 2003). A 'hit-and-run' interaction with tBid had been suggested (Eskes et al., 2000). Recruitment to the mitochondrial inner membrane Adenine Nucleotide Transporter (ANT) was reported to enhance Bax activation (Marzo et al., 1998) whilst Humanin, a short peptide of 24 amino acids, has been shown to bind and inhibit Bax activation (Guo et al., 2003). Interestingly there is a complete open reading frame for Humanin within the mitochondrial genome and it is suggested the sequence present in mammalian nuclear genomes arose by transfer from the mitochondrial genome. Humanin has also been recently shown to bind Bid and tBid (Zhai et al., 2005). The apoptosis-associated speck-like protein (ASC) has been shown to be a p53 target gene that interacts with Bax and has been shown to promote its activation (Ohtsuka et al., 2004) as has an interaction between Bax and Bif-1, and Endophilin B family protein (Cuddeback et al., 2001; Takahashi et al., 2005) whilst Bax activation has been suggested to be suppressed by an interaction with Clusterin (Zhang et al., 2005). Despite the size of this ever-growing list none have yet been proved essential in regulating Bax activation and in most cases the physiological relevance of the interactions reported remains to be fully demonstrated *in vivo*. Many of these proteins were identified on the basis or yeast two-hybrid screens or functional screens in yeast. An unbiased approach to identify proteins interacting with Bax during its activation in mammalian cells has not previously been reported. This chapter reports the strategy and results of such an approach.

6.2 Design of the purification strategy:

The identification of proteins interacting with Bax at the time when the protein is becoming active is predicted to provide important insights the molecule's regulation. In order to identify such candidates an unbiased proteomic approach was pursued. For such an analysis it may be advantageous if cells could be accumulated at the point when Bax molecules are first becoming active. Data presented in Chapter 4 suggests that over-expression of Bcl-2 pro-survival proteins is unlikely to augment this aim since they act to delay Bax from becoming active. The level of protection afforded by these proteins can eventually be breached, resulting in Bax activation, but when this occurs it happens just as in wild type cells (data not shown). A number viral proteins targeting Bax and Bak have recently been reported, these include vMIA (Arnoult et al., 2004; Poncet et al., 2004), F1L (Postigo et al., 2006; Wasilenko et al., 2005) and M11L (Su et al., 2006; Wang et al., 2004), but in each case these proteins were shown to act by constitutively targeting and sequestering either Bax or Bak and thereby preventing their normal activation. So

the former category delays Bax and Bak activation, while the later category removes Bax and Bak from their normal activation pathways, in neither case are these pro-survival proteins likely to aid the accumulation of cells with active Bax for a proteomic analysis. However, data presented in Chapter 4 demonstrates the Adenoviral E1B19k protein blocks Bax and Bak activation at a unique and potentially useful step. Following the induction of apoptosis, E1B19k-expressing cells still exhibit the initial stages of Bax activation, namely mitochondrial translocation and N-terminal conformational change. Importantly, at the population level, these events take place at the same rate as in control cells, indicating upstream signalling events are intact and reach Bax unopposed. E1B19k then blocks cell death by preventing only the later steps in Bax/Bak activation, namely the homo- and hetero-oligomerisation of Bax and Bak, loss of $\Delta\psi_m$ and Cyt-c release. Over time the initial activation of Bax takes place in an increasing proportion of cells, but these cells remain alive and accumulate with mitochondrially translocated and N-terminally activated Bax. This mitochondrial pool of Bax protein, stabilised by E1B19k, may be directly comparable to, or at least provide useful insights into, a step in Bax regulation that exists only transiently and in a small subset of wild type cells.

The rationale above explains why E1B19k-expressing cells may provide a unique entry point for a biochemical analysis of mitochondrially localised Bax. However, before such an analysis can be undertaken however, a further problem arises, which is how to activate Bax in as many cells as possible. Fas/CHX was used frequently used in the present study due of its acute and reproducible action; however, the use of anti-Fas IgM is economically unfeasible for treatment of large-scale cultures. A number of other potential cell death triggers, including H_2O_2 and UV irradiation were investigated, but all proved less efficient and less reproducible in initiating cell death in large-scale cell cultures. An alternative strategy was therefore pursued, relying on the use of mutations to constitutively activated Bax. This approach is outlined in Chapter 5 and led to the generation of four Bax mutants: S184V, L25P, AAA and AEE, of which L25P seemed the most promising in terms of promoting constitutive Bax activation. It was reasoned that, if expressed under the control of a tetracycline inducible promoter these Bax mutants would provide a way to generate activated Bax synchronously and in large numbers of cells. In combination with E1B19k, to prevent or delay full apoptosis, it was hoped this would provide an entry point with which to purify Bax at a critical step in its activation.

6.3 Characterisation of 293 T-REx cells TAP-tagged Bax clonal cell lines:

The proteomic purification strategy chosen was the Tandem Affinity Purification (TAP) tag system (Rigaut et al., 1999). The TAP method allows the purification of protein complexes

under native conditions, without prior knowledge of their composition or function. To this end the GFP-tag (27 kDa) on wild type Bax and the Bax mutants, characterised in the previous chapter, was exchanged for the similarly sized TAP tag (20 kDa).

The TAP tag consists of main components. The first element consists of tandem Protein A epitopes, which allows efficient recovery of the tagged protein and associated components by affinity purification on an IgG-linked bead matrix. This is followed by a cleavage site for the Tobacco Etch Virus (TEV) protease, which allows specific elution from the matrix under native conditions. The second element in the tag consists of a calmodulin binding protein (CBP) epitope, which allows a second round of affinity purification on a calmodulin-coated bead matrix, this is necessary to remove both the TEV protease as well as remaining trace contaminants. After washing bound material is again eluted under native conditions, this time by the chelation of Ca^{2+} ions with EGTA. The eluted tagged proteins, together with any co-purifying proteins, can then be analysed by SDS PAGE followed either by western blotting or mass spectrometry.

The cell line chosen for this analysis was Human Embryonic Kidney 293 cell line. 293 cells were originally generated by transformation using sheared fragments of Adenovirus DNA (Graham et al., 1977). As a consequence of this they acquired the E1B19k open reading frame and express high levels of E1B19k. They are also well suited to biochemical purifications being fast and densely growing cell line leading to particularly high protein yields relative to other commonly used cell lines. For efficient large-scale purifications it was preferable to use cell lines stably expressing the TAP tagged Bax fusion proteins. In order to prevent cells adapting to the inherent toxicity of constitutive Bax over-expression, which is substantially increased by some of the mutations, expression of the tagged proteins was made dependent on a tetracycline inducible expression system (T-REx) to enable their regulated expression in 293 cells stably expressing the Tetracycline Repressor (293 T-REx cells).

The generation of 293 T-Rex stable cell lines expressing TAP tagged Bax and Bax mutants is outlined in section 2.4.5. Prior to their use in purification experiments the 293 clonal cell lines were examined for the localisation by immunofluorescence microscopy to validate the distribution of the TAP tagged Bax protein. In all cases the distribution in the TAP-tagged Bax proteins in E1B19k-containg 293 clones was analogous to the equivalent GFP-tagged Bax protein in MCF10A E1B19k, as characterised in Chapter 5. This is illustrated by the location of the Bax-TAP L25P and Bax-TAP AEE, which, in the presence of E1B19k are shifted into mitochondrial localised foci or an ER-like distribution respective (Figure 6.1).

To ensure subsequent TAP purifications would yield meaningful results, two further analyses were performed on the 293 T-REx clonal cell lines to validate and characterise TAP-tagged Bax activity. Firstly, the effect of Bax induction on their cristae structure was examined by electron microscopy. Cells were treated for 12 hrs with 100 ng/ml doxycycline, which was sufficient to induce TAP-tagged Bax proteins to a high level. The cells were then harvested, fixed and prepared for electron microscopy. Representative images from five clonal lines expressing: TAP-Bax, TAP-Bax L25P, TAP-Bax AEE, Bax-TAP and Bax-TAP L25P are shown in Figure 6.2. This analysis revealed that, relative to a control cell line expressing the TAP tag alone (Figure 6.2, panel A), induction of TAP-tagged Bax proteins did not result in disruption of mitochondrial morphology or cristae ultrastructure. This result is likely to indicate that, despite high level Bax induction, and its presence in mitochondrially associated foci in cells expressing the L25P mutation, E1B19k is able prevent mitochondrial dysfunction at this time point. Although electron microscopy was not conducted at later times it was observed that between 18 and 24 hrs after induction of TAP tagged Bax most 293 clonal cell lines showed significant levels of death (data not shown). Since expression was maximal after approximately 8-10 hrs of induction, the later cell death is likely to reflect the eventual overloading of E1B19k's ability to block cell death. However, this analysis shows that at 12 hrs after induction, when TAP purifications were performed, the induced Bax proteins had yet to cause significant mitochondrial disruption.

Finally, the TAP-tagged Bax clones were also subjected to gel filtration analysis. The results for three cell lines expressing Bax-TAP, Bax-TAP L25P and Bax-TAP AEE are shown (Figure 6.3). Equal aliquots from fractions spanning the entire column volume were analysed by western blotting to visualise the elution profiles of: TAP-tagged Bax (41 kDa), endogenous Bax (21 kDa) and the alpha subunit of the F1F0 ATP Synthase, which is a 60 kDa protein but as a component of much larger macromolecular complexes at mitochondria (up to 670 kDa), and thereby provided a marker for the highest molecular weight range separated by the column. This analysis reveals that whilst endogenous Bax and wild type Bax-TAP elute at sizes close to their monomeric masses, Bax-TAP AEE and, to a greater extent, Bax-TAP L25P shift into higher molecular weight ranges. They also cause shifts in the elution profiles of both E1B19k and a small fraction of the endogenous Bax. This data therefore provides preliminary validation of the approach, suggesting that TAP-tagged Bax proteins, and in particular Bax-TAP L25P, could enter larger protein complexes than are accessible to the wild type Bax-TAP, which appears to remain monomeric.

In the literature it has often been assumed that the higher molecular weight fractions of Bax from apoptotic cells (Antonsson et al., 2001) are directly comparable to the Bax homo-

oligomers stabilised by protein cross-linkers (Mikhailov et al., 2003) and the foci observed by immunofluorescence analysis (Nechushtan et al., 2001). However, it has been reported that these foci are likely to contain around 1,000 to 20,000 Bax molecules (Nechushtan et al., 2001), thus making them far larger than either the dimers and tetramers stabilised by cross-linking or the 200-600 kDa material seen by gel filtration analysis described above. In addition the very large clusters of oligomeric Bax that form in the later stages of apoptosis have been reported to be CHAPS insoluble (Annis et al., 2005; Gilmore et al., 2000; Valentijn et al., 2003). It is possible that a fraction of the material seen at higher molecular weight ranges on Bax gel filtration profiles is a component of larger mitochondrial protein complexes. In support of this interpretation, Bcl-XL (Antonsson et al., 2001) and BHRF1 (this study, data not shown) have both been seen in high molecular weight fractions (~400-600 kDa) by gel filtration and yet there is no evidence that these proteins participate in the formation of Bax oligomers. It was reasoned that TAP purifications might assist in characterising the composition of these higher molecular weight complexes and these complexes are more accessible to Bax–TAP L25P than the wild type Bax-TAP, which appears to remain monomeric.

6.4 Tandem Affinity Purifications with Bax:

Triton X-100, a non-ionic detergent, causes oligomerisation Bax, whilst the zwitterionic detergent CHAPS does not perturb Bax conformation (Hsu and Youle, 1997; Hsu and Youle, 1998). Initial TAP purifications were performed with wild type Bax, tagged at the N-terminus and at the C-terminus, in both these detergent conditions (Figure 6.4). Analysis of the final TAP eluate by western blotting for Bax revealed an absence of the endogenous protein co-purifying with either TAP-Bax or Bax-TAP in CHAPS detergent (Figure 6.4 A). In good agreement with the published literature, TAP purifications in the presence of Triton induced co-association of Bax and approximately equal amounts of endogenous Bax were co-purified with the TAP-tagged proteins (Figure 6.4 B). When the final TAP eluate was analysed by SDS PAGE followed by silver staining, a noticeably less complex band pattern was visible in Triton versus CHAPS purified material (Figure 6.4 C). The protein content of most of the bands was below the level required for identification by mass spectrometry, although the identity of endogenous Bax in the Triton-purified material was confirmed. It was also apparent that there were more bands co-purifying with Bax-TAP and with TAP-Bax under CHAPS detergent conditions.

The structure / function analysis described in Chapter 5 resulted in the identification of a leucine residue within the N-terminally conformationally sensitive hα1 of Bax, which, when mutated to a helically disrupting proline residue, promoted activation of the N-terminally tagged GFP-Bax.

It was also determined that placing the GFP-tag at the C-terminus, Bax-GFP L25P, resulted in a substantial reduction in Bax activity and a constitutively cytoplasmic localisation. However, when expressed in the presence of E1B19k, the C-terminally tagged L25P mutant was induced to enter small mitochondrially associated foci (Figure 5.4), without a large increase in the protein's toxicity (Figure 5.6). In addition, when the GFP-tag was exchanged for the TAP-tag, Bax-TAP L25P, and expressed in E1B19k-expressing 293 cells a similar partial localisation into mitochondrially-associated foci was observed (Figure 6.1), resulting in a shift to higher molecular weight ranges in the protein's elution profile by gel filtration relative to the wild type control (Figure 6.3). When the behaviour of this mutant in TAP purifications was examined there was a noticeable increase in both the complexity and intensity in the resulting band pattern, relative to that observed with either the N- or C-terminally tagged wild type proteins, following analysis by SDS PAGE and silver staining, (Figure 6.5). From this experiment one of the co-purifying bands of approximately 19 kDa in size was identified as Adenoviral E1B19k. This provided an initial validation for the hypothesis presented in Chapter 5 that mitochondrial localisation of the Bax-GFP L25P in E1B19k-expressing cells was due to destabilisation of the protein promoting activation and it enters a mitochondrial localisation due it forming an E1B19k to inhibit its complete activation. In support of this, it has been previously demonstrated that E1B19k selectively binds the active conformation of Bax, and that this results in its translocation to mitochondria (Perez and White, 2000).

Other combinations of Bax mutations and N- and C-terminal tags were investigated, however, the Bax-TAP L25P combination consistently resulted in the purification of a more complex and more abundant range of co-purifying proteins (see below and data not shown). Therefore this variant was chosen for a preparative scale TAP purification experiment. Eluted proteins were analysed by SDS PAGE followed by staining with colloidal coomassie (Figure 6.6). Systematic identification of co-purifying proteins was achieved by subjecting the entire SDS PAGE separation range in 1 mm slices to tandem electrospray mass spectrometry. This resulted in the identification of the following protein or protein complexes as major co-purifying species: (i) components of the F1F0 ATP Synthase from the inner mitochondrial membrane, (ii) components of the OST48/Ribophonirn complex from the ER and an associated ER-lumenal chaperon, Calnexin, (iii) two inner mitochondrial chaperone proteins, the prohibitins (Figure 6.6).

The prominent representation of mitochondrial inner membrane proteins, namely the F1F0 ATP Synthase complex and prohibitins, in these initial TAP purification was surprising since Bcl-2 proteins, including Bax, are thought to be located at the outer mitochondrial membrane. However, it is know that in places the mitochondrial inner and outer membranes may come into

very close proximity and may even fuse in specialised structures known as contact sites (Crompton, 2000; Crompton et al., 2002). It is also thought that some Bcl-2 proteins localise to these contact sites, including tBid (Kim et al., 2004b; Lutter et al., 2001), and potentially Bax (Capano and Crompton, 2002). In addition, the number of mitochondrial contact sites has been observed to increase in apoptosis induced by Bax over-expression (He et al., 2003) and importantly, the ATP Synthase has been shown to be enriched at contact sites (Hoppel et al., 2002).

The Bax α5/α6 region is known to insert into membranes, with the apex of this region (residues 127 - 129 of human Bax), being thought to fully penetrate the lipid bilayer (Annis et al., 2005). It is therefore possible that this region of Bax could make contact with inner membrane proteins, particularly at contact sites. The AAA (K119A, K123A, K128A) charge neutralisation mutant and AEE (K119A, K123E, K128E) charge reversal mutant, introduced in Chapter 5, were selected specifically to alter the properties of the α5/α6 region (see section 5.2). It was therefore investigated whether, in TAP purification experiments, these Bax mutants were able to perturb any of the candidate interactions identified using the Bax-TAP L25P mutant. Based on its increased toxicity (see Section 5.5) and similarity to the bacterial toxin proteins, which constitutively insert into cellular membranes (Rosconi and London, 2002), it was predicted that the AAA mutation is able to bypass some levels of regulation wild type Bax is subjected to. It was therefore hypothesised that this mutation may disrupt or weaken interactions with inner membrane proteins. The AEE mutation was selected to make the α5/α6 region resemble that of the pro-survival proteins Bcl-2 and Bcl-XL. A model has been proposed whereby Bcl-XL and Bax compete for a shared, but as yet unidentified, mitochondrial target (Polcic and Forte, 2003). On the basis of this data it was hypothesised that if such a target protein was among those identified in the Bax-TAP L25P purifications, and the a5/a6 region of Bax mediated the interaction, then making this region of Bax more closely resemble that of Bcl-XL would enhance the interaction.

To test these predictions, parallel TAP purifications were conducted using the using the C-terminally tagged Bax mutant panel, S184V, L25P, AAA (two separate clones) and AEE, together with the wild type protein. Final TAP eluates were analysed by western blotting for some of the major co-purifying species identified by mass spectrometry (Figure 6.7 A). Levels of Bax-TAP in the final eluates, as an indication of the protein yield from the experiment, were approximately equal. However, assessment of the effect of the mutations on the levels of the candidate interacting proteins was not conclusive. In general, the L25P and AEE mutation performed consistently better than the other variants, namely WT, S184V and AAA. However, after several attempts at these experiments, it became clear that experimental variation

introduced by two rounds of affinity purification necessary for TAP purifications also had a substantial effect on the levels of candidate Bax interacting proteins detected. Therefore, whilst the trend was that L25P and AEE mutants enhanced the levels of co-purifying proteins, it cannot be concluded for certain that this was directly due to the mutations introduced into the Bax molecule. These purifications did however confirm the presence of bands, of the correct size, recognised by antibodies raised against the F1F0 ATP Synthase alpha, beta, d and OSCP subunits, Ribophorin I, Calnexin I and E1B19k in the TAP eluates. In addition, the presence of the F1F0 ATP Synthase beta subunit, BAP32, BAP37, Ribophorin II was also confirmed (data not shown). This data thereby acts as to initially validate the protein identification made by mass spectrometry (Figure 6.6). Finally, these experiments did show that the more toxic mutations, namely L25P, AAA and AEE, were consistently those co-purifying the highest levels of E1B19k, supporting data which suggests E1B19k specifically interacts with the active conformation of Bax (Perez and White, 2000).

Purifications with N-terminal tagged constructs were also attempted. In these experiments very little ATP Synthase, the major co-purifying complex in the C-terminal TAP data set, was detected (Figure 6.7 B). In this case the AAA and AEE mutations both consistently outperformed the other mutations, although the reason for this is not known. The low abundance of co-purifying proteins obtained with the N-terminal TAP mutant set in these experiments was in good agreement with earlier observations using only the wild type proteins (Figure 5.4 and 5.5). For these reasons the N-terminally TAP tagged Bax mutants were not pursued further.

6.5 Tandem Affinity Purifications with Bcl-XL:

An initial concern regarding the spectrum of proteins identified in Bax TAP purifications was their subcellular localisation, with abundant protein complexes from both mitochondrial inner membrane and endoplasmic reticulum proteins being highly represented. Whilst both can be explained in terms of known localisation of Bcl-2 proteins to mitochondrial contact sites (discussed above), and the recently established role for Bax at the ER (Scorrano et al., 2003; Zong et al., 2003), it was considered preferable to first try and validate these interactions in a heterologous system.

Therefore, in collaboration with Ingram Iaccarino (present location CNR, Naples, Italy), similar TAP purifications were undertaken with Bcl-XL fused to an N-terminal TAP tag. Following transfection and drug selection, cells were analysed for the ability of the over-expressed Bcl-XL to functionally protect from UV induced apoptosis (Figure 6.8 A). Cells were exposed to a

200 J/m^2 UV irradiation for 0, 2 or 4 hrs whole cell lysates were then prepared and analysed by western blotting for cleavage of the PARP protein, a marker of apoptosis (Figure 6.8 A). This result clearly demonstrates that the over-expressed Bcl-XL was functional despite the addition of the N-terminal TAP tag, causing a substantial reduction in PARP cleavage 4 hrs after irradiation. Following initial TAP purifications it was determined that purification of candidate Bcl-XL interacting proteins was significantly enhanced by the addition of a membrane fractionation step, prior to detergent solubilisation of the cells (Figure 6.8 B). Systematic identification of co-purifying proteins was achieved by subjecting the entire SDS PAGE separation range to tandem electrospray mass spectrometry. The complete data set of proteins identified in purification with Bax-TAP L25P from 293 T-REx cells and TAP-Bcl-XL from HeLa cells is shown in Table 6.1. Proteins highlighted bold are shared between the Bax and Bcl-XL data sets. Where possible, proteins of the same complex or subcellular localisation have been grouped together. The potential relevance of these proteins to Bax and Bcl-XL function and the regulation of apoptosis are discussed in section 6.7 and Chapter 7.

6.6 Preliminary validation of candidate Bax and Bcl-XL interacting proteins:

In order to validate some of the candidate interactions listed in Table 6.1 co-immunoprecipitation were performed. The F1F0 ATP Synthase was the most abundant co-purifying species in Bax-TAP L25P purifications and an antibody that allows the immunocapture of F1F0 ATP Synthase complex has been reported (Aggeler et al., 2002) and was used for the basis of these for co-immunoprecipitation assays from MCF10A cells treated with Fas/CHX or STS to induce apoptosis (Figure 6.9). Preliminary result indicates that there is an inducible interaction between endogenous F1F0 ATP-Synthase and Bax, under conditions where subunits of the ATP Synthase complex are immunoprecipitated evenly. In the experiment shown, the cells were harvested after 6 hrs of exposure to the apoptotic stimulus, at which time STS has induced substantially more death than Fas/CHX (data not shown). In support of this result, co-purification of Bcl-XL and the F1F0 ATP Synthase to a high degree of purity has recently been observed following a sequential biochemical fractionation strategy (Marie Hardwick, personal communication). Further characterisation of this interaction is ongoing.

From the Bcl-XL data set, further attempts were made to validate the interaction between XL and a small transport protein JM4 (see below for discussion). Again, preliminary data is shown in figure 6.9, indicates that over-expressed Myc-tagged JM4 co-immunoprecipitates with over-expressed Bcl-XL following transfection into HeLa cells. Further characterisation of this

interaction is on-going however, the related protein Rab7 has been seen to interact with Bcl-XL by far western (Abigail Hunt and Gerard Evan, personal communication) and there is preliminary evidence of a mutually exclusive binding of either JM4 or Rab7 to Bcl-XL (data not shown).

6.7 Discussion:

Evidence suggesting that Bcl-2 proteins, and Bax in particular, might interact with additional cellular proteins outside of the Bcl-2 family has steadily accumulated. In particular the existence of a mitochondrial target for Bax has been predicted both by biochemical fraction models (Roucou et al., 2002) and by experiments in yeast suggesting Bcl-XL and Bax may compete for a shared target (Polcic and Forte, 2003). Bcl-XL has been suggested to have survival functions independent of Bcl-2 family interactions (Minn et al., 1999). In addition, it has yet to be definitively shown the higher molecular weight range entered by Bax in gel filtration experiments represents only Bax and Bak oligomers and not additional protein complexes. Accumulating evidence suggests that Bax oligomerisation is the key event in its irreversible activation (Gross et al., 1998), and when this does occur it is likely to happen at mitochondrial membranes (Annis et al., 2005). Evidence from the present study suggests that Bax molecules may first become activated in a local subcellular region, implicating one or a small subset of mitochondria in being intimately involved in the Bax activation event.

In order to isolate candidate proteins interacting with Bax at the critical mitochondrial stages in its activation, a strategy was developed which allowed the Bax molecule to be accumulated in an active state at mitochondria using a mutation, L25P, while the expression of E1B19k blocked loss of cells due to apoptosis. TAP purifications were performed using a C-terminally tagged version of this mutant, Bax-TAP L25P expressed in 293 T-REx cells. Constitutive expression of E1B19k in 293 cells, caused Bax-TAP L25P to enter small mitochondrially-associated foci, (Figure 6.1), without significant disruption of mitochondrial ultrastructure (Figure 6.2). Bax-TAP L25P also displayed a shift to a higher molecular weight range on gel filtration profiles, relative to the wild type protein (Figure 6.3). In addition, and for comparison, TAP purifications were performed with N-terminally tagged Bcl-XL, which remained functional when over-expressed in HeLa cells. The combined data Bax and Bcl-XL purification shows a substantial degree of overlap, despite the use of different cell lines, different expression systems, and TAP tags placed at different ends of the molecules. This section considers the potential significance of some of the proteins identified in this screen as co-purifying with Bax and Bcl-XL. A more

general discussion considering the place of this data set in the field of apoptosis regulation as a whole follows in the final Chapter.

6.7.1 Known interactions - E1B19k and the BH3 only proteins:

The presence of high levels E1B19k in the Bax data set indicates that the L25P mutant protein has gained an active Bax conformation (Perez and White, 2000). It is likely that, following the induction of high levels of activated Bax, binding of E1B19k to Bax delays cell death in these cells, allowing them to be harvested for purifications. Strikingly within the Bax data set no Bcl-2 family members were detected. In contrast the Bcl-XL data set contained Bax and Bak, together with BH3-only proteins Bim, Puma, Bid and Bad. Strikingly, these are exclusively members of the subset of BH3-only proteins shown to have highest affinity for Bcl-XL in recent binding studies (Chen et al., 2005) (Figure 1.4 B). The presence of Bax indicates that perhaps mitochondrially localised Bax can be bound by Bcl-2 pro-survival proteins in an analogous manner as that now demonstrated conclusively for Bak (Willis et al., 2005) (Figure 1.4 C). BH3-only proteins, in particular, are low abundance proteins and of small molecular weight, therefore making them difficult to detect by mass spectrometry. The fact that these proteins were detected at levels allowing protein sequencing, and in concordance with recently published literature, indicates the purifications were working reliably and efficiently.

6.7.2 F1F0 ATP Synthase complex and other inner membrane proteins:

The F1F0 ATP Synthase complex is a highly conserved enzyme complex catalysing the terminal step in ATP synthesis. The mammalian complex contains at least 17 subunits. The F0 component acts as a proton channel embedded in the inner mitochondrial membrane. The F1 component catalyses either the synthesis or hydrolysis of ATP and is attached to the matrix-side of the F0. The F1F0 ATP Synthase was originally implicated in Bax function when the F0 b subunit was identified in a classic yeast genetic screen of mutations conferring Bax resistance, although no direct biochemical link was anticipated the time. Although this study was criticised for their failure to report the exact genetic defect, it was subsequently demonstrated that functional oxidative phorphorylation, in general, is required for Bax killing in yeast (Harris et al., 2000). Subunits of the F1F0 ATP Synthase complex were major components of both the Bax and Bcl-XL data sets. The functional significance of a direct biochemical interaction between Bax and the ATP Synthase is at present unclear. However, it is interesting to note that changes in $\Delta\psi_m$ occurring at the time of onset of apoptosis, as yet do not have a defined molecular mechanism. In the absence of sufficient flux through the electron transport chain both hydrolysis of ATP via reversal of the F1F0 ATP Synthase and regulated ATP^{4-}/ATP^{3-} exchange through ANT provide alternative mechanisms by which $\Delta\psi_m$ can be maintained. It is possible Bax and Bcl-XL have as yet undefined roles in coordinating (Bcl-XL) or disrupting (Bax) the metabolic mechanisms by which ATP production and maintenance of $\Delta\psi_m$ are coordinated.

6.7.3 The Ribophorin / OST48 / DAD1 complex:

The Ribophorin / OST complex catalyses the first step in N-linked glycosylation of proteins. Calnexin is an associated chaperone. The smallest subunit of this complex, DAD1, was named after it was originally identified as Defender Against apoptotic cell Death . Originally characterised in CHO cells (Kelleher and Gilmore, 1997). DAD1 has also been reported to interact with Mcl-1 in a yeast two hybrid assay (Makishima et al., 2000). Glycosylation defects may have as yet unidentified links to the initiation of apoptosis. Inhibition of N-linked glycosylation in yeast has been reported to result in a range of phenotypes similar to those seen during apoptotic cell death of mammalian cells, such as DNA fragmentation and phosphatidylserine exposure, and these could be blocked by Bcl-2(Hauptmann et al., 2006).

6.7.4 VDAC and ANT:

Both mammalian isoforms of VDAC were specifically detected in the Bcl-XL data set, but not with Bax. This supports existing data suggesting that VDAC2, a low abundance isoform, can specifically interact with the active conformation of Bak to prevent oligomerisation of the protein (Cheng et al., 2003). It has also been reported that Bax can regulate with VDAC (Shimizu et al., 1999), but more recent evidence argues against this (Rostovtseva et al., 2004). Conversely the presence of Adenine Nucleotide Transporter (ANT) was specific to the Bax purification data set. ANT has been directly implicated in promoting Bax function (Marzo et al., 1998), however, its presence could also be explained due to the large amount of F1F0 ATP Synthase purified, since ANT is known to co-purify with this respiratory complex (Ko et al., 2003).

6.7.5 Rab7/JM4 and secretory pathway proteins:

The small GTPase Rab7, has recently been implicated in the degradation of nutrient transporters in response to growth factor withdrawal (Edinger et al., 2003). Under these conditions, Rab7 deficiency leads to prolonged cell autonomous survival in the absence of growth factors. Another small candidate regulator of the endocytic pathway identified was JM4 which as has family of proteins bearing a prenylated Rab acceptor 1 (PRA1) motif. (Schweneker et al., 2005).

6.7.6 Proteins involved in Ca^{2+} regulation:

Whilst mitochondrial contact sites (discussed above) and the close proximity of the ER to mitochondria (Figure 6.2, red arrows) (Collins et al., 2002; Rizzuto et al., 1998) provide a possible explanation physiological explanation. In addition to the close physical proximity of the organelles, a pool of Bax and Bak molecules have both been reported localise to the ER (Scorrano et al., 2003; Zong et al., 2003). Genetic studies have indicated that Bax and Bak can promote release of Ca^{2+} from the ER (Zong et al., 2003), whilst over-expression of Bcl-2 promotes Ca^{2+} release by unregulated leak from the ER (Oakes et al., 2005). In this respect it is

also interesting that a SEC61 complex component (Sec61 beta), as well as the Signal receptor delta and signal peptidase proteins were identified in the Bcl-XL data set. The SEC61 complex forms the core of the mammalian endoplasmic reticulum (ER) translocon, a transmembrane channel for the translocation of proteins across the ER membrane, but has also recently been implicated in mediating ER Ca^{2+} leak (Van Coppenolle et al., 2004). Both Bcl-2 and Bcl-XL have been reported to interact with the IP3 receptor (Chen et al., 2004; White et al., 2005), which is present in the Bax data set. Also MG29 has been reported to be a small regulator of the Ryanodine receptor, a relative of the IP3 receptor, and been reported to promote apoptosis through up-regulation of ER Ca^{2+} leak (Pan et al., 2004).

The proteins identified in these analyses require further validation. However, the presence of known Bcl-2 family interacting proteins and proteins previously implicated in the regulation of apoptosis provides at least a partial validation of the approach. The substantial overlap between the Bax and Bcl-XL data sets despite the use of different cell lines and the proteins being tagged at different ends also indicates many of these proteins may interact with multi-domain Bcl-2 proteins more generally. Each interaction will need to be confirmed by co-immunoprecipitation and the relevance to the apoptotic program assessed in function assays. However, the range of metabolic and transport proteins identified and not previously implicated in Bcl-2 function provides initial evidence that Bax regulation, and that of the Bcl-2 family more generally, may be more closely integrated into the control of cell metabolism and physiology than previously anticipated.

Figure 6.1 Distribution of TAP-tagged Bax proteins in 293 T-REx clonal cell lines.

The distributions of TAP-tagged Bax proteins in 293 T-REx clonal cell lines were identical to those of the analogous GFP-tagged proteins in MCF10A E1B19k cells. Two of the 293 T-REx clonal cell lines generated are shown: Bax-TAP L25P (clone 3.13, top row) and Bax-TAP AAA (clone 4.9, bottom row). Cells were plated on glass coverslips and treated with 100 ng/ml doxycycline for 12 hrs to induce expression of the tagged Bax protein. Cells were then loaded with Mitotracker to reveal the location of energised mitochondria, fixed and stained using a FITC-coupled secondary antibody alone. The secondary antibody recognises the TAP tag since Protein A epitopes within the TAP tag bind to the constant region of the antibody's heavy chain. Cells were mounted and imaged by confocal microscopy. Scale bars represent 10 μm.

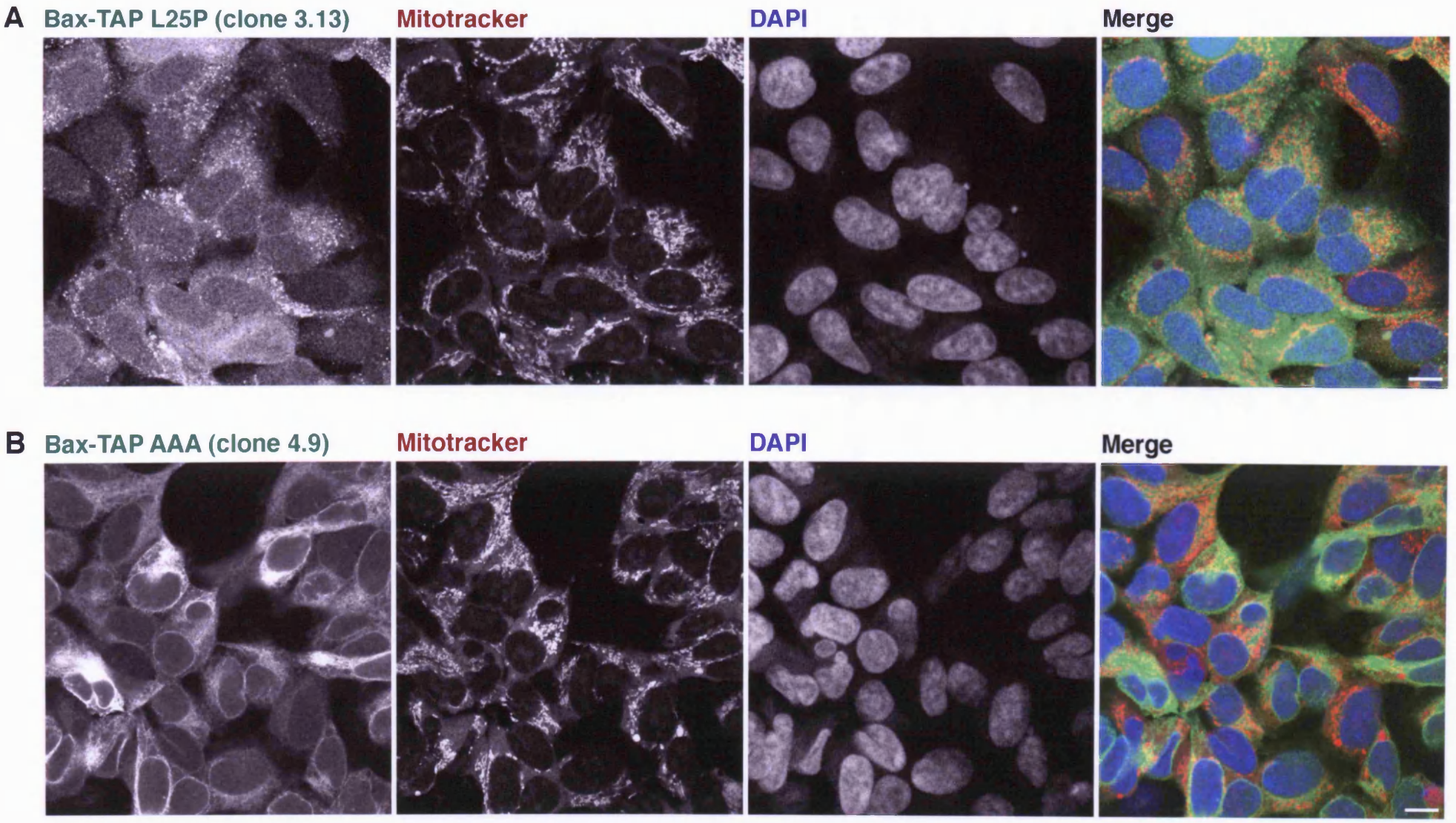
A
Bax-TAP L25P (clone 3.13)
Mitotracker
DAPI
Merge
B
Bax-TAP AAA (clone 4.9)
Mitotracker
DAPI
Merge

Figure 6.2 Expression of TAP-tagged Bax proteins does not change mitochondrial morphology in 293 T-REx clonal cell lines.

Analysis of 293 T-Rex clonal cell lines by electron microscopy confirmed that induction of TAP-tagged Bax proteins did not cause significant disruption to mitochondria. 293 T-REx cells were treated with 100 ng/ml doxycycline for 12 hrs to induce expression of the TAP-tagged Bax proteins, then fixed and prepared for electron microscopy. **(A)** Control cell line expressing the TAP tag alone demonstrating normal mitochondrial morphology with tightly aligned cristae membranes. This morphology is unchanged following the induction of: **(B)** wild type (w.t.) TAP-Bax (which is mostly cytoplasmic); **(C)** TAP-Bax L25P (which forms small mitochondrially-associated foci); **(D)** TAP-Bax AEE Bax (which shows a partial enrichment at mitochondria without forming foci); **(E)** wild type (w.t.) Bax-TAP (which is cytoplasmic); **(F)** Bax-TAP L25P (which forms small mitochondrially-associated foci). In all images scale bars represent 0.5 μm. Areas where mitochondria are in close proximity to the endoplasmic reticulum are highlighted with red arrows (see section 6.5 and Chapter 7 discussion).

A TAP control (clone 11.22)

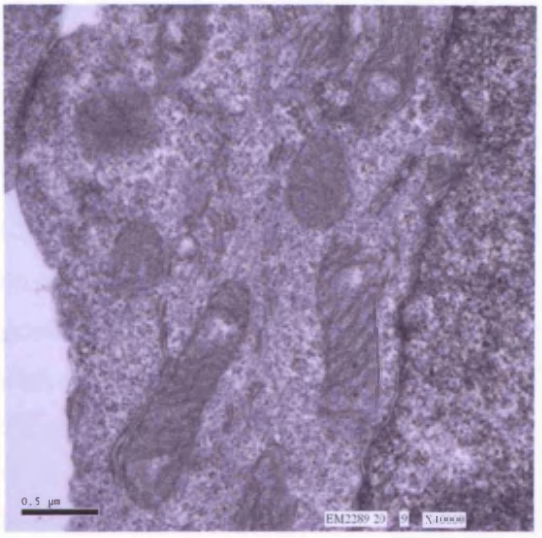

B TAP-Bax w.t. (clone 6.18)

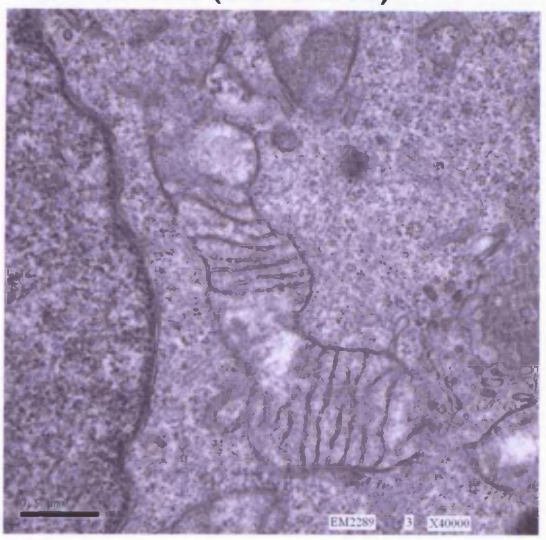

C TAP-Bax L25P (clone 8.21)

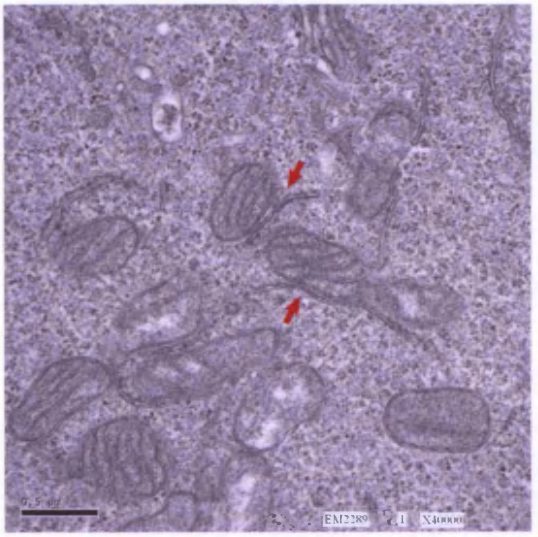

D TAP-Bax AEE (clone 10.3)

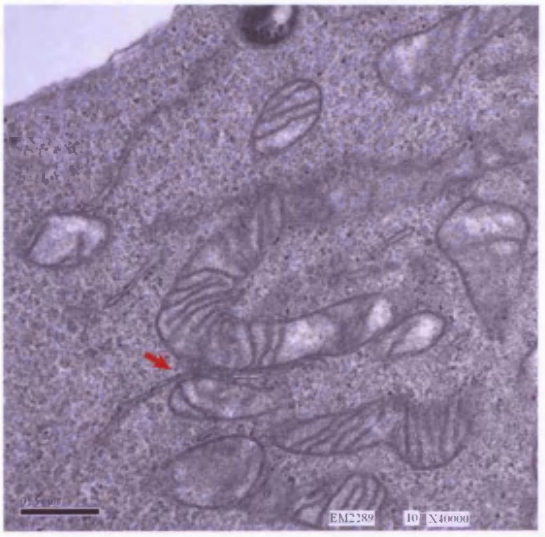

E Bax-TAP w.t. (clone 8.10)

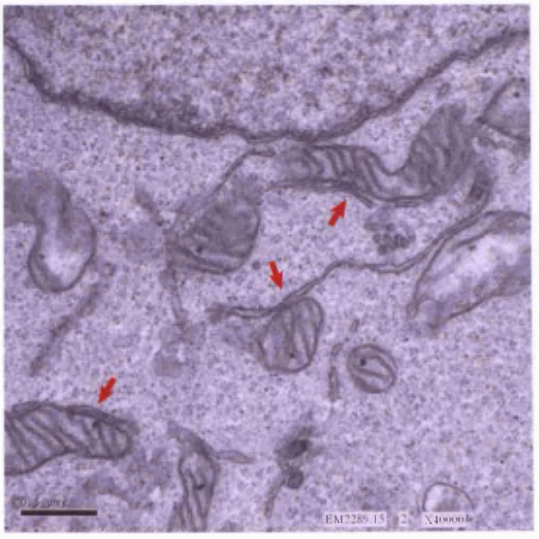

F Bax-TAP L25P (clone B.12)

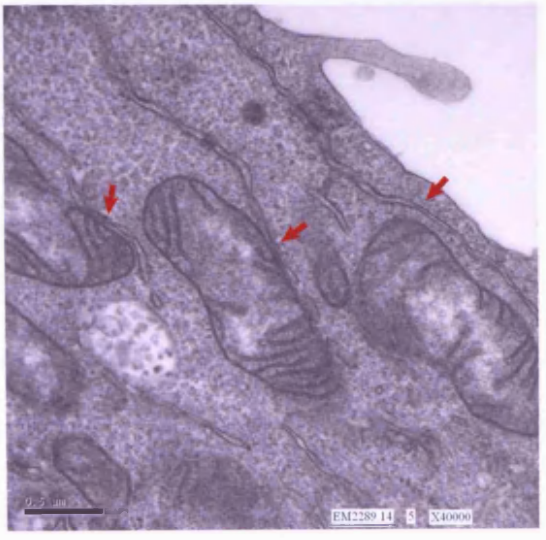

Figure 6.3 The gel filtration profile of TAP-tagged Bax is altered by Bax mutations.
Gel filtration analysis of 293 T-REx clonal cell lines reveals Bax-TAP L25P and Bax-TAP AEE mutants have altered elution profiles relative to that of Bax-TAP wild type (w.t.). 293 T-REx cells were treated with 100 ng/ml doxycycline to induce expression of the indicated TAP-tagged Bax protein. Cells were then harvested and lysed in an equal volume of 2% CHAPS lysis buffer and analysed by gel filtration. 10 μl aliquots of the indicated fractions were analysed by SDS PAGE followed by western blotting with: anti-Bax (2D2), an antibody raised against the alpha subunit of the F1F0 ATP Synthase (alpha) and anti-E1B19k. The TAP tagged protein is recognised by all antibodies due to Protein A epitopes within the TAP tag. In each case a longer exposure of the Bax elution profile is shown to reveal the presence of Bax in higher molecular weight fractions. **(A)** Bax-TAP wild type control, which is predominantly cytoplasmic; **(B)** Bax-TAP L25P, which forms small mitochondrially-associated foci; **(C)** Bax-TAP AEE, which shows a partial enrichment at mitochondria without forming foci.

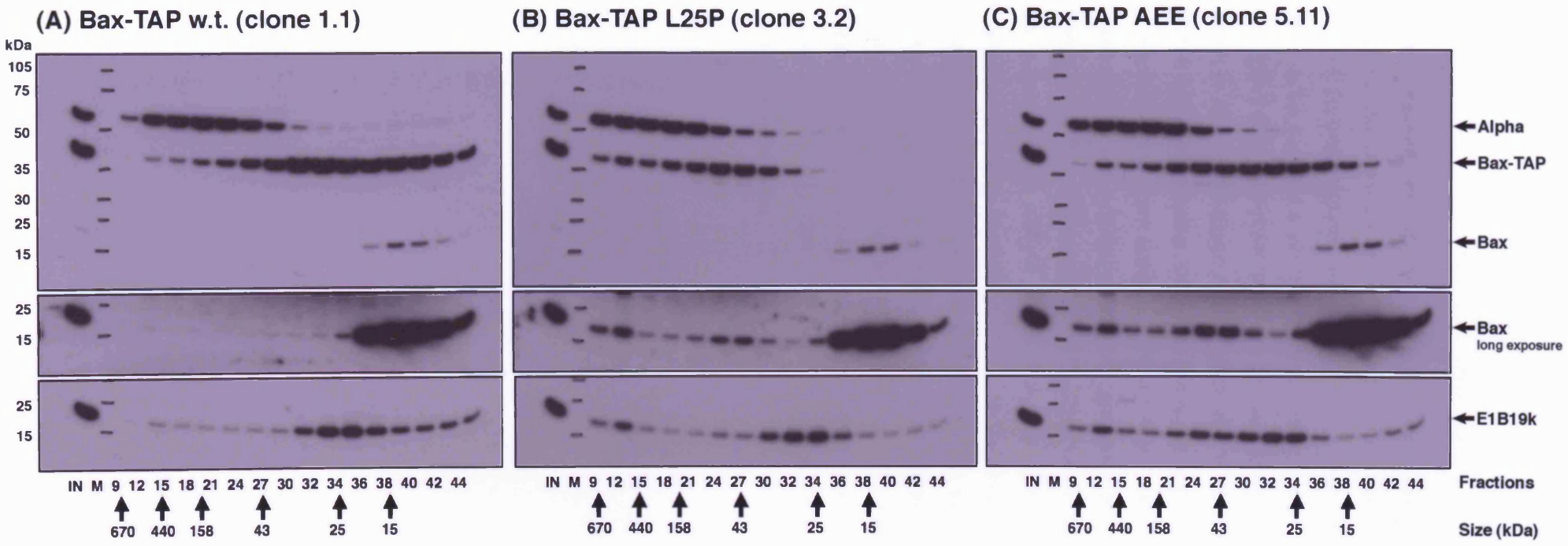
(A) Bax-TAP w.t. (clone 1.1)
(B) Bax-TAP L25P (clone 3.2)
(C) Bax-TAP AEE (clone 5.11)
kDa
105
75
50
35
30
25
15
25
15
25
15
IN M 9 12 15 18 21 24 27 30 32 34 36 38 40 42 44
670 440 158 43 25 15
Alpha
Bax-TAP
Bax
Bax
long exposure
E1B19k
Fractions
Size (kDa)

Figure 6.4 Effect of detergents on the profile of proteins purified with TAP-tagged Bax.
TAP purifications in the presence of the zwitterionic detergent CHAPS resulted in a distinct profile of purified proteins without endogenous Bax whilst the presence of the non-ionic detergent Triton X-100 resulted a simpler band pattern and large amounts of endogenous Bax are co-purified. 293 T-REx cells (TAP-Bax clone 8o, Bax-TAP clone 10f and a TAP control clone 12c) were grown in 15 x 15 cm tissue culture plates and expression of the TAP tagged protein induced with 100 ng/ml doxycycline for 12 hrs. Cells were then harvested and used for TAP purifications. Equal fractions were collected at each stage in the TAP purification and used for diagnostic western blots with anti-Bax (2D2). **(A)** purification in CHAPS detergent, there is no endogenous Bax in the final eluate (lane 5); **(B)** purification in Triton X-100 detergent there are approximately equal amounts of TAP tagged Bax and endogenous Bax in the final eluate (lane 5, compare red boxes to those in part (A)). In both cases the TAP tagged protein and endogenous Bax can be seen in Lane 1. The decrease in size of the TAP-tagged Bax from Lane 3 onwards is due to loss of the tandem Protein A epitopes due to TEV cleavage. **(C)** Final eluates from the TAP purifications were analysed by SDS PAGE and visualised by silver staining. M indicates lanes containing molecular weight markers. Labelled bands: blue arrow is TAP-Bax, green arrow is Bax-TAP, pink arrow is endogenous Bax, red arrows are bands submitted for mass spectrometry.

A

CHAPS

Diagnostic blots:

1 IgG column IN
2 IgG column FT
3 TEV eluate / calmodulin IN
4 Calmodulin column FT
5 Calmodulin column eluate
6 Final concentrated eluate

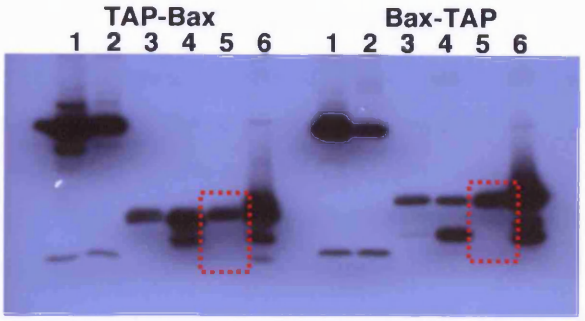

B

Triton X-100

Diagnostic blots:

1 IgG column IN
2 IgG column FT
3 TEV eluate / calmodulin IN
4 Calmodulin column FT
5 Calmodulin column eluate
6 Final concentrated eluate

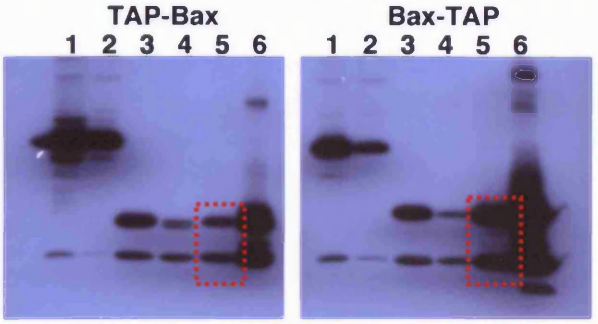

C

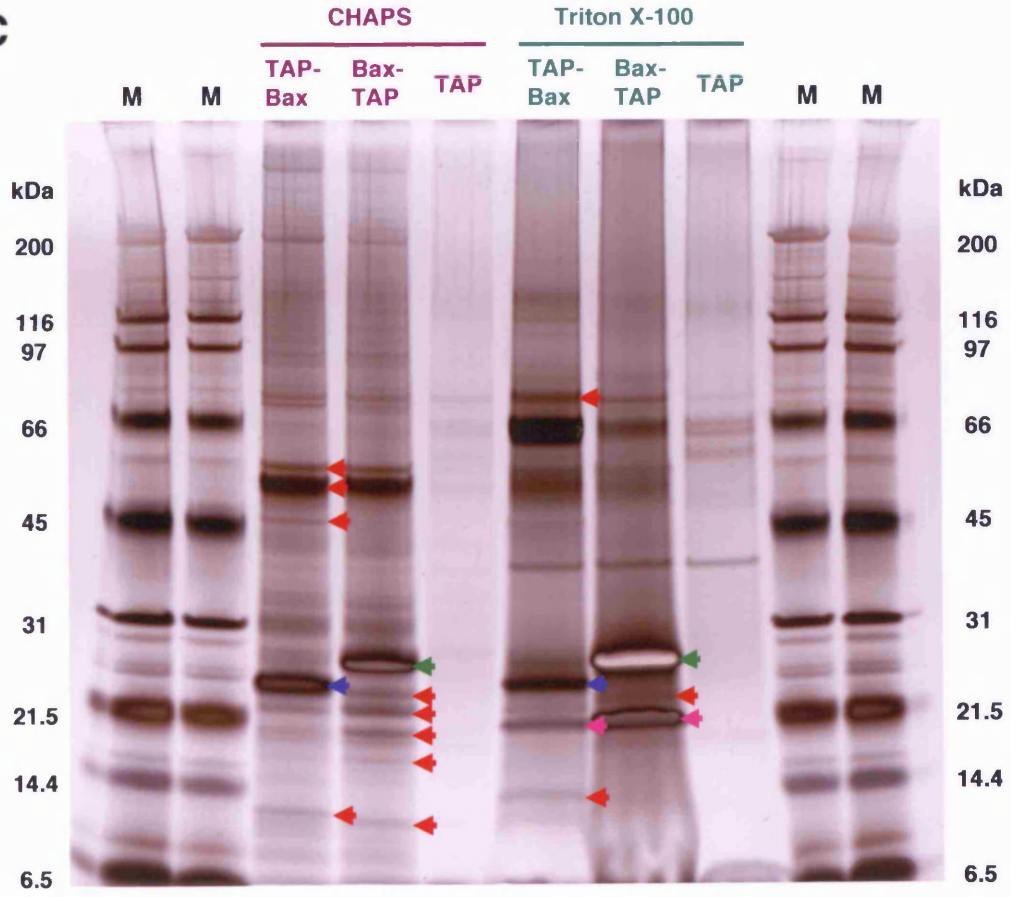

Figure 6.5 The Bax-TAP L25P construct enhances the profile of purified proteins.

C-terminally TAP-tagged Bax consistently resulted in the purification of a more complex band pattern and the staining intensity was enhanced by the use of the L25P mutation. 293 T-REx cells (Lane 1: TAP-Bax clone 8o, Lane 2: Bax-TAP clone 10f, Lane 3: TAP control clone 12c and Lane 4: TAP-Bax L25P clone B12) were grown in 15 x 15 cm tissue culture plates and expression of the TAP tagged protein induced with 100 ng/ml doxycycline for 12 hrs. Cells were then harvested and used for TAP purifications. Final eluates were analysed by SDS PAGE and visualised by silver staining. M indicates lane containing molecular weight markers. Labelled bands: blue arrow is TAP-Bax, green arrow is Bax-TAP, red arrows are bands submitted for mass spectrometry.

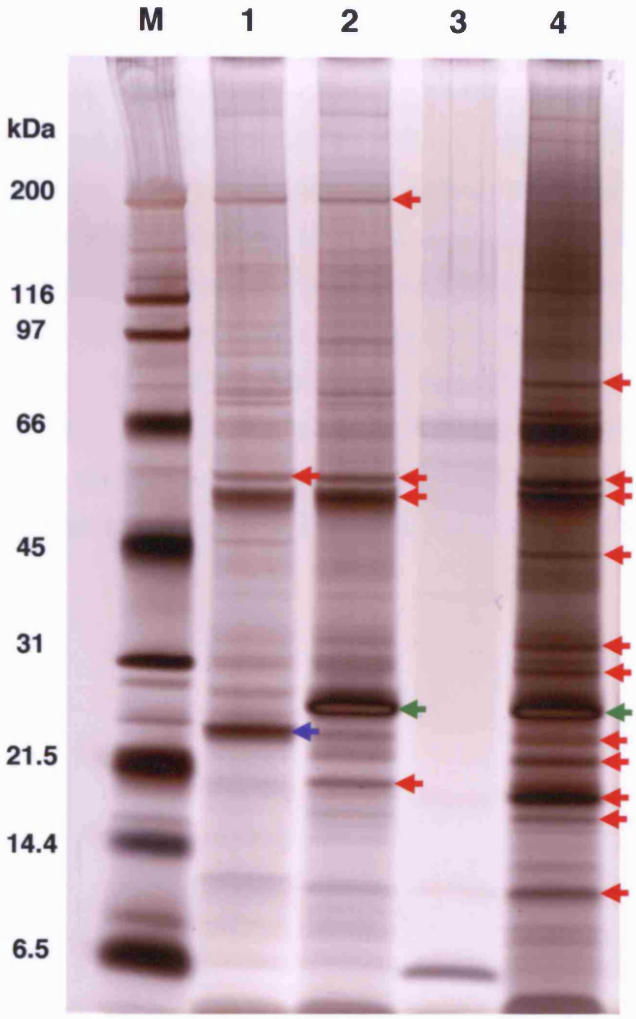

TAP purification final eluates:

Lane 1: TAP-Bax, clone 8o

Lane 2: Bax-TAP, clone 10f

Lane 3: TAP control, clone 12c

Lane 4: TAP-Bax L25P, clone B12

Figure 6.6 Summary of proteins identified by mass spectrometry in a preparative scale TAP purification with Bax-TAP L25P.

Preparative scale TAP purification with Bax-TAP L25P resulted in the identification of E1B19k, the F1F0 ATP Synthase and the Ribophorin (OST48) complex as major co-purifying species. 293 T-REx Bax-TAP L25P cells (clone B12) were grown in 60 x 15 cm tissue culture plates and expression of the TAP tagged protein induced with 100 ng/ml doxycycline for 12 hrs. Cells were then harvested and used for TAP purifications. 20 plates were used in each of 3 parallel purifications and the final eluates combined. **(A)** SDS PAGE analysis of the TAP purified proteins visualised by staining with colloidal coomassie. Labelled bands: green arrow is TAP-Bax, pink is E1B19k, red arrows are bands submitted for mass spectrometry; **(B)** Cartoon representation showing the subcellular localisation and subunit composition of the major protein complexes identified by mass spectrometry: the F1F0 ATP Synthase (F1 subunits in green, F0 subunits in orange), the ribophorin (RI, RII, OST48, Dad1) complex with the associated chaperone Calnexin and two mitochondrial chaperones, the prohibitins BAP32 and BAP37.

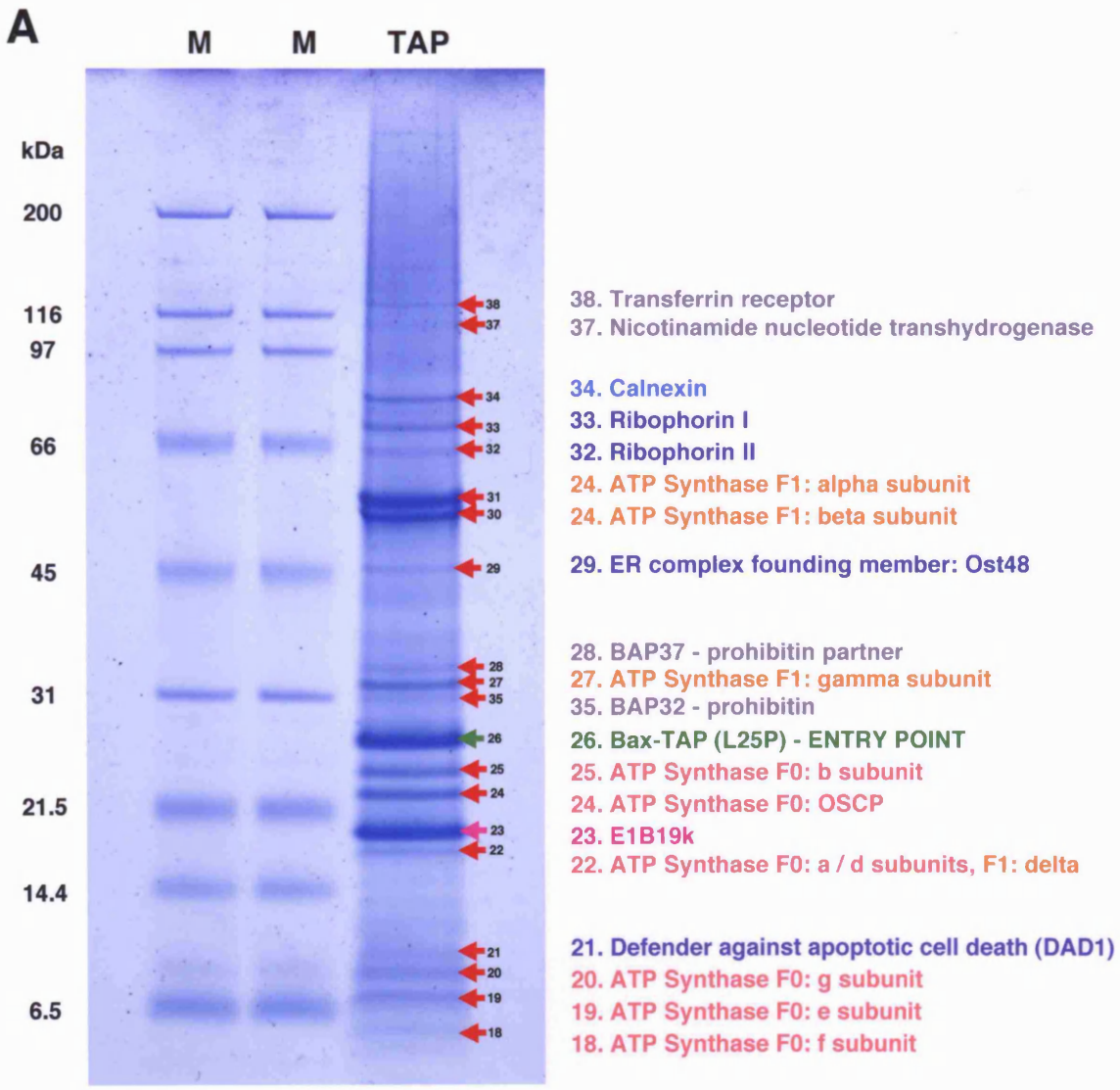
A
M
M
TAP
kDa
200
116
97
66
45
31
21.5
14.4
6.5
38
37
34
33
32
31
30
29
28
27
35
26
25
24
23
22
21
20
19
18
38. Transferrin receptor
37. Nicotinamide nucleotide transhydrogenase
34. Calnexin
33. Ribophorin I
32. Ribophorin II
24. ATP Synthase F1: alpha subunit
24. ATP Synthase F1: beta subunit
29. ER complex founding member: Ost48
28. BAP37 - prohibitin partner
27. ATP Synthase F1: gamma subunit
35. BAP32 - prohibitin
26. Bax-TAP (L25P) - ENTRY POINT
25. ATP Synthase F0: b subunit
24. ATP Synthase F0: OSCP
23. E1B19k
22. ATP Synthase F0: a / d subunits, F1: delta
21. Defender against apoptotic cell death (DAD1)
20. ATP Synthase F0: g subunit
19. ATP Synthase F0: e subunit
18. ATP Synthase F0: f subunit

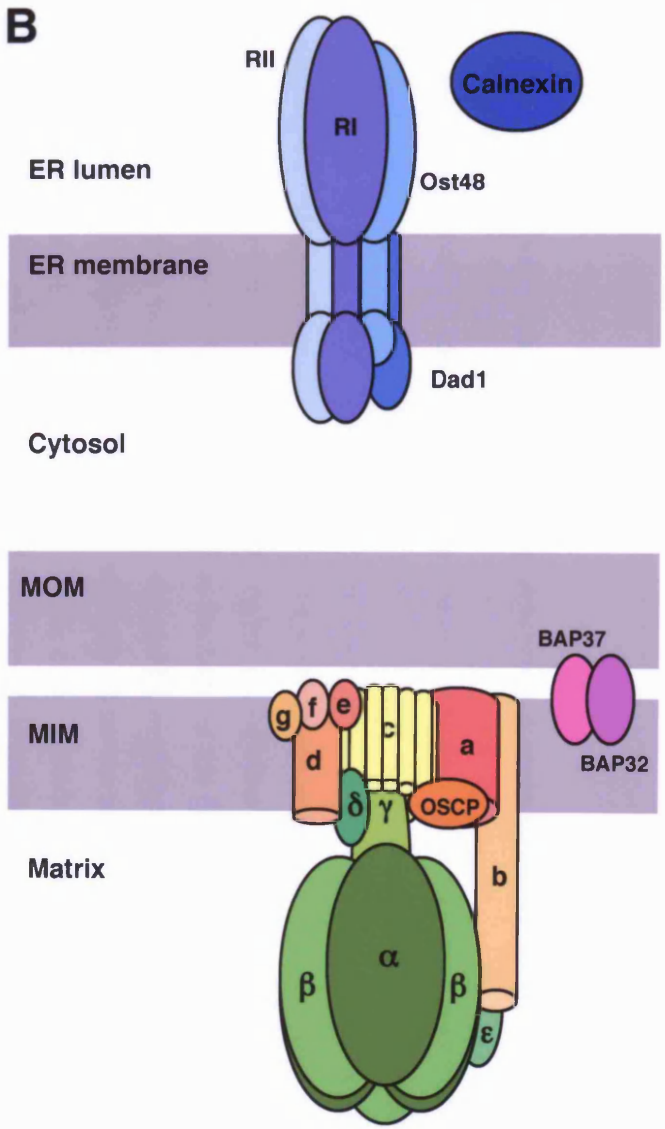
B
RII
RI
Calnexin
ER lumen
Ost48
ER membrane
Dad1
Cytosol
MOM
BAP37
MIM
BAP32
Matrix
g
f
e
c
a
d
δ
γ
OSCP
b
α
β
β
ε

Figure 6.7 Western blot confirmation of the presence of proteins identified by mass spectrometry.

The presence of proteins identified by mass spectrometry was confirmed by western blotting with antibodies raised against: subunits of the F1F0 ATP Synthase complex, Ribophorin I, Calnexin and E1B19k. 293 T-REx clonal cell lines expressing TAP-tagged Bax proteins containing the indicated mutation were grown in 15 x 15 cm tissue culture plates and expression of the TAP tagged protein induced with 100 ng/ml doxycycline for 12 hrs. Cells were then harvested and used for TAP purifications. Equal fractions of the final eluates were analysed by SDS PAGE followed by western blotting using the indicated antibodies. **(A)** C-terminal TAP tag: higher levels of co-purifying proteins were consistently observed using Bax-TAP L25P and AEE mutants, although most could be detected using any of the variants. Two separate clones of the Bax-TAP AAA mutant are shown (AAA 1 and AAA 2). **(B)** N-terminal TAP tag: The N-terminally tagged Bax variants were much less efficient in TAP purifications with relatively minor amounts of the F1F0 ATP Synthase alpha subunit only detectable using the TAP-Bax AAA and AEE mutants.

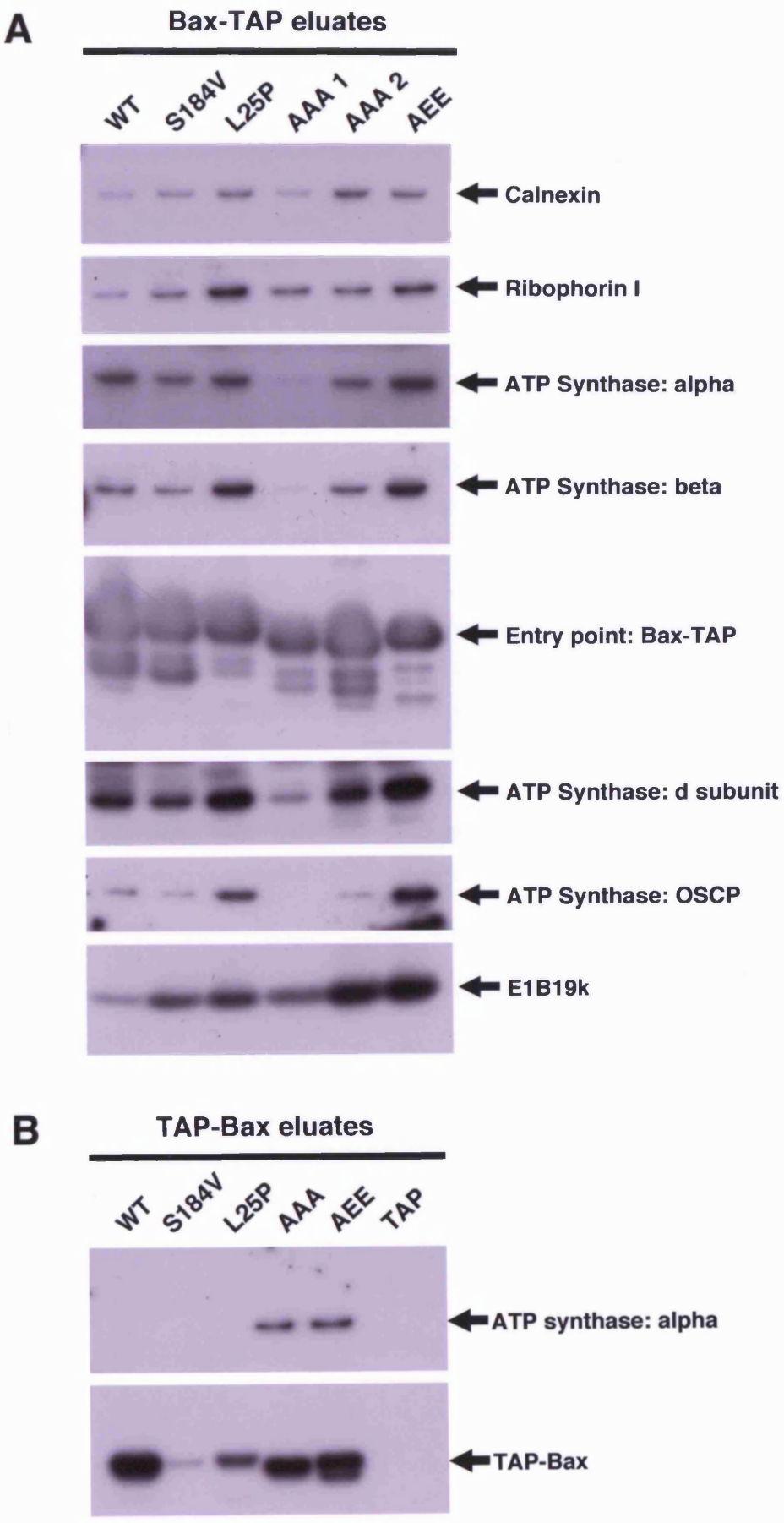
A
Bax-TAP eluates
WT
S184V
L25P
AAA 1
AAA 2
AEE
Calnexin
Ribophorin I
ATP Synthase: alpha
ATP Synthase: beta
Entry point: Bax-TAP
ATP Synthase: d subunit
ATP Synthase: OSCP
E1B19k
B
TAP-Bax eluates
WT
S184V
L25P
AAA
AEE
TAP
ATP synthase: alpha
TAP-Bax

Figure 6.8 HeLa cells over-expressing TAP-Bcl-XL are protected from apoptosis and can be used for TAP purifications.

HeLa cells expressing TAP-Bcl-XL were protected from UV-induced apoptosis and subsequently used in TAP purifications to isolate candidate Bcl-XL interacting proteins. **(A)** HeLa cells stably over-expressing either the TAP tag alone or TAP-Bcl-XL were treated with UV irradiation (200 J/m^2 for 0, 2 or 4 hrs) to induce apoptosis. Whole cell lysates were prepared from these cells were analysed by SDS PAGE followed by western blotting for using an anti-PARP antibody. **(B)** HeLa TAP-Bcl-XL cells were grown in 30 x 15 cm and used for TAP purifications. 15 plates were used for each of 2 parallel purifications and the final eluates combined, analysed by SDS PAGE and visualised by staining with colloidal coomassie. The profile of co-purifying proteins was enhanced by the addition of a membrane fractionation step. Briefly, cells were first lysed in hypotonic lysis buffer: 20 mM Hepes (pH 7.5), 1 mM EGTA, 10 mM KCl, 5 mM MgCl2, 1mM DTT with dounce homogenisation and membranes pelleted by centrifugation at 9500 x g for 30 mins. The resulting membrane pellet was resuspended in 1% CHAPS lysis buffer and TAP purification was performed as described previously (membrane). The cytosolic supernatant was also used for TAP purification (cytosol). M indicates lane containing molecular weight markers. Bands were cut for identification from by mass spectrometry from the membrane purification only. Data produced in collaboration with Ingram Iaccarino, current address: Institute of Genetics and Biophysics - CNR, Naples, Italy.

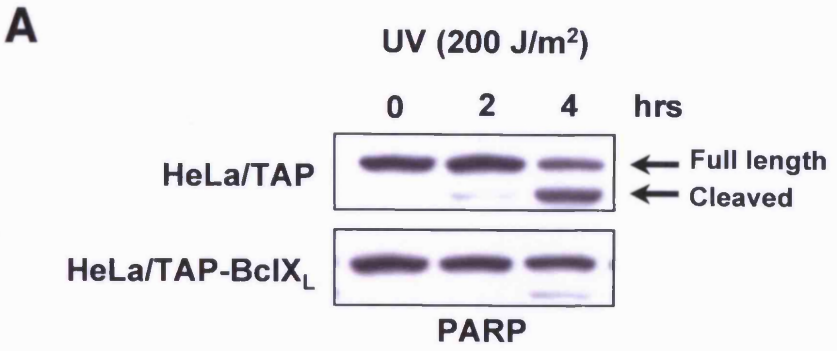
A
UV (200 J/m2)
0
2
4
hrs
HeLa/TAP
Full length
Cleaved
HeLa/TAP-BclXL
PARP

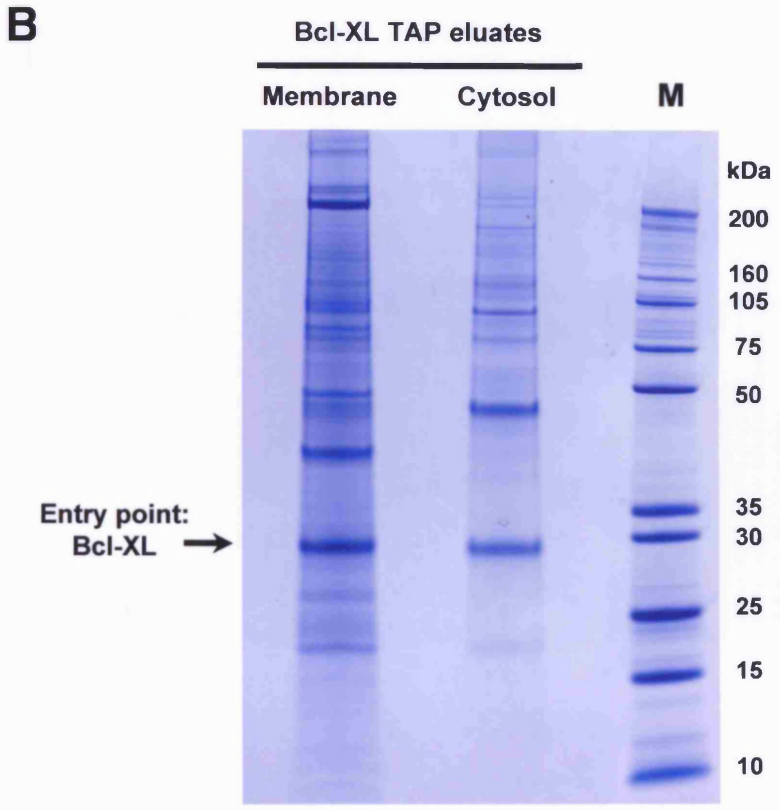
B
Bcl-XL TAP eluates
Membrane
Cytosol
M
kDa
200
160
105
75
50
35
30
25
15
10
Entry point:
Bcl-XL

Table 6.1 Proteins identified in TAP purifications from 293 T-REx Bax-TAP L25P and HeLa TAP-Bcl-XL cells.

BAX DATA SET IDs:	Other names	Size
F1: alpha subunit	**F0F1 ATP synthase**	**59.7**
F1: beta subunit	**F0F1 ATP synthase**	**56.5**
F1: epsilon	F0F1 ATP synthase	5.6
F1: gamma	**F0F1 ATP synthase**	**32.9**
F1: delta	**F0F1 ATP synthase**	**17.5**
F0: a subunit	**F0F1 ATP synthase**	**24.8**
F0: b subunit	**F0F1 ATP synthase**	**28.9**
F0: c subunit	F0F1 ATP synthase	7.6
F0: OSCP subunit	**F0F1 ATP synthase**	**20.9**
F0: d subunit	**F0F1 ATP synthase**	**18.5**
F0: e subunit	**F0F1 ATP synthase**	**7.9**
F0: g subunit	**F0F1 ATP synthase**	**12.8**
F0: f subunit	**F0F1 ATP synthase**	**10.9**
F0: A6L subunit	F0F1 ATP synthase	8.0
F0: F6 subunit	F0F1 ATP synthase	8.9
E1B19k	E1B protein, small T-antigen	20.6
Adenine nucleotide translocator	ANT1	33.0
BAP32	PHB, prohibitin 1	29.8
BAP37	**REA, prohibitin 2**	**33.4**
Nicotinamide nucleotide transhydrogenase	NAD(P) transhydrogenase	113.9
NADH dehydrogenase 1 beta subcomplex, 9, 22kDa	NDUFB9	21.8
CAD trifunctional protein	**CSPase/ATCase/DHOase**	**242.8**
Cytochrome c oxidase Subunit II	**MTCO2, COII**	**25.5**
Cytochrome c oxidase Subunit IV	**MTCO1, COI**	**19.6**
Transferrin receptor	**p90, CD71**	**84.8**
Ribophorin I	**RPN1**	**68.5**
Ribophorin II	RPN2	69.3
Oligosaccharyltransferase	**OST48**	**50.7**
DAD1	Defender against apoptotic cell death	12.4
Calnexin	**Calnexin**	**67.5**
Signal sequence receptor gamma	Translocon-associated protein gamma	21.1
Signal recognition particle	SRPR	69.9
IP3 receptor	**Type I, II and III**	**~310**
SERCA2	**SR/ER Ca2+ transporting ATPase 2**	**114.7**
MG29	Mitsugumin 29	30.2
Vesicle transport-related protein	Sec1 family domain containing 1	72.3
Vesicle trafficking protein sec22b	**SEC22L1**	**24.7**
Transmembrane trafficking protein	**TMP21**	**25.0**
JM4	**PRA1 domain family, member 2**	**19.2**
Putative sulfhydryl oxidase (Fe/S proteins)	Quiescin Q6-like 1	74.4
ZW10 homolog, centromere/kinetochore protein	ZW10	88.8
Mannosyl-oligosaccharide glucosidase	Glucosidase 1	91.8
Transitional endoplasmic reticulum ATPase	Valosin-containing protein	89.3
Cytoskeleton-associated protein 4	CKAP4	66.0
Solute carrier family 25, member 13	Citrin	74.1
Histone H4		11.4
Neutral amino acid transporter		
SPFH domain family, member 1	SPFH1	38.9
Progesterone receptor membrane component 1	PGRMC1	21.7
Opioid receptor, sigma 1	OPRS1	25.1
Hypothetical protein MGC5508	**Mitsugumin 23**	**26.2**
Alpha tubulin		
Beta tubulin		
Alpha-1-antitrypsin precursor		
Lamin B2		

BCL-XL DATA SET IDs:	Other names	Size
F1: alpha subunit	**F0F1 ATP synthase**	**59.7**
F1: beta subunit	**F0F1 ATP synthase**	**56.5**
F1: delta	**F0F1 ATP synthase**	**17.5**
F1: gamma	**F0F1 ATP synthase**	**32.9**
F0: a subunit	**F0F1 ATP synthase**	**24.8**
F0: b subunit	**F0F1 ATP synthase**	**28.9**
F0: OSCP subunit	**F0F1 ATP synthase**	**20.9**
F0: d subunit	**F0F1 ATP synthase**	**18.5**
F0: e subunit	**F0F1 ATP synthase**	**7.9**
F0: g subunit	**F0F1 ATP synthase**	**12.8**
F0: f subunit	**F0F1 ATP synthase**	**10.9**
Bak	Bcl2 antagonist killer 1	23.4
Bax	Bcl2-associated X protein	21.2
Bad	Bcl2L8, Bcl-2 binding component 6	18.4
Bid	BH3 interacting domain death agonist	22.0
PUMA	Bcl2 binding component 3	20.5
Bim	Bcl2-like 11, Bcl2L11	22.2
VDAC1	Porin	30.8
VDAC2		38.1
BAP37	**REA, prohibitin 2**	**33.4**
Carbamoyl phosphate synthetase 1	CPS1	164.8
Phosphofructokinase, platlet	PFK-C, PFKF	85.5
Cytochrome b5 outer membrane isoform		16.3
Manose-P-dolichol utilization defect 1	Lec35, SL15	26.7
Solute carrier family 3, member 2	MDU1, 4F2 antigen heavy chain	57.9
Na+/K+ ATPase alpha 1 subunit	Na,K-ATPase	81.7
CAD trifunctional protein	**CSPase/ATCase/DHOase**	**242.8**
Cytochrome c oxidase Subunit II	**MTCO2, COII**	**25.5**
Cytochrome c oxidase Subunit IV	**MTCO1, COI**	**19.6**
Transferrin receptor	**Transferrin receptor**	**84.8**
Ribophorin I	**RPN1**	**68.5**
Oligosaccharyltransferase	**OST48**	**50.7**
Calnexin	**CNX**	**67.5**
Protein translocation complex beta	SEC61 beta subunit	9.8
ER lumen protein retaining receptor 1	KDEL receptor 1	24.5
Signal sequence receptor delta	SSR4, TRAPD	19.0
Signal peptidase 18kD subunit		18.0
SERCA2	**SR/ER Ca2+ transporting ATPase 2**	**114.7**
Small GTP binding protein Rab7		23.5
Ras-related protein Rab7A		23.2
ER-Golgi intermediate compartment 32kD protein	KIAA1181	36.9
Vesicle associated membrane protein 3	Synaptobrevin 3	11.3
Transmem. emp24 protein transport domain containing 5	TMED5	19.1
Vesicle trafficking protein sec22b	**SEC22L1**	**24.7**
Transmembrane trafficking protein	**TMP21**	**25.0**
JM4	**PRA1 domain family, member 2**	**19.2**
Interferon induced transmembrane protein	LEU13, IFI17	17.0
Delta-2-ISPD		
Stomatin like 2	SLP2	45.5
Mesenchymal stem cell protein DSCD75	LOC51337	23.9
E2IG5	Growth and transformation-dependent protein	16.7
Tricaboxylate carrier protein	SFXN1, Sideroflexin 1	35.6
Hypothetical protein MGC5508	**Mitsugumin 23**	**26.2**
Hypothetical protein LOC203547		11.3
Hypothetical protein MGC14697	Upregulated during skeletal muscle growth 5	6.4
Hypothetical protein LOC493856	LOC493856	15.3

Note: proteins listed in **bold** were present in both analyses.

Figure 6.9 Preliminary validation of interactions identified in TAP experiments by co-immunoprecipitation.

Preliminary evidence suggests an inducible interaction between endogenous Bax and the F1F0 ATP synthase and between over-expressed Myc-tagged JM4 and Bcl-XL. **(A)** MCF10A cells (empty vector control or E1B19k-expressing) were treated STS (250 nM) or Fas (250 ng/ml) plus CHX (2 μg/ml) for 6 hrs to induce apoptosis. Cells were then lysed in 1% CHAPS buffer and used in co-immunoprecipitation assays with an anti-F1F0 ATP Synthase antibody (gift from R.Capaldi, University of Orgeon). Equal fractions of inputs and final eluates were analysed by SDS PAGE followed by western blotting with the indicated antibodies. **(B)** HeLa cells were transfected with Myc-tagged JM4 and untagged Bcl-XL as indicated. 24 hrs after transfection cells were lysed and used in co-immunoprecipitation assays with an anti-Myc antibody (9E10, CR-UK research services). Equal fractions of inputs and final eluates were analysed by SDS PAGE followed by western blotting with either anti-Bcl-XL or anti-myc antibodies as indicated. Data in part (B) supplied by Ingram Iaccarino, current address: Institute of Genetics and Biophysics - CNR, Naples, Italy.

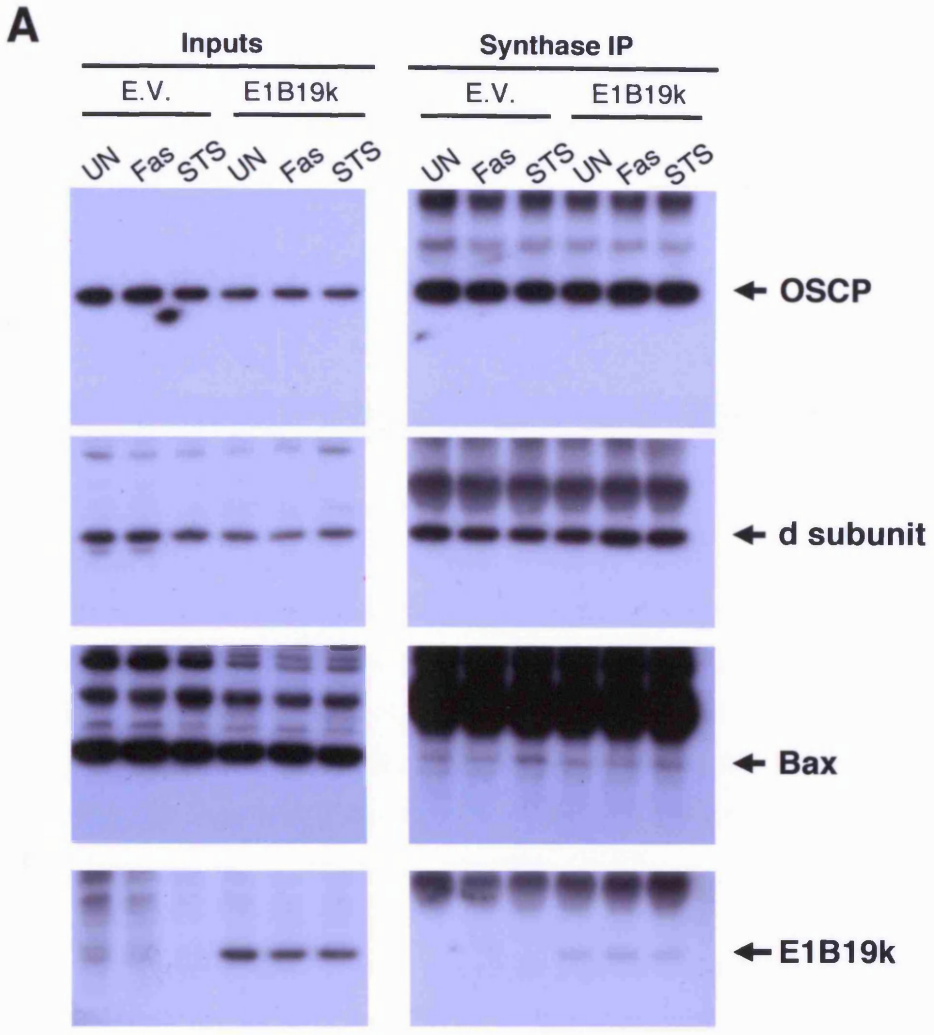
A
Inputs
Synthase IP
E.V.
E1B19k
E.V.
E1B19k
UN
Fas
STS
UN
Fas
STS
UN
Fas
STS
UN
Fas
STS
OSCP
d subunit
Bax
E1B19k

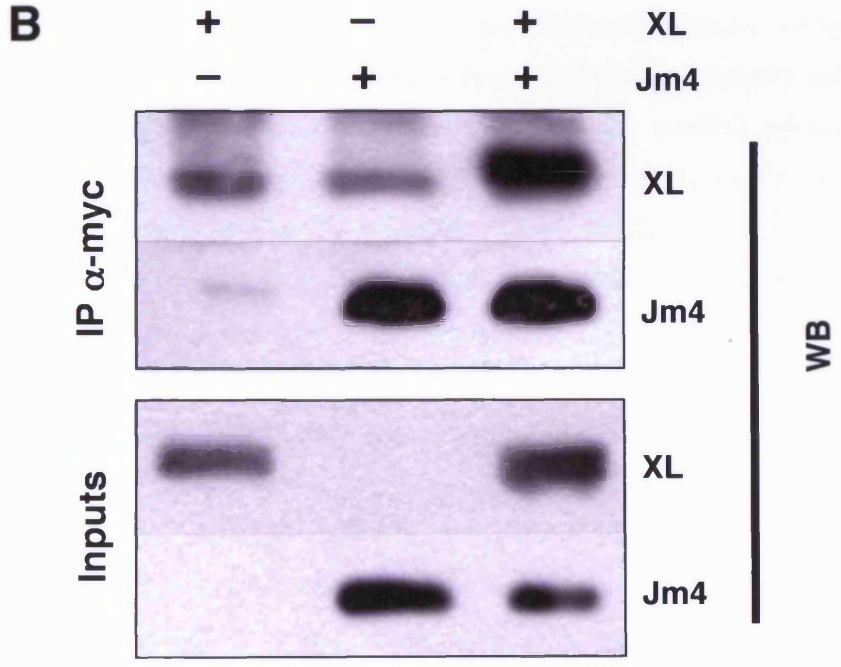
B
+
−
+
XL
−
+
+
Jm4
IP α-myc
XL
Jm4
Inputs
XL
Jm4
WB

Chapter 7 – General discussion

7.1 Progress made in this thesis:

This thesis deals with the regulation of the pro-apoptotic Bcl-2 family member Bax. At the time this work was begun the generation of *Bax-/-Bak-/-* doubly deficient animals had recently provided genetic proof that the presence of either Bax, or the related protein Bak, was required for apoptotic cell death mediated by mitochondrial dysfunction (Lindsten et al., 2000; Wei et al., 2001). Yet, despite a significant body of work in this area, both the mechanism of action of these proteins, and the process by which they become active, remained a matter of debate and does so to this day. The experiments described here were initiated in order to gain further insights into the process of Bax regulation and activation.

The Bcl-2 family of proteins are critically placed at a mitochondrial proximal step in the apoptotic signalling pathway to mediate what is widely considered the irreversible step in apoptotic cell death, namely the initiation of mitochondrial dysfunction and accompanying release of Cyt-c. Recently the roles of some of the proteins in this family have been substantially clarified. It now seems likely that the BH3-only proteins act as ligands, each activated by a specific range of cellular stress responses or developmentally programmed cues (Cory et al., 2003) (Figure 1.4 A). Once active, the BH3-only proteins selectively target and inhibit pro-survival proteins, such as Bcl-XL (Chen et al., 2005) (Figure 1.4 B). This inhibition of the pro-survival proteins leads to the activation of Bax and Bak. For Bak, the mechanism of activation has been partially clarified. Bak is constitutively localised to mitochondria in healthy cells and held in check by direct physical interaction with Bcl-XL and Mcl-1. Upon receipt of an apoptotic signal this binding is disrupted by BH3-only proteins, thus releasing Bak to initiate mitochondrial dysfunction (Willis et al., 2005) (Figure 1.4 C). However, there is no evidence of an analogous mechanism for Bax. When purified in the absence of detergents Bax is monomeric (Antonsson et al., 2000; Hsu and Youle, 1997; Hsu and Youle, 1998). Activating interactions with some BH3-only proteins, namely Bid and Bim, have been suggested but a stable interaction of Bax with these proteins has not been detected (Sundararajan and White, 2001; Wei et al., 2000).

A number of lines of evidence indicate that the regulation and function of Bcl-2 family proteins may not be entirely explained by intra-family interactions. For example, there is evidence to suggest that Bax and Bcl-XL can compete for a shared cellular target in mammalian cells (Hsu et al., 1997b) and when the proteins are expressed in yeast (Polcic and Forte, 2003). The existence of a Bax-binding partner at mitochondria has also been inferred from *in vitro* reconstitution data (Roucou et al., 2002). For other family members, Bcl-w fails to localise to mitochondria when expressed without the last 10 C-terminal residues. This protein is biologically inert even though it binds and sequesters BH3-only proteins avidly (Denisov et al., 2003; Hinds et al., 2003), suggesting additional pro-survival functions at mitochondria beyond its ability to bind BH3-only ligands. In addition, a Bcl-XL mutant that failed to interact with Bax retained pro-survival function in both yeast and mammalian cells (Minn et al., 1999). A growing number of reports have also suggested that Bcl-2 proteins may be complexed with other cellular proteins in healthy cells, for example Bak was found to be bound by VDAC2 (Cheng et al., 2003), Mcl-1 has been found to interact with an E3 ubiquitin ligase, Mule/ARF-BP1, which catalyses its poly-ubiquitylation and degradation following the binding of the BH3-only protein Noxa (Warr et al., 2005; Zhong et al., 2005). A novel role is emerging for a cytoplasmic pool of p53 that interacts with Bcl-XL (Mihara et al., 2003), and upon release by binding of the BH3-only protein Puma, may be able to directly activate Bax (Chipuk et al., 2005). Notably, this pool of p53 molecules is detectable within 30 mins following irradiation and is accompanied by an early wave of caspase-3 activation, contrasting with the p53 transcriptionally controlled effects which occur at later times: PUMA (2 hrs), Noxa (4 hrs), Bax (8 hrs) (Erster et al., 2004).

If regulation of Bax is to be explained, at least in part, by interactions with proteins outside of the Bcl-2 family, several lines of evidence indicate such interactions take place at cellular membranes. It has recently been shown that Bax inserts into membranes and that oligomerisation is likely to be driven by the association of transmembrane monomers in the plane of the membrane (Annis et al., 2005). This mechanism differs from that of some bacterial toxins which are thought to form pores via the concerted membrane insertion of pre-formed oligomers (Heuck et al., 2000). However, the exact mechanism of membrane insertion for more structurally related toxin proteins, such as the Diphtheria toxin is not yet known. Bcl-2 has also been shown to insert into both ER and mitochondrial membranes upon receipt of a death trigger or binding of a BH3 peptide (Kim et al., 2004a), and membrane insertion following the receipt of an apoptotic signal has also been shown for Bcl-w (Wilson-Annan et al., 2003).

The data presented in this thesis was generated in order to gain further insights into the mechanisms of Bax regulation and activation. Chapter 3 showed the results of a detailed

microscopy-based analysis Bax activation in U2OS and MCF10A cells. The premise of these experiments was that observing Bax activation at high temporal and spatial resolution might reveal clues about how the protein is regulated. The data collected suggested that, following a low dose of UV irradiation, Bax can pre-exist at mitochondria, and is not yet fully active. Similar observations have also been made by others in an anoikis model (Valentijn et al., 2003). When Bax activation did occur it was a rapid event, correlating with loss of $\Delta\psi_m$. Pre-enrichment of Bax to mitochondria was seen to be neither sufficient nor required for complete Bax activation as detected by the formation of bright fluorescence foci and loss of $\Delta\psi_m$. Some evidence that Bax activation may initiate locally and then become rapidly propagated across the cell was also obtained. Further analysis of these data was however complicated by the extremely rapid nature of the process, with Bax activation typically initiating > 5 hours after the addition apoptotic trigger and yet $\Delta\psi_m$ loss being complete within 5 mins. Evidence of the local initiation and propagation of Bax activation in wild type cells was therefore only obtained in the more polarised cells shown in Figures 3.9 and 3.10, although the spreading loss of $\Delta\psi_m$ was commonly observed in E1B19k-expressing cells (see Sections 4.6 and 4.8). It is possible this mechanism may be more generally applicable in wild type cells but that it occurs too rapidly to be seen at a 1 frame per minute image acquisition rate, except in highly polarised cells where it propagates over larger distances and therefore exists for longer. A more sophisticated imaging system allowing more rapid acquisition cycles, eg. 20 frames per minute, would potentially allow this question to be definitively addressed. Further attempts to quantify the live cell recordings generated were confounded by movements of the cells being imaged. The experiments were performed with a 63X objective to obtain high resolution images of mitochondria, however, at this resolution even small cell movements, occurring either through migration or in response to changes in the monolayer as nearby cells underwent apoptosis, resulted in significant movement of cells out of a defined region of interest defined by either the cell perimeter or to contain a subset of mitochondria. Attempts to quantify the rate of increase in Bax intensity at mitochondria, appearance of Bax foci and loss of $\Delta\psi_m$ using two separate analysis software packages were unable to reproducibly measure these changes while taking into account cell movements. A limited quantification of $\Delta\psi_m$ loss showing complete loss within 5 mins in wild type cells, and a partial recovery after initial decrease in some E1B19k-expressing cells is shown in Figure 4.14. Even in these cases there are caveats in interpretation of $\Delta\psi_m$ traces beyond 5-10 minutes after GFP-Bax activation due to movement of the cells (see Section 4.6 for further details).

Data presented in Chapter 3 establishes the assay and microscopy system that is used in Chapter 4, in combination with E1B19k and BHRF1 expression to perturb Bax activation in MCF10A cells in response to Fas/CHX-induced apoptosis. Together these data led to the model shown in

Figure 4.17 in which E1B19k blocks Bax activation at a step subsequent to its N-terminal conformational change and mitochondrial translocation. This block is therefore later than the block afforded by BHRF1-expression when these events are also prevented. More generally the data is supportive of a model in which the crucial event in Bax activation is the dimerisation and oligomerisation of Bax molecules. This is in agreement with a previous study in which enforced dimerisation of Bax induced apoptosis (Gross et al., 1998). It is possible the potent ability of E1B19k to protect MCF10A cells from Fas/CHX-induced Bax activation is explained by the ability of E1B19k to bind and directly prevent co-association of Bax molecules (Figures 4.7 and 6.6). Substantial areas of uncertainty and controversy do however remain regarding the mechanism of action of E1B19k and BHRF1. For example, BHRF1 does not contain a prominent BH3-binding groove seen in the other family members and, consistent with this, is not able to efficiently bind BH3 peptides from Bax, Bak, Bad and Bid (Huang et al., 2003). It may be that peptide-binding studies do not reflect the interactions formed by BHRF1 *in vivo*, or that BHRF1 interacts with cellular Bcl-2 proteins by a different mechanism not recapitulated using BH3 peptides alone. Nevertheless, BHRF1 may also have a distinct anti-apoptotic function, independent of its binding to other BH3-containing proteins. In this respect, it was interesting that BHRF1 was also seen in high molecular weight fractions of ~670 kDa by gel filtration (data not shown). Determining the composition of such complexes may help elucidate at exactly which step BHRF1 acts in the pathway downstream of Fas death receptor activation. BHRF1 could, for example, play a role in directly inhibiting the activity of initiator caspases such as caspase-8, alternatively it could perturb mitochondrial physiology in as yet undefined ways. In either case, BHRF1 is likely to exert its effects from the mitochondria since both untagged and N-terminally GFP-tagged BHRF1 exhibit an exclusively mitochondrial localisation, as determined by confocal microscopy (data not shown). In addition, understanding how BHRF1 is able to offer such a greater level of protection than cellular sequence homologues Bcl-2 and Bcl-XL (Figure 4.2) may provide important insights into understanding the pro-survival functions of the cellular Bcl-2 proteins.

For E1B19k significant questions regarding its precise biological functions also remain. Although the protein predominantly localises to endoplasmic reticulum and nuclear membranes (Supplementary Figure 5.7) it can also redistribute to mitochondria following Bax activation (Perez and White, 2000 and data not shown). The block conferred by E1B19k-expression on both Bax and Bak activation occurs subsequently to their N-terminal conformational change, when both proteins are located at the mitochondria. A strong interaction between Bax L25P and E1B19k, in approximately 1:1 stoichiometry, was consistently observed in TAP purifications (Figure 6.6) and by co-immunoprecipitation (Figure 4.7 B) and has been previously reported between Bak and E1B19k (Sundararajan et al., 2001). The interaction between Bax L25P and

E1B19k was resistant to 1% SDS (data not shown). Together these data suggest that E1B19k is likely to block Bax and Bak activation by directly binding the N-terminally active conformations before homo- or hetero-dimerisation can occurs. However, GFP-E1B19k could also sometimes be seen to have a partial mitochondrial localisation even in healthy cells and redistribution to mitochondria in response to an apoptotic trigger appeared to involve only a small fraction of total GFP-E1B19k (data not shown). Viral proteins are often promiscuous in the interactions they form with cellular proteins and E1B19k may also have other biological activities at the ER and nuclear membranes, as well as at mitochondria. In addition further experiments will be needed to determine whether the candidate Bax-interacting proteins purified in the presence of E1B19k are present through a direct interaction with Bax. Many could be present due to indirect interactions (see below) and some may primarily be E1B19k-interacting proteins.

Mitochondrial ultrastructural analysis was performed in the presence of viral proteins to block cell death and this analysis revealed that changes in cristae morphology occurred independently of Bax and Bak activation (Figure 4.16). This finding places changes in mitochondrial ultrastructure in an upstream or parallel pathway to Bax and Bak activation. In the MCF10A cell system used, tBid was also efficiently generated following treatment with Fas/CHX in the presence of both E1B19k and BHRF1 to block cell death (Figure 4.3). Therefore, the mitochondrial remodelling observed could be tBid-dependent effect, in agreement with a previous report (Scorrano et al., 2002). Although this finding has not been pursued further a genetic approach, knocking down the levels of Bid with RNA interference, could provide a way to directly test this hypothesis. The ultrastructural analysis performed on E1B19k-expressing MCF10A cells also illustrates how this system may be analogous to the murine DKO cells in which Bax and Bak have been genetically deleted.

The analysis of mitochondrial ultrastructure also revealed the appearance of prominent electron dense granules in the mitochondrial matrix of cells treated with Fas/CHX. These are thought to be calcium phosphate deposits and may represent a rapidly reversible mitochondrial Ca^{2+} buffering system (David, 1999; Pivovarova et al., 1999). The reversibility of the precipitates was not investigated in the present study, however, these Ca^{2+} precipitates could provide a large source of Ca^{2+} available for release upon permeabilisation of the mitochondria. Ca^{2+} signals are known to be propagated by mitochondria (Ichas et al., 1997), and Ca^{2+} overload of mitochondria induces permeability transition (Bernardi, 1999). It has also been observed that Ca^{2+} waves can occur at around the time of onset of cell death (Carvalho et al., 2004; Pacher and Hajnoczky, 2001). There is therefore substantial evidence suggesting that the feed-forward propagation of Bax activation observed in the present study, whereby Bax activation can initiate locally and

then propagate across the cell, may be mediated by a mitochondria Ca^{2+} wave. The existence of such a mechanism would have the advantage of coordinating recruitment of all mitochondria, especially in large and polarised cells, into the apoptotic program. It also possible that Ca^{2+} precipitates could have both protective and pro-apoptotic functions. For example under physiological conditions they may serve as a fast, reversible Ca^{2+} buffer system, however, under stress conditions of Ca^{2+} overload, they might continue to increase in size and number until the counter ion (ie. phosphate) is exhausted. At this point a rapid and uncontrolled rise in mitochondrial Ca^{2+} could result in the initiation of mitochondrial permeability transition.

If the electron dense granules observed in the present study are truly calcium precipitates the question arises as to the origin of the calcium. The ability of mitochondria to uptake large amounts Ca^{2+}, driven either by oxidative phosphorylation of respiratory substrates for hydrolysis of adenosine 5'-triphosphate (ATP) has been known since the 1950s (Carafoli, 2003). Unlike that of other ions and metabolites, Ca^{2+} uptake by mitochondria is not mediated by pumps or exchangers but by a 'uniporter', although its molecular identity remains unknown (Nicholls and Crompton, 1980). Ca^{2+} uptake is driven by $\Delta\psi_m$, which is around 150-200 mV negative compared to the cytosol. If Ca^{2+} accumulation were governed solely by the Nernst equation, the concentration in the matrix would be around 10^6 times greater than that in the cytosol. This does not occur due to the presence of antiporters that allow the slow release of Ca^{2+} in exchange for Na^+ or H^+ ions (Nicholls and Crompton, 1980). Therefore, mitochondrial Ca^{2+} levels are maintained by a combination of membrane potential driven uptake and concentration dependent release. This futile cycle establishes a 'mitochondrial set-point' for the Ca^{2+} level in energised healthy mitochondria. In reality the rate of cycling is low, and therefore not energetically wasteful, due to both the low Ca^{2+} affinity of the uniporter and the low extra-mitochondrial Ca^{2+} concentration (around $1\mu M$). However, mitochondria are still able to rapidly accumulate Ca^{2+} under physiological conditions (Rizzuto et al., 1992) and this directly affects their metabolic activity (Brini et al., 1999; Hajnoczky et al., 1995). This is due to the proximity of mitochondria to regions of Ca^{2+} release, namely inositol 1,4,5-trisphosphate (IP3) receptor-gated ER Ca^{2+} stores. In these regions, or 'hotspots' there is a microenvironment where the Ca^{2+} concentration exceeds that of the bulk cytosol by over an order of magnitude (Rizzuto et al., 1993). In this respect, it is interesting that several proteins involved in Ca^{2+} regulation were co-purified in Bax and Bcl-XL TAP experiments (see section 6.7.7 for details).

A model invoking the feed-forward spread of Bax activation leads to the question of how an initiation site might be selected. An interesting observation made during the course of this work was that the first signs of GFP-Bax activation and loss of $\Delta\psi_m$ reproducibly occurred in the cell periphery (see Figures 3.9, 3.10 and 4.13 for examples). It has recently been demonstrated that

substantial functional heterogeneity exists between mitochondria in the same cell, with a greater proportion of highly energised mitochondria in the cell periphery (Collins et al., 2002). Since the mitochondrial Ca^{2+} uniporter is driven by $\Delta\psi_m$, this has also been shown to translate into a functional difference. In response to histamine-induced Ca^{2+} release peripheral mitochondrial were observed to accumulate substantially more Ca^{2+} than those in the perinuclear region (Collins et al., 2002). This difference occurs despite those mitochondria in the perinuclear region being embedded in a higher concentration of ER network (Collins et al., 2002). The results therefore indicate that, under some circumstances, $\Delta\psi_m$ and the nature of the Ca^{2+} signal may play a more prominent role in determining mitochondrial Ca^{2+} uptake than proximity to the Ca^{2+} source. It is also a possible explanation why peripheral mitochondrial may experience Ca^{2+} overload leading to membrane permeability transition before those in the perinuclear region. Accurate Ca^{2+} imaging requires a rapid rate of image acquisition than was possible in the present study. However, beyond this requirement the validity of these hypotheses could be addressed by use of Ca^{2+}-free culture media and the addition of Ca^{2+} chelators such as EGTA or emptying of ER Ca^{2+} stores with thapsigargin, in combination with a cytoplasmic Ca^{2+} indicator or the mitochondrial pericam. Live cell imaging and electron microscopy analysis under these conditions would be able to determine: (a) whether the appearance of the electron dense granules is a Ca^{2+}-dependent process, (b) whether rapid and efficient cell-wide wide recruitment of mitochondria into the apoptotic program is dependent on prior accumulation mitochondrial Ca^{2+} and (c) whether a wave of mitochondrial Ca^{2+} release accompanies the initiation of apoptosis and Bax activation or loss of $\Delta\psi_m$.

The data presented in Chapters 3 and 4 supports the view that monomeric Bax can exist at the mitochondrial membrane and is not necessarily fully active. However, enforced dimerisation of Bax kills cells (Gross et al, 1998) and oligomerisation of Bax always accompanied full activation and mitochondrial dysfunction. Therefore, determining how and why the first Bax molecules enter into dimers and higher order oligomers is crucial to understanding Bax activation. In the present study, Bax activation has been seen to initiate in a discrete area of the cell, indicating a possible mitochondrial origin for these events, as opposed to synchronous cell-wide Bax activation. In addition, Myc-/- cells have been demonstrated to have increased resistance to Bax toxicity and cytosol switching experiments involving mitochondria purified from Myc-/- cells indicated that this property was inherent to the mitochondria (Annis et al., 2005). Together, these observations suggest that events taking place at the membranes of individual mitochondria and properties intrinsic to mitochondria may be critical in regulating the activity of Bax and other Bcl-2 family proteins. A proteomic approach, the TAP purification method, was therefore used in an attempt to isolate candidate Bax interacting proteins. To enrich for proteins which may be involved in Bax regulation at mitochondria, the effect of

mutations which promoted the activation and translocation of Bax to mitochondria was also investigated. It was reasoned that such mutant proteins, when placed under an inducible promote system, would allow the synchronous activation of Bax in all cells in a culture.

The effect of four mutations on the localisation and toxicity of Bax are reported in Chapter 5. When Bax was tagged at the N-terminus these mutations each had the effect of altering the protein localisation. The S184V mutation resulted in a constitutive mitochondrial localisation of a GFP-Bax, as has been previously reported (Nechushtan et al., 1999). A mutation in which the N-terminal helix was disrupted by an L25P mutation appeared to be activating, enhancing Bax toxicity and resulting in an the formation of bright mitochondrially-associated foci, although, in some cells, GFP-Bax L25P was also seen to be partially cytoplasmic or evenly distributed along the mitochondrial network. It therefore seems likely the L25P mutation promotes Bax activation and this is in good agreement with the finding that deletion of the entire N-terminus of Bax also results in enhanced toxicity (Goping et al., 1998). Mutations in the $\alpha 5/\alpha 6$ region of Bax were also found to alter the localisation and toxicity of GFP-Bax. The GFP-Bax AAA appeared to enter mitochondrially-associated foci constitutively whilst the GFP-Bax AEE showed a partial mitochondrial enrichment. When GFP was fused to the C-terminus of Bax all mutants were cytoplasmic, with the exception of the AAA mutant, which still formed mitochondrially associated foci. Finally, two of the C-terminally tagged mutants, Bax-GFP L25P and Bax-GFP AAA were altered by co-expression of E1B19k, with the L25P mutant forming small mitochondrially associated foci and the AAA gaining an ER-like distribution (Figure 5.4). Therefore the C-terminal GFP tag proved a barrier to Bax activation and mitochondrial localisation. However, when compared with untagged constructs, the N-terminally tagged versions showed a modest increase in toxicity (Figure 5.6 A). This could mean that whilst the C-terminal tag is inhibitory, the addition of an N-terminal tag may promote Bax activation.

The shift in localisation of the C-terminal L25P and AAA constructs in the presence of E1B19k was an unexpected result. This could indicate that these mutations destabilise the Bax molecule sufficiently to induce the formation of aggregates or precipitates at particular sub-cellular locations. At least for the L25P mutation this seems unlikely since it formed a stable cytoplasmic distribution in the absence of E1B19k, however it cannot be excluded on the data presented for the AAA mutation. An alternative explanation is that these Bax proteins are destabilised by their respective mutations sufficiently to have a higher binding affinity for E1B19k, which only binds to Bax after an initial conformational change has occurred. In this case the localisations may be explained if the AAA mutation is recruited to the normal location of the majority of E1B19k, namely the ER, whilst the L25P mutation complexes with E1B19k at mitochondria, the normal site of Bax activation and Bax-E1B19k interaction. In support of

this interpretation both mutations strongly associate with E1B19k by TAP (Figure 6.7 A) and co-immunoprecipitation (data not shown).

At present it remains uncertain whether mitochondrial associated clusters formed by GFP-tagged L25P and AAA Bax mutant proteins are analogous to the mitochondrially-associated foci formed by the endogenous protein in apoptotic cells. In addition, the FACS based Annexin/PI assay used is not ideal for the quantification of relative toxicity of the mutant Bax proteins since this can also vary with both expression time and expression level, neither of which were constant between the mutant constructs tested. To clarify these issues a number of further experiments would be possible. An *in vitro* assay in which the same amount of each mutant protein could be tested for ability to cause Cyt-c release from purified mitochondria would be helpful in assessing the relative toxicity of the proteins. It would also be informative to complement the confocal localisation study with a sub-cellular fractionation approach to determine the distribution of the mutant proteins across subcellular compartments such as the mitochondria, ER and cytosol. This assay can also be extended with the use of alkali extraction of proteins not fully integrated into cellular membranes. Such an approach could yield significant additional information about the nature of the distributions of the mutant Bax proteins observed by microscopy. Finally, it may also be useful to investigate the localisations and activities of the untagged mutant proteins using the panel of endogenous antibodies previously characterised. When used for immunoprecipitation assays this may also reveal the extent to which the mutations induce conformational change within Bax molecules.

The behaviour of all mutant Bax proteins, both N- and C-terminally tagged, in TAP purification experiments was investigated. This revealed that C-terminally TAP tagged Bax proteins consistently produced a more complex profile of co-purifying proteins than the N-terminally tagged versions. The reason for this is not entirely clear since the wild type, S184V and AEE mutants were predominantly cytosolic and therefore expected to be monomeric. One possibility is that interactions, artificial or biologically relevant, may be formed post-lysis in these cases. An alternative explanation is that whilst the bulk of the over-expressed complex remains monomeric, these C-terminally tagged mutant proteins are still able enter larger molecular weight complexes, albeit at low efficiency. This interpretation is supported by their entry of a proportion of the over-expressed mutant proteins into higher molecular weight ranges in gel filtration assays when compared to the wild type version (Figure 6.3). There is no ideal place to tag Bax: the N-terminus of the protein is conformationally sensitive and may therefore be the site of important protein-protein interactions whilst the addition of a tag to the C-terminus of Bax impairs the protein's activity and limits its association with mitochondria, perhaps by preventing insertion of the hα9 into the mitochondrial membrane. Of all the tag and mutation

combinations tested for TAP purifications, experiments performed using the combination of C-terminally tagged Bax-TAP and the L25P mutation consistently produced the most complex and abundant band pattern. This mutation also entered small mitochondrially associated foci and higher molecular weight complexes by gel filtration, both of which were interesting since the primary aim of the screen was to isolate proteins involved in Bax activation. For these reasons it was this combination which was selected for a preparative scale experiment and systematic identification of co-purifying proteins by mass spectrometry. However, based on the data collected from TAP purification experiments alone is not possible to know whether the proteins identified by mass spectrometry are real Bax interacting proteins. They could also be present due to incomplete solubilisation of cellular membranes, precipitation or aggregation of the mutant Bax proteins or artificially induced interactions due to the high levels of Bax over-expression used. Candidate Bax interacting proteins from this initial screen therefore need to either be confirmed or eliminated in subsequent experiments using different techniques.

Other Bax mutant and TAP tag combinations were investigated in more detail in smaller scale TAP purifications. It was hoped these mutant proteins, due to their differing subcellular distributions and apoptotic activities, might either disrupt or enhance specific interactions identified from the Bax-TAP L25P data set. In these experiments the L25P and AEE mutations, in the context of Bax-TAP, performed consistently better than the other mutations in terms of the abundance of the co-purifying species (Figure 6.7 and data not shown), however, this line of investigation ultimately proved unsuccessful as no clear effect of a particular mutation on a particular subset of bands could be identified. It was concluded that whilst the TAP purification method is a powerful approach for initial proteomic screening, the experiments are too complex and lack sufficient reproducibility to be useful in asking more subtle questions, such as the ability of a mutation to disrupt or enhance a particular protein interaction. However, it remains possible that the panel of Bax mutants generated could be useful in screening and validating candidate interactors in co-immunoprecipitation assays or pull-down assays using *in vitro* purified Bax proteins. At present this possibility has not been investigated further.

A partial validation of some of the mass spectrometry data presented in Figure 6.6 came from an TAP purifications with a second Bcl-2 family protein, Bcl-XL. These experiments used an N-terminally tagged TAP-Bcl-XL expressed constitutively expressed in HeLa cells. The data from both screens reveals a substantial degree of overlap between proteins co-purifying with Bax-TAP L25P in 293 T-REx cells and TAP-Bax-XL in HeLa cells (Table 6.1). In addition, the presence of known Bcl-2 family interacting proteins, and in particular the BH3-only proteins interacting with Bcl-XL, which are low abundance and small molecular weight proteins, indicate the purification strategy was working well.

The F1F0 ATP Synthase represented a major co-purifying species in both Bax and Bcl-XL purifications. However, this is also a highly abundant complex at the mitochondrial membrane. It was therefore a concern as to whether this result represented a specific interaction with Bcl-2 family proteins or was the result of artificial over-expression of the tagged proteins or incomplete solubilisation of mitochondrial membranes. One approach pursued in order to further address this question involved the addition of chemical cross-linkers to Bax TAP purifications. It was reasoned that if a direct interaction exists between the F1F0 ATP Synthase and Bax it would most likely be mediated by a single subunit that could be fixed by the addition of a cross-linker following the TEV cleavage step in the TAP purifications. These experiments were indeed successful in stabilising higher molecular weight protein products containing Bax, as assessed by western blotting (data not shown). However, these products then had to be separated away from other co-purifying proteins of the same molecular weight. This was achieved by the addition of SDS to 1% in order to dissociate any proteins not covalently linked by the cross-linker. The SDS was then diluted to 0.1% and Bax-containing species recovered using an anti-Bax N20 linked agarose. However, when higher molecular weight Bax-containing species were analysed by mass spectrometry and by western blotting with antibodies raised against F1F0 ATP Synthase components, no subunits were identified other than Bax and E1B19k which appeared to have been stabilised in higher order dimers and multimers (data not shown). Nevertheless, the same approach using other chemical cross-linkers with different length spacer arms and reactive groups may yet prove to be useful in isolating proteins directly interacting with Bax.

An alternative approach to validate interactions with co-purifying proteins is to use a traditional biochemical purification strategy in which multiple chromatography steps are used to separate the proteins of interest. Such an approach has been successfully used to shown that Bcl-XL and the F1F0 ATP Synthase are co-enriched over multiple co the F1F0 ATP Synthase (M. Hardwick, Johns Hopkins, personal communication). Additionally, experiments with protein cross-linkers and SDS dissociation described above also revealed the association between Bax and the a subunit of the F0 ATP Synthase is resistant to 1% SDS, as is the interaction with E1B19k (data not shown). This observation makes it less likely the Bax-F1F0 ATP Synthase result is simply due to incomplete solubilisation of mitochondrial membranes in CHAPS detergent. There are unlikely to be many intermediate components if the association is resistant to 1% SDS. When taken together with earlier observations that Bax toxicity in yeast is dependent on functional oxidative phosphorylation (Gross et al., 2000; Harris et al., 2000) it remains possible that the co-association of Bcl-2 proteins Bax and Bcl-XL with the F1F0 ATP Synthase may not be artifactual.

Unfortunately, experiments to show the presence of the F1F0 ATP Synthase in Bax co-immunoprecipitations were confounded by the extremely high abundance of F1F0 ATP Synthase in cells, meaning it was difficult to wash out of control samples and yet retain any specific interactions (data not shown). However, preliminary indications indicate that the reverse experiment may be possible, showing that Bax co-immunoprecipitates with the endogenous F1F0 ATP Synthase following an apoptotic trigger (Figure 6.9). Co-immunoprecipitation assays with some of the less abundant proteins in the list of candidates may prove to be less challenging.

Several other approaches to could be used in order to identify potential direct interactions from the TAP data sets. One possibility is to screen the TAP eluates by far western using recombinant Bax and Bcl-XL. A similar approach has been used to detect an interaction between Bcl-XL and Rab7 (A. Hunt, UCSF, personal communication). Alternatively candidate protein interactions could also be tested in a pair wise fashion using either the yeast two hybrid or the related split-ubiquitin yeast assay systems, the later also being suitable for analysing interactions between membrane proteins.

Ultimately however, full validation of candidate interaction will require the development of activity based assay and investigation of the relevance of the interaction within the boarded context of mammalian apoptotic pathways and Bcl-2 family function. Such experiments could initially be based on RNAi or over-expression of candidate proteins in an attempt to determine if they have an effect on apoptotic responses. For some of the TAP proteins identified this will be complicated if they are known to be subunits within larger complexes. However, some of the candidate proteins identified have known enzymatic activities, such as recycling of growth factor receptors, protein glycosylation and ATP synthesis and for these proteins assays to directly measure their activity could be developed.

7.2 Concluding remarks:

This study was initiated to gain further insights into the regulation of Bax, one of the key players in the decision to commit to apoptosis. Previous models invoked to explain Bax and Bcl-2 family regulation have predominantly focused on the interplay between Bcl-2 family members themselves, with the mitochondria becoming involved solely as the targets of Bcl-2 family action (Figure 7.1 A). Instead, the data presented in this thesis suggests the mitochondria may play a more central role in influencing the decision to initiate the apoptotic program

(Figure 7.1 B). In this alternative view the pro-survival Bcl-2 proteins may have roles in regulating cellular metabolism and in particular mitochondrial physiology prior to the receipt of an apoptotic signal. Under the right conditions Bax and Bak may be able to intercept the same signals to which Bcl-2 family proteins are normally responsive but then initiate the apoptotic program. Such a model is consistent with a view that the apoptotic program in mammalian cells may be a late evolutionary addition to ensure rapid and co-ordinated removal of unwanted and damaged cells but is directly coupled to basic cellular stress responses common to all eukaryotic cells.

Figure 7.1 Model for the regulation of Bax activation.

(A) Traditional model for Bax activation. The decision to initiate mitochondrial dysfunction and apoptosis is controlled exclusively by Bcl-2 family proteins. **(B)** Alternative model for Bax activation. Data presented in this thesis implicates mitochondrial metabolic proteins, mitochondrial Ca^{2+} accumulation and mitochondrial structural changes as candidate upstream triggers for Bax activation and regulation. Bax and Bak are shown inactive (green), following their N-terminal conformational activation (orange) and in their oligomerised state (red). The position of blocks imposed by E1B19k and BHRF1 are also shown.

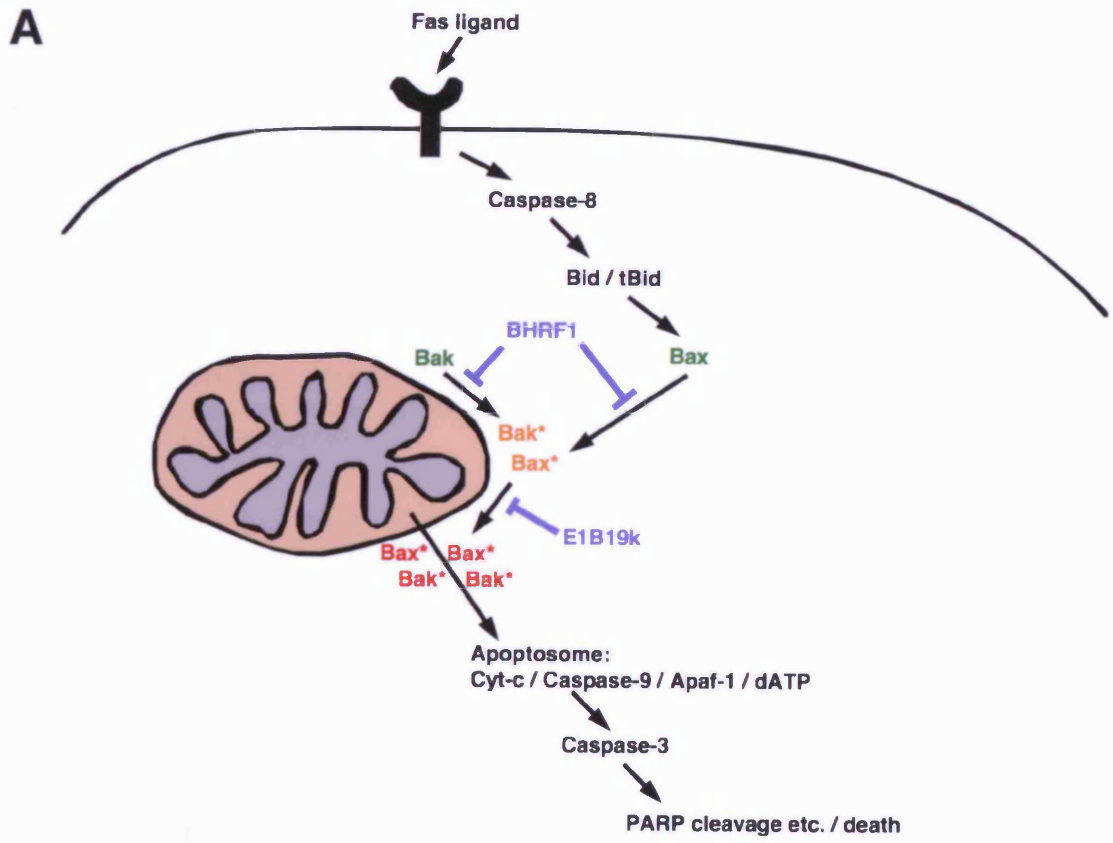
A
Fas ligand
Caspase-8
Bid / tBid
BHRF1
Bak
Bax
Bak*
Bax*
E1B19k
Bax* Bax*
Bak* Bak*
Apoptosome:
Cyt-c / Caspase-9 / Apaf-1 / dATP
Caspase-3
PARP cleavage etc. / death

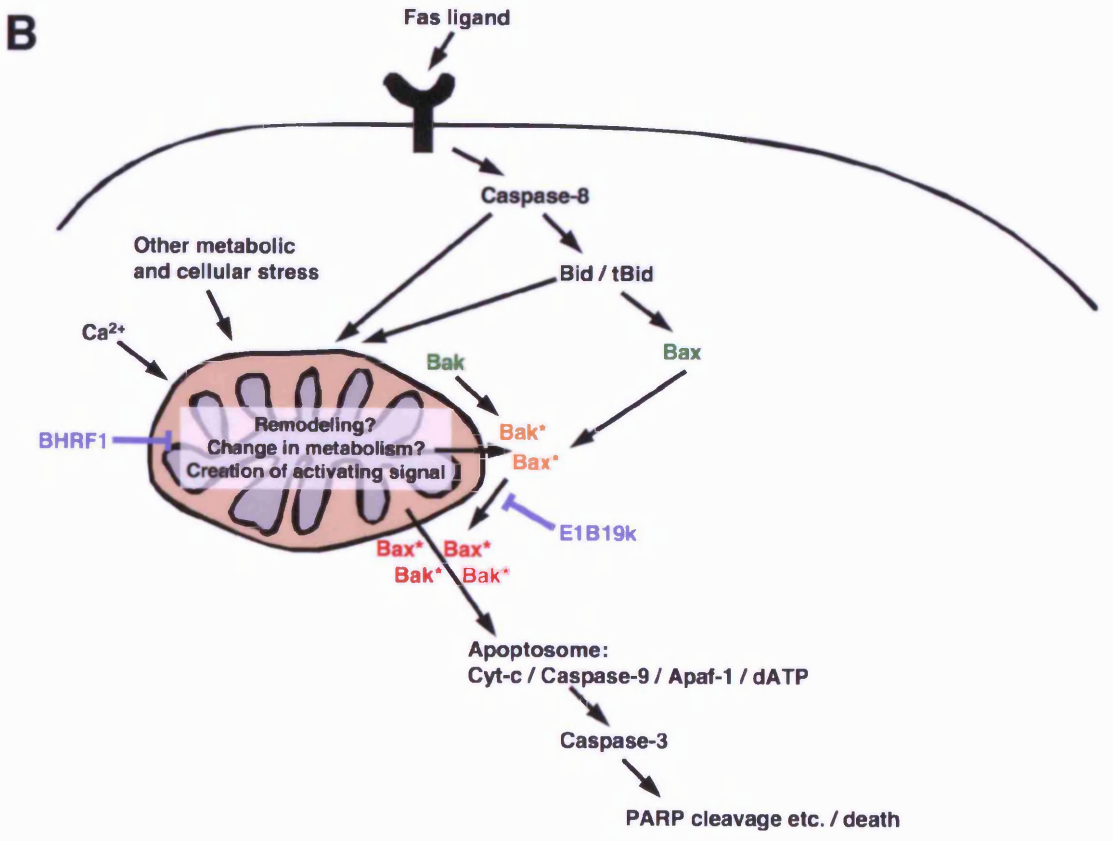
B
Fas ligand
Caspase-8
Other metabolic
and cellular stress
Bid / tBid
Ca2+
Bak
Bax
BHRF1
Remodeling?
Change in metabolism?
Creation of activating signal
Bak*
Bax*
E1B19k
Bax* Bax*
Bak* Bak*
Apoptosome:
Cyt-c / Caspase-9 / Apaf-1 / dATP
Caspase-3
PARP cleavage etc. / death

References:

Aggeler, R., Coons, J., Taylor, S. W., Ghosh, S. S., Garcia, J. J., Capaldi, R. A., and Marusich, M. F. (2002). A functionally active human F1F0 ATPase can be purified by immunocapture from heart tissue and fibroblast cell lines. Subunit structure and activity studies. J Biol Chem *277*, 33906-33912.

Annis, M. G., Soucie, E. L., Dlugosz, P. J., Cruz-Aguado, J. A., Penn, L. Z., Leber, B., and Andrews, D. W. (2005). Bax forms multispanning monomers that oligomerize to permeabilize membranes during apoptosis. Embo J *24*, 2096-2103.

Antonsson, B., Conti, F., Ciavatta, A., Montessuit, S., Lewis, S., Martinou, I., Bernasconi, L., Bernard, A., Mermod, J. J., Mazzei, G., *et al.* (1997). Inhibition of Bax channel-forming activity by Bcl-2. Science *277*, 370-372.

Antonsson, B., Montessuit, S., Lauper, S., Eskes, R., and Martinou, J. C. (2000). Bax oligomerization is required for channel-forming activity in liposomes and to trigger cytochrome c release from mitochondria. Biochem J *345 Pt 2*, 271-278.

Antonsson, B., Montessuit, S., Sanchez, B., and Martinou, J. C. (2001). Bax is present as a high molecular weight oligomer/complex in the mitochondrial membrane of apoptotic cells. J Biol Chem *276*, 11615-11623.

Arnoult, D., Bartle, L. M., Skaletskaya, A., Poncet, D., Zamzami, N., Park, P. U., Sharpe, J., Youle, R. J., and Goldmacher, V. S. (2004). Cytomegalovirus cell death suppressor vMIA blocks Bax- but not Bak-mediated apoptosis by binding and sequestering Bax at mitochondria. Proc Natl Acad Sci U S A *101*, 7988-7993.

Arnoult, D., Rismanchi, N., Grodet, A., Roberts, R. G., Seeburg, D. P., Estaquier, J., Sheng, M., and Blackstone, C. (2005). Bax/Bak-dependent release of DDP/TIMM8a promotes Drp1-mediated mitochondrial fission and mitoptosis during programmed cell death. Curr Biol *15*, 2112-2118.

Ashkenazi, A., and Dixit, V. M. (1998). Death receptors: signaling and modulation. Science *281*, 1305-1308.

Bernardi, P. (1999). Mitochondrial transport of cations: channels, exchangers, and permeability transition. Physiol Rev *79*, 1127-1155.

Berridge, M. J., Lipp, P., and Bootman, M. D. (2000). The versatility and universality of calcium signalling. Nat Rev Mol Cell Biol *1*, 11-21.

Boatright, K. M., and Salvesen, G. S. (2003). Mechanisms of caspase activation. Curr Opin Cell Biol *15*, 725-731.

Boise, L. H., Gonzalez-Garcia, M., Postema, C. E., Ding, L., Lindsten, T., Turka, L. A., Mao, X., Nunez, G., and Thompson, C. B. (1993). bcl-x, a bcl-2-related gene that functions as a dominant regulator of apoptotic cell death. Cell *74*, 597-608.

Bouillet, P., Metcalf, D., Huang, D. C., Tarlinton, D. M., Kay, T. W., Kontgen, F., Adams, J. M., and Strasser, A. (1999). Proapoptotic Bcl-2 relative Bim required for certain apoptotic responses, leukocyte homeostasis, and to preclude autoimmunity. Science *286*, 1735-1738.

Bouillet, P., Purton, J. F., Godfrey, D. I., Zhang, L. C., Coultas, L., Puthalakath, H., Pellegrini, M., Cory, S., Adams, J. M., and Strasser, A. (2002). BH3-only Bcl-2 family member Bim is required for apoptosis of autoreactive thymocytes. Nature *415*, 922-926.

Brimmell, M., Mendiola, R., Mangion, J., and Packham, G. (1998). BAX frameshift mutations in cell lines derived from human haemopoietic malignancies are associated with resistance to apoptosis and microsatellite instability. Oncogene *16*, 1803-1812.

Brini, M., Pinton, P., King, M. P., Davidson, M., Schon, E. A., and Rizzuto, R. (1999). A calcium signaling defect in the pathogenesis of a mitochondrial DNA inherited oxidative phosphorylation deficiency. Nat Med *5*, 951-954.

Capano, M., and Crompton, M. (2002). Biphasic translocation of Bax to mitochondria. Biochem J *367*, 169-178.

Carafoli, E. (2003). Historical review: mitochondria and calcium: ups and downs of an unusual relationship. Trends Biochem Sci *28*, 175-181.

Cartron, P. F., Gallenne, T., Bougras, G., Gautier, F., Manero, F., Vusio, P., Meflah, K., Vallette, F. M., and Juin, P. (2004). The first alpha helix of Bax plays a necessary role in its ligand-induced activation by the BH3-only proteins Bid and PUMA. Mol Cell *16*, 807-818.

Cartron, P. F., Priault, M., Oliver, L., Meflah, K., Manon, S., and Vallette, F. M. (2003). The N-terminal end of Bax contains a mitochondrial-targeting signal. J Biol Chem *278*, 11633-11641.

Carvalho, A. C., Sharpe, J., Rosenstock, T. R., Teles, A. F., Youle, R. J., and Smaili, S. S. (2004). Bax affects intracellular Ca2+ stores and induces Ca2+ wave propagation. Cell Death Differ *11*, 1265-1276.

Chai, J., Wu, Q., Shiozaki, E., Srinivasula, S. M., Alnemri, E. S., and Shi, Y. (2001). Crystal structure of a procaspase-7 zymogen: mechanisms of activation and substrate binding. Cell *107*, 399-407.

Chandra, D., Choy, G., Deng, X., Bhatia, B., Daniel, P., and Tang, D. G. (2004). Association of active caspase 8 with the mitochondrial membrane during apoptosis: potential roles in cleaving BAP31 and caspase 3 and mediating mitochondrion-endoplasmic reticulum cross talk in etoposide-induced cell death. Mol Cell Biol *24*, 6592-6607.

Chang, D. W., Xing, Z., Pan, Y., Algeciras-Schimnich, A., Barnhart, B. C., Yaish-Ohad, S., Peter, M. E., and Yang, X. (2002). c-FLIP(L) is a dual function regulator for caspase-8 activation and CD95-mediated apoptosis. Embo J *21*, 3704-3714.

Chen, L., Willis, S. N., Wei, A., Smith, B. J., Fletcher, J. I., Hinds, M. G., Colman, P. M., Day, C. L., Adams, J. M., and Huang, D. C. (2005). Differential targeting of prosurvival Bcl-2 proteins by their BH3-only ligands allows complementary apoptotic function. Mol Cell *17*, 393-403.

Chen, R., Valencia, I., Zhong, F., McColl, K. S., Roderick, H. L., Bootman, M. D., Berridge, M. J., Conway, S. J., Holmes, A. B., Mignery, G. A., *et al.* (2004). Bcl-2 functionally interacts with inositol 1,4,5-trisphosphate receptors to regulate calcium release from the ER in response to inositol 1,4,5-trisphosphate. J Cell Biol *166*, 193-203.

Cheng, E. H., Kirsch, D. G., Clem, R. J., Ravi, R., Kastan, M. B., Bedi, A., Ueno, K., and Hardwick, J. M. (1997). Conversion of Bcl-2 to a Bax-like death effector by caspases. Science *278*, 1966-1968.

Cheng, E. H., Levine, B., Boise, L. H., Thompson, C. B., and Hardwick, J. M. (1996). Bax-independent inhibition of apoptosis by Bcl-XL. Nature *379*, 554-556.

Cheng, E. H., Sheiko, T. V., Fisher, J. K., Craigen, W. J., and Korsmeyer, S. J. (2003). VDAC2 inhibits BAK activation and mitochondrial apoptosis. Science *301*, 513-517.

Cheng, E. H., Wei, M. C., Weiler, S., Flavell, R. A., Mak, T. W., Lindsten, T., and Korsmeyer, S. J. (2001). BCL-2, BCL-X(L) sequester BH3 domain-only molecules preventing BAX- and BAK-mediated mitochondrial apoptosis. Mol Cell *8*, 705-711.

Chipuk, J. E., Bouchier-Hayes, L., Kuwana, T., Newmeyer, D. D., and Green, D. R. (2005). PUMA couples the nuclear and cytoplasmic proapoptotic function of p53. Science *309*, 1732-1735.

Chittenden, T., Flemington, C., Houghton, A. B., Ebb, R. G., Gallo, G. J., Elangovan, B., Chinnadurai, G., and Lutz, R. J. (1995a). A conserved domain in Bak, distinct from BH1 and BH2, mediates cell death and protein binding functions. Embo J *14*, 5589-5596.

Chittenden, T., Harrington, E. A., O'Connor, R., Flemington, C., Lutz, R. J., Evan, G. I., and Guild, B. C. (1995b). Induction of apoptosis by the Bcl-2 homologue Bak. Nature *374*, 733-736.

Choi, S. S., Park, I. C., Yun, J. W., Sung, Y. C., Hong, S. I., and Shin, H. S. (1995). A novel Bcl-2 related gene, Bfl-1, is overexpressed in stomach cancer and preferentially expressed in bone marrow. Oncogene *11*, 1693-1698.

Chou, J. J., Li, H., Salvesen, G. S., Yuan, J., and Wagner, G. (1999). Solution structure of BID, an intracellular amplifier of apoptotic signaling. Cell *96*, 615-624.

Clarke, P. G., and Clarke, S. (1996). Nineteenth century research on naturally occurring cell death and related phenomena. Anat Embryol (Berl) *193*, 81-99.

Clem, R. J., Fechheimer, M., and Miller, L. K. (1991). Prevention of apoptosis by a baculovirus gene during infection of insect cells. Science *254*, 1388-1390.

Collins, T. J., Berridge, M. J., Lipp, P., and Bootman, M. D. (2002). Mitochondria are morphologically and functionally heterogeneous within cells. Embo J *21*, 1616-1627.

Conradt, B., and Horvitz, H. R. (1998). The C. elegans protein EGL-1 is required for programmed cell death and interacts with the Bcl-2-like protein CED-9. Cell *93*, 519-529.

Cory, S., Huang, D. C., and Adams, J. M. (2003). The Bcl-2 family: roles in cell survival and oncogenesis. Oncogene *22*, 8590-8607.

Crompton, M. (2000). Mitochondrial intermembrane junctional complexes and their role in cell death. J Physiol *529 Pt 1*, 11-21.

Crompton, M., Barksby, E., Johnson, N., and Capano, M. (2002). Mitochondrial intermembrane junctional complexes and their involvement in cell death. Biochimie *84*, 143-152.

Csordas, G., Madesh, M., Antonsson, B., and Hajnoczky, G. (2002). tcBid promotes Ca(2+) signal propagation to the mitochondria: control of Ca(2+) permeation through the outer mitochondrial membrane. Embo J *21*, 2198-2206.

Cuddeback, S. M., Yamaguchi, H., Komatsu, K., Miyashita, T., Yamada, M., Wu, C., Singh, S., and Wang, H. G. (2001). Molecular cloning and characterization of Bif-1. A novel Src homology 3 domain-containing protein that associates with Bax. J Biol Chem *276*, 20559-20565.

Danial, N. N., Gramm, C. F., Scorrano, L., Zhang, C. Y., Krauss, S., Ranger, A. M., Datta, S. R., Greenberg, M. E., Licklider, L. J., Lowell, B. B., *et al.* (2003). BAD and glucokinase reside in a mitochondrial complex that integrates glycolysis and apoptosis. Nature *424*, 952-956.

David, G. (1999). Mitochondrial clearance of cytosolic Ca(2+) in stimulated lizard motor nerve terminals proceeds without progressive elevation of mitochondrial matrix [Ca(2+)]. J Neurosci *19*, 7495-7506.

Day, C. L., Chen, L., Richardson, S. J., Harrison, P. J., Huang, D. C., and Hinds, M. G. (2005). Solution structure of prosurvival Mcl-1 and characterization of its binding by proapoptotic BH3-only ligands. J Biol Chem *280*, 4738-4744.

Degterev, A., Boyce, M., and Yuan, J. (2003). A decade of caspases. Oncogene *22*, 8543-8567.

Dejean, L. M., Martinez-Caballero, S., Guo, L., Hughes, C., Teijido, O., Ducret, T., Ichas, F., Korsmeyer, S. J., Antonsson, B., Jonas, E. A., and Kinnally, K. W. (2005). Oligomeric Bax is a component of the putative cytochrome c release channel MAC, mitochondrial apoptosis-induced channel. Mol Biol Cell *16*, 2424-2432.

Denisov, A. Y., Madiraju, M. S., Chen, G., Khadir, A., Beauparlant, P., Attardo, G., Shore, G. C., and Gehring, K. (2003). Solution structure of human BCL-w: modulation of ligand binding by the C-terminal helix. J Biol Chem *278*, 21124-21128.

Desagher, S., Osen-Sand, A., Nichols, A., Eskes, R., Montessuit, S., Lauper, S., Maundrell, K., Antonsson, B., and Martinou, J. C. (1999). Bid-induced conformational change of Bax is responsible for mitochondrial cytochrome c release during apoptosis. J Cell Biol *144*, 891-901.

Deshmukh, M., Du, C., Wang, X., and Johnson, E. M., Jr. (2002). Exogenous smac induces competence and permits caspase activation in sympathetic neurons. J Neurosci *22*, 8018-8027.

Deveraux, Q. L., Takahashi, R., Salvesen, G. S., and Reed, J. C. (1997). X-linked IAP is a direct inhibitor of cell-death proteases. Nature *388*, 300-304.

Dijkers, P. F., Medema, R. H., Lammers, J. W., Koenderman, L., and Coffer, P. J. (2000). Expression of the pro-apoptotic Bcl-2 family member Bim is regulated by the forkhead transcription factor FKHR-L1. Curr Biol *10*, 1201-1204.

Du, C., Fang, M., Li, Y., Li, L., and Wang, X. (2000). Smac, a mitochondrial protein that promotes cytochrome c-dependent caspase activation by eliminating IAP inhibition. Cell *102*, 33-42.

Edinger, A. L., Cinalli, R. M., and Thompson, C. B. (2003). Rab7 prevents growth factor-independent survival by inhibiting cell-autonomous nutrient transporter expression. Dev Cell *5*, 571-582.

Enari, M., Sakahira, H., Yokoyama, H., Okawa, K., Iwamatsu, A., and Nagata, S. (1998). A caspase-activated DNase that degrades DNA during apoptosis, and its inhibitor ICAD. Nature *391*, 43-50.

Epand, R. F., Martinou, J. C., Montessuit, S., Epand, R. M., and Yip, C. M. (2002). Direct evidence for membrane pore formation by the apoptotic protein Bax. Biochem Biophys Res Commun *298*, 744-749.

Erster, S., Mihara, M., Kim, R. H., Petrenko, O., and Moll, U. M. (2004). In vivo mitochondrial p53 translocation triggers a rapid first wave of cell death in response to DNA damage that can precede p53 target gene activation. Mol Cell Biol *24*, 6728-6741.

Eskes, R., Desagher, S., Antonsson, B., and Martinou, J. C. (2000). Bid induces the oligomerization and insertion of Bax into the outer mitochondrial membrane. Mol Cell Biol *20*, 929-935.

Fadok, V. A., Bratton, D. L., Rose, D. M., Pearson, A., Ezekewitz, R. A., and Henson, P. M. (2000). A receptor for phosphatidylserine-specific clearance of apoptotic cells. Nature *405*, 85-90.

Falnes, P. O., and Sandvig, K. (2000). Penetration of protein toxins into cells. Curr Opin Cell Biol *12*, 407-413.

Frank, S., Gaume, B., Bergmann-Leitner, E. S., Leitner, W. W., Robert, E. G., Catez, F., Smith, C. L., and Youle, R. J. (2001). The role of dynamin-related protein 1, a mediator of mitochondrial fission, in apoptosis. Dev Cell *1*, 515-525.

Frey, T. G., and Mannella, C. A. (2000). The internal structure of mitochondria. Trends Biochem Sci *25*, 319-324.

Frisch, S. M., and Mymryk, J. S. (2002). Adenovirus-5 E1A: paradox and paradigm. Nat Rev Mol Cell Biol *3*, 441-452.

Gibson, L., Holmgreen, S. P., Huang, D. C., Bernard, O., Copeland, N. G., Jenkins, N. A., Sutherland, G. R., Baker, E., Adams, J. M., and Cory, S. (1996). bcl-w, a novel member of the bcl-2 family, promotes cell survival. Oncogene *13*, 665-675.

Gilkerson, R. W., Selker, J. M., and Capaldi, R. A. (2003). The cristal membrane of mitochondria is the principal site of oxidative phosphorylation. FEBS Lett *546*, 355-358.

Gilmore, A. P., Metcalfe, A. D., Romer, L. H., and Streuli, C. H. (2000). Integrin-mediated survival signals regulate the apoptotic function of Bax through its conformation and subcellular localization. J Cell Biol *149*, 431-446.

Goldstein, J. C., Munoz-Pinedo, C., Ricci, J. E., Adams, S. R., Kelekar, A., Schuler, M., Tsien, R. Y., and Green, D. R. (2005). Cytochrome c is released in a single step during apoptosis. Cell Death Differ *12*, 453-462.

Goldstein, J. C., Waterhouse, N. J., Juin, P., Evan, G. I., and Green, D. R. (2000). The coordinate release of cytochrome c during apoptosis is rapid, complete and kinetically invariant. Nat Cell Biol *2*, 156-162.

Goping, I. S., Gross, A., Lavoie, J. N., Nguyen, M., Jemmerson, R., Roth, K., Korsmeyer, S. J., and Shore, G. C. (1998). Regulated targeting of BAX to mitochondria. J Cell Biol *143*, 207-215.

Graham, F. L., Smiley, J., Russell, W. C., and Nairn, R. (1977). Characteristics of a human cell line transformed by DNA from human adenovirus type 5. J Gen Virol *36*, 59-74.

Greenawalt, J. W., Rossi, C. S., and Lehninger, A. L. (1964). Effect of Active Accumulation of Calcium and Phosphate Ions on the Structure of Rat Liver Mitochondria. J Cell Biol *23*, 21-38.

Griffiths, G. J., Dubrez, L., Morgan, C. P., Jones, N. A., Whitehouse, J., Corfe, B. M., Dive, C., and Hickman, J. A. (1999). Cell damage-induced conformational changes of the pro-apoptotic protein Bak in vivo precede the onset of apoptosis. J Cell Biol *144*, 903-914.

Gross, A., Jockel, J., Wei, M. C., and Korsmeyer, S. J. (1998). Enforced dimerization of BAX results in its translocation, mitochondrial dysfunction and apoptosis. Embo J *17*, 3878-3885.

Gross, A., Pilcher, K., Blachly-Dyson, E., Basso, E., Jockel, J., Bassik, M. C., Korsmeyer, S. J., and Forte, M. (2000). Biochemical and genetic analysis of the mitochondrial response of yeast to BAX and BCL-X(L). Mol Cell Biol *20*, 3125-3136.

Gumienny, T. L., Brugnera, E., Tosello-Trampont, A. C., Kinchen, J. M., Haney, L. B., Nishiwaki, K., Walk, S. F., Nemergut, M. E., Macara, I. G., Francis, R., *et al.* (2001). CED-12/ELMO, a novel member of the CrkII/Dock180/Rac pathway, is required for phagocytosis and cell migration. Cell *107*, 27-41.

Guo, B., Zhai, D., Cabezas, E., Welsh, K., Nouraini, S., Satterthwait, A. C., and Reed, J. C. (2003). Humanin peptide suppresses apoptosis by interfering with Bax activation. Nature *423*, 456-461.

Hajnoczky, G., Robb-Gaspers, L. D., Seitz, M. B., and Thomas, A. P. (1995). Decoding of cytosolic calcium oscillations in the mitochondria. Cell *82*, 415-424.

Haldar, S., Basu, A., and Croce, C. M. (1998). Serine-70 is one of the critical sites for drug-induced Bcl2 phosphorylation in cancer cells. Cancer Res *58*, 1609-1615.

Han, J., Modha, D., and White, E. (1998). Interaction of E1B 19K with Bax is required to block Bax-induced loss of mitochondrial membrane potential and apoptosis. Oncogene *17*, 2993-3005.

Han, J., Sabbatini, P., Perez, D., Rao, L., Modha, D., and White, E. (1996). The E1B 19K protein blocks apoptosis by interacting with and inhibiting the p53-inducible and death-promoting Bax protein. Genes Dev *10*, 461-477.

Hanahan, D., and Weinberg, R. A. (2000). The hallmarks of cancer. Cell *100*, 57-70.

Harlin, H., Reffey, S. B., Duckett, C. S., Lindsten, T., and Thompson, C. B. (2001). Characterization of XIAP-deficient mice. Mol Cell Biol *21*, 3604-3608.

Harrington, E. A., Bennett, M. R., Fanidi, A., and Evan, G. I. (1994a). c-Myc-induced apoptosis in fibroblasts is inhibited by specific cytokines. Embo J *13*, 3286-3295.

Harrington, E. A., Fanidi, A., and Evan, G. I. (1994b). Oncogenes and cell death. Curr Opin Genet Dev *4*, 120-129.

Harris, M. H., Vander Heiden, M. G., Kron, S. J., and Thompson, C. B. (2000). Role of oxidative phosphorylation in Bax toxicity. Mol Cell Biol *20*, 3590-3596.

Hauptmann, P., Riel, C., Kunz-Schughart, L. A., Frohlich, K. U., Madeo, F., and Lehle, L. (2006). Defects in N-glycosylation induce apoptosis in yeast. Mol Microbiol *59*, 765-778.

He, L., Perkins, G. A., Poblenz, A. T., Harris, J. B., Hung, M., Ellisman, M. H., and Fox, D. A. (2003). Bcl-xL overexpression blocks bax-mediated mitochondrial contact site formation and apoptosis in rod photoreceptors of lead-exposed mice. Proc Natl Acad Sci U S A *100*, 1022-1027.

Hedgecock, E. M., Sulston, J. E., and Thomson, J. N. (1983). Mutations affecting programmed cell deaths in the nematode Caenorhabditis elegans. Science *220*, 1277-1279.

Hemann, M. T., Zilfou, J. T., Zhao, Z., Burgess, D. J., Hannon, G. J., and Lowe, S. W. (2004). Suppression of tumorigenesis by the p53 target PUMA. Proc Natl Acad Sci U S A *101*, 9333-9338.

Hengartner, M. O., and Horvitz, H. R. (1994). C. elegans cell survival gene ced-9 encodes a functional homolog of the mammalian proto-oncogene bcl-2. Cell *76*, 665-676.

Heuck, A. P., Hotze, E. M., Tweten, R. K., and Johnson, A. E. (2000). Mechanism of membrane insertion of a multimeric beta-barrel protein: perfringolysin O creates a pore using ordered and coupled conformational changes. Mol Cell *6*, 1233-1242.

Hinds, M. G., Lackmann, M., Skea, G. L., Harrison, P. J., Huang, D. C., and Day, C. L. (2003). The structure of Bcl-w reveals a role for the C-terminal residues in modulating biological activity. Embo J *22*, 1497-1507.

Hoeppner, D. J., Hengartner, M. O., and Schnabel, R. (2001). Engulfment genes cooperate with ced-3 to promote cell death in Caenorhabditis elegans. Nature *412*, 202-206.

Hofmann, E. R., Milstein, S., Boulton, S. J., Ye, M., Hofmann, J. J., Stergiou, L., Gartner, A., Vidal, M., and Hengartner, M. O. (2002). Caenorhabditis elegans HUS-1 is a DNA damage checkpoint protein required for genome stability and EGL-1-mediated apoptosis. Curr Biol *12*, 1908-1918.

Hoppel, C., Kerner, J., Turkaly, P., Minkler, P., and Tandler, B. (2002). Isolation of hepatic mitochondrial contact sites: previously unrecognized inner membrane components. Anal Biochem *302*, 60-69.

Hsu, S. Y., Kaipia, A., McGee, E., Lomeli, M., and Hsueh, A. J. (1997a). Bok is a pro-apoptotic Bcl-2 protein with restricted expression in reproductive tissues and heterodimerizes with selective anti-apoptotic Bcl-2 family members. Proc Natl Acad Sci U S A *94*, 12401-12406.

Hsu, Y. T., Wolter, K. G., and Youle, R. J. (1997b). Cytosol-to-membrane redistribution of Bax and Bcl-X(L) during apoptosis. Proc Natl Acad Sci U S A *94*, 3668-3672.

Hsu, Y. T., and Youle, R. J. (1997). Nonionic detergents induce dimerization among members of the Bcl-2 family. J Biol Chem *272*, 13829-13834.

Hsu, Y. T., and Youle, R. J. (1998). Bax in murine thymus is a soluble monomeric protein that displays differential detergent-induced conformations. J Biol Chem *273*, 10777-10783.

Huang, Q., Petros, A. M., Virgin, H. W., Fesik, S. W., and Olejniczak, E. T. (2003). Solution structure of the BHRF1 protein from Epstein-Barr virus, a homolog of human Bcl-2. J Mol Biol *332*, 1123-1130.

Ichas, F., Jouaville, L. S., and Mazat, J. P. (1997). Mitochondria are excitable organelles capable of generating and conveying electrical and calcium signals. Cell *89*, 1145-1153.

Igney, F. H., and Krammer, P. H. (2002). Death and anti-death: tumour resistance to apoptosis. Nat Rev Cancer *2*, 277-288.

Jagasia, R., Grote, P., Westermann, B., and Conradt, B. (2005). DRP-1-mediated mitochondrial fragmentation during EGL-1-induced cell death in C. elegans. Nature *433*, 754-760.

Jeffers, J. R., Parganas, E., Lee, Y., Yang, C., Wang, J., Brennan, J., MacLean, K. H., Han, J., Chittenden, T., Ihle, J. N., *et al.* (2003). Puma is an essential mediator of p53-dependent and -independent apoptotic pathways. Cancer Cell *4*, 321-328.

Jeong, S. Y., Gaume, B., Lee, Y. J., Hsu, Y. T., Ryu, S. W., Yoon, S. H., and Youle, R. J. (2004). Bcl-x(L) sequesters its C-terminal membrane anchor in soluble, cytosolic homodimers. Embo J *23*, 2146-2155.

Johnstone, R. W., Ruefli, A. A., and Lowe, S. W. (2002). Apoptosis: a link between cancer genetics and chemotherapy. Cell *108*, 153-164.

Jurgensmeier, J. M., Xie, Z., Deveraux, Q., Ellerby, L., Bredesen, D., and Reed, J. C. (1998). Bax directly induces release of cytochrome c from isolated mitochondria. Proc Natl Acad Sci U S A *95*, 4997-5002.

Karbowski, M., Jeong, S. Y., and Youle, R. J. (2004). Endophilin B1 is required for the maintenance of mitochondrial morphology. J Cell Biol *166*, 1027-1039.

Karbowski, M., Lee, Y. J., Gaume, B., Jeong, S. Y., Frank, S., Nechushtan, A., Santel, A., Fuller, M., Smith, C. L., and Youle, R. J. (2002). Spatial and temporal association of Bax with mitochondrial fission sites, Drp1, and Mfn2 during apoptosis. J Cell Biol *159*, 931-938.

Kawanishi, M. (1997). Epstein-Barr virus BHRF1 protein protects intestine 407 epithelial cells from apoptosis induced by tumor necrosis factor alpha and anti-Fas antibody. J Virol *71*, 3319-3322.

Kelleher, D. J., and Gilmore, R. (1997). DAD1, the defender against apoptotic cell death, is a subunit of the mammalian oligosaccharyltransferase. Proc Natl Acad Sci U S A *94*, 4994-4999.

Kerr, J. F., Wyllie, A. H., and Currie, A. R. (1972). Apoptosis: a basic biological phenomenon with wide-ranging implications in tissue kinetics. Br J Cancer *26*, 239-257.

Kiefer, M. C., Brauer, M. J., Powers, V. C., Wu, J. J., Umansky, S. R., Tomei, L. D., and Barr, P. J. (1995). Modulation of apoptosis by the widely distributed Bcl-2 homologue Bak. Nature *374*, 736-739.

Kim, P. K., Annis, M. G., Dlugosz, P. J., Leber, B., and Andrews, D. W. (2004a). During apoptosis bcl-2 changes membrane topology at both the endoplasmic reticulum and mitochondria. Mol Cell *14*, 523-529.

Kim, T. H., Zhao, Y., Ding, W. X., Shin, J. N., He, X., Seo, Y. W., Chen, J., Rabinowich, H., Amoscato, A. A., and Yin, X. M. (2004b). Bid-cardiolipin interaction at mitochondrial contact site contributes to mitochondrial cristae reorganization and cytochrome C release. Mol Biol Cell *15*, 3061-3072.

Kischkel, F. C., Hellbardt, S., Behrmann, I., Germer, M., Pawlita, M., Krammer, P. H., and Peter, M. E. (1995). Cytotoxicity-dependent APO-1 (Fas/CD95)-associated proteins form a death-inducing signaling complex (DISC) with the receptor. Embo J *14*, 5579-5588.

Kluck, R. M., Esposti, M. D., Perkins, G., Renken, C., Kuwana, T., Bossy-Wetzel, E., Goldberg, M., Allen, T., Barber, M. J., Green, D. R., and Newmeyer, D. D. (1999). The pro-apoptotic proteins, Bid and Bax, cause a limited permeabilization of the mitochondrial outer membrane that is enhanced by cytosol. J Cell Biol *147*, 809-822.

Knudson, C. M., Tung, K. S., Tourtellotte, W. G., Brown, G. A., and Korsmeyer, S. J. (1995). Bax-deficient mice with lymphoid hyperplasia and male germ cell death. Science *270*, 96-99.

Ko, Y. H., Delannoy, M., Hullihen, J., Chiu, W., and Pedersen, P. L. (2003). Mitochondrial ATP synthasome. Cristae-enriched membranes and a multiwell detergent screening assay yield dispersed single complexes containing the ATP synthase and carriers for Pi and ADP/ATP. J Biol Chem *278*, 12305-12309.

Kohn, A. D., Barthel, A., Kovacina, K. S., Boge, A., Wallach, B., Summers, S. A., Birnbaum, M. J., Scott, P. H., Lawrence, J. C., Jr., and Roth, R. A. (1998). Construction and characterization of a conditionally active version of the serine/threonine kinase Akt. J Biol Chem *273*, 11937-11943.

Koopman, G., Reutelingsperger, C. P., Kuijten, G. A., Keehnen, R. M., Pals, S. T., and van Oers, M. H. (1994). Annexin V for flow cytometric detection of phosphatidylserine expression on B cells undergoing apoptosis. Blood *84*, 1415-1420.

Korsmeyer, S. J., Wei, M. C., Saito, M., Weiler, S., Oh, K. J., and Schlesinger, P. H. (2000). Pro-apoptotic cascade activates BID, which oligomerizes BAK or BAX into pores that result in the release of cytochrome c. Cell Death Differ *7*, 1166-1173.

Kozopas, K. M., Yang, T., Buchan, H. L., Zhou, P., and Craig, R. W. (1993). MCL1, a gene expressed in programmed myeloid cell differentiation, has sequence similarity to BCL2. Proc Natl Acad Sci U S A *90*, 3516-3520.

Kranz, R., Lill, R., Goldman, B., Bonnard, G., and Merchant, S. (1998). Molecular mechanisms of cytochrome c biogenesis: three distinct systems. Mol Microbiol *29*, 383-396.

Kuwana, T., Bouchier-Hayes, L., Chipuk, J. E., Bonzon, C., Sullivan, B. A., Green, D. R., and Newmeyer, D. D. (2005). BH3 domains of BH3-only proteins differentially regulate Bax-mediated mitochondrial membrane permeabilization both directly and indirectly. Mol Cell *17*, 525-535.

Kuwana, T., Mackey, M. R., Perkins, G., Ellisman, M. H., Latterich, M., Schneiter, R., Green, D. R., and Newmeyer, D. D. (2002). Bid, Bax, and lipids cooperate to form supramolecular openings in the outer mitochondrial membrane. Cell *111*, 331-342.

Lazebnik, Y. (2001). Why do regulators of apoptosis look like bacterial toxins? Curr Biol *11*, R767-768.

LeBlanc, H. N., and Ashkenazi, A. (2003). Apo2L/TRAIL and its death and decoy receptors. Cell Death Differ *10*, 66-75.

Lei, K., and Davis, R. J. (2003). JNK phosphorylation of Bim-related members of the Bcl2 family induces Bax-dependent apoptosis. Proc Natl Acad Sci U S A *100*, 2432-2437.

Lemasters, J. J., Nieminen, A. L., Qian, T., Trost, L. C., Elmore, S. P., Nishimura, Y., Crowe, R. A., Cascio, W. E., Bradham, C. A., Brenner, D. A., and Herman, B. (1998). The mitochondrial permeability transition in cell death: a common mechanism in necrosis, apoptosis and autophagy. Biochim Biophys Acta *1366*, 177-196.

Letai, A., Bassik, M. C., Walensky, L. D., Sorcinelli, M. D., Weiler, S., and Korsmeyer, S. J. (2002). Distinct BH3 domains either sensitize or activate mitochondrial apoptosis, serving as prototype cancer therapeutics. Cancer Cell *2*, 183-192.

Ley, R., Ewings, K. E., Hadfield, K., and Cook, S. J. (2005). Regulatory phosphorylation of Bim: sorting out the ERK from the JNK. Cell Death Differ *12*, 1008-1014.

Li, H., Zhu, H., Xu, C. J., and Yuan, J. (1998). Cleavage of BID by caspase 8 mediates the mitochondrial damage in the Fas pathway of apoptosis. Cell *94*, 491-501.

Li, L. Y., Luo, X., and Wang, X. (2001). Endonuclease G is an apoptotic DNase when released from mitochondria. Nature *412*, 95-99.

Li, P., Nijhawan, D., Budihardjo, I., Srinivasula, S. M., Ahmad, M., Alnemri, E. S., and Wang, X. (1997). Cytochrome c and dATP-dependent formation of Apaf-1/caspase-9 complex initiates an apoptotic protease cascade. Cell *91*, 479-489.

Lindsten, T., Ross, A. J., King, A., Zong, W. X., Rathmell, J. C., Shiels, H. A., Ulrich, E., Waymire, K. G., Mahar, P., Frauwirth, K., *et al.* (2000). The combined functions of proapoptotic Bcl-2 family members bak and bax are essential for normal development of multiple tissues. Mol Cell *6*, 1389-1399.

Liu, Q. A., and Hengartner, M. O. (1998). Candidate adaptor protein CED-6 promotes the engulfment of apoptotic cells in C. elegans. Cell *93*, 961-972.

Liu, X., Dai, S., Zhu, Y., Marrack, P., and Kappler, J. W. (2003). The structure of a Bcl-xL/Bim fragment complex: implications for Bim function. Immunity *19*, 341-352.

Liu, X., Kim, C. N., Yang, J., Jemmerson, R., and Wang, X. (1996). Induction of apoptotic program in cell-free extracts: requirement for dATP and cytochrome c. Cell *86*, 147-157.

Liu, X., Zou, H., Slaughter, C., and Wang, X. (1997). DFF, a heterodimeric protein that functions downstream of caspase-3 to trigger DNA fragmentation during apoptosis. Cell *89*, 175-184.

Liu, X. H., Castelli, J. C., and Youle, R. J. (1999). Receptor-mediated uptake of an extracellular Bcl-x(L) fusion protein inhibits apoptosis. Proc Natl Acad Sci U S A *96*, 9563-9567.

Lockshin, R. A., and Williams, C. M. (1965). Programmed Cell Death--I. Cytology of Degeneration in the Intersegmental Muscles of the Pernyi Silkmoth. J Insect Physiol *11*, 123-133.

Loew, L. M., Tuft, R. A., Carrington, W., and Fay, F. S. (1993). Imaging in five dimensions: time-dependent membrane potentials in individual mitochondria. Biophys J *65*, 2396-2407.

Lum, M. G., and Nagley, P. (2003). Two phases of signalling between mitochondria during apoptosis leading to early depolarisation and delayed cytochrome c release. J Cell Sci *116*, 1437-1447.

Luo, X., Budihardjo, I., Zou, H., Slaughter, C., and Wang, X. (1998). Bid, a Bcl2 interacting protein, mediates cytochrome c release from mitochondria in response to activation of cell surface death receptors. Cell *94*, 481-490.

Lutter, M., Perkins, G. A., and Wang, X. (2001). The pro-apoptotic Bcl-2 family member tBid localizes to mitochondrial contact sites. BMC Cell Biol *2*, 22.

Lutz, W., Leon, J., and Eilers, M. (2002). Contributions of Myc to tumorigenesis. Biochim Biophys Acta *1602*, 61-71.

Makin, G. W., Corfe, B. M., Griffiths, G. J., Thistlethwaite, A., Hickman, J. A., and Dive, C. (2001). Damage-induced Bax N-terminal change, translocation to mitochondria and formation of Bax dimers/complexes occur regardless of cell fate. Embo J *20*, 6306-6315.

Makishima, T., Yoshimi, M., Komiyama, S., Hara, N., and Nishimoto, T. (2000). A subunit of the mammalian oligosaccharyltransferase, DAD1, interacts with Mcl-1, one of the bcl-2 protein family. J Biochem (Tokyo) *128*, 399-405.

Mannella, C. A., Pfeiffer, D. R., Bradshaw, P. C., Moraru, II, Slepchenko, B., Loew, L. M., Hsieh, C. E., Buttle, K., and Marko, M. (2001). Topology of the mitochondrial inner membrane: dynamics and bioenergetic implications. IUBMB Life *52*, 93-100.

Marchetti, P., Hirsch, T., Zamzami, N., Castedo, M., Decaudin, D., Susin, S. A., Masse, B., and Kroemer, G. (1996). Mitochondrial permeability transition triggers lymphocyte apoptosis. J Immunol *157*, 4830-4836.

Marzo, I., Brenner, C., Zamzami, N., Jurgensmeier, J. M., Susin, S. A., Vieira, H. L., Prevost, M. C., Xie, Z., Matsuyama, S., Reed, J. C., and Kroemer, G. (1998). Bax and adenine nucleotide translocator cooperate in the mitochondrial control of apoptosis. Science *281*, 2027-2031.

Matsuyama, S., Schendel, S. L., Xie, Z., and Reed, J. C. (1998). Cytoprotection by Bcl-2 requires the pore-forming alpha5 and alpha6 helices. J Biol Chem *273*, 30995-31001.

McDonnell, J. M., Fushman, D., Milliman, C. L., Korsmeyer, S. J., and Cowburn, D. (1999). Solution structure of the proapoptotic molecule BID: a structural basis for apoptotic agonists and antagonists. Cell *96*, 625-634.

McDonnell, T. J., Deane, N., Platt, F. M., Nunez, G., Jaeger, U., McKearn, J. P., and Korsmeyer, S. J. (1989). bcl-2-immunoglobulin transgenic mice demonstrate extended B cell survival and follicular lymphoproliferation. Cell *57*, 79-88.

McDonnell, T. J., and Korsmeyer, S. J. (1991). Progression from lymphoid hyperplasia to high-grade malignant lymphoma in mice transgenic for the t(14; 18). Nature *349*, 254-256.

McIlroy, D., Tanaka, M., Sakahira, H., Fukuyama, H., Suzuki, M., Yamamura, K., Ohsawa, Y., Uchiyama, Y., and Nagata, S. (2000). An auxiliary mode of apoptotic DNA fragmentation provided by phagocytes. Genes Dev *14*, 549-558.

Meergans, T., Hildebrandt, A. K., Horak, D., Haenisch, C., and Wendel, A. (2000). The short prodomain influences caspase-3 activation in HeLa cells. Biochem J *349*, 135-140.

Mela, L., and Hess, B. (1982). Influence of inorganic phosphate on the kinetics of heart mitochondrial calcium accumulation. Biochem Biophys Res Commun *106*, 1280-1285.

Micheau, O., and Tschopp, J. (2003). Induction of TNF receptor I-mediated apoptosis via two sequential signaling complexes. Cell *114*, 181-190.

Mihara, M., Erster, S., Zaika, A., Petrenko, O., Chittenden, T., Pancoska, P., and Moll, U. M. (2003). p53 has a direct apoptogenic role at the mitochondria. Mol Cell *11*, 577-590.

Mikhailov, V., Mikhailova, M., Degenhardt, K., Venkatachalam, M. A., White, E., and Saikumar, P. (2003). Association of Bax and Bak homo-oligomers in mitochondria. Bax requirement for Bak reorganization and cytochrome c release. J Biol Chem *278*, 5367-5376.

Minn, A. J., Kettlun, C. S., Liang, H., Kelekar, A., Vander Heiden, M. G., Chang, B. S., Fesik, S. W., Fill, M., and Thompson, C. B. (1999). Bcl-xL regulates apoptosis by heterodimerization-dependent and -independent mechanisms. Embo J *18*, 632-643.

Minn, A. J., Velez, P., Schendel, S. L., Liang, H., Muchmore, S. W., Fesik, S. W., Fill, M., and Thompson, C. B. (1997). Bcl-x(L) forms an ion channel in synthetic lipid membranes. Nature *385*, 353-357.

Miura, M., Zhu, H., Rotello, R., Hartwieg, E. A., and Yuan, J. (1993). Induction of apoptosis in fibroblasts by IL-1 beta-converting enzyme, a mammalian homolog of the C. elegans cell death gene ced-3. Cell *75*, 653-660.

Muchmore, S. W., Sattler, M., Liang, H., Meadows, R. P., Harlan, J. E., Yoon, H. S., Nettesheim, D., Chang, B. S., Thompson, C. B., Wong, S. L., *et al.* (1996). X-ray and NMR structure of human Bcl-xL, an inhibitor of programmed cell death. Nature *381*, 335-341.

Nagai, T., Sawano, A., Park, E. S., and Miyawaki, A. (2001). Circularly permuted green fluorescent proteins engineered to sense Ca2+. Proc Natl Acad Sci U S A *98*, 3197-3202.

Nechushtan, A., Smith, C. L., Hsu, Y. T., and Youle, R. J. (1999). Conformation of the Bax C-terminus regulates subcellular location and cell death. Embo J *18*, 2330-2341.

Nechushtan, A., Smith, C. L., Lamensdorf, I., Yoon, S. H., and Youle, R. J. (2001). Bax and Bak coalesce into novel mitochondria-associated clusters during apoptosis. J Cell Biol *153*, 1265-1276.

Newmeyer, D. D., Farschon, D. M., and Reed, J. C. (1994). Cell-free apoptosis in Xenopus egg extracts: inhibition by Bcl-2 and requirement for an organelle fraction enriched in mitochondria. Cell *79*, 353-364.

Nicholls, D. G., and Crompton, M. (1980). Mitochondrial calcium transport. FEBS Lett *111*, 261-268.

Nomura, M., Shimizu, S., Sugiyama, T., Narita, M., Ito, T., Matsuda, H., and Tsujimoto, Y. (2003). 14-3-3 Interacts directly with and negatively regulates pro-apoptotic Bax. J Biol Chem *278*, 2058-2065.

Nouraini, S., Six, E., Matsuyama, S., Krajewski, S., and Reed, J. C. (2000). The putative pore-forming domain of Bax regulates mitochondrial localization and interaction with Bcl-X(L). Mol Cell Biol *20*, 1604-1615.

O'Reilly, C. M., Fogarty, K. E., Drummond, R. M., Tuft, R. A., and Walsh, J. V., Jr. (2003). Quantitative analysis of spontaneous mitochondrial depolarizations. Biophys J *85*, 3350-3357.

Oakes, S. A., Scorrano, L., Opferman, J. T., Bassik, M. C., Nishino, M., Pozzan, T., and Korsmeyer, S. J. (2005). Proapoptotic BAX and BAK regulate the type 1 inositol trisphosphate receptor and calcium leak from the endoplasmic reticulum. Proc Natl Acad Sci U S A *102*, 105-110.

Oda, E., Ohki, R., Murasawa, H., Nemoto, J., Shibue, T., Yamashita, T., Tokino, T., Taniguchi, T., and Tanaka, N. (2000). Noxa, a BH3-only member of the Bcl-2 family and candidate mediator of p53-induced apoptosis. Science *288*, 1053-1058.

Ohtsuka, T., Ryu, H., Minamishima, Y. A., Macip, S., Sagara, J., Nakayama, K. I., Aaronson, S. A., and Lee, S. W. (2004). ASC is a Bax adaptor and regulates the p53-Bax mitochondrial apoptosis pathway. Nat Cell Biol *6*, 121-128.

Okada, H., Suh, W. K., Jin, J., Woo, M., Du, C., Elia, A., Duncan, G. S., Wakeham, A., Itie, A., Lowe, S. W., *et al.* (2002). Generation and characterization of Smac/DIABLO-deficient mice. Mol Cell Biol *22*, 3509-3517.

Oltvai, Z. N., Milliman, C. L., and Korsmeyer, S. J. (1993). Bcl-2 heterodimerizes in vivo with a conserved homolog, Bax, that accelerates programmed cell death. Cell *74*, 609-619.

Pacher, P., and Hajnoczky, G. (2001). Propagation of the apoptotic signal by mitochondrial waves. Embo J *20*, 4107-4121.

Pan, Z., Hirata, Y., Nagaraj, R. Y., Zhao, J., Nishi, M., Hayek, S. M., Bhat, M. B., Takeshima, H., and Ma, J. (2004). Co-expression of MG29 and ryanodine receptor leads to apoptotic cell death: effect mediated by intracellular Ca2+ release. J Biol Chem *279*, 19387-19390.

Pavlov, E. V., Priault, M., Pietkiewicz, D., Cheng, E. H., Antonsson, B., Manon, S., Korsmeyer, S. J., Mannella, C. A., and Kinnally, K. W. (2001). A novel, high conductance channel of mitochondria linked to apoptosis in mammalian cells and Bax expression in yeast. J Cell Biol *155*, 725-731.

Perez, D., and White, E. (2000). TNF-alpha signals apoptosis through a bid-dependent conformational change in Bax that is inhibited by E1B 19K. Mol Cell *6*, 53-63.

Petit, P. X., Lecoeur, H., Zorn, E., Dauguet, C., Mignotte, B., and Gougeon, M. L. (1995). Alterations in mitochondrial structure and function are early events of dexamethasone-induced thymocyte apoptosis. J Cell Biol *130*, 157-167.

Petros, A. M., Medek, A., Nettesheim, D. G., Kim, D. H., Yoon, H. S., Swift, K., Matayoshi, E. D., Oltersdorf, T., and Fesik, S. W. (2001). Solution structure of the antiapoptotic protein bcl-2. Proc Natl Acad Sci U S A *98*, 3012-3017.

Petros, A. M., Nettesheim, D. G., Wang, Y., Olejniczak, E. T., Meadows, R. P., Mack, J., Swift, K., Matayoshi, E. D., Zhang, H., Thompson, C. B., and Fesik, S. W. (2000). Rationale for Bcl-xL/Bad peptide complex formation from structure, mutagenesis, and biophysical studies. Protein Sci *9*, 2528-2534.

Pivovarova, N. B., Hongpaisan, J., Andrews, S. B., and Friel, D. D. (1999). Depolarization-induced mitochondrial Ca accumulation in sympathetic neurons: spatial and temporal characteristics. J Neurosci *19*, 6372-6384.

Polcic, P., and Forte, M. (2003). Response of yeast to the regulated expression of proteins in the Bcl-2 family. Biochem J *374*, 393-402.

Poncet, D., Larochette, N., Pauleau, A. L., Boya, P., Jalil, A. A., Cartron, P. F., Vallette, F., Schnebelen, C., Bartle, L. M., Skaletskaya, A., *et al.* (2004). An anti-apoptotic viral protein that recruits Bax to mitochondria. J Biol Chem *279*, 22605-22614.

Postigo, A., Cross, J. R., Downward, J., and Way, M. (2006). Interaction of F1L with the BH3 domain of Bak is responsible for inhibiting vaccinia-induced apoptosis. Cell Death Differ.

Putcha, G. V., Moulder, K. L., Golden, J. P., Bouillet, P., Adams, J. A., Strasser, A., and Johnson, E. M. (2001). Induction of BIM, a proapoptotic BH3-only BCL-2 family member, is critical for neuronal apoptosis. Neuron *29*, 615-628.

Puthalakath, H., Huang, D. C., O'Reilly, L. A., King, S. M., and Strasser, A. (1999). The proapoptotic activity of the Bcl-2 family member Bim is regulated by interaction with the dynein motor complex. Mol Cell *3*, 287-296.

Puthalakath, H., Villunger, A., O'Reilly, L. A., Beaumont, J. G., Coultas, L., Cheney, R. E., Huang, D. C., and Strasser, A. (2001). Bmf: a proapoptotic BH3-only protein regulated by interaction with the myosin V actin motor complex, activated by anoikis. Science *293*, 1829-1832.

Reddien, P. W., and Horvitz, H. R. (2000). CED-2/CrkII and CED-10/Rac control phagocytosis and cell migration in Caenorhabditis elegans. Nat Cell Biol *2*, 131-136.

Rigaut, G., Shevchenko, A., Rutz, B., Wilm, M., Mann, M., and Seraphin, B. (1999). A generic protein purification method for protein complex characterization and proteome exploration. Nat Biotechnol *17*, 1030-1032.

Rizzuto, R., Brini, M., Murgia, M., and Pozzan, T. (1993). Microdomains with high Ca2+ close to IP3-sensitive channels that are sensed by neighboring mitochondria. Science *262*, 744-747.

Rizzuto, R., Duchen, M. R., and Pozzan, T. (2004). Flirting in little space: the ER/mitochondria Ca2+ liaison. Sci STKE *2004*, re1.

Rizzuto, R., Pinton, P., Carrington, W., Fay, F. S., Fogarty, K. E., Lifshitz, L. M., Tuft, R. A., and Pozzan, T. (1998). Close contacts with the endoplasmic reticulum as determinants of mitochondrial Ca2+ responses. Science *280*, 1763-1766.

Rizzuto, R., Simpson, A. W., Brini, M., and Pozzan, T. (1992). Rapid changes of mitochondrial Ca2+ revealed by specifically targeted recombinant aequorin. Nature *358*, 325-327.

Rodriguez, J., and Lazebnik, Y. (1999). Caspase-9 and APAF-1 form an active holoenzyme. Genes Dev *13*, 3179-3184.

Rosconi, M. P., and London, E. (2002). Topography of helices 5-7 in membrane-inserted diphtheria toxin T domain: identification and insertion boundaries of two hydrophobic sequences that do not form a stable transmembrane hairpin. J Biol Chem *277*, 16517-16527.

Rosse, T., Olivier, R., Monney, L., Rager, M., Conus, S., Fellay, I., Jansen, B., and Borner, C. (1998). Bcl-2 prolongs cell survival after Bax-induced release of cytochrome c. Nature *391*, 496-499.

Rostovtseva, T. K., Antonsson, B., Suzuki, M., Youle, R. J., Colombini, M., and Bezrukov, S. M. (2004). Bid, but not Bax, regulates VDAC channels. J Biol Chem *279*, 13575-13583.

Roucou, X., Montessuit, S., Antonsson, B., and Martinou, J. C. (2002). Bax oligomerization in mitochondrial membranes requires tBid (caspase-8-cleaved Bid) and a mitochondrial protein. Biochem J *368*, 915-921.

Saito, M., Korsmeyer, S. J., and Schlesinger, P. H. (2000). BAX-dependent transport of cytochrome c reconstituted in pure liposomes. Nat Cell Biol *2*, 553-555.

Salvesen, G. S., and Duckett, C. S. (2002). IAP proteins: blocking the road to death's door. Nat Rev Mol Cell Biol *3*, 401-410.

Samuel, T., Weber, H. O., Rauch, P., Verdoodt, B., Eppel, J. T., McShea, A., Hermeking, H., and Funk, J. O. (2001). The G2/M regulator 14-3-3sigma prevents apoptosis through sequestration of Bax. J Biol Chem *276*, 45201-45206.

Sattler, M., Liang, H., Nettesheim, D., Meadows, R. P., Harlan, J. E., Eberstadt, M., Yoon, H. S., Shuker, S. B., Chang, B. S., Minn, A. J., *et al.* (1997). Structure of Bcl-xL-Bak peptide complex: recognition between regulators of apoptosis. Science *275*, 983-986.

Saunders, J. W., Jr. (1966). Death in embryonic systems. Science *154*, 604-612.

Savill, J., and Fadok, V. (2000). Corpse clearance defines the meaning of cell death. Nature *407*, 784-788.

Sawada, M., Sun, W., Hayes, P., Leskov, K., Boothman, D. A., and Matsuyama, S. (2003). Ku70 suppresses the apoptotic translocation of Bax to mitochondria. Nat Cell Biol *5*, 320-329.

Scaffidi, C., Fulda, S., Srinivasan, A., Friesen, C., Li, F., Tomaselli, K. J., Debatin, K. M., Krammer, P. H., and Peter, M. E. (1998). Two CD95 (APO-1/Fas) signaling pathways. Embo J *17*, 1675-1687.

Schlesinger, P. H., Gross, A., Yin, X. M., Yamamoto, K., Saito, M., Waksman, G., and Korsmeyer, S. J. (1997). Comparison of the ion channel characteristics of proapoptotic BAX and antiapoptotic BCL-2. Proc Natl Acad Sci U S A *94*, 11357-11362.

Schweneker, M., Bachmann, A. S., and Moelling, K. (2005). JM4 is a four-transmembrane protein binding to the CCR5 receptor. FEBS Lett *579*, 1751-1758.

Scorrano, L., Ashiya, M., Buttle, K., Weiler, S., Oakes, S. A., Mannella, C. A., and Korsmeyer, S. J. (2002). A distinct pathway remodels mitochondrial cristae and mobilizes cytochrome c during apoptosis. Dev Cell *2*, 55-67.

Scorrano, L., Oakes, S. A., Opferman, J. T., Cheng, E. H., Sorcinelli, M. D., Pozzan, T., and Korsmeyer, S. J. (2003). BAX and BAK regulation of endoplasmic reticulum Ca2+: a control point for apoptosis. Science *300*, 135-139.

Sheridan, J. W., Bishop, C. J., and Simmons, R. J. (1981). Biophysical and morphological correlates of kinetic change and death in a starved human melanoma cell line. J Cell Sci *49*, 119-137.

Shi, Y. (2002). Mechanisms of caspase activation and inhibition during apoptosis. Mol Cell *9*, 459-470.

Shimizu, S., Narita, M., and Tsujimoto, Y. (1999). Bcl-2 family proteins regulate the release of apoptogenic cytochrome c by the mitochondrial channel VDAC. Nature *399*, 483-487.

Simpson, P. B., and Russell, J. T. (1996). Mitochondria support inositol 1,4,5-trisphosphate-mediated Ca2+ waves in cultured oligodendrocytes. J Biol Chem *271*, 33493-33501.

Smaili, S. S., Hsu, Y. T., Sanders, K. M., Russell, J. T., and Youle, R. J. (2001). Bax translocation to mitochondria subsequent to a rapid loss of mitochondrial membrane potential. Cell Death Differ *8*, 909-920.

Somlyo, A. P., Somlyo, A. V., and Shuman, H. (1979). Electron probe analysis of vascular smooth muscle. Composition of mitochondria, nuclei, and cytoplasm. J Cell Biol *81*, 316-335.

Soucie, E. L., Annis, M. G., Sedivy, J., Filmus, J., Leber, B., Andrews, D. W., and Penn, L. Z. (2001). Myc potentiates apoptosis by stimulating Bax activity at the mitochondria. Mol Cell Biol *21*, 4725-4736.

Stennicke, H. R., Deveraux, Q. L., Humke, E. W., Reed, J. C., Dixit, V. M., and Salvesen, G. S. (1999). Caspase-9 can be activated without proteolytic processing. J Biol Chem *274*, 8359-8362.

Strasser, A., Harris, A. W., Bath, M. L., and Cory, S. (1990). Novel primitive lymphoid tumours induced in transgenic mice by cooperation between myc and bcl-2. Nature *348*, 331-333.

Strasser, A., Harris, A. W., Huang, D. C., Krammer, P. H., and Cory, S. (1995). Bcl-2 and Fas/APO-1 regulate distinct pathways to lymphocyte apoptosis. Embo J *14*, 6136-6147.

Stroud, R. M., Reiling, K., Wiener, M., and Freymann, D. (1998). Ion-channel-forming colicins. Curr Opin Struct Biol *8*, 525-533.

Su, J., Wang, G., Barrett, J. W., Irvine, T. S., Gao, X., and McFadden, G. (2006). Myxoma virus M11L blocks apoptosis through inhibition of conformational activation of Bax at the mitochondria. J Virol *80*, 1140-1151.

Sulston, J. E. (1976). Post-embryonic development in the ventral cord of Caenorhabditis elegans. Philos Trans R Soc Lond B Biol Sci *275*, 287-297.

Sundararajan, R., Cuconati, A., Nelson, D., and White, E. (2001). Tumor necrosis factor-alpha induces Bax-Bak interaction and apoptosis, which is inhibited by adenovirus E1B 19K. J Biol Chem *276*, 45120-45127.

Sundararajan, R., and White, E. (2001). E1B 19K blocks Bax oligomerization and tumor necrosis factor alpha-mediated apoptosis. J Virol *75*, 7506-7516.

Susin, S. A., Lorenzo, H. K., Zamzami, N., Marzo, I., Snow, B. E., Brothers, G. M., Mangion, J., Jacotot, E., Costantini, P., Loeffler, M., *et al.* (1999). Molecular characterization of mitochondrial apoptosis-inducing factor. Nature *397*, 441-446.

Suzuki, M., Youle, R. J., and Tjandra, N. (2000). Structure of Bax: coregulation of dimer formation and intracellular localization. Cell *103*, 645-654.

Suzuki, Y., Imai, Y., Nakayama, H., Takahashi, K., Takio, K., and Takahashi, R. (2001). A serine protease, HtrA2, is released from the mitochondria and interacts with XIAP, inducing cell death. Mol Cell *8*, 613-621.

Tafani, M., Cohn, J. A., Karpinich, N. O., Rothman, R. J., Russo, M. A., and Farber, J. L. (2002). Regulation of intracellular pH mediates Bax activation in HeLa cells treated with staurosporine or tumor necrosis factor-alpha. J Biol Chem *277*, 49569-49576.

Takahashi, Y., Karbowski, M., Yamaguchi, H., Kazi, A., Wu, J., Sebti, S. M., Youle, R. J., and Wang, H. G. (2005). Loss of Bif-1 suppresses Bax/Bak conformational change and mitochondrial apoptosis. Mol Cell Biol *25*, 9369-9382.

Terrones, O., Antonsson, B., Yamaguchi, H., Wang, H. G., Liu, J., Lee, R. M., Herrmann, A., and Basanez, G. (2004). Lipidic pore formation by the concerted action of proapoptotic BAX and tBID. J Biol Chem *279*, 30081-30091.

Tinel, H., Cancela, J. M., Mogami, H., Gerasimenko, J. V., Gerasimenko, O. V., Tepikin, A. V., and Petersen, O. H. (1999). Active mitochondria surrounding the pancreatic acinar granule region prevent spreading of inositol trisphosphate-evoked local cytosolic Ca(2+) signals. Embo J *18*, 4999-5008.

Tsujimoto, Y., Finger, L. R., Yunis, J., Nowell, P. C., and Croce, C. M. (1984). Cloning of the chromosome breakpoint of neoplastic B cells with the t(14;18) chromosome translocation. Science *226*, 1097-1099.

Valentijn, A. J., Metcalfe, A. D., Kott, J., Streuli, C. H., and Gilmore, A. P. (2003). Spatial and temporal changes in Bax subcellular localization during anoikis. J Cell Biol *162*, 599-612.

Van Coppenolle, F., Vanden Abeele, F., Slomianny, C., Flourakis, M., Hesketh, J., Dewailly, E., and Prevarskaya, N. (2004). Ribosome-translocon complex mediates calcium leakage from endoplasmic reticulum stores. J Cell Sci *117*, 4135-4142.

Vander Heiden, M. G., Chandel, N. S., Williamson, E. K., Schumacker, P. T., and Thompson, C. B. (1997). Bcl-xL regulates the membrane potential and volume homeostasis of mitochondria. Cell *91*, 627-637.

Vaux, D. L., Cory, S., and Adams, J. M. (1988). Bcl-2 gene promotes haemopoietic cell survival and cooperates with c-myc to immortalize pre-B cells. Nature *335*, 440-442.

Vaux, D. L., and Silke, J. (2005). IAPs, RINGs and ubiquitylation. Nat Rev Mol Cell Biol *6*, 287-297.

Verhagen, A. M., Ekert, P. G., Pakusch, M., Silke, J., Connolly, L. M., Reid, G. E., Moritz, R. L., Simpson, R. J., and Vaux, D. L. (2000). Identification of DIABLO, a mammalian protein that promotes apoptosis by binding to and antagonizing IAP proteins. Cell *102*, 43-53.

Villunger, A., Michalak, E. M., Coultas, L., Mullauer, F., Bock, G., Ausserlechner, M. J., Adams, J. M., and Strasser, A. (2003). p53- and drug-induced apoptotic responses mediated by BH3-only proteins puma and noxa. Science *302*, 1036-1038.

Vousden, K. H., and Lu, X. (2002). Live or let die: the cell's response to p53. Nat Rev Cancer *2*, 594-604.

Wang, G., Barrett, J. W., Nazarian, S. H., Everett, H., Gao, X., Bleackley, C., Colwill, K., Moran, M. F., and McFadden, G. (2004). Myxoma virus M11L prevents apoptosis through constitutive interaction with Bak. J Virol *78*, 7097-7111.

Warr, M. R., Acoca, S., Liu, Z., Germain, M., Watson, M., Blanchette, M., Wing, S. S., and Shore, G. C. (2005). BH3-ligand regulates access of MCL-1 to its E3 ligase. FEBS Lett *579*, 5603-5608.

Wasilenko, S. T., Banadyga, L., Bond, D., and Barry, M. (2005). The vaccinia virus F1L protein interacts with the proapoptotic protein Bak and inhibits Bak activation. J Virol *79*, 14031-14043.

Wei, M. C., Lindsten, T., Mootha, V. K., Weiler, S., Gross, A., Ashiya, M., Thompson, C. B., and Korsmeyer, S. J. (2000). tBID, a membrane-targeted death ligand, oligomerizes BAK to release cytochrome c. Genes Dev *14*, 2060-2071.

Wei, M. C., Zong, W. X., Cheng, E. H., Lindsten, T., Panoutsakopoulou, V., Ross, A. J., Roth, K. A., MacGregor, G. R., Thompson, C. B., and Korsmeyer, S. J. (2001). Proapoptotic BAX and BAK: a requisite gateway to mitochondrial dysfunction and death. Science *292*, 727-730.

White, C., Li, C., Yang, J., Petrenko, N. B., Madesh, M., Thompson, C. B., and Foskett, J. K. (2005). The endoplasmic reticulum gateway to apoptosis by Bcl-X(L) modulation of the InsP3R. Nat Cell Biol *7*, 1021-1028.

White, E., Blose, S. H., and Stillman, B. W. (1984). Nuclear envelope localization of an adenovirus tumor antigen maintains the integrity of cellular DNA. Mol Cell Biol *4*, 2865-2875.

Willis, S. N., and Adams, J. M. (2005). Life in the balance: how BH3-only proteins induce apoptosis. Curr Opin Cell Biol *17*, 617-625.

Willis, S. N., Chen, L., Dewson, G., Wei, A., Naik, E., Fletcher, J. I., Adams, J. M., and Huang, D. C. (2005). Proapoptotic Bak is sequestered by Mcl-1 and Bcl-xL, but not Bcl-2, until displaced by BH3-only proteins. Genes Dev *19*, 1294-1305.

Wilson-Annan, J., O'Reilly, L. A., Crawford, S. A., Hausmann, G., Beaumont, J. G., Parma, L. P., Chen, L., Lackmann, M., Lithgow, T., Hinds, M. G., *et al.* (2003). Proapoptotic BH3-only proteins trigger membrane integration of prosurvival Bcl-w and neutralize its activity. J Cell Biol *162*, 877-887.

Wolter, K. G., Hsu, Y. T., Smith, C. L., Nechushtan, A., Xi, X. G., and Youle, R. J. (1997). Movement of Bax from the cytosol to mitochondria during apoptosis. J Cell Biol *139*, 1281-1292.

Wu, Y. C., and Horvitz, H. R. (1998a). C. elegans phagocytosis and cell-migration protein CED-5 is similar to human DOCK180. Nature *392*, 501-504.

Wu, Y. C., and Horvitz, H. R. (1998b). The C. elegans cell corpse engulfment gene ced-7 encodes a protein similar to ABC transporters. Cell *93*, 951-960.

Xiang, J., Chao, D. T., and Korsmeyer, S. J. (1996). BAX-induced cell death may not require interleukin 1 beta-converting enzyme-like proteases. Proc Natl Acad Sci U S A *93*, 14559-14563.

Yin, X. M., Wang, K., Gross, A., Zhao, Y., Zinkel, S., Klocke, B., Roth, K. A., and Korsmeyer, S. J. (1999). Bid-deficient mice are resistant to Fas-induced hepatocellular apoptosis. Nature *400*, 886-891.

Youle, R. J., and Karbowski, M. (2005). Mitochondrial fission in apoptosis. Nat Rev Mol Cell Biol *6*, 657-663.

Yu, J., Zhang, L., Hwang, P. M., Kinzler, K. W., and Vogelstein, B. (2001). PUMA induces the rapid apoptosis of colorectal cancer cells. Mol Cell *7*, 673-682.

Yu, S. W., Wang, H., Poitras, M. F., Coombs, C., Bowers, W. J., Federoff, H. J., Poirier, G. G., Dawson, T. M., and Dawson, V. L. (2002). Mediation of poly(ADP-ribose) polymerase-1-dependent cell death by apoptosis-inducing factor. Science *297*, 259-263.

Zamzami, N., Marchetti, P., Castedo, M., Zanin, C., Vayssiere, J. L., Petit, P. X., and Kroemer, G. (1995). Reduction in mitochondrial potential constitutes an early irreversible step of programmed lymphocyte death in vivo. J Exp Med *181*, 1661-1672.

Zha, J., Harada, H., Yang, E., Jockel, J., and Korsmeyer, S. J. (1996). Serine phosphorylation of death agonist BAD in response to survival factor results in binding to 14-3-3 not BCL-X(L). Cell *87*, 619-628.

Zha, J., Weiler, S., Oh, K. J., Wei, M. C., and Korsmeyer, S. J. (2000). Posttranslational N-myristoylation of BID as a molecular switch for targeting mitochondria and apoptosis. Science *290*, 1761-1765.

Zhai, D., Luciano, F., Zhu, X., Guo, B., Satterthwait, A. C., and Reed, J. C. (2005). Humanin binds and nullifies Bid activity by blocking its activation of Bax and Bak. J Biol Chem *280*, 15815-15824.

Zhang, H., Kim, J. K., Edwards, C. A., Xu, Z., Taichman, R., and Wang, C. Y. (2005). Clusterin inhibits apoptosis by interacting with activated Bax. Nat Cell Biol *7*, 909-915.

Zhang, J., Campbell, R. E., Ting, A. Y., and Tsien, R. Y. (2002). Creating new fluorescent probes for cell biology. Nat Rev Mol Cell Biol *3*, 906-918.

Zhong, Q., Gao, W., Du, F., and Wang, X. (2005). Mule/ARF-BP1, a BH3-only E3 ubiquitin ligase, catalyzes the polyubiquitination of Mcl-1 and regulates apoptosis. Cell *121*, 1085-1095.

Zhou, Z., Hartwieg, E., and Horvitz, H. R. (2001). CED-1 is a transmembrane receptor that mediates cell corpse engulfment in C. elegans. Cell *104*, 43-56.

Zhu, Y., Swanson, B. J., Wang, M., Hildeman, D. A., Schaefer, B. C., Liu, X., Suzuki, H., Mihara, K., Kappler, J., and Marrack, P. (2004). Constitutive association of the proapoptotic protein Bim with Bcl-2-related proteins on mitochondria in T cells. Proc Natl Acad Sci U S A *101*, 7681-7686.

Zong, W. X., Li, C., Hatzivassiliou, G., Lindsten, T., Yu, Q. C., Yuan, J., and Thompson, C. B. (2003). Bax and Bak can localize to the endoplasmic reticulum to initiate apoptosis. J Cell Biol *162*, 59-69.

Zong, W. X., Lindsten, T., Ross, A. J., MacGregor, G. R., and Thompson, C. B. (2001). BH3-only proteins that bind pro-survival Bcl-2 family members fail to induce apoptosis in the absence of Bax and Bak. Genes Dev *15*, 1481-1486.

Zong, W. X., and Thompson, C. B. (2006). Necrotic death as a cell fate. Genes Dev *20*, 1-15.

Zou, H., Henzel, W. J., Liu, X., Lutschg, A., and Wang, X. (1997). Apaf-1, a human protein homologous to C. elegans CED-4, participates in cytochrome c-dependent activation of caspase-3. Cell *90*, 405-413.

Appendix

Supplementary data figures.

Supplementary Figure 3.13 C

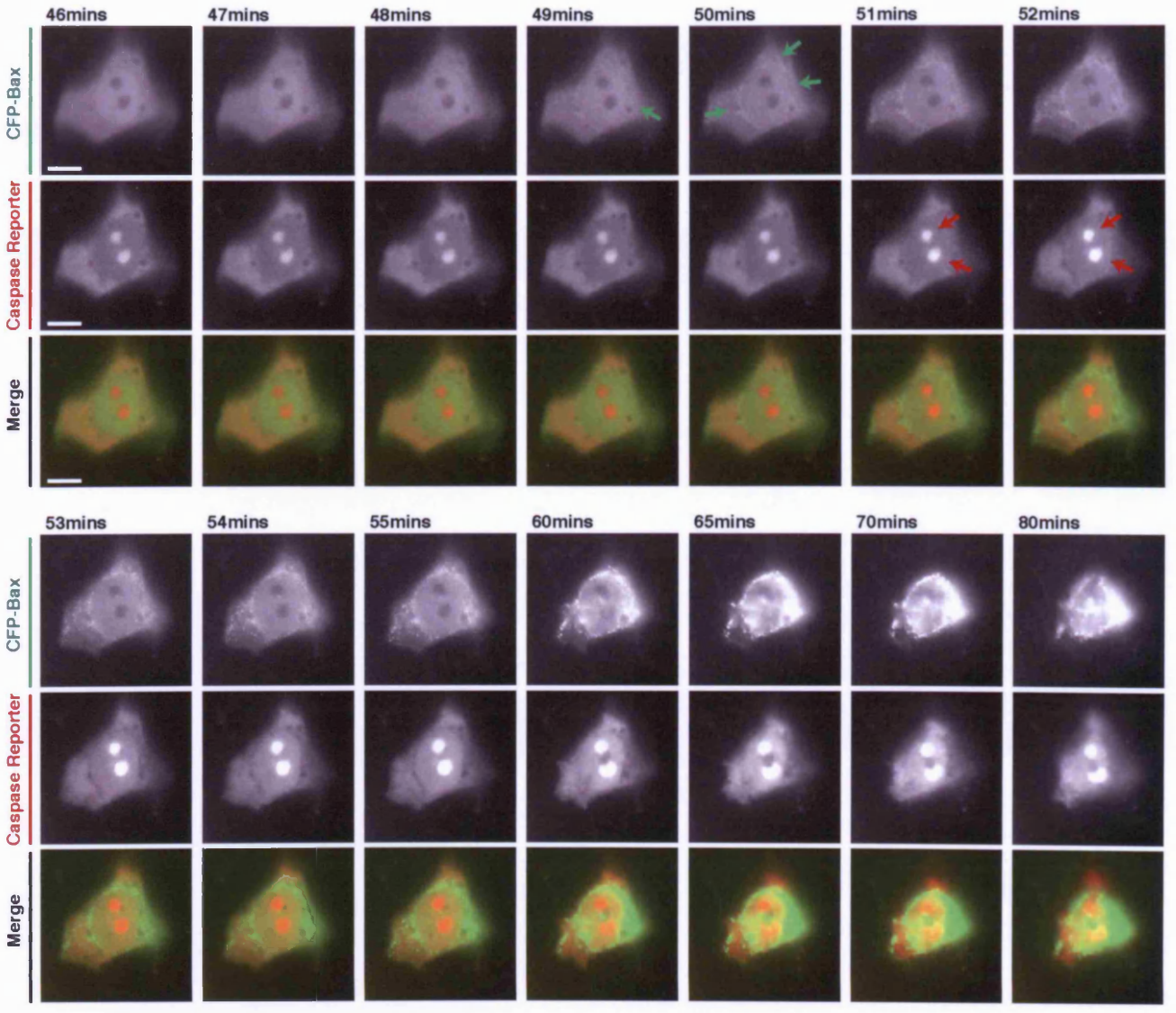

Supplementary Figure 3.13 D

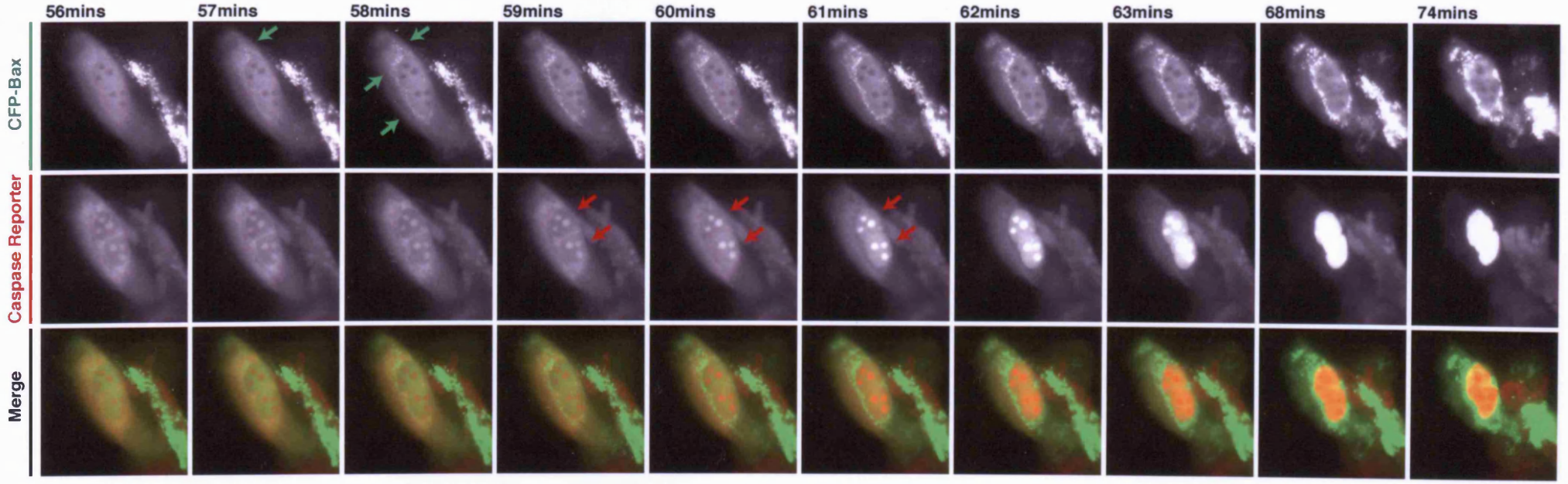

Supplementary Figure 3.14 D and E

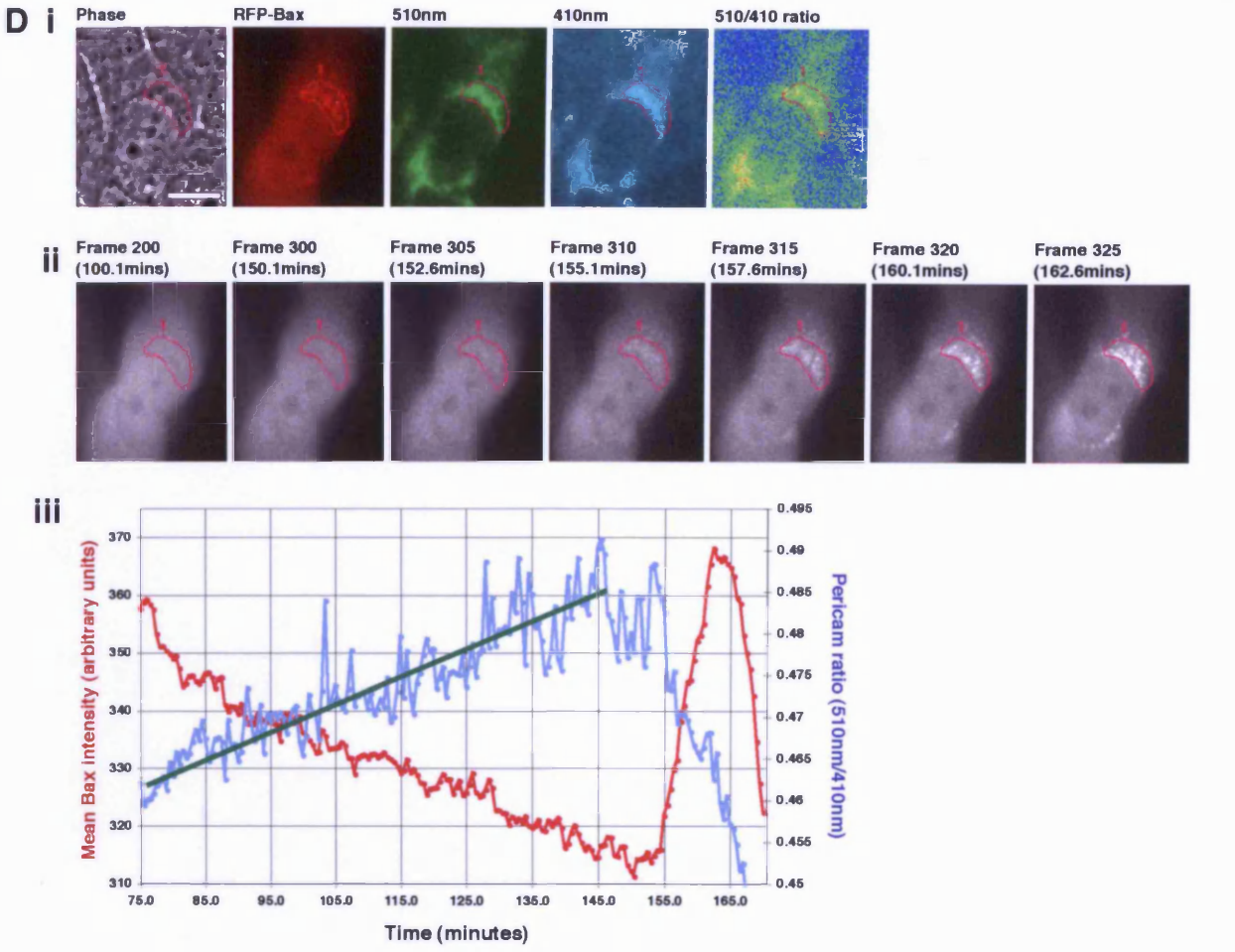

Supplementary Figure 4.11 C

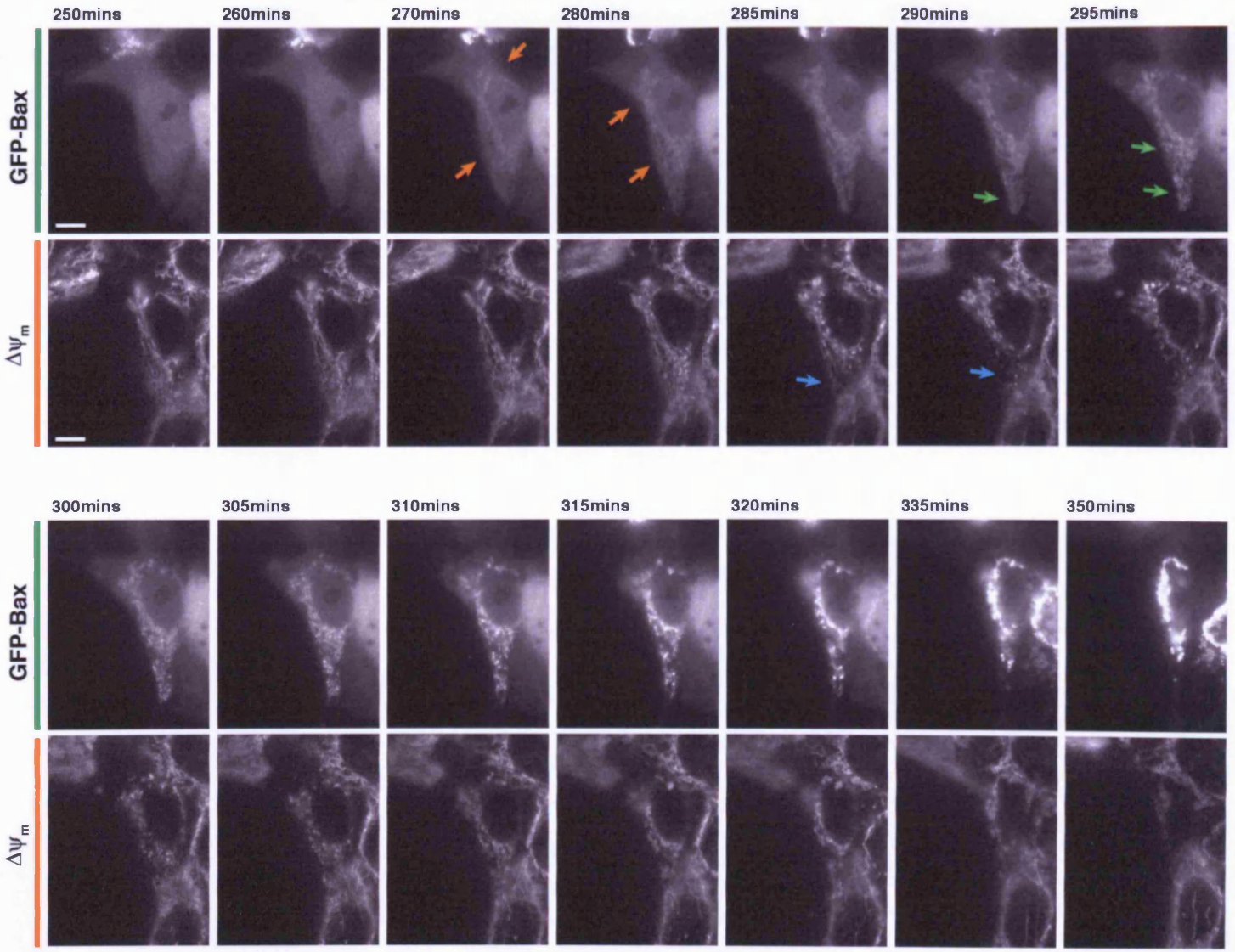

Supplementary Figure 4.13 C and D

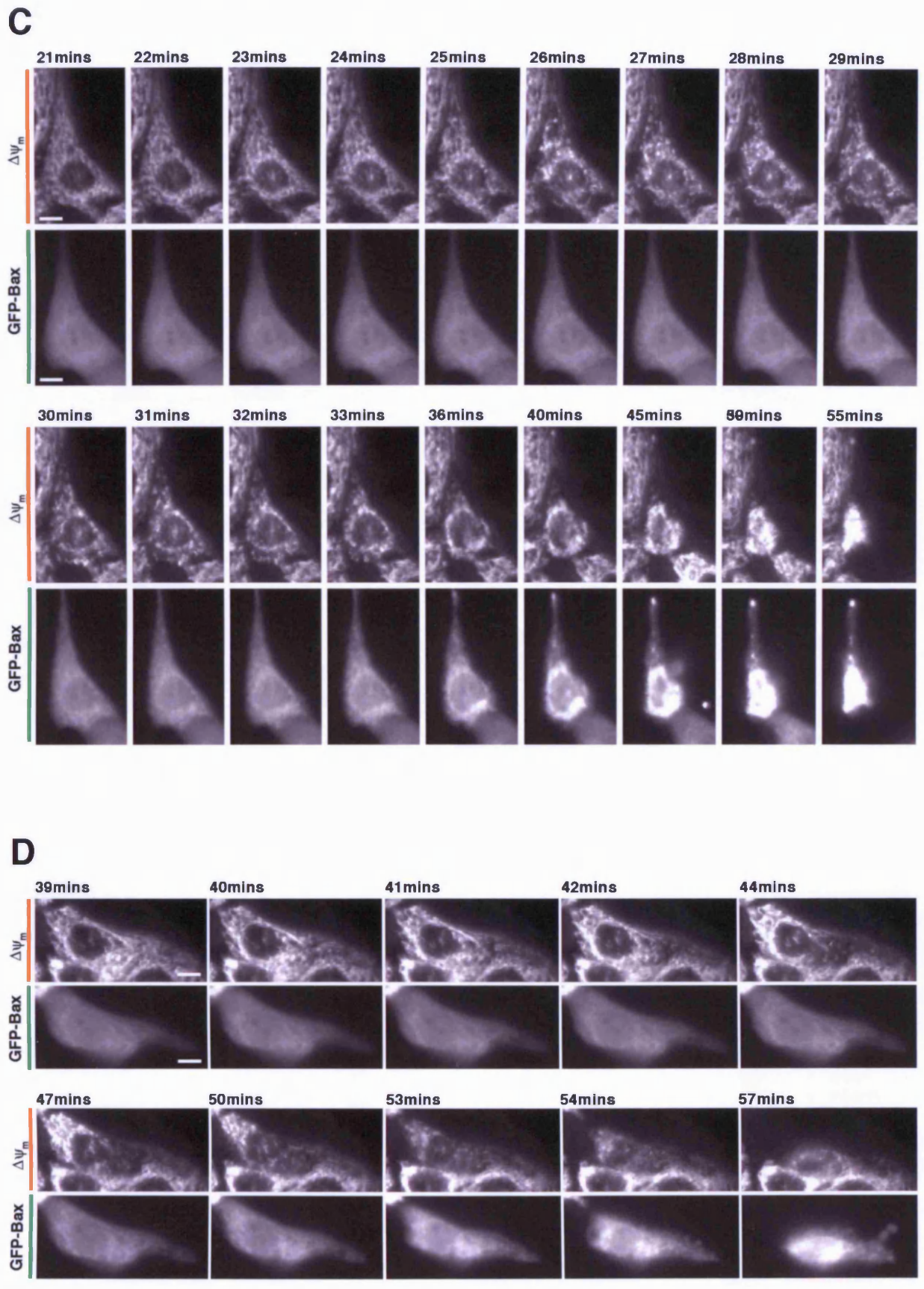

Supplementary Figure 4.16 C, D and E

C

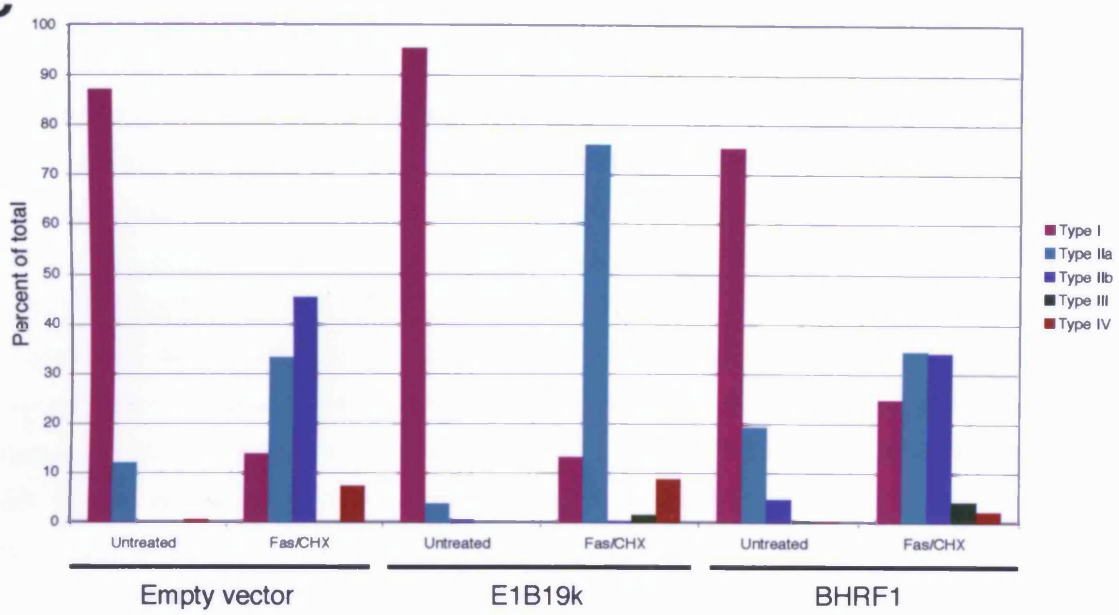

D

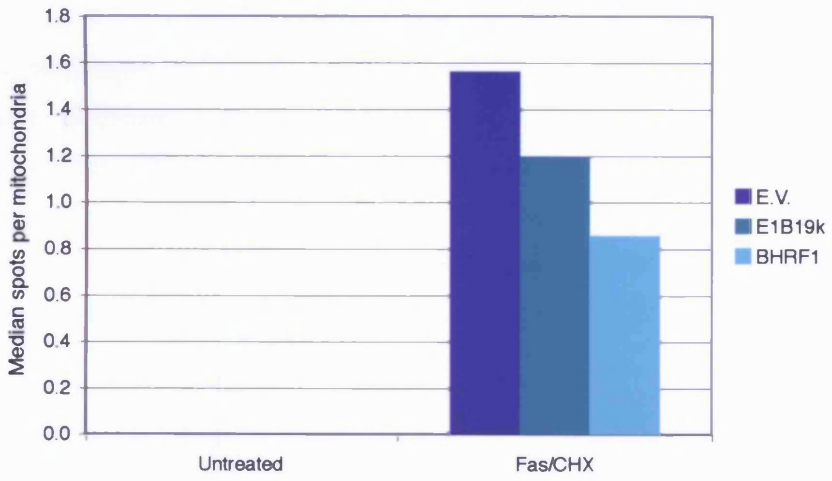

E

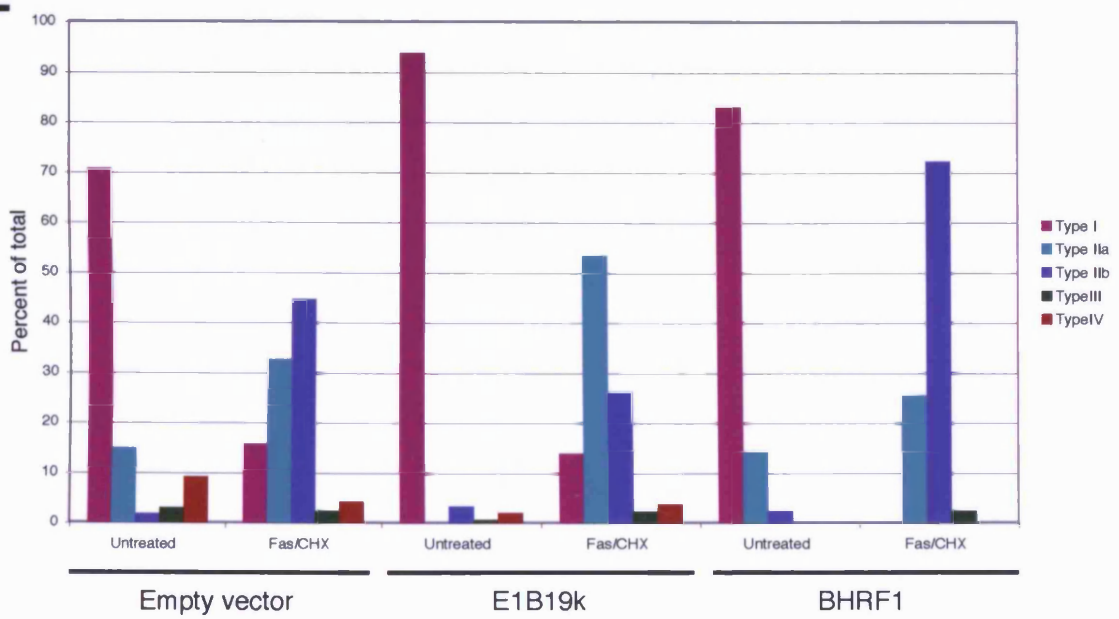

Supplementary Figure 5.7: data added in support.

Bax-GFP AAA shows an ER-like distribution in MCF10A E1B19k cells.

The localisation of Bax-GFP AAA in E1B19k-expressing MCF10A cells is similar to that of an ER marker construct and that of YFP-E1B19k, and fails to co-localise with mitochondria. **(A)** MCF10A E1B19k cells were transfected with Bax-GFP AAA. 24 hrs later cells were loaded with Mitotracker, fixed and mounted for confocal microscopy. The GFP-Bax AAA construct demonstrates a reticular distribution throughout the cytoplasm and enrichment around the nucleus, both characteristics of an ER localisation. **(B)** MCF10A cells were transfected with an ER marker construct (pEGFP-ER, Clontech) and then prepared as in (A). The resulting distribution of the marker construct is very similar to that shown for Bax-GFP AAA in part (A). **(C)** MCF10A E1B19k cells were loaded with Mitotracker, fixed and immunostained using an anti-E1B19k antibody and FITC-coupled secondary antibody. The E1B19k antibody is not recommended for immunofluorescence experiments by the manufacturer but nevertheless shows an enrichment of E1B19k around the cell nucleus, and some evidence of a reticularised cytoplasmic distribution. **(D)** MCF10A cells were transfected with a YFP-E1B19k fusion construct (D.Hancock, CR-UK). 24 hrs later cells were fixed and mounted for confocal microscopy. The over-expressed YFP-E1B19k shows a similar nuclear enrichment and reticularised cytoplasmic distribution as shown in parts (A) and (B). In all images scale bars represent 10 μm.

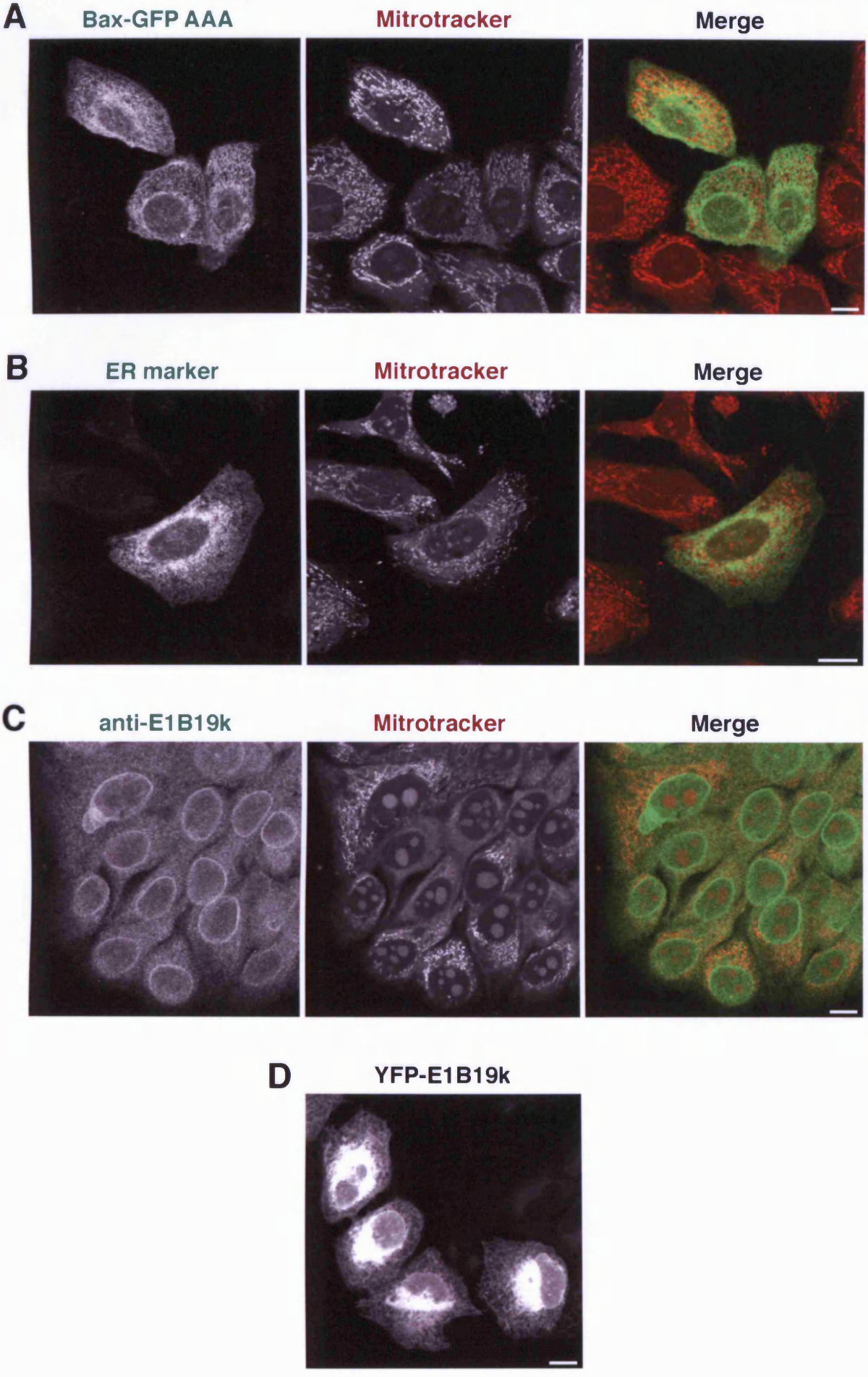
A
Bax-GFP AAA
Mitrotracker
Merge
B
ER marker
Mitrotracker
Merge
C
anti-E1B19k
Mitrotracker
Merge
D
YFP-E1B19k